Dissertation

Experimental and numerical study on pull-out resistance of flip-type earth anchors under different ground conditions, and its application to slope stability

Graduate School of
Natural Science & Technology
Kanazawa University

Division of Environmental Design

Student ID No. 1824052010
Name: Shota Yoshida
Chief advisor: Prof. Hiroshi Masuya
Date of Submission: September, 2021

Abstract

Anchors have been widely used for supporting structures on the ground and on the water. Anchors that are installed in the soil are largely called earth anchors or ground anchors. Anchors can be broadly divided into those that are used with grout and those that are not. There are 2 types of anchors among the anchors installed without grouting. One is pre-embedded in the ground and another is driven directly into the ground.

A typical pre-embedded earth anchors are plate anchors. The plate anchors are pre-embedded in the ground and are expected to have pull-out resistance due to the bearing resistance of the plate. The earth anchors can be used for a wide variety of purposes, such as embankment reinforcement, retaining wall reinforcement, tower support, and so on.

Among those anchors that are directly driven into the ground, there are percussion anchors which are rotate and open in the ground when tensile force acts. Percussion anchors are called “flip anchors” in this study. Unlike grouted ground anchors and plate anchors, flip anchors do not require curing period of grout. And because grouting is unnecessary, cement, water, and related equipment are not required. The required machines and resources are limited; thus, it is possible to respond immediately in the event of disasters. In addition, dust and muddy water accompanied with drilling and grouting are not generated. Flip anchors minimize the efforts and time required for installation and are environmentally friendly. Flip anchors have many advantages and have been used mainly in Europe, the United States, and Australia.

Although the workability is better, there are only a limited number of references directly referring to flip anchors. Moreover, there are still no popular design guidelines such as those found on ground anchors and soil nails. That makes further field application of flip anchors difficult. Even so, there are many studies that can be used for the study of flip anchors, including those of plate anchors. However, as a major premise, it is necessary to confirm that the flip anchors really behaves like the plate anchors after sufficiently open in the ground.

Thus, in this study, pull-out experiments of flip anchors similar to those of the plate anchors were conducted under the condition that the characteristics of the flip anchor to open in the soil were taken into consideration. Three installation conditions, such as “Opened”, “Closed”, and “Driven” were prepared to simulate a practical installation condition of flip anchors. And the experimental results conducted under these conditions can also be compared with those of plate anchors.

In laboratories, pull-out experiments on dense sand ground were conducted. Three-dimensional pull-out experiments using actual flip anchors, and two-dimensional pull-out experiments using model plate or flip anchors were conducted. In the two-dimensional vertical and diagonal pull-out experiments on the model sand ground, in addition to the relationship between pull-out force and pull-out displacement, the displacement of soil particles during the experiments was observed by photos during the experiments to model ground failure pattern.

Full-scale vertical pull-out experiments using actual flip anchors in fields were conducted on a sand ground and a clayey ground. From the results of the field experiments and ground failure patterns observed in the laboratory experiments, 3D ground failure patterns were modelled to estimate pull-out resistance of flip anchors in sand.

In addition, to investigate the slope reinforcement effect of flip anchors, a loading experiment on the model slope was conducted using model plate anchors in a plane strain condition or actual

small flip anchors in a three-dimensional condition.

The pull-out experiments performed on the sandy ground was also simulated by numerical analysis using FEM. Through the series of experiments and numerical analysis, estimation methods of pull-out resistance of flip anchors by limit equilibrium method and FEM analysis were proposed.

In sand, pull-out resistance F_{max} of flip anchors increased as projected area of an anchor A increased; whereas, maximum pull-out pressure p_{max} of the flip anchors increased as A became smaller. F_{max} of Driven and Closed anchors, which are corresponding to the practical installation of flip anchors, reached about 80% of that of horizontally embedded plate anchors (Opened anchors) within the experimental conditions in this study. Pull-out displacement w required for the flip anchors to attain F_{max} was the same amount as a length of an anchor plate L or about 1.5 times that amount.

Ground failure pattern in the pull-out experiments was simply modelled based on the observations of ground deformation during the pull-out experiments in a plane strain condition. F_{max} calculated from the proposed model qualitatively agreed well with measured F_{max} of each pull-out condition. The ground failure pattern of the flip (plate) anchors changes from "shallow anchor" model to "deep anchor" model at critical embedment ratio $(H/L)_{cr}$: where H is an installation depth of an anchor and L is a length of an anchor plate. Thus, the 2D ground failure model was extended to 3D ground failure models for a "shallow anchor" or "deep anchor", respectively.

Using the limit equilibrium method (LEM) based on the 3D models and finite element method (FEM), pull-out resistance of flip anchors in sand were estimated. The calculated values of F_{max} were compared with the measured values of field experiments and calculated values based on the empirical method using breakout factor f_q. The calculated values of F_{max} based on the three estimation methods were all agreed well with each other. Furthermore, the calculated values were agreed well with measured values of F_{max} in the field experiments. The both estimation methods based on the 3D models and FEM could be promising ways to estimate F_{max} of flip anchors in sand, as long as the w required for a plate anchor sufficiently opens is taken into the consideration for H/L.

In clay, pull-out behavior of flip anchors is quite different from that in sand. In clay, F_{max} of a flip anchor was proportional to A. This indicates that p_{max} acting on the anchor head was equivalent regardless of A. As an estimation method of pull-out resistance of flip anchors in clay, the interpretation method for T-bar penetration test is applied. It is because pulling a flip anchor throughout clay is just reverse way of pushing T-bar into the clay. The predicted p range estimated from the values of undrained shear strength of the soil c_u from the vane shear tests and bearing factor of T-bar N_b of 10.5 agreed well with the measured p range of the field experiment. Thus, the estimation method based on the interpretation of T-bar penetration test can be a promising way to estimate pull-out resistance of flip anchors in clay ground.

Finally, an application of flip anchors to slope stability was verified by experimental and numerical study using FEM. From the results of the loading experiments on the shoulder of the model slope ground, flip anchors were found to be effective for slope stability as well. The results of the experiments well agreed with the FEM simulations using the Mohr-Coulomb model. Not only the reinforcement effect but also the displacement of the ground and tensile force acting on anchor rods can be well obtained by FEM analysis. Thus, reinforcement effect of flip anchors can be analyzed by finite element method. In the case of slope reinforcement, the dilatancy of the soil greatly affects the reinforcement effect.

In the scope of this study, the pull-out resistance of flip anchors installed at various grounds conditions, angles, and depths has not been all investigated. From this study, it was found that the

research of pre-embedded plate anchors can be employed in the design of flip anchors, as long as the displacement of flip anchors to open are taken into consideration. Thus, for the conditions that could not be verified in this study, a number of studies on plate anchors, which are performed under other conditions, can be effectively utilized for flip anchors.

Construction of flip anchors can be designed by FEM, but the analysis results are greatly affected by the parameters, thus it is necessary to accurately consider the effects of the parameters for field application. Especially in the case of slopes, the setting of the dilatancy angle has a great influence. In this study, the shoulder of the slope is loaded to analyze the slope stability, but for practical purposes, the effect of flip anchors on slope stability should also be verified using the shear strength reduction (SSR) method.

Although the results of this study were obtained under limited conditions, this study complements the research of plate anchors, and are expected to contribute to the further field application of flip anchors.

Acknowledgements

First and foremost I am extremely grateful to my predecessor supervisor, Emeritus Prof. Tatsunori Matsumoto for his invaluable advice, dedicated support, and patience during my PhD study. His immense knowledge and plentiful experience in world-wide have encouraged me in all the time of my academic research. I have learned more than just about research from his enthusiastic supervisions. This research could not complete, or even begin without his dedicated supports. The three years under his guidance have been an irreplaceable experience for my life. I am very proud of being one of his students.

I would like to extend my gratitude to my chief advisor Prof. Hiroshi Masuya. He gave me advice from the view point of structural engineering. His advice led me to see the research from new perspective. I am grateful his supervising me.

I would also like to express my sincere thankfulness to Asst. Prof. Dr. Xi Xiong. She reviewed and guide my technical papers with her profound knowledge of geotechnical engineering. I learned a lot from her advice and discussion with her. Having her guidance in a timely manner was one of the luckiest things in my research activities.

I would like to thank Assoc. Prof. Shun-ichi Kobayashi for his support at the beginning of my research. And his keen advice helped improve my research.

I also highly appreciate Mr. Shinya Shimono, a technician of the Geotechnical Laboratory. His technical skills allowed me to realize the idea of laboratory experiments.

My research was also supported by students of the laboratory, Dr. Hoang Thi Lua, M. Eng. Dao Xuan Khang, M. Eng. Wentao Guo, Mr. Kanno Masanori, Mr. Kazuki Komura, Ms. Minami Watanabe, and many others.

I would like to express many of my thanks to Daisho Co., Ltd. to which I belong. Daisho Co., Ltd. offered opportunities for field experiments. With the cooperation of Daisho's experienced teams, the field experiments were conducted successfully.

Finally, I would like to express my gratitude to my parents, my wife and my children. Their tremendous understanding and encouragement in the past few years made it possible for me to complete this dissertation.

Shota Yoshida

Kanazawa University

September, 2021

Contents

List of Figures

Chapter 1

Chapter 2

Chapter 3

Chapter 4

Chapter 5

Chapter 6

List of Tables

Chapter 2

Chapter 3

Chapter 4

Chapter 5

Chapter 6

List of Notations

A = projected area of an anchor;
B = breadth of an anchor plate;
B_c = fixed breadth of an anchor for calculation;
c = cohesion of soil;
c_u = undrained shear strength;
D_r = relative density;
E = young's modulus;
E' = modulus of elasity;
EA = axial stiffness;
E_c = constrained modulus;
e = void ratio
e_{max} = maximum void ratio
e_{min} = minimum void ratio
e_{init} = initial void ratio
F = pull-out force;
F_{max} = maximum pull-out force (pull-out resistance);
$F_{max(s)}$ = maximum pull-out resistance of shallow anchor;
$F_{max(d)}$ = maximum pull-out resistance of deep anchor;
F_c = breakout factor for a shallow anchor in clay;
F_c^* = breakout factor for a deep anchor in clay;
$F_{(R)}^*$ = breakout factor for a rectangular deep anchor;
$F_{(S)}^*$ = breakout factor for a square deep anchor;
f_q = breakout factor for shallow anchor in sand;
f_q^* = breakout factor for deep anchor in sand;
H = installation depth of an anchor;
H_{cr} = critical installation depth of an anchor;
(H/L) = embedment ratio;
$(H/L)_{cr}$ = critical embedment ratio;
h = anchor length;
K_0 = coefficient of lateral earth pressure at rest;
K_p = coefficient of passive earth pressure;
K_{pv} = vertical component of passive earth pressure;
K_u = nominal uplift coefficient;
L = length of an anchor plate;
l = length of a slip line;
m = coefficient related to shape factor;
N = normal force;
N_b = bearing factor of T-bar;
P = vertical load;
p = pressure;
p_{max} = maximum pressure;
Q_u = ultimate pull-out capacity;
S = frictional resistance;
s = shape factor;
T = tensile force;
W = weight of soil;
W_a = weight of an anchor;
w = pull-out (or settlement) displacement;
w_c = water content of the ground;
α = pull-out angle;
β = installation angle of an anchor plate;
ΔF = incremental pull-out force;
ΔP = incremental vertical load;
Δw = incremental displacement;
ϕ = friction angle of soil;
ϕ_p = friction angle of soil at peak strength;
ϕ_r = friction angle of soil at residual strength;
γ = unit weight;
γ_{unsat} = unit weight of unsaturated soil;
ν = poisson's ratio;
ρ_d = dry density;
ρ_{dmax} = maximum dry density;
ρ_{dmin} = minimum dry density;
ρ_s = density of soil particle;
θ = angle of a slip line;
$\bar{\sigma}'_0$ = average effective stress between $(H\text{-}H_{cr})$;
σ_n = normal stress;
σ_{ref} = reference stress;
σ_v = effective vertical stress;
τ = shear stress;
$\omega = 90° - \theta$;
ψ = dilatancy angle;

Chapter 1
Introduction

1.1 Background and motivation of the study

Anchors have been widely used for supporting structures on the ground or the water. Anchors that are installed in the soil are largely called earth anchors or ground anchors. The types of the anchors can be broadly divided into those that are used with grout and those that are not. Among the anchors installed without grouting, there are mainly 2 types of anchors. One is pre-embedded in the ground and another is driven or penetrated directly into the ground.

A typical pre-embedded anchors are plate anchors (Fig.1.1). The plate anchors are expected to have pull-out resistance due to the bearing resistance in the ground. The plate anchors can be used for a wide variety of purposes, such as embankment reinforcement, retaining wall reinforcement, tower support, and so on.

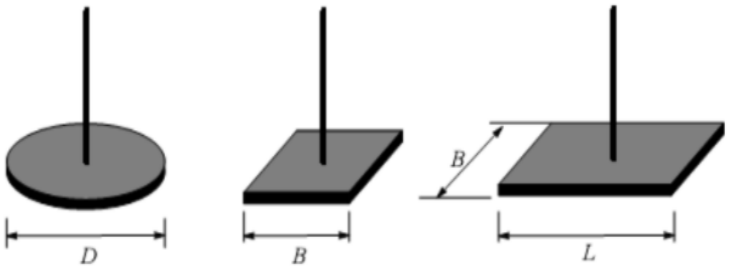

Fig. 1.1. Examples of pre-embedded plate anchors (Niroumand et al., 2010).

Among those anchors that are directly driven or penetrated into the ground, there are largely 2 types of anchors, which are often called “percussion anchors” and “helical anchors”. Percussion anchors rotate and open in the ground when tensile force acts. The pull-out resistance is obtained by the bearing resistance like the plate anchor, but it differs from the plate anchor in that it rotates to open after being driven into the soil.

Percussion anchors are called “flip anchors” in this study (Figs.1.2 & 1.3).

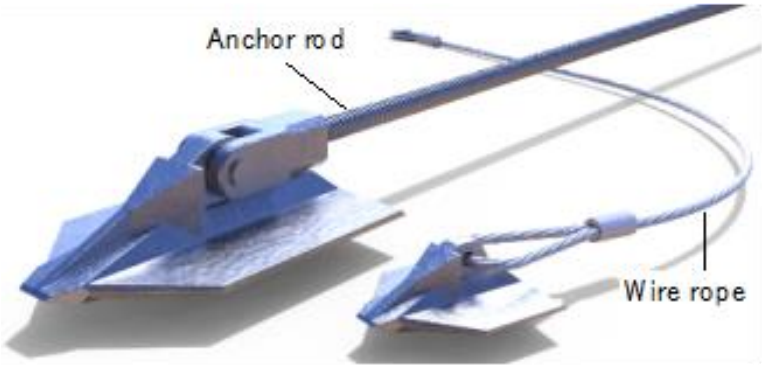

Fig. 1.2. Examples of flip anchors (Anchoring Rope and Rigging Pty Ltd., 2021).

Fig. 1.3. Installation of flip anchors (Anchoring Rope and Rigging Pty Ltd., 2021).

The anchors directly penetrated into the ground are often called helical anchors (Fig. 1.4). Helical anchors are equipped with multiple circular plates on the pile are directly penetrated into the ground. The helical anchors obtain pull-out resistance by the bearing resistance of the plates.

(a) (b)

Fig. 1.4. Helical anchors (piles) by (a) Foundation Technologies Inc. (2021), (b) Lazarte et al. (2015).

The anchors installed with grout are generally called (grouted) ground anchors (Fig. 1.5). The ground anchors are composed of a bonded part and unbonded part, and support the unstable ground so as to be sandwiched by pre-stress. Ground anchors are popular measures for reinforcing retaining walls, slopes (Fig. 1.6), and so on (Fig. 1.7).

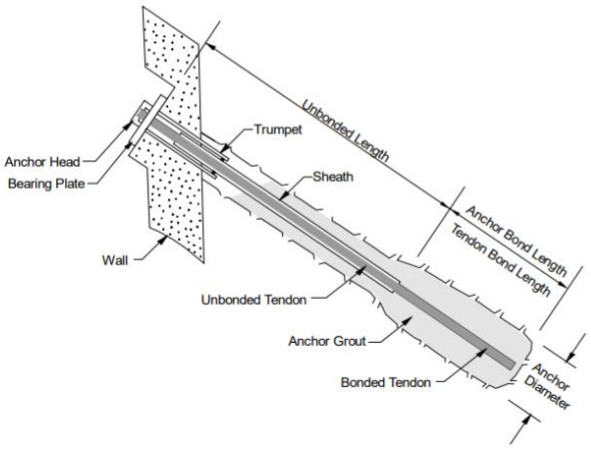

Fig. 1.5. Components of grouted ground anchors (Sabatini et al., 1999).

Fig. 1.6. Application of grouted ground anchors for slope stabilization (Daisho Co., Ltd., 2021).

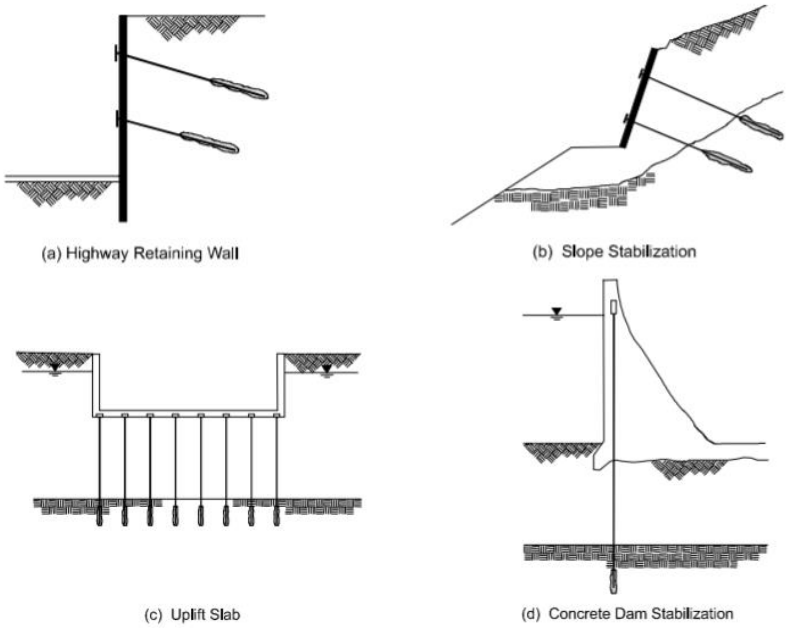

Fig. 1.7. Applications of ground anchors and anchored systems (Sabatini et al., 1999).

Soil nails are technically different from anchors, but often applied to reinforce slopes or walls. Soil nails differ from the ground anchors in that the reinforcing bars inserted into the ground are completely bonded with grout and that pre-stress is not applied (Fig. 1.8). The soil nails obtain pull-out resistance by the peripheral frictional resistance between the grout and the ground (Fig. 1.9). The nails are inserted into boreholes like ground anchors (Fig. 1.10). Soil nails are smaller scale construction than ground anchors.

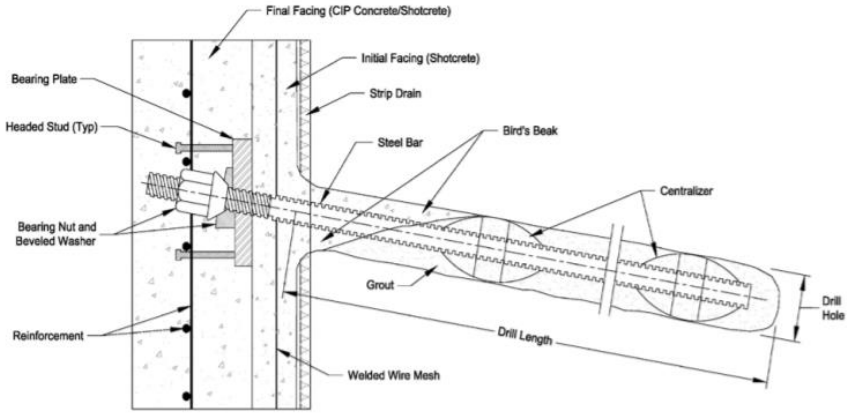

Fig. 1.8. Components of Soil nails (Lazarte et al., 2015).

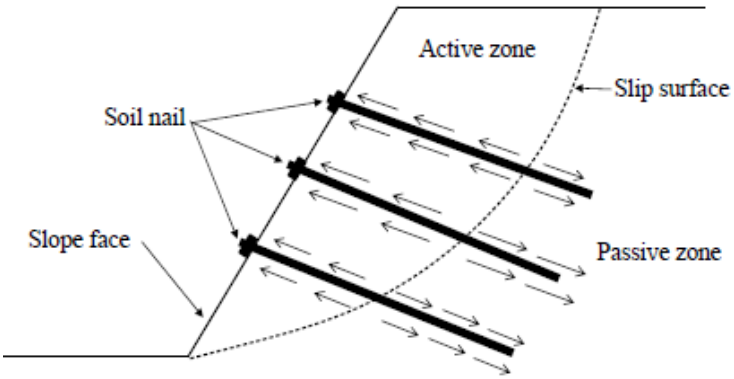

Fig. 1.9. Functions of Soil nails (Ismail et al., 2018).

Fig. 1.10. Construction (drilling) of soil nails (Daisho Co., Ltd., 2021).

The above-mentioned anchors have been applied to variety of supports. Demands for supporting and reinforcing structures or slopes are expected to increase further because the damage caused by slope failures or falling of structures has become more serious recently due to heavy rains, cyclones and typhoons caused by abnormal climate around the world. In situations where the occurrence of such disasters is unpredictable, and the areas where damage is expected are scattered on a small scale, anchors that can be easily installed and immediately exert a reinforcing effect are useful.

Among above-mentioned anchors, flip anchors are suitable for the urgent restoration works from slope failures for example, and preventive measures against collapse of structures or slope failures immediately before disasters. It is because drilling and grouting are not required for flip anchors, the installation and reinforcement are completed immediately. As shown in Fig. 1.11, flip anchors are driven directly into the ground in the closed anchor head state. After being driven to the designed depth, an anchor head rotates and opens when tensile force acts on the anchor, so that obtain pull-out resistance.

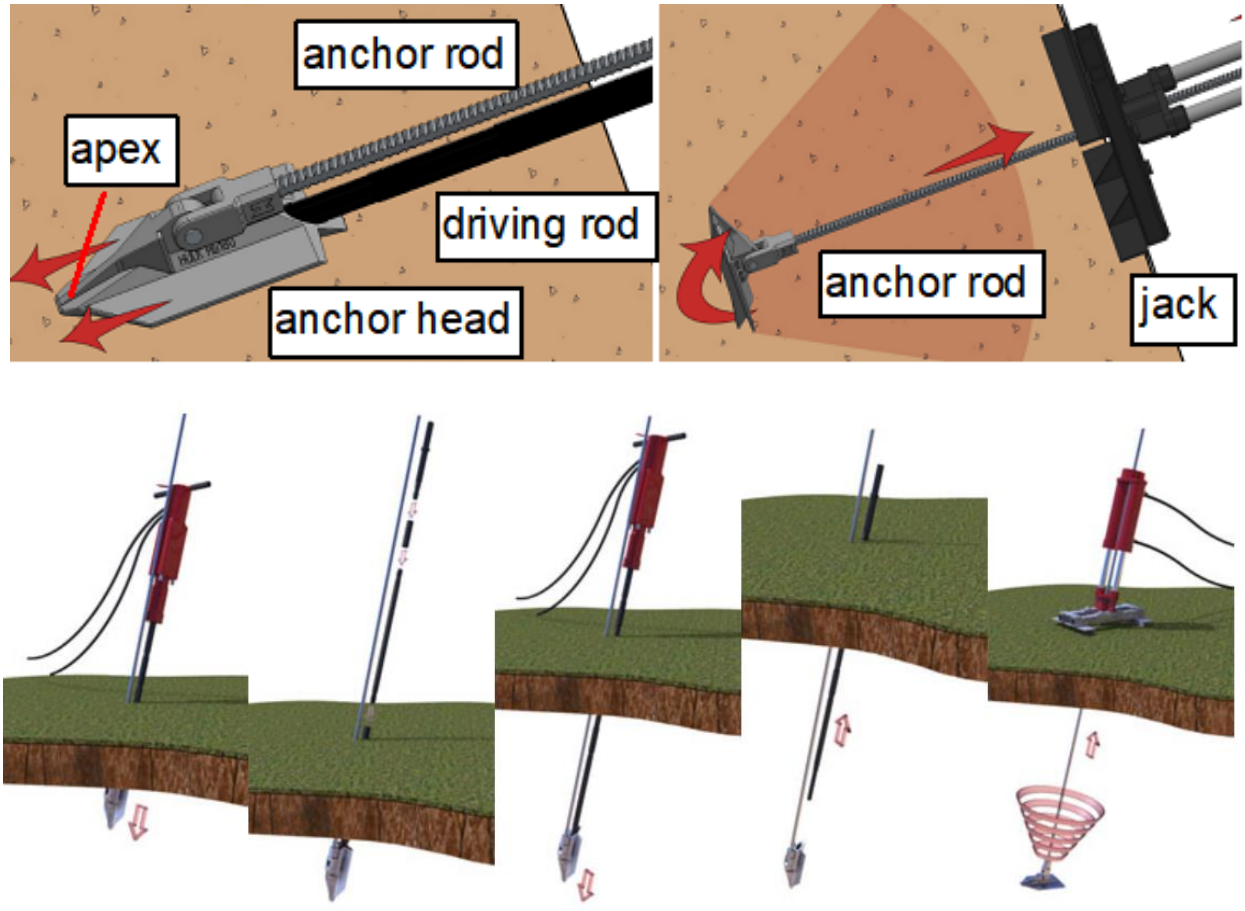

Fig. 1.11. Installation procedures of a flip anchor (Anchoring Rope And Rigging Pty. Ltd., 2021).

Unlike grouted ground anchors, flip anchors do not require curing period of grout. Because grouting is unnecessary, cement, water, and related equipment are not required. The required machines and resources for the installation are limited; thus, it is possible to respond immediately in the event of disasters. In addition, dust and muddy water accompanied with drilling and grouting are

not generated. Flip anchors minimize the efforts, material, and time required for the installation, and are environmentally friendly.

Figure 1.12 shows examples of applications of flip anchors.

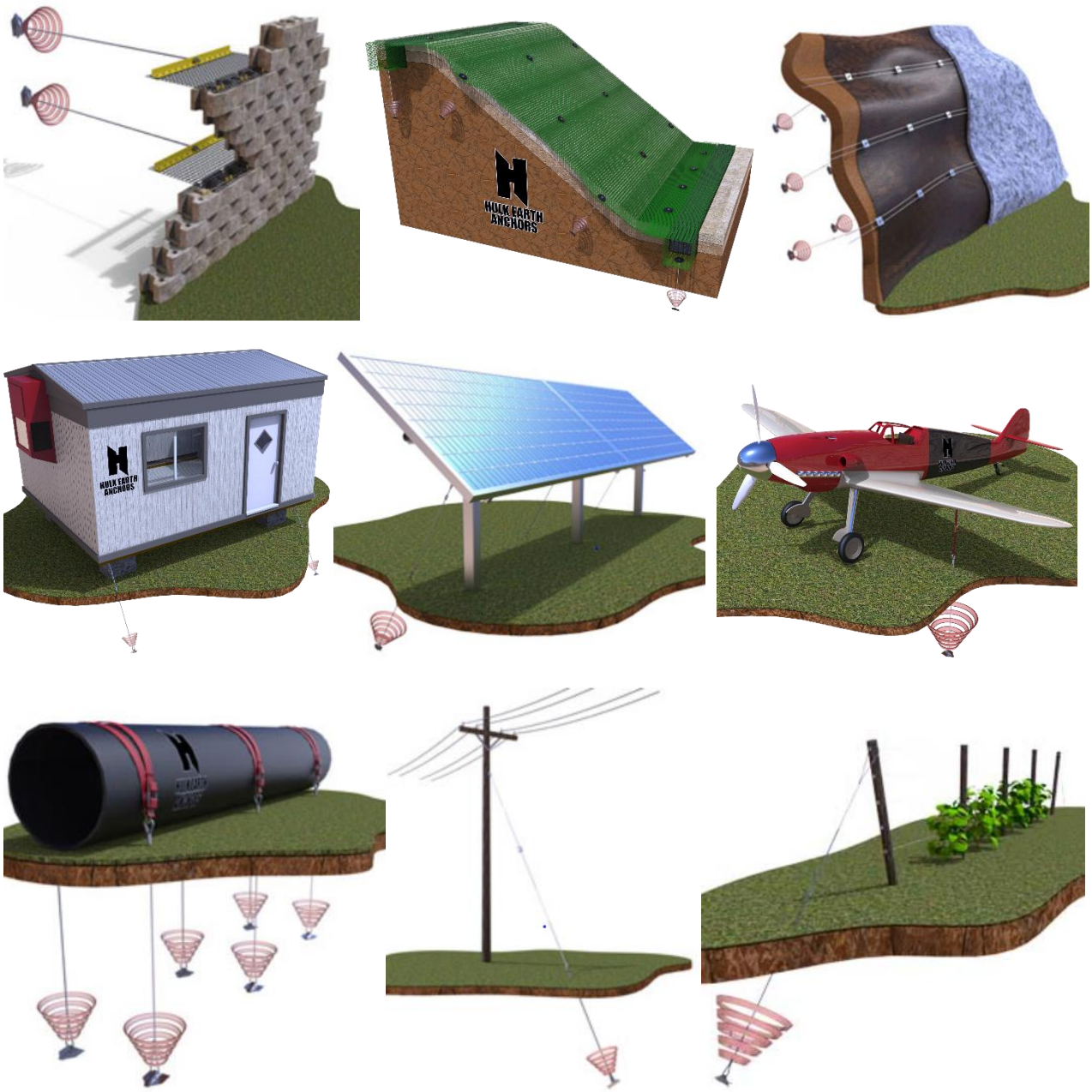

Fig. 1.12. Application examples of flip anchors (Anchoring Rope And Rigging Pty. Ltd, 2021).

Flip anchors have many advantages and have been used mainly in Europe, the United States, and Australia. Although flip anchors have excellent workability, estimating pull-out resistance depending on ground conditions seems to be difficult, due to its specific mechanism compared to general pre-embedded plate anchors. A number of previous research on pull-out capacity of the plate anchors were conducted so far. And some studies on helical anchors can be found although there are fewer than plate anchors; however, there are few studies on flip anchors. Moreover, there are still no

popular design guidelines such as those found on ground anchors and soil nails. That makes further field application of flip anchors difficult.

Thus, in this study, a series of experimental and numerical studies were conducted to investigate the fundamental mechanism of the pull-out resistance of flip anchors.

1.2 Scope of the study

This study focused on providing insights into the mechanism of pull-out resistance of flip-type (percussion) earth anchors based on experimental results in sand and clay.

Pull-out experiments of flip anchors were conducted both in laboratories and fields, considering the unique feature that the anchor head rotates and opens in the ground. From the relationship between pull-out force and pull-out displacement, the behavior including pull-out resistance of flip anchors was investigated.

In laboratories, pull-out experiments on dense dry sand ground were conducted. Three-dimensional pull-out experiments using actual flip anchors, and two-dimensional pull-out experiments using model plate or flip anchors were conducted. In the two-dimensional vertical and diagonal pull-out experiments on the sand ground, the displacement of soil particles during the experiments was observed by taking photos during the pull-out of the anchors to model ground failure pattern.

In fields, full-scale vertical pull-out experiments using actual flip anchors were conducted on sand and clay.

To study the slope reinforcement effect of flip anchors, a loading experiment on the model slope was conducted using model plate anchors in a plane strain condition, or actual small flip anchors in a three-dimensional condition.

Furthermore, the above experiments performed on the sandy ground was also simulated by numerical analysis using FEM.

Through a series of experiments, including model and full-scale pull-out experiments, and numerical simulations, experimental results on the pull-out resistance of flip anchors were obtained. Because three installation conditions prepared for flip anchors: “Opened”, “Closed”, and “Driven”, experimental results can be compared with the those on plate anchors in previous studies. With reference to those experimental results and research on plate anchors, estimation methods of pull-out resistance of flip anchors on sand and clay grounds were proposed. And its application to slope stability was examined.

1.3 Thesis structure

Chapter 1 is an introduction of this thesis.

Chapter 2 is a review of literature related to flip anchors and case studies of application of flip anchors by mainly some private companies.

Chapter 3 describes the results of pull-out experiments using actual flip anchors. Chapter 3 consists of the following three experiments.

- *Section 3.2.* Vertical pull-out experiments of 3 sizes of actual flip anchors on a model sand ground in a laboratory.
- *Section 3.3.* Vertical pull-out experiments of 5 sizes of actual flip anchors on full-scale sand

ground in a field.

- *Section 3.4.* Vertical pull-out experiments of 5 sizes of actual flip anchors on a full-scale ground consisted of sand and clay layer in a field. Estimation method of pull-out resistance of flip anchors in clay was proposed.

In **Chapter 4**, pull-out experiments in sand grounds under plane strain conditions using model plate or model flip anchors were conducted while observing the ground failure pattern.

- *Section 4.2.* Push-up experiments of a horizontal model plate anchor (trap door).
- *Section 4.3.* Vertical and diagonal pull-out experiments of model flip anchors.

In **Chapter 5**, based on the above experimental results, estimation methods for pull-out resistance of flip anchors in sand by LEM and FEM were proposed.

In **Chapter 6**, an application of flip anchors to slope stability was considered by loading experiments on a shoulder of a model slope made of sand. The experiments were conducted using model plate anchors in a plane strain condition, or using actual small flip anchors in a three-dimensional condition. The experiments in a plane strain condition were simulated by FEM analysis.

Chapter 7 is a summary and recommendation of this thesis.

References in Chapter 1

Anchoring Rope And Rigging Pty. Ltd. (2021). https://www.hulkearthanchors.com.

Daisho Co., Ltd. (2021). https://sd-daisho.com.

Foundation Technologies Inc. (2021). https://www.foundationtechnologies.com/products/chance-helical-piles/.

Ismail M. A. M., Min N. S., Abidin M. H. Z., and Madun A. (2018). Subsurface characterization using geophysical seismic refraction survey for slope stabilization design with soil nailing. Journal of Physics: Conference Series, 995(1), 8 pp.

Lazarte C. A., Robinson H., Gómez J. E., Baxter A., Cadden A., and Berg R. (2015). Geotechnical engineering circular No. 7 Soil nail walls - reference manual, U.S. Department of Transportation Federal Highway Administration, 425 pp.

Niroumand H., Kassim K. A., and Nazir R. (2010). Experimental studies on horizontal anchor plates in cohesive soil. Electronic Journal of Geotechnical Engineering. 15, pp. 879-886.

Sabatini P.J., Pass D.G., Bachus R.C. (1999). Geotechnical engineering circular No. 4 Ground anchors and anchored systems. U.S. Department of Transportation Federal Highway Administration, 304 pp.

Chapter 2
Literature review

2.1 Introduction

Few studies have been found on the pull-out resistance of flip anchors. In this study, because when a flip anchor fully opens in the ground, it will be in the same state as pre-embedded plate anchor, the studies of plate anchors were referred to as the closest reference on flip anchors. The behaviors of pre-embedded plate anchors, such as square, rectangular, circular, and strip anchors in sandy or clayey ground conditions, have been well investigated in previous studies. A number of experimental studies have been conducted to investigate pull-out resistance of the plate anchors. And ground failure patterns related to the uplift of the anchors were observed and modelled. Pull-out resistance and ground failure patterns were studied by numerical analysis as well.

Among the studies on plate anchors, pull-out experiments of plate anchors on sand grounds were conducted more than those on clay grounds. In experimental studies on both ground conditions, most of the studies conducted in laboratories using small model anchor plates. Centrifuge experiments were also conducted considering scale effects. Compared to that, there are few cases of full-scale field experiments using actual plate anchors. In the sandy ground, there are some examples of full-scal pull-out experiments in the early days of research, but in clay ground, there are few can be found.

Through those studies, methods and procedures for calculating pull-out resistance of plate anchors have been proposed in both sand and clay. The pull-out resistance of the plate anchor largely depends on the shape of the ground failure pattern by the pull-out of the anchor. Because the failure pattern accompanied with the uplift of plate anchors depends on the ground or pull-out conditions, many experimental and numerical studies have been conducted still recently. In this chapter, the literature is reviewed.

2.2 Research on pull-out resistance of plate anchors in sand

For the estimation of pull-out resistance of plate anchors in sand, there are mainly three types of approaches using: ground failure models, empirical relationships, or numerical analysis

Ground failure patterns can be modelled from the observation of the ground during the pull-out experiments. Based on the model, pull-out resistance of plate anchors can be estimated. There are following 3 major early theories.

Majer (1955) proposed the frictional cylinder model (Fig. 2.1). The model assumes that the ground fails in a cylindrical shape with the anchor plate at the bottom. The pull-out resistance is calculated from the sum of the weight of the cylindrical soil above the anchor plate and the frictional resistance of the peripheral surface of the soil cylinder.

Mors (1959) proposed the cone model (Fig. 2.2). The model assumes that truncated-cone-shaped soil mass with an apex angle of $90°+\phi/2$ (ϕ: internal friction angle). In this model, only the weight of the soil in the truncated cone is considered to obtain the pull-out resistance.

Balla (1961) observed a failure pattern consisting of curved failure lines from the edge of the anchor (Fig. 2.3). The curved lines meet the ground surface at an angle of approximately $45°-\phi/2$. The

pull-out resistance is calculated from the weight of the soil mass and the friction along the curved failure lines based on the Kötter's equation.

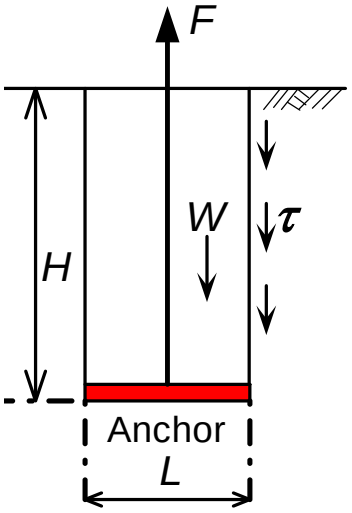

Fig. 2.1. Soil cylinder model (Majer, 1955).

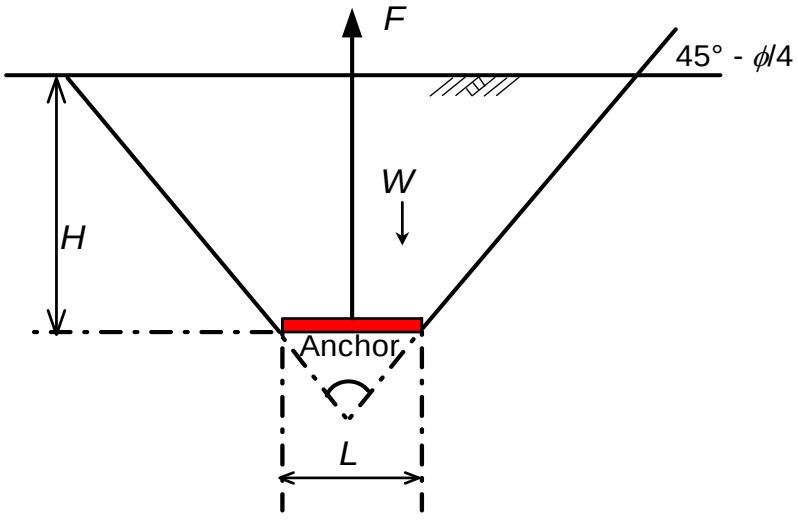

Fig. 2.2. Cone model (Mors, 1959).

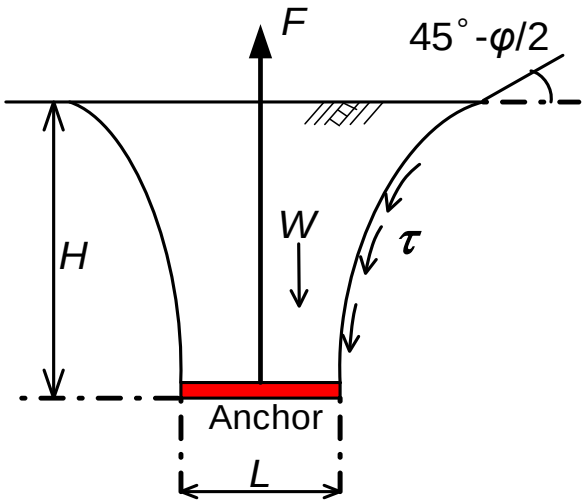

Fig. 2.3. Model by Balla (1961).

In general, the ground failure pattern accompanied with the pull-out of the plate anchors changes at a certain critical embedded depth (Meyerhof & Adams, 1968). For square and rectangular anchors, the embedment ratio H/L (= B) is usually applied because the critical embedded depth depends on the size of an anchor. The border of distinguishing failure patterns is expressed as critical embedment ratio $(H/L)_{cr}$ (Das et al., 1977): where H is an embedment depth of an anchor, L is a length of an anchor plate, B is a breadth of an anchor plate. For circular anchor, H/L (= B) is usually replaced by H/d (= h): where d or h is a diameter of a circular anchor.

An anchor embedded shallower than the $(H/L)_{cr}$ is regarded as "shallow anchor", and an anchor embedded equal to or deeper than the $(H/L)_{cr}$ is regarded as "deep anchor". The clear difference between "shallow anchor" and "deep anchor" is whether the slip lines that are generated by an uplift of an anchor reach the ground surface or not. The failure pattern can be observed in pull-out experiments in a plane strain condition, for example, the ground failure patterns have been observed by photos taken during the experiments. A kind of particle image velocimetry (PIV) analysis was employed to observe ground failure patterns in push-up test on a trap door (Tanaka & Sakai, 1993) or digital image correlation (DIC) methods were employed by pull-out test of anchors (Liu et al., 2012). In a three-dimensional condition, cracks and heaving of the ground surface were observed in the experiments to find $(H/L)_{cr}$ (Baker & Kondner, 1966).

The value of $(H/L)_{cr}$ depends on the ground conditions. In dense sand ground, for example, $(H/L)_{cr}$ of 6 was pointed out by Baker and Kondner (1966). In the study, based on the results of pull-out experiments, empirical theories to estimate pull-out resistance of plate anchors for "shallow anchor" or "deep anchor" conditions in sand ground were proposed.

Shallow anchor

Mariupol'skii (1965) estimated pull-out resistance separately for shallow anchor or deep anchor. For shallow anchor, compression process of the cylindrical column of soil is considered (Fig. 2.4). As compression proceeds, the vertical compressive stress increase. An increase frictional resistance in the soil column leads to the development of sufficient tensile stresses so that slip lines occur in the form of a cone with curved lines. The pull-out resistance is calculated from the weight of the anchor and soil in the truncated cone, and frictional and cohesive force along the external surface.

Veesaert (1977) estimated pull-out resistance from the weight of the anchor, the weight of sand within the failure zone, and the shearing resistance along the failure plane (Fig. 2.5). The truncated cone model has an apex angle ϕ. Veesaert assumed that the normal stress acting on the surface of the cone was a linear function of depth, i.e., the K_0 is assumed to be constant with depth.

Vesić (1971) applied the theory of cavity expansion to the calculation of pull-out resistance of plate anchors (Fig. 2.6). Pull-out resistance can be calculated from vertical component of force inside the cavity, weight of the soil, and vertical component of internal force.

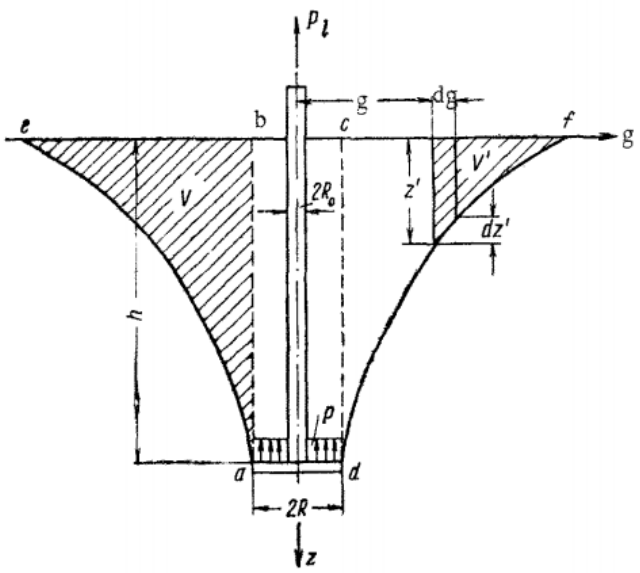

Fig. 2.4. Model by Mariupol'skii (1965) for shallow anchors.

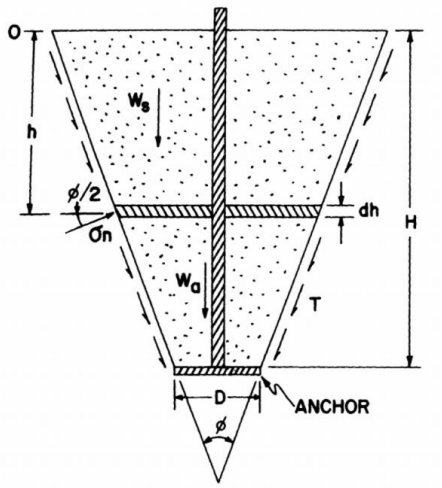

Fig. 2.5. Model by Veesaert (1977).

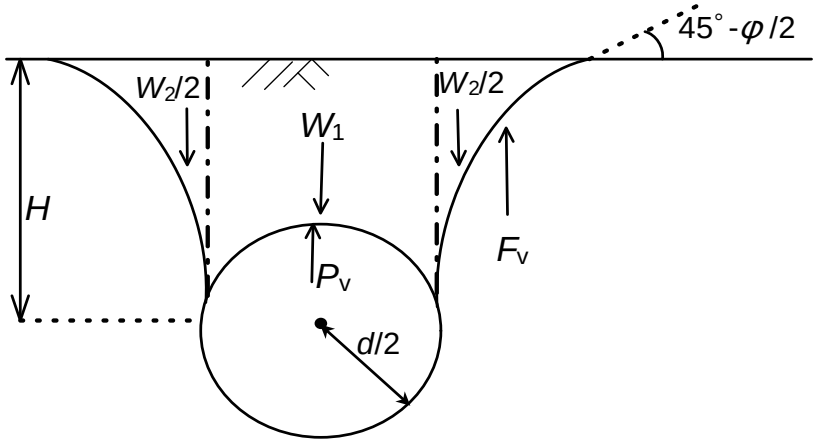

Fig. 2.6. Model by Vesić (1971) for shallow anchors.

Deep anchor

In case of a deep anchor, the above models cannot be applied because slip lines do not reach the ground surface in a deep anchor condition. Following are examples of deep anchor models.

Tagaya et al. (1988a) proposed that the highly compressed wedge I formed above the anchor pushes the radial shear zone II sideways into the plastic zone III (Fig. 2.7).

Mariupol'skii (1965) assumed that pulling the anchor under deep anchor condition required force equivalent to force to expand a cavity having the same volume created by pulling the anchor plate (Fig. 2.8).

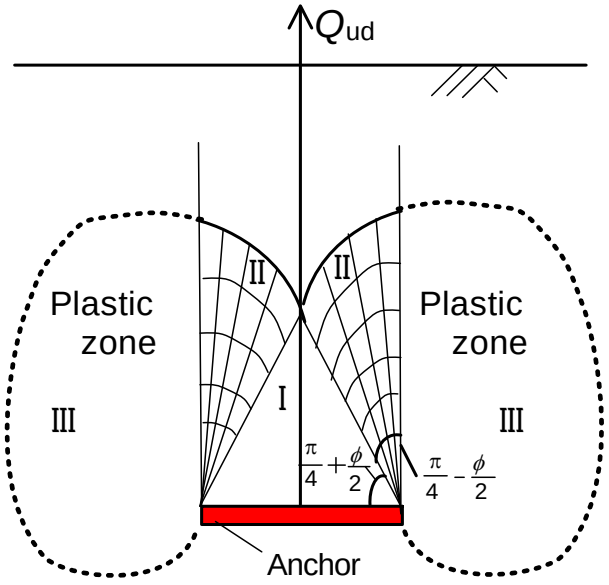

Fig. 2.7. Model by Tagaya et al. (1988a) for deep anchor.

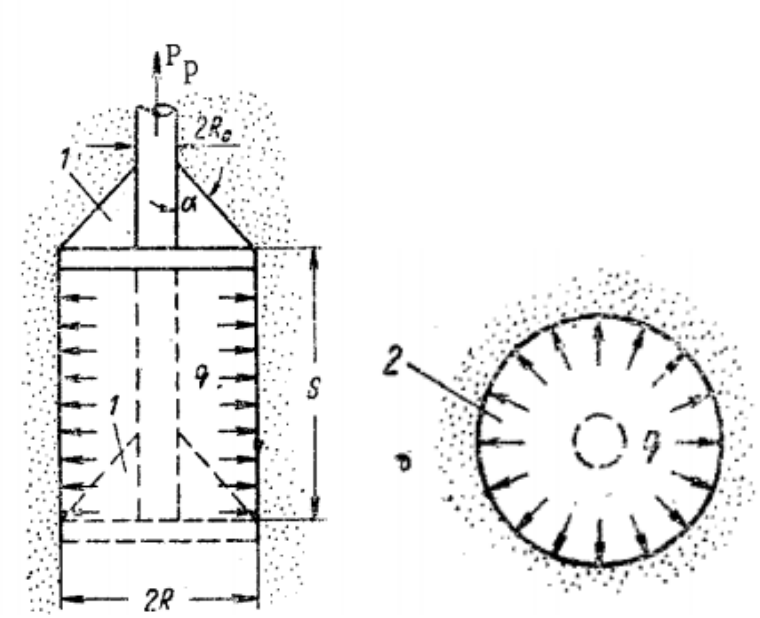

Fig. 2.8. Model by Mariupol'skii (1965) for deep anchor.

As shown in Figs. 2.9 & 2.10, Baker and Kondner (1966) gave results of a number of pull-out experiments of small-scale model earth anchors. And two full-scale field experiments of Webb-Lipow type anchors were presented as well. Empirical relationships among anchor size, embedment depth of anchor, and pull-out capacity of circular anchors buried in dense uniform sand were developed by dimensional analysis techniques. Especially, embedement ratio *(h*/*d*) was studied in a range of field application of earth anchors to define the transition point from a shallow failure to a deep failure.

The border of the (*h*/*d*) was defined as 6 for dense sand based on the tendencies of relationships between pull-out force and pull-out displacement, and observations of the deformation of the ground surface during pulling an anchor.

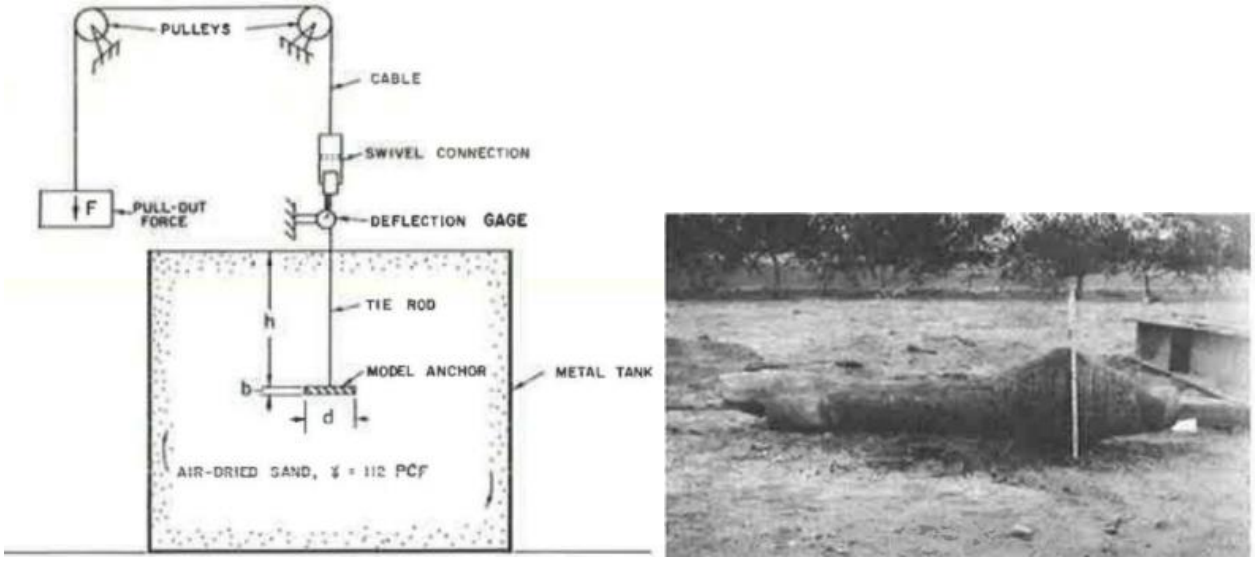

(a) Model anchor experiment setup (b) Field anchor after testing

Fig. 2.9. Pull-out experiments of model and field anchors (Baker & Kondner, 1966).

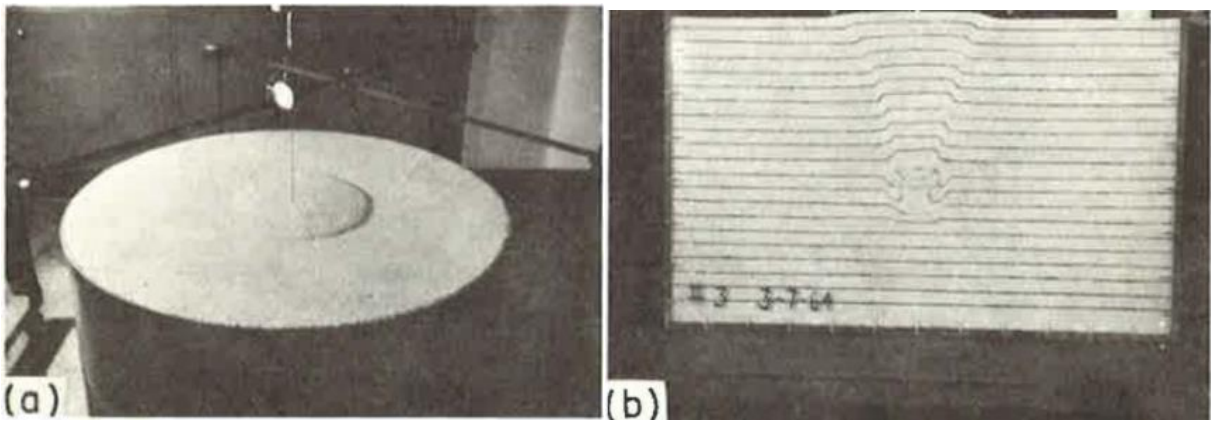

(a) Failure circle developed by shallow anchor (*h*/*d* < 6) (b) Two-dimensional failure surface developed by 76.2 mm wider than the anchor

Fig. 2.10. Observed 2D & 3D ground failure pattern (Baker & Kondner, 1966).

Using dimentionless factors, Baker and Kondner (1966) derived empirical formulas for calculating pull-out resistance for shallow and deep anchor. For shallow anchor in dense sand ground ($\phi = 42°$), the estiamted results were well agreed with values form Balla's theory.

A number of other pull-out experiments in laboratories have been conducted under different experimental conditions, such as Saeedy (1971), Das and Seely (1975), Das and Jones (1982), Murray and Gededes (1987), and Niroumand et al. (2010).

Some studies, such as Ovesen (1979), Tagaya et al. (1988b), Tanaka and Sakai (1993), Sakai and Tanaka (1998) pointed out, and examine the problem of scale effect on the results of experimental studies using small scale model anchors.

Instead of conducting field experiments that cost much, some model experiments in a centrifuge force field were conducted, such as Dickin and Leung (1983), Dickin (1988), Tagaya et al. (1988b).

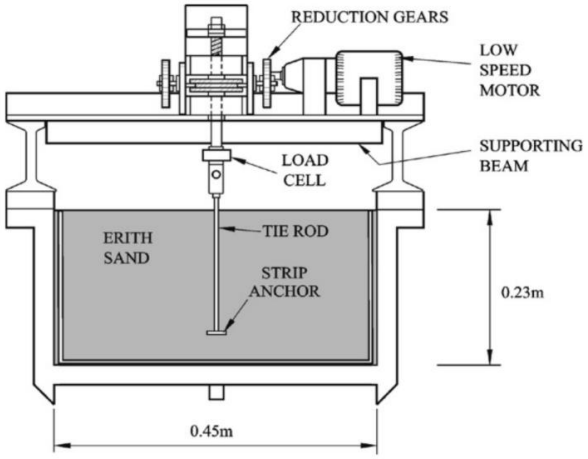

Fig. 2.11. Centrifuge package arrangement for uplift tests on strip anchors (Dickin, 1988).

Dickin (1988) conducted centrifuge experiments using 25 mm wide, 3 mm thick model anchor plates with aspect ratios L/B = 1, 2, 5, and 8 at H/B from 1 to 8 in loose and dense sand grounds (Fig. 2.11). The anchors were subjected to accelerations of 40 gravities in flight. The experienced stress levels were similar to those around 1.0 m wide prototype anchors.

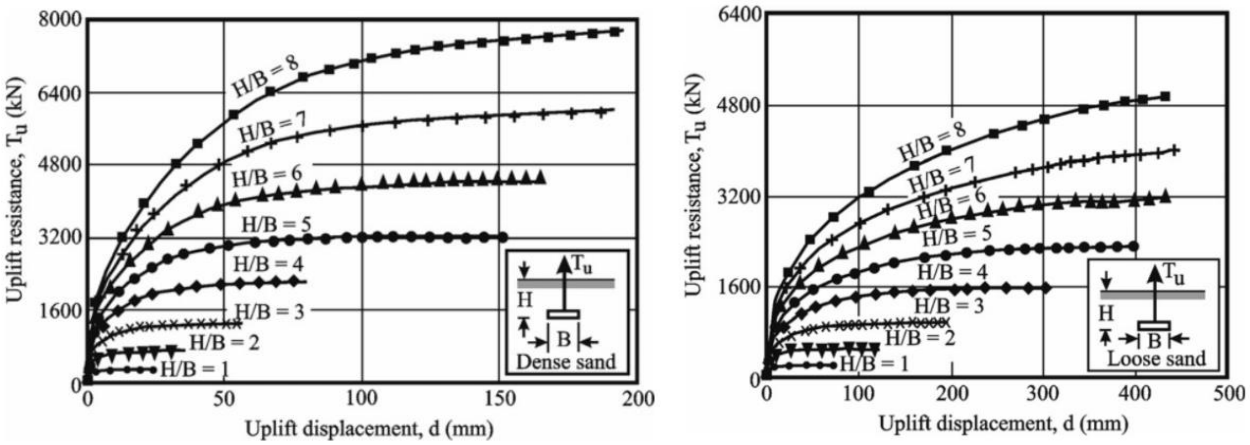

(a) Dense sand (16 kN/m^3) (b) Loose sand (14.5 kN/m^3)

Fig. 2.12. Influence of embedment ratio on the uplift load response of strip anchors in dense or loose sand (Dickin, 1988).

As shown in Fig. 2.12, Pull-out resistance of strip anchors become larger with increasing H/B both in dense and loose sand. In loose sand, the anchors require much larger pull-out displacement to attain peak pull-out resistance. And for anchors at larger H/B, the peak values of resistance do not appear clearly even with large displacement.

Ilamparuthi et al. (2002) investigated pull-out behavior of relatively large scale model circular plate anchors up to 400 mm in diameter. The anchors were embedded in loose, medium-dense, or dense dry sand ground. The experimental results were compared from various points of view including the observation of the deformation of the ground. The following critical embedment depth $(H/D)_{CR}$ were derived depending on the ground conditions. A relationship between $(H/D)_{CR}$ and ϕ were plotted from the results of the experiments in Fig. 2.13 and listed in Table 2.1: where δ is the displacement at peak pullout load, N_{qf} is breakout factor, H is embedment depth, D is the diameter of the anchor. In Table 2.2, previous value of $(H/D)_{CR}$ was compared with the values in the research.

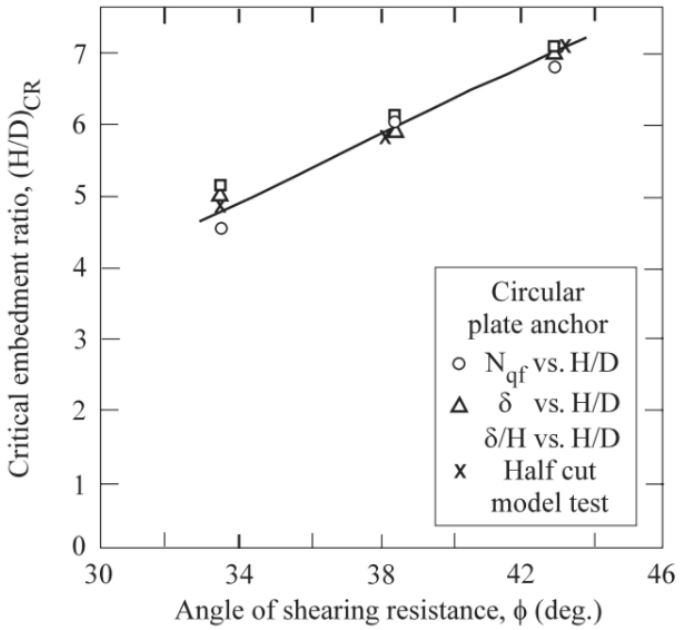

Fig. 2.13. Comparison of alternative estimations of critical embedment ratio for circular plate anchors in sand (Ilamparuthi et al., 2002).

Table 2.1. Critical embedment ratios for circular plate anchors calculated by various methods by (Ilamparuthi et al., 2002).

	Critical embedment ratio		
Means of determination	ϕ = 33.5°	ϕ = 38.5°	ϕ = 43.0°
Load vs. displacement	4.0	5.9	6.3
N_{qf} vs. H/D	4.5	5.5	6.6
δ vs. H/D	5.0	5.8	6.8
δ/H vs. H/D	5.1	5.9	6.9
Surface heave	4.0	5.9	>6.0
Rupture surface in half-cut model test	4.9	5.8	6.9

Table 2.2. Comparison of critical embedment ratios obtained from the present investigations with those from published results (Ilamparuthi et al., 2002).

Authors	Angle of shearing resistance, ϕ (°)	Critical embedment ratio	
		Published results	Present investigation
Baker and Kondner 1966	42	6	6.6
Vesic 1971	Loose	3	4.8
	Dense	10	6.8
Meyerhof and Adams 1968	30	4	4.0
	35	5	5.1
	40	7	6.2
	45	9	7.5
Clemence and Veesaert 1977	41	5	6.4
Sutherland et al. 1982	33.6	4.3	4.8
	36.5	7.8	5.4
	41.5	10.5	6.5
Tagaya et al. 1988	32	6	4.4
	42	8	6.6

Merifield et al. (2006) estimates anchor break-out factor N_γ for horizontal square and circular anchors by rigorous numerical analysis for various friction angles of soil ϕ. From the research, the break-out factor N_γ increase non-linearly with an increasing H/B (Fig, 2.14). The rate of increase is the greatest where $\phi > 30°$. Dimensionless shape factor effecting on pull-out resistance of plate anchors was examined and proposed. The application of semi-empirical estimation techniques based on laboratory experiments sometimes do not work well due to problems such as scale effect. The calculation results by limit equilibrium techniques do not match well with the results of the analysis by the author. Thus, the author explains the effectiveness of numerical analysis to estimate pull-out resistance of plate anchors.

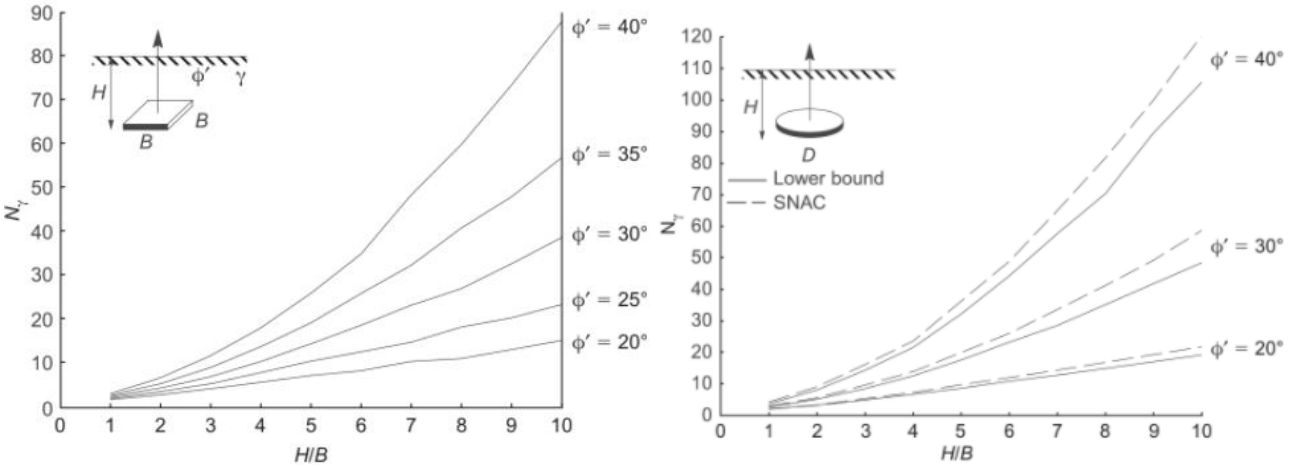

Fig. 2.14. Lower-bound break-out factors for square and circular anchors in cohensionless soil (Merifield et al., 2006).

Dickin and Laman (2007) conducted FEM analysis, using Hardening Soil Model. The anchors and grounds were modelled with very fine mesh or coarse mesh, as shown in Fig. 2.15. The results were compared with the results of centrifugal experiments (Fig. 2.16). The influence of mesh coarseness and a value of K_0 was found to be a minor influence on the results. The response of the soil above a strip anchor is dependent on H/B. The displacement contours can be obtained from FEM analysis (Fig. 2.17). For shallow anchor (Fig. 2.17a), the soil displacements extend to the ground surface whereas the displacement for deep anchor (Fig. 2.17b) is more localized.

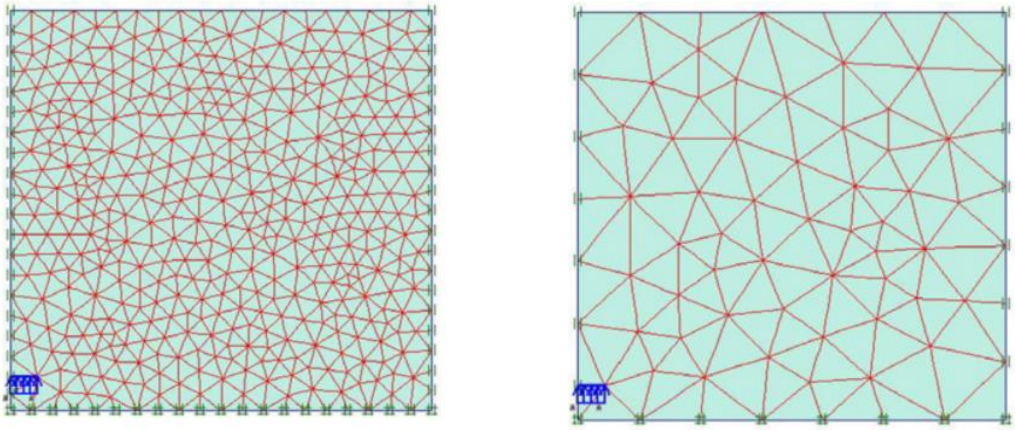

(a) Very fine mesh (b) Coarse mesh

Fig. 2.15. Mesh of FEM analysis of a strip anchor with H/B = 7 (Dickin and Laman, 2007).

The results from numerical analysis were reasonably agreed with the result of centrifuge experiments by Dickin (1988) in both shallow anchor case (H/B = 3) and deep anchor case (H/B = 7).

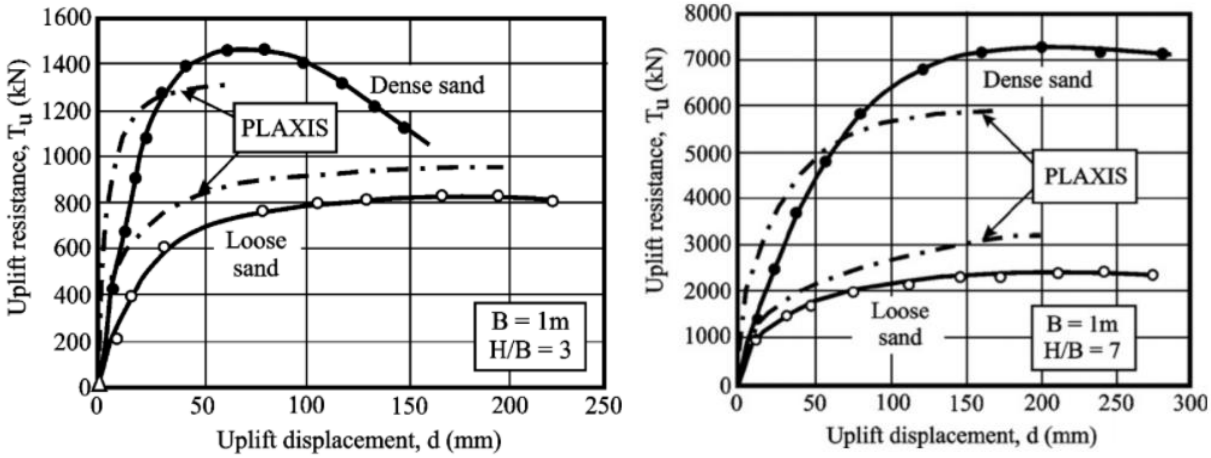

(a) H/B = 3 (b) H/B=7

Fig. 2.16. Comparison of the results by FEM and centrifuge experiments (Dickin and Laman, 2007).

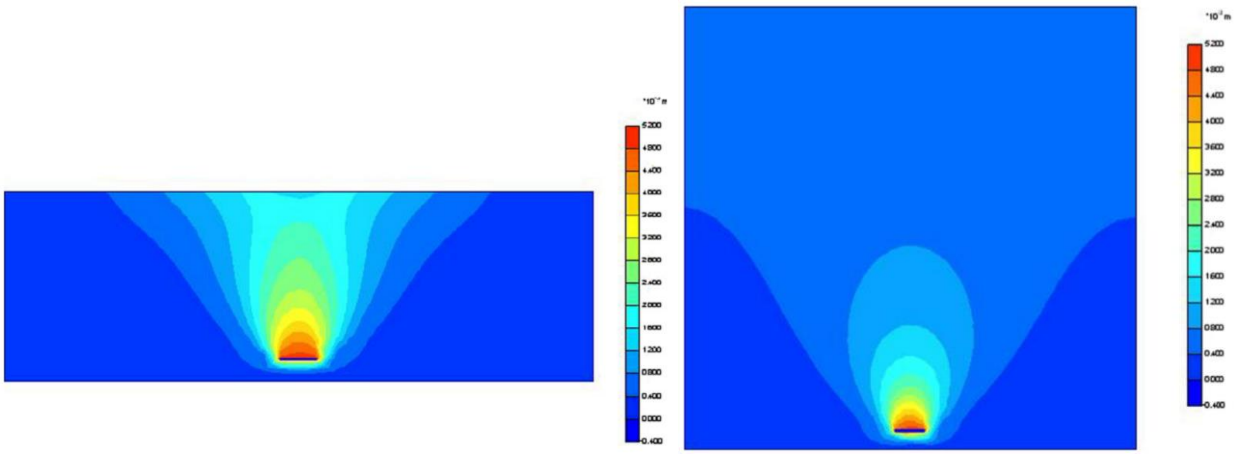

(a) H/B = 5 (b) H/B = 15

Fig. 2.17. Displacement contours for a strip anchor at H/B = 5 in dense sand (Dickin and Laman, 2007).

Other numerical analysis in sand ground was also conducted by other studies, such as Tagaya et al. (1983), Kouzer and Kumar (2009), Mokhbi et al. (2018), and Riyad et al. (2020).

Liu et al. (2012) presented an experimental investigation on sand deformation around uplift plate anchors in sand ground by using digital image correlation (DIC). As shown in Fig. 2.18, ground failure pattern by the pull-out of the anchor is influenced by the ground density. In loose sand, the ground failure pattern could shift from "shallow anchor" pattern to "deep anchor" pattern at smaller H / D than that in dense sand.

Discrete-element method (DEM) simulations were applied to investigate the behavior of plate anchors by Evans and Zhang (2019). The DEM model consisted of spherical particles and boundary walls (Fig. 2.19). In this study, system and particle scale analyses of plate anchors embedded in granular soils were conducted. Consistency in results across DEM simulations, experimental tests, and empirical equations was demonstrated. Anchor failure mechanisms were analyzed by investigating particle-scale response to anchor uplift.

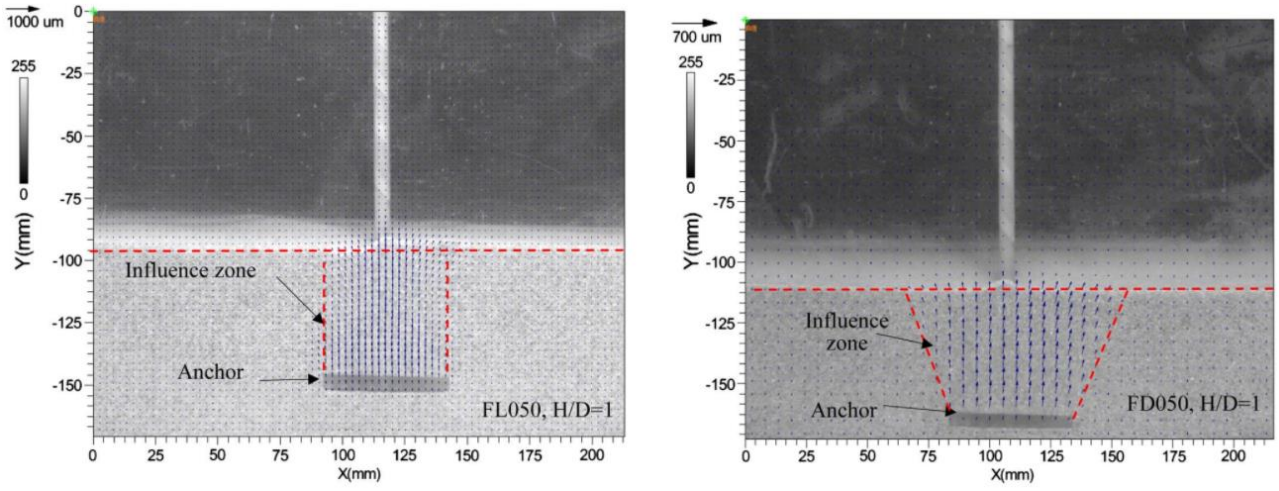

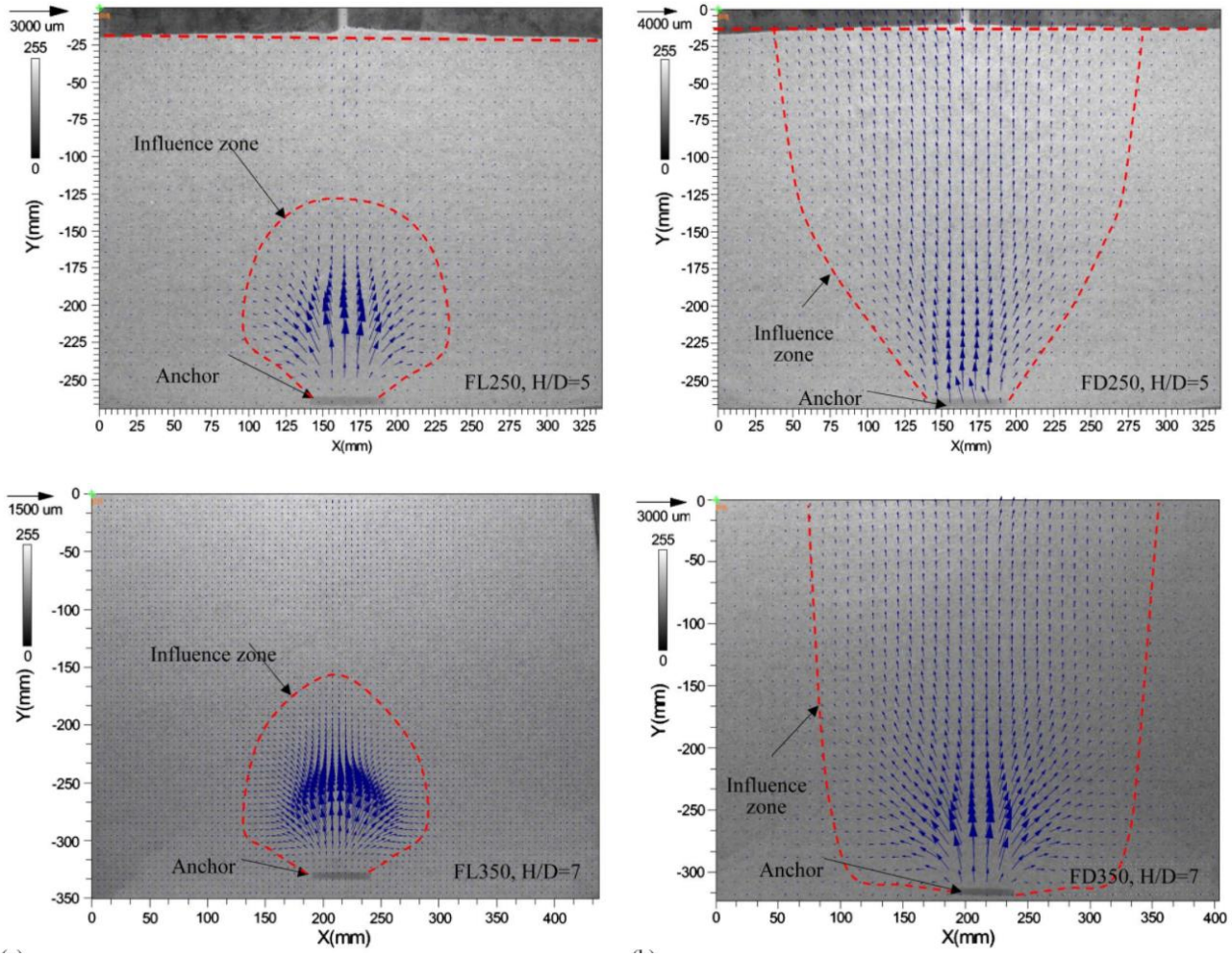

(a) Loose sand (b) Dense sand

Fig. 2.18. Influence of anchor embedment depth on soil displacement field (Liu et al., 2012).

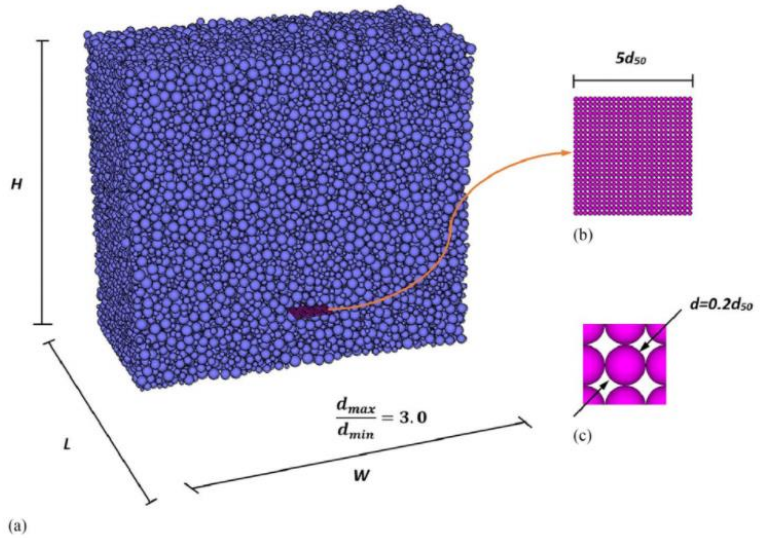

Fig. 2.19. DEM model: (a) granular assembly; (b) plate anchor; and (c) plate anchor ball. (Evans & Zhang, 2019).

2.3 Research on pull-out resistance of plate anchors in clay

When estimating pull-out resistance of plate anchors in clay, unlike in sand, the shape of ground failure pattern is not so important because the pull-out resistance usually is not estimated from the ground failure model. For anchors in clay ground, the maximum pull-out pressure p_{max} acting on a plate anchor has been generally estimated from the undrained shear strength c_u as $p_{max} = F_c c_u$: where F_c is breakout factor. Thus, for the estimation p_{max} in clay, the method of finding F_c that affects the value is important. The F_c was back calculated from the results of laboratory experiments.

Vesić (1971) gave Eq. (2.1) for estimating pull-out capacity of plate anchors in clay. For undrained condition, $\phi = 0$, $c = c_u$

$$Q_u = A(\gamma H + c_u F_c) \tag{2.1}$$

where Q_u is net ultimate uplift capacity, A is the area of an anchor plate, γ is the unit weight of the soil.

As shown in Table 2.3, Vesić (1971) presented values of breakout factor F_c for circular and strip anchor with embedment ratio. F_c increases with increasing H/h (= B), and become constant as a peak value F_c^* at $(H/h)_{cr}$.
where h is a diameter of a circular anchor, B is a length of a strip anchor.

Table 2.3. Theoretical values of F_c for shallow foundations in clay (Das, 1978).

H/B	0.5	1	1.5	2.5	5
Circular	1.76	3.80	6.12	11.6	30.3
Continuous ($B/L = 0$)	0.81	1.61	2.42	4.04	8.07

*After Vesić (1971)

Based on the experimental results, Meyrhof (1973) presented the relationship between F_c and H/B for circular, square, and strip anchors.

As shown in Fig. 2.20, Das (1978, 1980) compared the previous experimental results to see the variation of breakout factor. Das (1980) suggested an estimation procedure of ultimate uplift capacity of plate anchors, including shape factor, in clay.

Merifield et al. (2003) evaluated an effect of anchor shape on the pull-out capacity of horizontal anchors in clay using three-dimensional numerical analysis (Fig. 2.21). According to the research, an anchor behave as shallow anchor or deep anchor, depending on the overburden ratio $\gamma H/c_u$. Merifield suggests the procedure for estimation of uplift capacity of plate anchors in clay. From the relationships between breakout factor $N_c\gamma$ and H/B, the limiting value of breakout factor N_{c*} was obtained as 11.9 for square anchor and 12.56 for circular anchor.

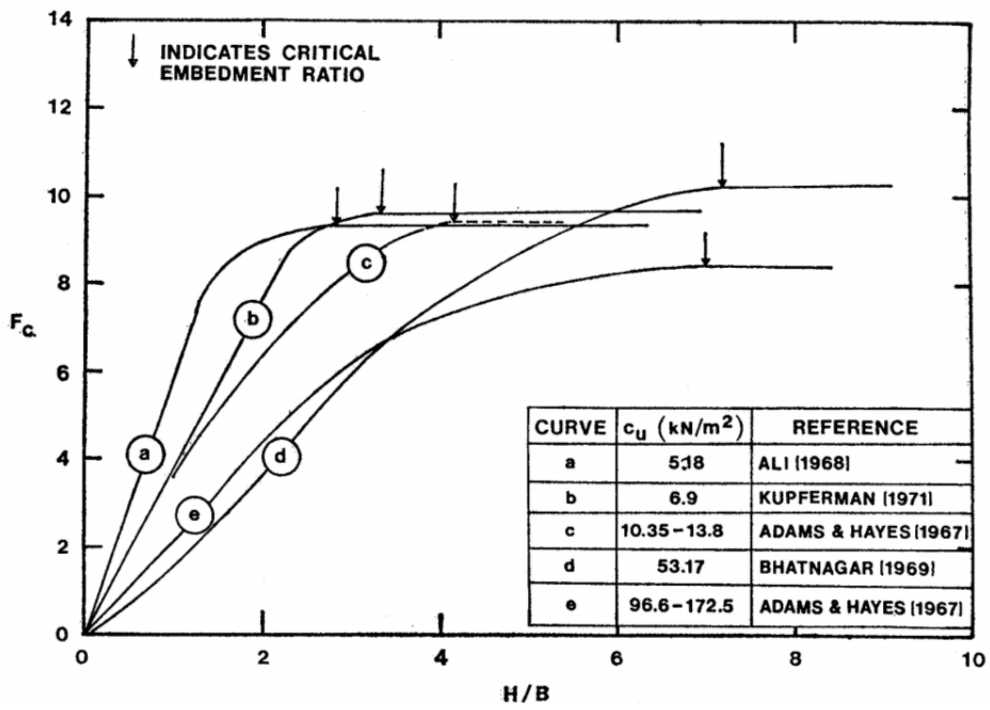

Fig. 2.20. Comparison of breakout factors with *H*/*B* for various experimental observations in clay (Das, 1980).

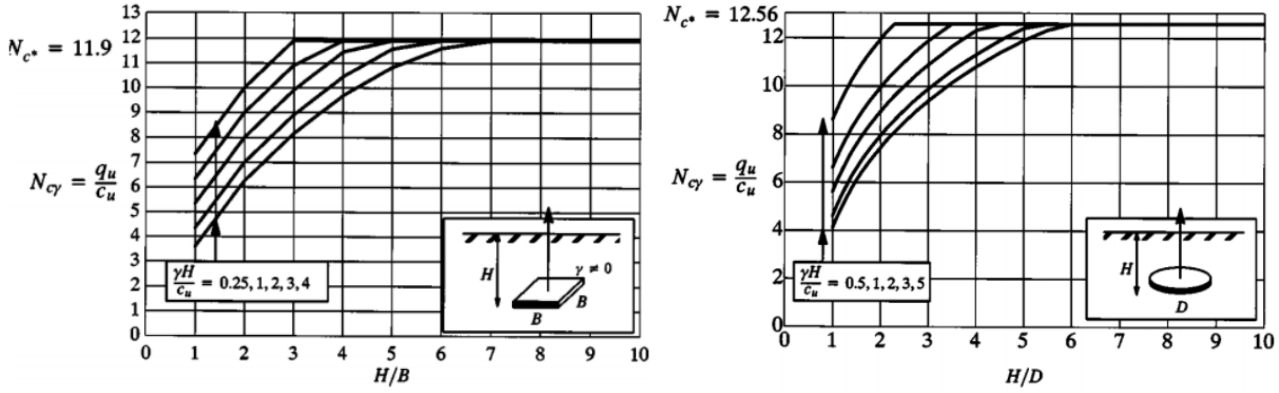

(a) square anchor (b) circular anchor

Fig. 2.21. Effect of overburden pressure in clay by Merifield et al. (2003).

Rowe and Davis (1982) conducted numerical study on the behavior of horizontal plate anchors in homogeneous, isotropic saturated clay. The study shows that significant pull-out displacement are required before ultimate collapse. Other numerical studies were conducted by such as Charlton et.al (2016), and Chen et. al (2013).

Han et al. (2016) conducted centrifuge experiments and observed soil deformation around an anchor plate in clay ground under sustained loading using PIV method, and conducted two-dimensional large deformation finite element (LDFE) analyses of the experiment. The study investigated that under which sustained loading may lead to failure and whether the soil at the base of the plate breaks away.

2.4 Research and case studies on applications of flip anchors

Niroumand and Kassim (2013) conducted experimental study using a flip anchor (called irregular shape anchor in the study) (Fig. 2.22). In the study, the flip anchor was driven into the model ground consisted of dense (ϕ = 42°, D_r = 75%) or loose (ϕ = 35°, D_r = 25%) dry sand and pulled by a winch (Fig. 2.23). The unit weight of the sand was 16.95 kN/m^3 and 14.90 kN/m^3, respectively. The embedment ratio H/L varied between 1 and 4.

As shown in Fig. 2.24, pull-out resistance increased significantly as H/L increased. Smaller H/L gives a smaller pull-out resistance at a smaller displacement.

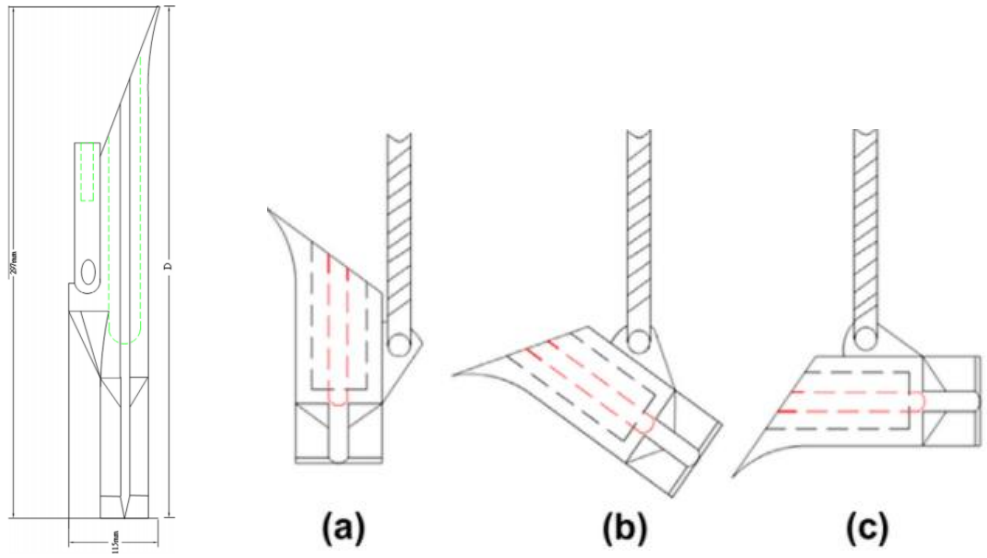

Fig. 2.22. Irregular shape anchor (length D = 297 mm) dimensions and rotation steps (Niroumand & Kassim, 2013).

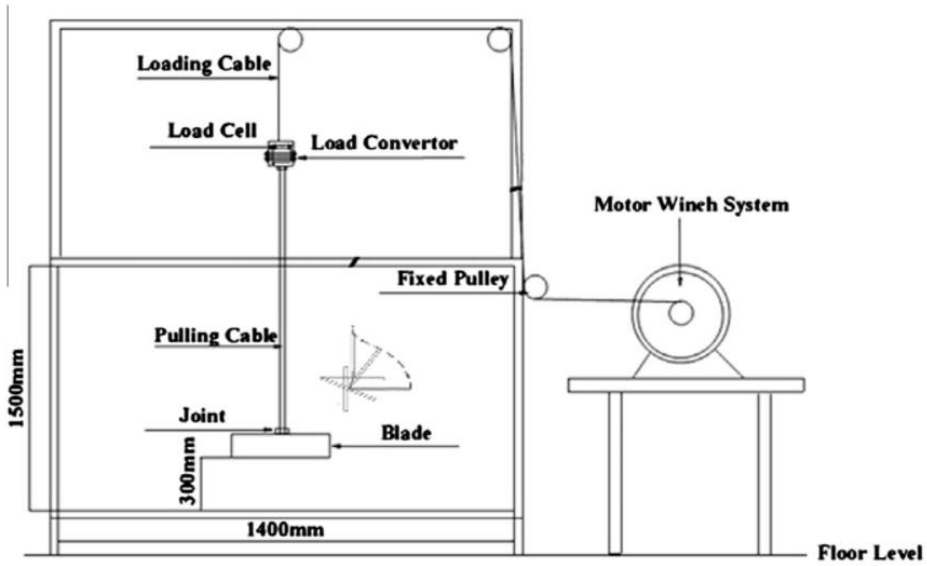

Fig. 2.23. Schematic diagram of pullout test arrangement (Niroumand & Kassim, 2013).

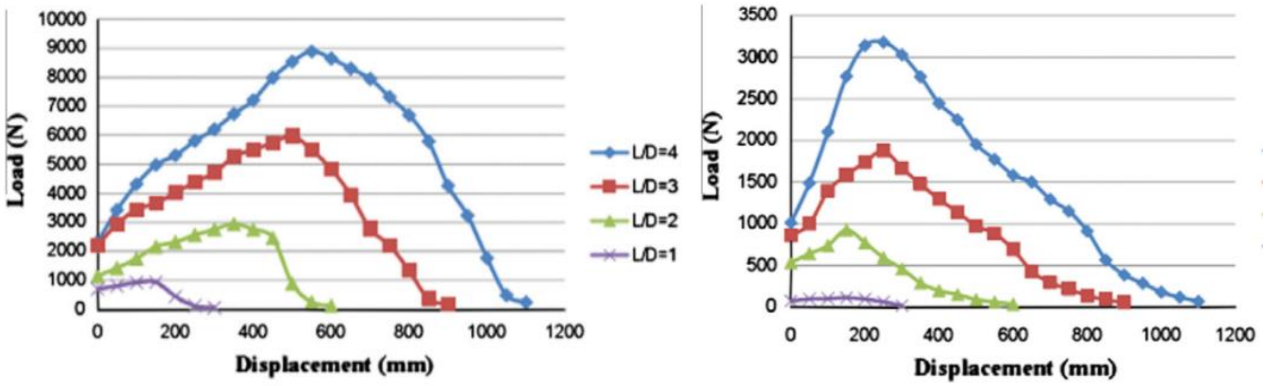

(a) Dense sand (b) Loose sand

Fig. 2.24. Variations of pullout load with embedment ratio *L*/*D* (= embedment depth / length of an anchor head) for the irregular shape anchor (Niroumand & Kassim, 2013).

There is an installation and design guide for earth anchors including flip anchors (Copstead & Studier, 1990). However, it focused on the design process and installation procedure, not the fundamental mechanism of pull-out resistance of flip anchors itself.

Although there are few studies, flip anchors have been applied to many sites, mainly in Europe, the United States and Australia. Titi and Helwany (2007) reported investigations on approaches to resist surficial slope instability. The case of flip anchor (Fig. 2.25) was introduced as one of the construction methods that contribute to slope stability (Figs. 2.25-27).

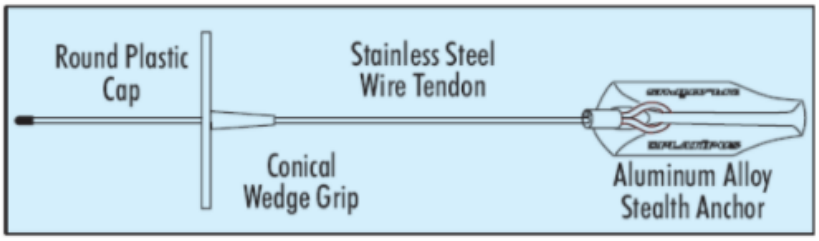

Fig. 2.25. A flip anchor (Platipus anchor) system designed for slope stabilization (Titi & Helwany, 2007).

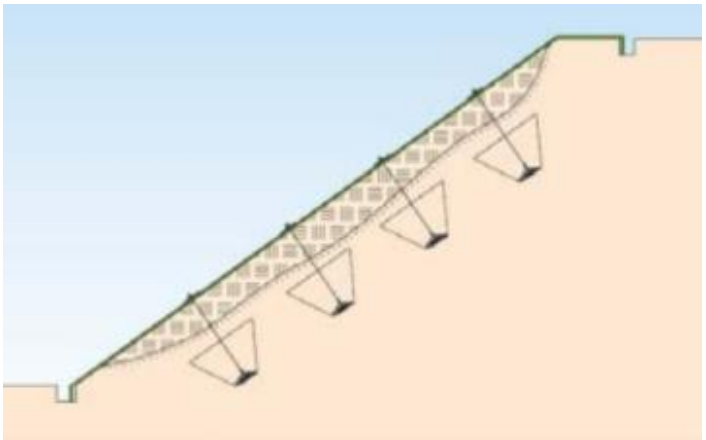

Fig. 2.26. Surficial slope failure stabilization by earth anchoring (flip anchor) systems (Titi &Helwany, 2007).

(a) Surficial slope failure (b) Slope repair using earth anchors

Fig. 2.27. Slope failure and repair work using flip anchors (Platipus anchors) (Titi & Helwany, 2007).

Koerner (2015) examined methods using soil nails or flip anchors connected to a geosynthetic surface to stabilize slopes (Fig. 2.28). Both laboratory (Fig. 2.29) and field (Fig. 2.30) experiments were conducted.

This kind of system was developed widely with different surface material, and nails and anchors. Flip anchors have been one of the options as an anchor for the anchored covering system. These methods have well-accepted theoretical background such as simplified Bishop method and the COE wedge method.

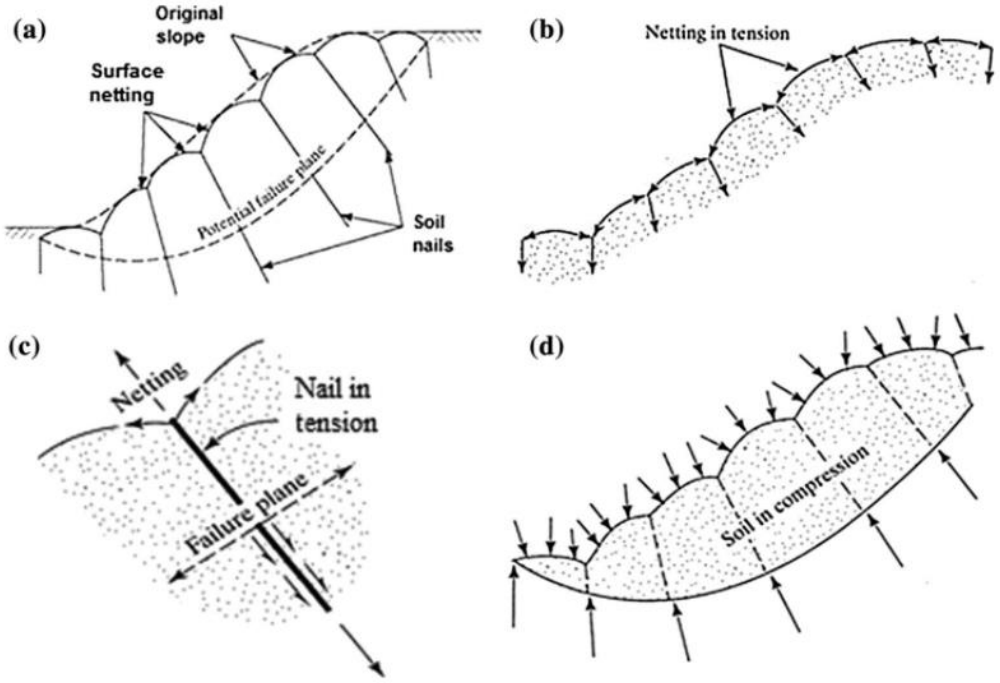

Fig. 2.28. Concept of nailed or anchored geosynthetic covering system (Koerner, 2015).

Fig. 2.29. Laboratory testing of specially designed knit geotextile (Koerner, 2015).

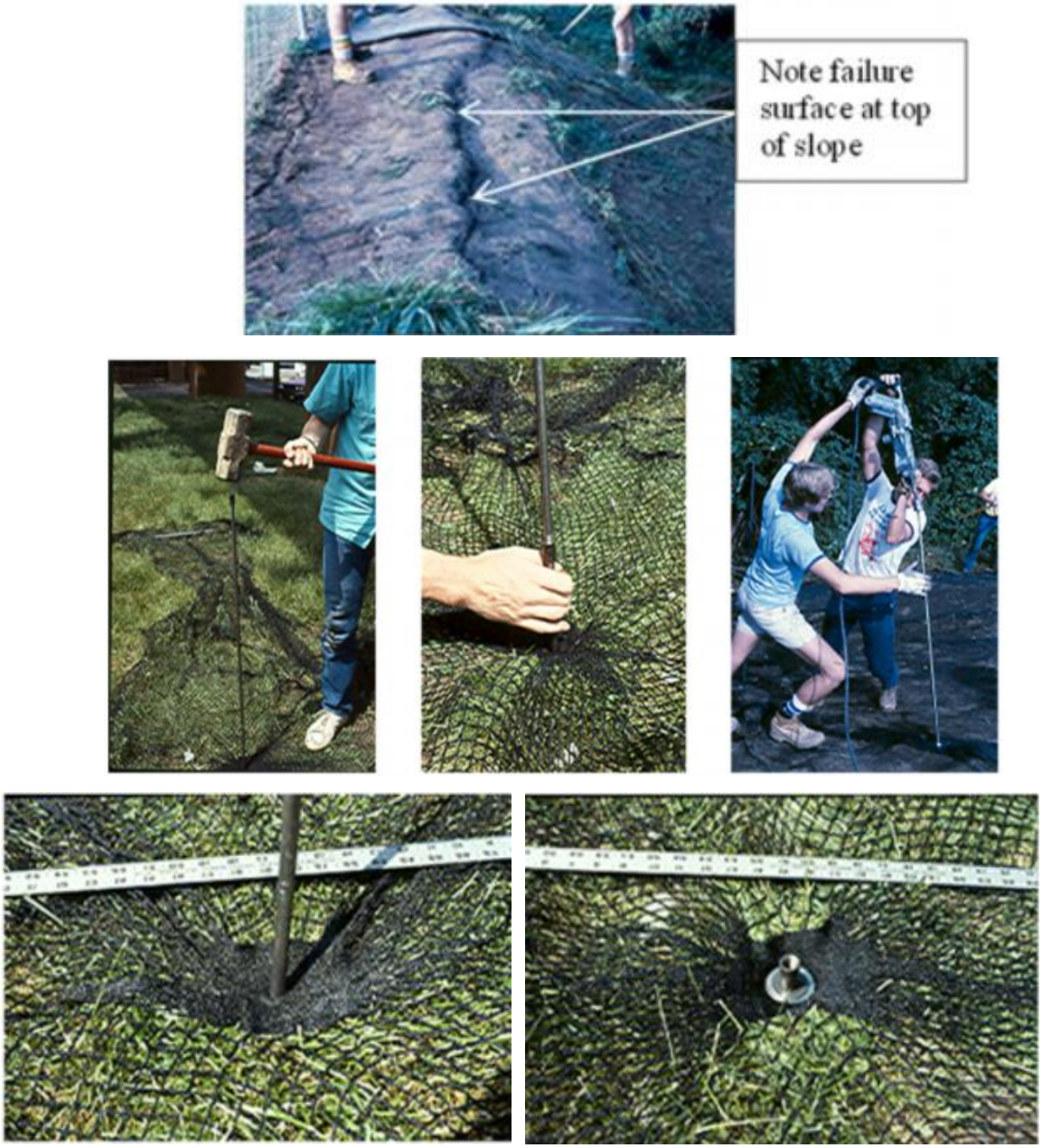

Fig. 2.30. Field deployment of anchored geosynthetic covering system using flip anchors on unstable silty clay slope (Koerner, 2015).

William and Paramaguru (2017) presented a case study where flip anchors (Platipus anchors) have been successfully adopted as temporary reinforcement, to facilitate construction of the embankment (Figs. 2.31 & 2.32). Flip anchors (Platipus anchors) were found to provide a cost effective solution that met the installation space constraints and the program constraints of the project.

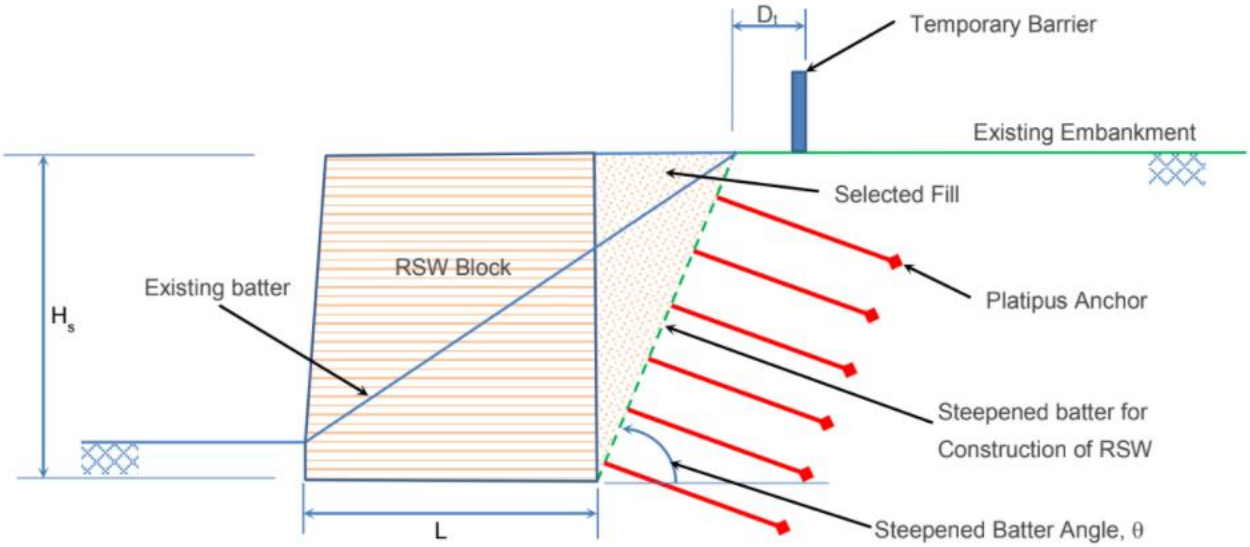

Fig. 2.31. Layout of temporary excavations and anchor arrangements (William and Paramaguru, 2017).

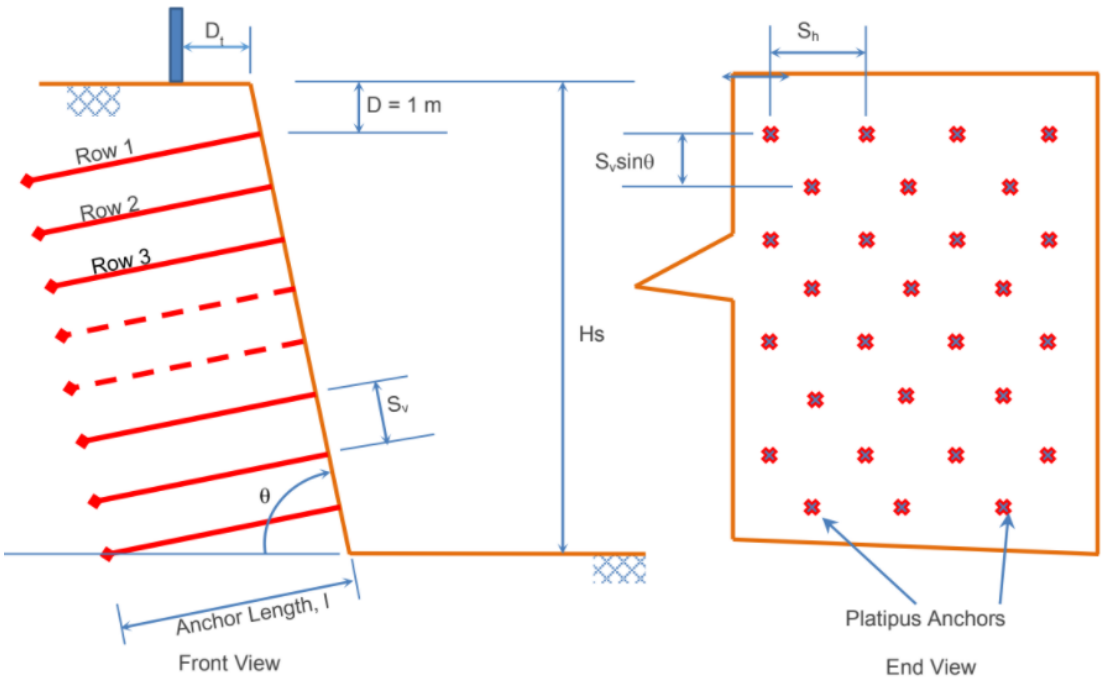

Fig. 2.32. Typical layout of flip (Platipus) anchors in a temporary slope (William & Paramaguru, 2017).

By the stability analysis (Fig. 2.33) and FEM analysis (Fig. 2.34), the temporary anchor work could be managed in the field not to affect the permanent works, such as by local movement of anchor locations. The convenience and effectiveness of flip anchors for temporary application have been proven.

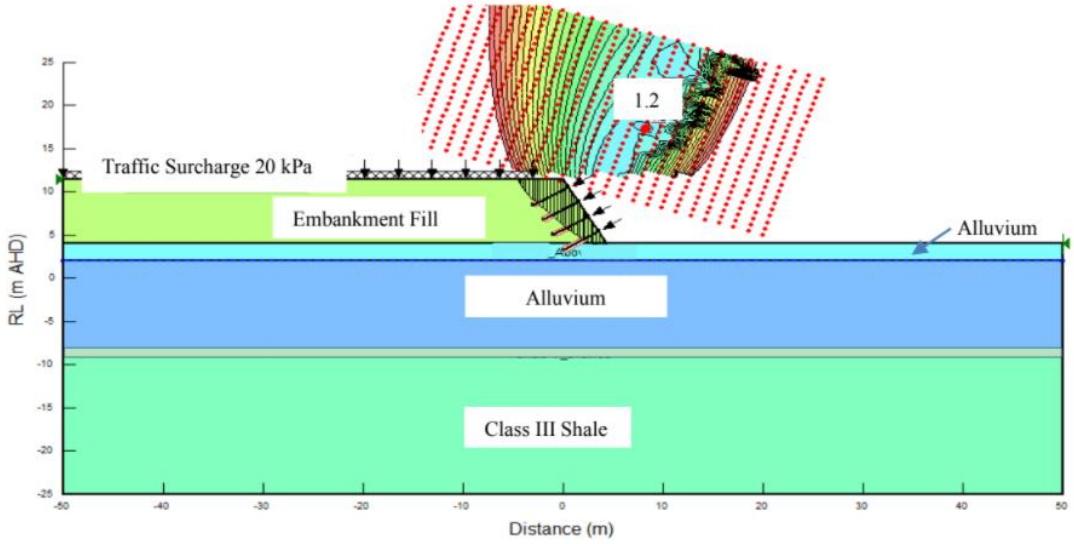

Fig. 2.33. Example slope stability assessment (William & Paramaguru, 2017).

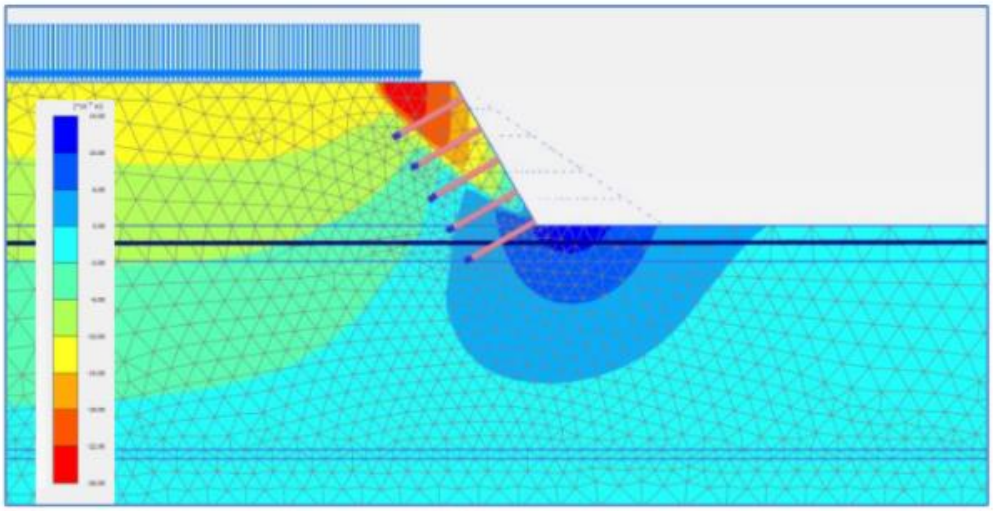

Fig. 2.34. Ground movement assessment (William & Paramaguru, 2017).

As examples of Figs. 2.35-2.38, a number of on-site applications of flip anchors have been reported by private companies, such as Anchoring Rope and Rigging Pty. Ltd. (2021), Williams Form Engineering Corp. (2021), Platipus Anchors Limited (2021).

Fig. 2.35. Application of flip anchors (HULK anchors) to reinforce the platform six at Redfern Station NSW, Australia, (Anchoring Rope and Rigging Pty. Ltd., 2021).

Fig. 2.36. Application of flip anchors (HULK anchors) to support transmission tower, tents for festival (Anchoring Rope and Rigging Pty. Ltd., 2021).

Fig. 2.37. Application of flip anchors (Platipus anchors) to support M4 Motorway, Sydney, Australia, (Platipus Anchors Limited, 2021).

Fig. 2.38. Application of flip anchors (Mantaray anchors) to support a slope along Guanella Pass (Williams Form Engineering Corp., 2021).

2.5 Summary of Chapter 2

This chapter provided a brief review of past studies related to flip anchors. Few studies on pull-out resistance of flip anchors was found. In contrast, many studies on pre-embedded plate anchors have been conducted. Because when a flip anchor opens sufficiently in the ground, the anchor would be in a similar condition to a pre-embedded plate anchor, experimental methods and results on plate anchors can be referred to as research related to flip anchors.

Many pull-out experiments of model plate anchors were conducted in sandy or clayey model grounds in laboratories. Considering scale effects, some centrifugal experiments were conducted, but there are few full-scale pull-out experiments using actual plate anchors. The ground failure patterns caused by the uplift of a plate anchor were observed during the pull-out experiments. From those experimental results, some empirical theories to calculate pull-out resistance of plate anchors in sand have been proposed. In recent years, numerical analysis such as by FEM has also been conducted to examine the previous empirical theories, or to study displacement or stress of the ground caused by the plate anchors.

Regarding research on flip anchors, Niroumand and Kassim (2013) conducted pull-out experiments of a flip (irregular shaped) anchor. In dense or loose dry sand grounds, pull-out resistance of flip anchors was investigated for different embedment ratio. Some private construction companies have reported field application cases of flip anchors

Because there are only a limited number of literature directly referring to flip anchors, previous studies on plate anchors were referenced in this study. Pull-out experiments of flip anchors similar to those of the plate anchors were conducted. For comparing the results of pull-out experiments of flip anchors with those of plate anchors, experimental conditions reflecting the characteristics of flip anchors that rotate and open in the ground were prepared. Three installation conditions: “Opened”, “Closed”, and “Driven”, made it possible to investigate fundamental performance of flip anchors. Besides, those experimental results on flip anchors were able to be compared with those of plate anchors in past studies.

References in Chapter 2

Anchoring Rope and Rigging Pty. Ltd. (2021). https://www.arandr.com.au/articles/projects.

Baker W. H., and Kondner R. L. (1966). Pullout load capacity of a circular earth anchor buried in sand. Highway Research Record, 108, pp. 1-10.

Balla A. (1961). The resistance to breaking-out of mushroom foundations for pylons. Proceedings of the 5th international conference on Soil Mechanics and Foundation Engineering, 1, pp. 569-576.

Copstead R. L., and Studier D. D. (1990). An earth anchor system: installation and design guide. United States Department of Agriculture General technical report PNW-GTR-257, 41 pp..

Charlton T.S., Rouainia M., and Gens A. (2016). Numerical analysis of suction embedded plate anchors in structured clay. Applied Ocean Research, 61, pp. 156-166.

Chen Z., Tho K. K, Leung C. F., and Chow Y. K. (2013). Influence of overburden pressure and soil rigidity on uplift behavior of square plate anchor in uniform clay. Computers and Geotechnics, 52, pp.71-81.

Das B. M., and Seeley G. R. (1975). Breakout resistance of shallow horizontal anchors. Journal of the Geotechnical Engineering Division, 101(9), pp. 999-1003.

Das B. M, Seely G. R., and Das S. C. (1977). Ultimate resistance of deep vertical anchor in sand. Soils and Foundations, 17(2), pp.52-56.

Das B.M. (1978). Model tests for uplift capacity of foundations in clay. Soils and Foundations, 18(2), pp. 17-24.

Das B.M. (1980). A procedure for estimation of ultimate uplift capacity of foundations in clay. Soils and Foundations, 20(1), pp.77-82.

Das B. M., and Jones A. D. (1982). Uplift capacity of rectangular foundations in sand. Transportation Research Record, 884, pp. 54-58.

Dickin E.A., and Leung C.F. (1983). Centrifugal model tests on vertical anchor plates. Journal of Geotechnical Engineering, 109(12), pp. 1503-1525.

Dickin E.A. (1988). Uplift behavior of horizontal anchor plates in sand. Journal of Geotechnical Engineering, 114(11), pp. 1300-1317.

Dickin E. A., and Laman M. (2007). Uplift response of strip anchors in cohesionless soil. Advances in Engineering Software, 38(8), pp. 618-625.

Evans T. M., and Zhang N. (2019). Three-dimensional simulations of plate anchor pullout in granular materials. International Journal of Geomechanics, 19(4), pp. 1-14.

Han C., Wang D., Gaudin C., O'Loughlin C.D., and Cassidy M.J. (2016). Behaviour of vertically loaded plate anchors under sustained uplift. Géotechnique, 66(8), pp. 681-693.

Ilamparuthi K., Dickin E.A., and Muthukrisnaiah K. (2002). Experimental investigation of the uplift behaviour of circular plate anchors embedded in sand. Canadian Geotechnical Journal, 39(3), pp. 648-664.

Koerner R. M. (2015). In-situ stabilization of soil slopes using nailed or anchored geosynthetics. International Journal of Geosynthetics and Ground Engineering, 1(2), pp. 1-9.

Kouzer K. M., and Kumar J. (2009). Vertical uplift capacity of two interfering horizontal anchors in sand using an upper bound limit analysis. Computers and Geotechnics, 36(6), pp. 1084-1089.

Mariupol'skii L. G. (1965). The bearing capacity of anchor foundations. Soil Mechanics and

Foundation Engineering, 2, pp. 26-32.
Liu J., Liu M., and Zhu Z. (2012). Sand deformation around an uplift plate anchor. Journal of Geotechnical and Geoenvironmental Engineering, 138(6), pp. 728-737.
Majer J. (1955). Zur berechnung von zugfundamenten. Osterreichister. Bauzeitschift. 10(5), pp. 85-90.
Merifield R.S., Lyamin A.V., Sloan S.W., and Yu H.S. (2003). Three-dimensional lower bound solutions for stability of plate anchors in clay. Journal of Geotechnical and Geoenvironmental Engineering, 129(3), pp. 243-253.
Merifield R.S., Lyamin A.V., and Sloan S.W. (2006). Three-dimensional lower-bound solutions for the stability of plate anchors in sand. Géotechnique, 56(2), pp. 123-132.
Meyerhof G. G., and Adams J. I. (1968). The ultimate uplift capacity of foundations. Canadian Geotechnical Journal, 5(4), pp. 225-244.
Mokhbi H., Mellas M., Mabrouki A., and Pereira J. M. (2018). Three-dimensional numerical and analytical study of horizontal group of square anchor plates in sand. Acta Geotechnica, 13(6), pp. 159-174.
Mors H. (1959). Das Verhalten von Mastgruendungen bei Zugbeanspruchung. Bautechnik, 39(10), pp. 367-378.
Murray E. J., and Geddes J. D. (1987). Uplift of anchor plates in sand. Journal of Geotechinical Engineering, 113(3), pp. 202-215.
Niroumand H., Kassim K. A., and Nazir R. (2010). Anchor plates in two-layered cohesion less soils. American Journal of Applied Sciences, 7(10), pp. 1396-1399.
Niroumand H., and Kassim K. A. (2013). Pullout capacity of irregular shape anchor in sand. Measurement, 46(10), pp. 3876-3882.
Ovesen N. K. (1979). The use of physical models in design: the scaling law relationship. Proceedings of 7th European Conference on Soil Mechanics and Foundation Engineering, 4, pp. 318-323.
Platipus Anchors Limited. (2021). https://platipus-anchors.com/wp-content/uploads/2017/09/Platipus-ARGS-Brochure-080817.pdf.
Riyad A. S. M., Rokonuzzaman M., and Sakai T., (2020). Effect of using different approximation models to the exact Mohr–Coulomb material model in the FE simulation of Anchor Foundations in sand. International Journal of Geo-Engineering, 11(11). pp. 1-21.
Rowe R. K., and Davis E. H. (1982). The behaviour of anchor plates in clay. Géotechnique, 32(1), pp. 9-23.
Saeedy H. S. (1971). Analytical and experimental stability of earth anchors. Dissertation of Graduate colledge of the Oklahoma State University.
Sakai T., and Tanaka T. (1998). Scale effect of a shollow circular anchor in dense sand. Soils and Foundations, 38(2), pp. 93-99.
Tagaya K., Tanaka A., and Aboshi H. (1983). Application of finite element method to pullout resistance of buried anchor. Soils and Foundations, 23(3), pp. 91-104.
Tagaya K., Scott R.F., and Aboshi H. (1988a). Pullout resistance of buried anchor in sand. Soils and Foundations, 28(3), pp. 114-130.
Tagaya K., Scott R.F., and Aboshi H. (1988b). Scale effect in anchor pullout test by centrifugal technique. Soils and Foundations, 28(3), pp. 1-12.
Tanaka T., and Sakai T. (1993). Progressive failure and scale effect of trap-door problems with granular materials. Soils and Foundations, 33(1), pp. 11-22.

Titi H. H., and Helwany S. (2007). Investigation of vertical members to resist surficial slope instabilities. Wisconsin highway research program project ID 0092-05-09, 84 pp.

Veesaert C. J. (1977). Dynamic pullout resistance of anchors buried in dry sand. Masters theses of Graduate school of the University of Missouri-Rolla.

Vesić A. S. (1971). Breakout Resistance of Objects Embedded in Ocean Bottom. Journal of the Soil Mechanics and Foundations Division, 97(9), pp. 1183-1205.

Williams Form Engineering Corp. (2021). https://www.williamsform.com/soil/manta-ray-anchors/manta-ray-job-001/.

William T. M., and Paramaguru L. (2017). Use of temporary anchors in reinforced soil wall construction for the M4 motorway widening. Australian Geomechanics Society Sydney Chapter Symposium November.

Chapter 3
Experimental studies on pull-out resistance of flip-type earth anchors using actual anchors

3.1 Introduction

3.1.1 Overview of the experiments

In this chapter, a series of pull-out experiments using actual flip anchors were conducted in three-dimensional conditions to investigate behavior and pull-out resistance of flip anchors installed in sand or clay grounds. Based on the experimental results, estimation methods of pull-out resistance of flip anchors in sand and clay were proposed. The pull-out experiments on sand grounds were conducted both in a laboratory and a field. The experiments in a clayey ground were conducted only in a field.

The experiment was first conducted in a small-scale model sand ground in a laboratory. In a laboratory, three sizes of actual flip anchors were used for pull-out experiments.

Subsequently, to install the flip anchors deeper, pull-out experiment was conducted in a full-scale sand ground. The full-scale pull-out experiments were conducted using five sizes of actual flip anchors. By comparing the differences between the results of the laboratory and the field experiments, the fundamental characteristics of pull-out resistance of flip anchors in sand grounds was investigated.

In sand grounds, to reflect the property of flip anchors that rotate and open in the ground, 3 types of installation conditions (Opened, Closed, Pushed-in or Driven) were prepared. Regarding installation conditions, “Opened” embedded condition imitates the state of flip anchors fully opened in the ground after rotating (Fig. 3.1c). “Opened” condition is also equivalent to the embedded conditions of general horizontal plate anchors that have been studied a lot in the past. “Closed” embedded condition imitates the state after being driven in the ground (Fig. 3.1b). “Driven” and “Pushed-in” (Fig. 3.1a) conditions are practical installation process. The anchors are driven or pushed into the ground directly.

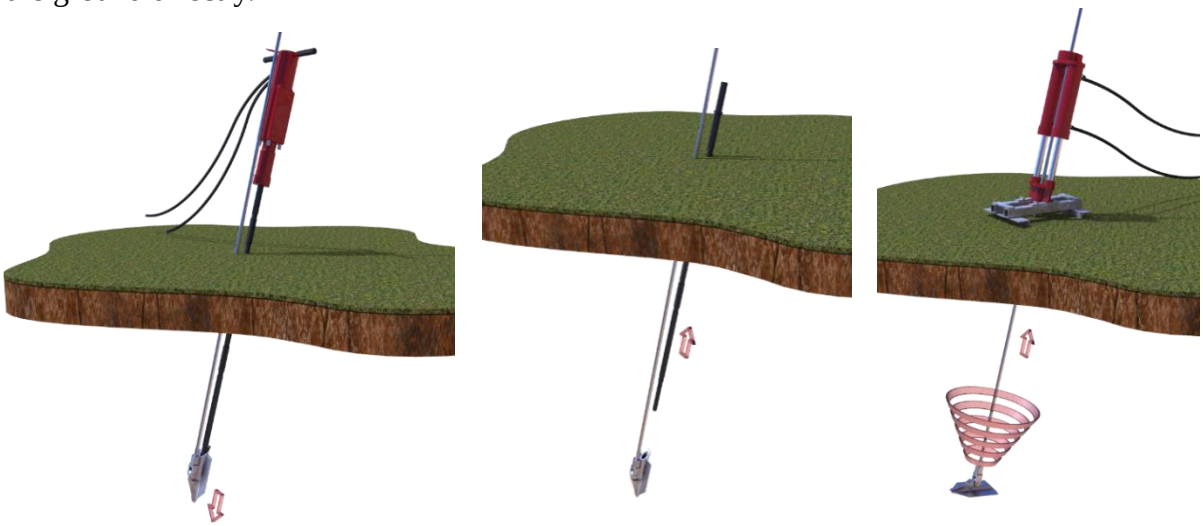

(a) Drive an anchor into the ground (b) Pull out a driving rod (c) Apply tensile force to rotate anchor

Fig. 3.1. Installation procedures of a flip anchor (a → b → c).

Under these installation conditions, pull-out experiments were conducted while changing the embedment (installation) depth *H* or anchor size. By comparing the results in each condition, pull-out resistance of flip anchors was able to be examined considering its unique features. In addition to that, the experimental results of flip anchors were able to be compared with previous research on plate anchors by preparing the three installation conditions.

After the experiments in sand grounds condition, the pull-out experiments in a ground consisting of sandy and clayey soil layers were conducted to investigate the pull-out resistance of flip anchors in clay. In the experiment in a clayey ground, the flip anchors were installed only under Driven condition by a percussion device because the ground was not a modelled ground.

3.1.2 Actual flip-type earth anchors used in the experiments

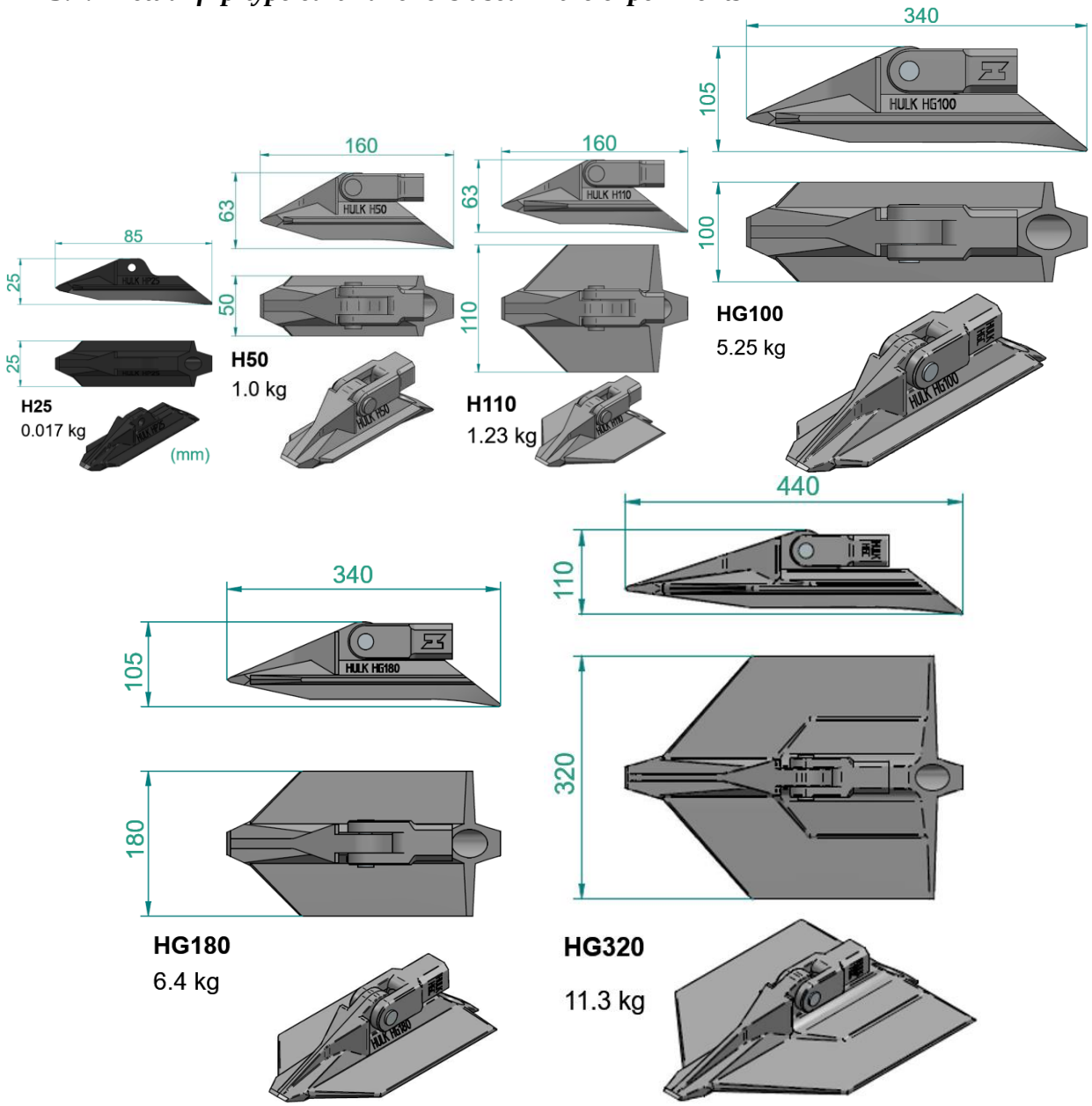

Fig. 3.2. Specifications of flip anchors used in this experiments (Anchoring Rope and Rigging Pty. Ltd., 2021).

In laboratory pull-out experiments, three types of H25 (S), H50 (M), and H110 (L) anchors were used. In the field experiments, five types of actual anchors, H50, H110, HG100, HG180, and HG320 were used. Figure 3.2 shows specification of flip anchors used in this study. H25 anchor is made of plastic and the other anchors are made of ductile iron. In the laboratory experiments, wire ropes having a diameter of 3 mm or rods (M12) were attached to the anchors, and in field experiments, steel rods (M12, M16, or M24) were attached to the anchors according to the anchor size.

3.2 Pull-out experiments of flip-type earth anchors embedded or pushed in a model sand ground

3.2.1 Introduction

Unlike the studies on pull-out resistance of plate anchors, the number of studies on the same for flip anchors are limited. Niroumand and Kassim (2013) conducted pull-out experiments of a flip (irregular shaped) anchor in a dense or loose dry sand ground. The experiment focused on its irregular shape rather than the unique mechanism, which rotates and opens in the ground when the anchor is pulled.

In this study, 3 sizes of flip anchors were installed with different installation conditions: Opened, Closed, and Pushed-in, to investigate pull-out resistance of flip anchors in sand.

3.2.2 Outline of the experiments

Three sizes of actual flip anchors (Fig. 3.3) were used in the pull-out experiments. Dimensions of the anchors are also indicated in Fig 3.3. They are named S, M, and L anchors, according to the size of projected area *A*. S anchor is made of plastic and M and L anchors are made of ductile iron,

The experiments were conducted in different anchor sizes, anchor installation depths *H*, and installation conditions (Opened, Closed, Pushed-in). The flip anchors were embedded in the model ground in “Opened” or “Closed” state while ground preparation, or pushed into the ground as “Pushed-in” condition after ground preparation.

Fig. 3.3. Actual flip anchors (S, M, L) used for pull-out experiments in a laboratory.

The model ground (Fig. 3.4) was prepared in a rigid rectangular soil box with a height of 530 mm, a length of 800 mm and a width of 500 mm. Dry silica sand # 6 was used for the model ground. Physical and mechanical properties of the sand are listed in Table 3.1.

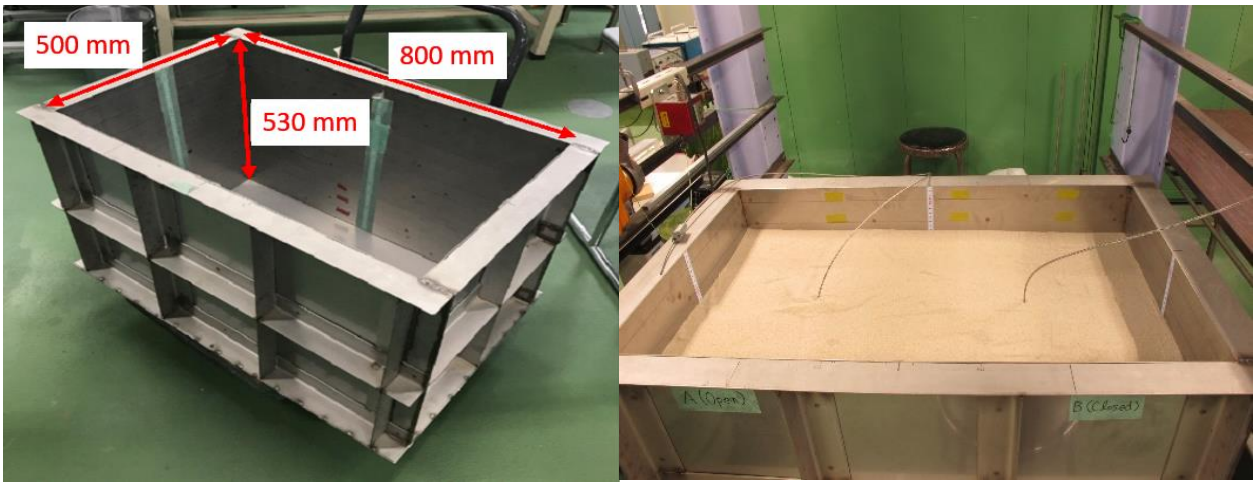

Fig. 3.4. A soil box and a model ground for pull-out experiments in a laboratory.

Table 3.1. Physical and mechanical properties of dry silica sand #6.

Density of soil particle, ρ_s (g/cm^3)	2.67
Maximum dry density, ρ_{dmax} (g/cm^3)	1.604
Minimum dry density, ρ_{dmin} (g/cm^3)	1.268
Maximum void ratio, e_{max}	1.089
Minimum void ratio, e_{min}	0.652
Int. friction angle at peak strength, ϕ_p (deg)	38.6
Int. friction angle at residual strength, ϕ_r (deg)	34.8

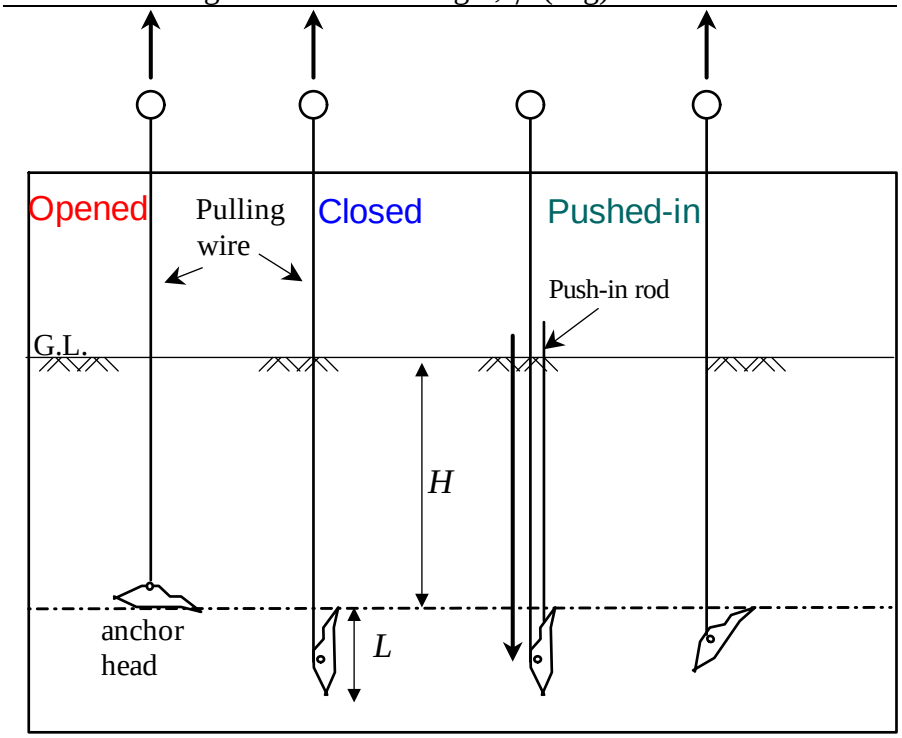

Fig. 3.5. Three installation conditions (Opened, Closed, Pushed-in) of actual flip anchors for pull-out experiments in the model sand ground.

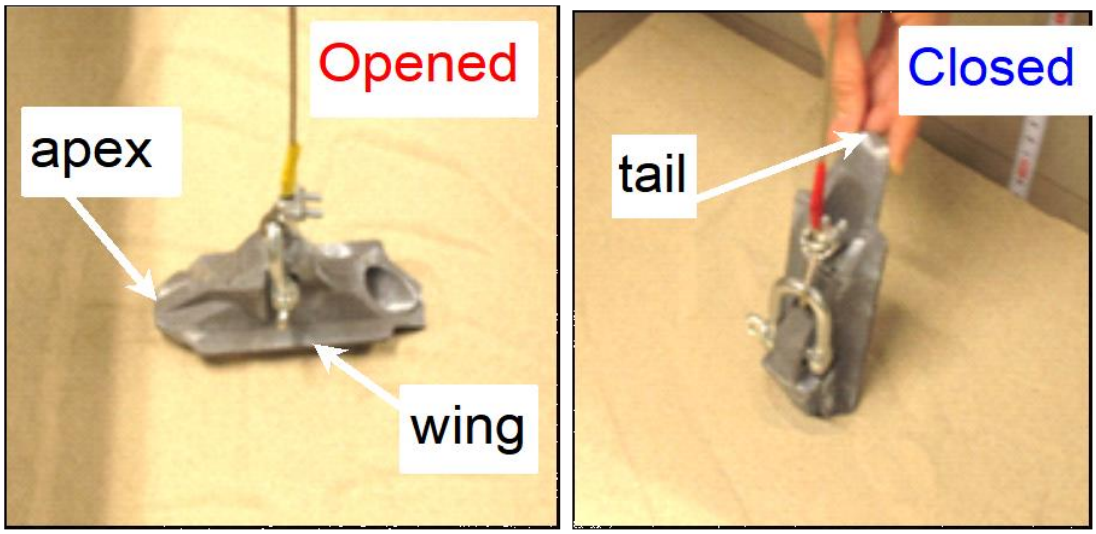

Fig. 3.6. Opened and Closed embedment conditions of the flip anchors.

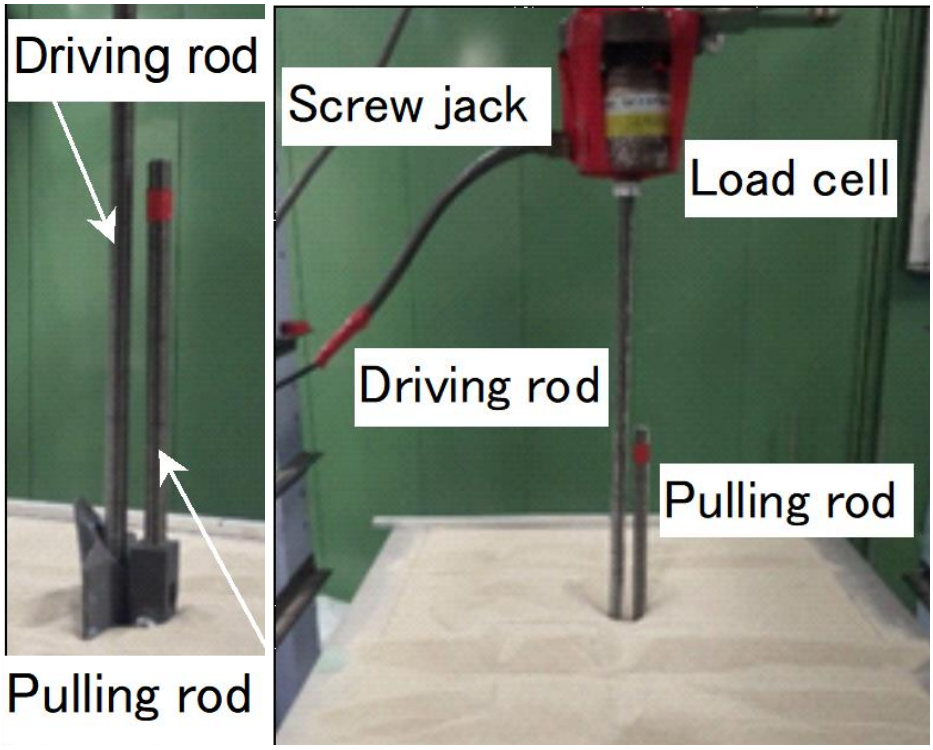

Fig. 3.7. Equipment for pushing the flip anchors in Pushed-in condition.

The model ground was prepared with 10 soil layers of 50 mm thick and a top layer of 30 mm thick. The sand was put into the soil box for each layer, and the layer was compacted to get a designed density (relative density D_r = 82%, dry density ρ_d = 1.533 g/cm^3). This procedure was repeated to complete the model ground of 530 mm high. The strength parameters of the sand were obtained by direct shear tests.

Experimental conditions and cases are described in Fig. 3.5 and Table 3.2. Embedment depth H were 150 mm, 250 mm, and 395 mm for S anchor, and 200 mm, 250 mm, and 290 mm for M & L anchors.

As shown in Fig. 3.6, in Opened & Closed condition, an anchor was buried in the model ground with its anchor head opened or closed while the ground preparation. As shown in Fig.3.7, under Pushed-in condition, the anchors were pushed into the model ground with its head closed to a designated depth by a screw jack set on a driving rod.

In Opened condition, *H* is the depth from the ground surface to the bottom of the anchor installed horizontally. Meanwhile, in Closed and Pushed-in conditions, *H* is the depth from the ground surface to a tail of the anchor installed vertically. It is because that Closed and Pushed-in anchor is thought to rotate around the tail to open, then finally has a same *H* as an Opened anchor.

Table 3.2. Experimental cases & results of pull-out experiments using actual flip anchors in the model sand ground.

Anchor	Installation Condition	Installation depth, *H* (mm)
S	Opened	150
S	Opened	250
S	Opened	395
S	Closed	150
S	Closed	250
S	Closed	395
S	Pushed-in	150
S	Pushed-in	250
M	Opened	200
M	Opened	250
M	Opened	290
M	Closed	200
M	Closed	250
M	Closed	290
M	Pushed-in	200
M	Pushed-in	250
M	Pushed-in	290
L	Opened	200
L	Opened	250
L	Opened	290
L	Closed	200
L	Closed	250
L	Closed	290
L	Pushed-in	200
L	Pushed-in	250
L	Pushed-in	290

Common to all conditions, the anchors were pulled out using equipment shown in Fig. 3.8. A pair of H-shaped steel bars was placed on the soil box. And, a bearing stand having a centre-hole, a hydraulic jack and a load cell were set on the H-shaped steel beam. The pulling rod was passed through the centre-holes, and a load cell was attached on a top of the rod. Because of this loading system, reaction force of the anchor was not transmitted from bearing stand to the ground surface.

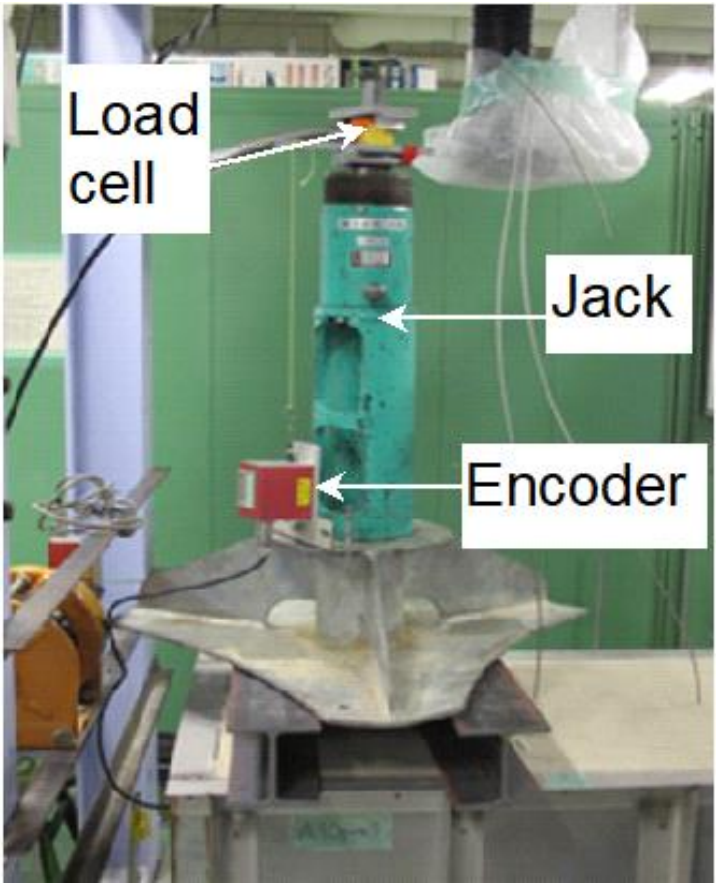

Fig. 3.8. A set-up for pulling out the flip anchors.

3.2.3 Results of the experiments

Relationship between pull-out force F and pull-out displacement w

Figures 3.9-3.11 show relationship between pull-out force *F* and pull-out displacement *w* of the anchors compared by each anchor size in each installation condition at *H* = 250 mm. The projected area *A* of M and L anchor are about 4 and 7 times larger than *A* of S anchor, respectively (Fig.3.3).

Figure 3.9 shows relationship between *F* and *w* of Opened anchors. *F* of M anchor was smaller than *F* of L anchor, but it was not smaller in proportional to their ratio of *A*. Contrary to the expectations, *F* of Opened S anchor having *A* of only about 15% of *A* of L anchor, was comparable with *F* of L anchor. M and L anchor softened immediately after the peak value, while S anchor maintained the peak value for longer than the other anchors. M and L anchors attained their peak values with about a half amount of *w* than S anchors.

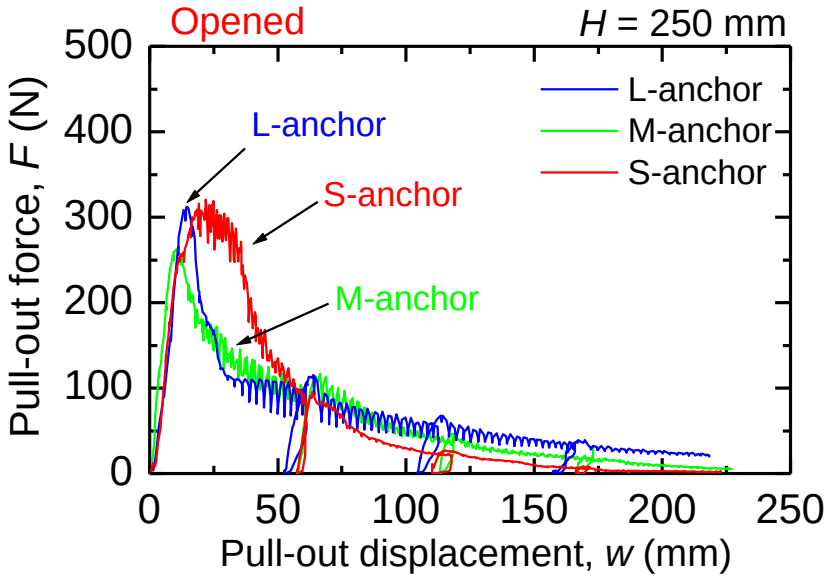

Fig. 3.9. *F* vs. *w* of Opened anchors at *H* = 250 mm.

Figure 3.10 shows relationship between *F* and *w* of Closed anchors. Maximum pull-out force F_{max} was larger in the order of the anchor size. F_{max} of M and L anchors were almost equal and 1.7 times larger than F_{max} of S anchor.

For S anchor, F_{max} of Closed anchors were about 80% of F_{max} of Opened anchors. Contrary to the expectations, F_{max} of Closed M and L anchors were about 150% of F_{max} of Opened M and L anchors. *w* of Closed anchor until F_{max} were about equal for all anchors. Closed M and L anchors maintained pull-out resistance even when pulled out about 50 mm, while Opened anchors softened immediately. Closed S anchor maintained resistance even when it was pulled out 100 mm.

Closed anchors showed much more stable pull-out resistance not softening immediately after the peak than Opened anchors.

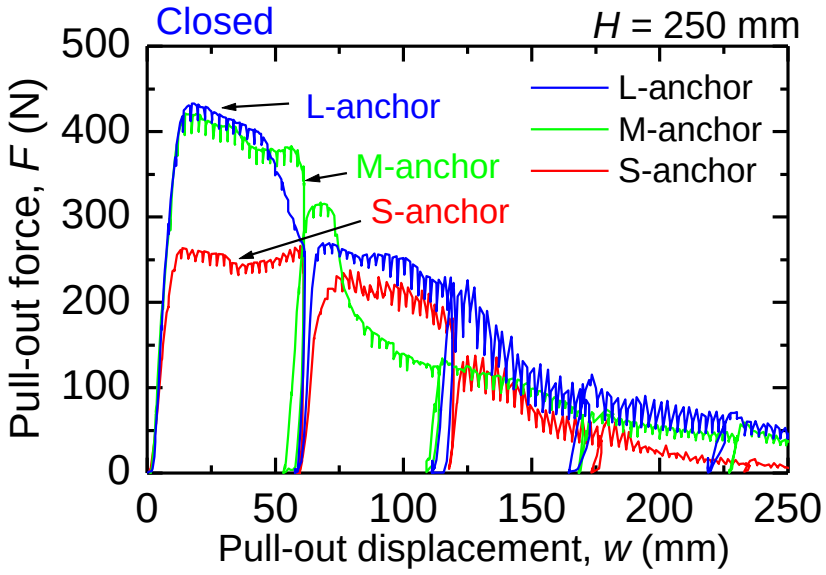

Fig. 3.10. *F* vs. *w* of Closed anchors at *H* = 250 mm.

Figure 3.11 shows relationship between F and w of Pushed-in anchors. Same as Closed anchors, F_{max} was larger in the order of the anchor size. F_{max} of Pushed-in M and L anchors were almost equivalent and 2 times larger than F_{max} of Pushed-in S anchor. w of Pushed-in M, L anchors until F_{max} was almost equal. S anchor required larger w to attain F_{max}. F_{max} of Pushed-in M, L anchors reached about 90% of F_{max} of each Opened anchor (Fig.3.9). In Pushed-in conditions, no rapid softening behavior occurred after passing F_{max}.

F_{max} of Pushed-in anchors were about 50% - 60% of Closed anchors possibly because and the depth of the model ground was too small for the actual anchors. The ground could be disturbed and weakened during push-in process due to the small H. This point will be discussed later.

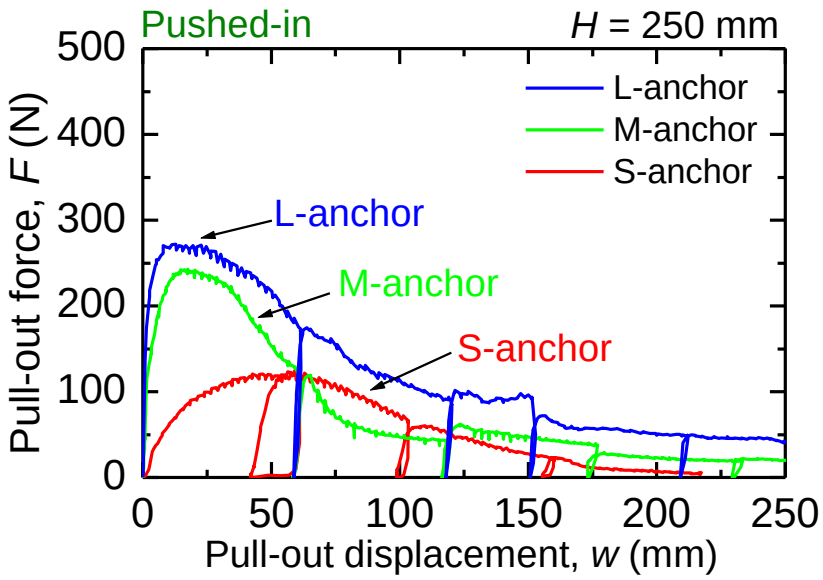

Fig. 3.11. F vs. w of Pushed-in anchors at H = 250 mm.

S anchor

Figure 3.12 shows F vs. w of Opened S anchor installed at H = 150, 250, 395 mm. Overall, as H increased, F_{max} increased. At H = 395 mm, even if w increased, F did not soften immediately and tended to be relatively stable compared to the other shallower Opened anchors.

Figure 3.13 shows the same for Closed S anchors. F_{max} of Closed S anchors were slightly smaller than F_{max} of Opened S anchors, but the pull-out resistance were maintained longer than Opened S anchors (Fig.3.12).

F_{max} of Opened and Closed S anchor at H = 395 mm was about 2.5 times F_{max} at H = 250 mm. H of the former was 1.6 times F_{max} of the latter. F_{max} of Opened and Closed S anchors at H = 250 mm was about 2.4 times F_{max} at H = 150 mm. H of the former was 1.7 times larger than H of the latter. Thus, it can be seen that F_{max} of Opened and Closed S anchors did not increase in proportion to H, but increased exponentially as H increases.

At the deepest installation depth of H = 395 mm, Opened S anchor maintained relatively tenacious pull-out resistance even with w about 100 mm. It indicates that Opened anchor also does not soften easily with enough H.

Figure 3.14 shows F vs. w of Pushed-in S anchors at H = 150 and 250 mm. F_{max} of Pushed-in S anchor were 50% of F_{max} of Closed anchors (Fig.3.13). F_{max} of Pushed-in S anchors were extremely small for Opened and Closed S anchors.

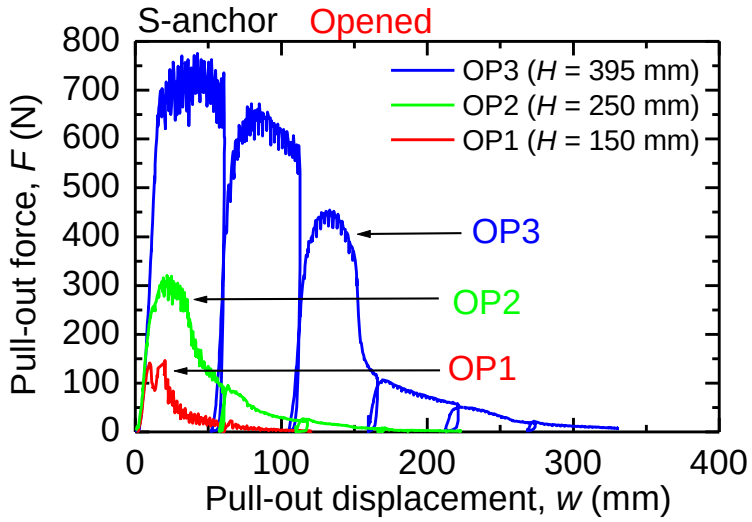

Fig. 3.12. *F* vs. *w* of Opened S anchors at different *H*.

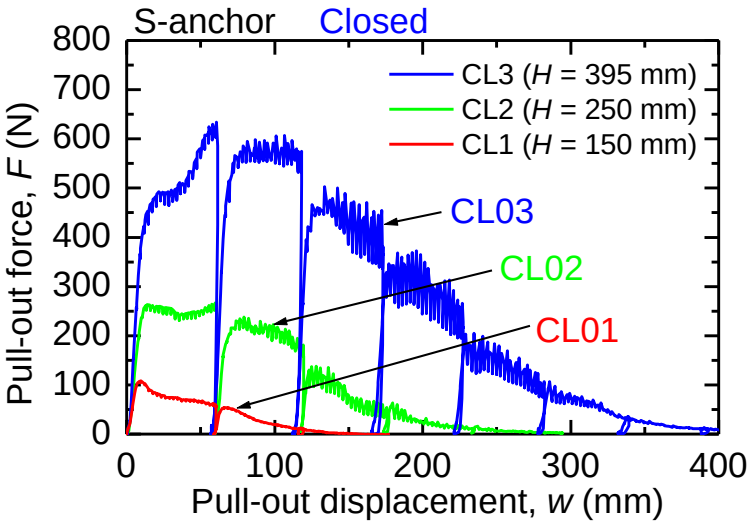

Fig. 3.13. *F* vs. *w* of Closed S anchors at different *H*.

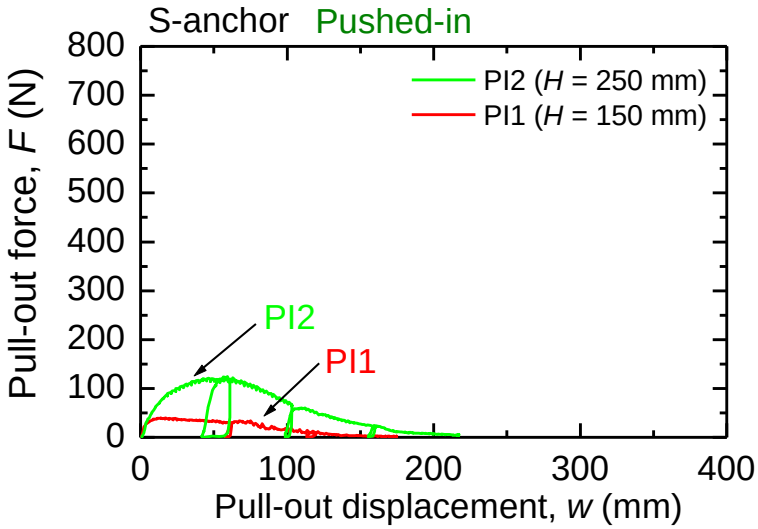

Fig. 3.14. *F* vs. *w* of Pushed-in S anchors at different *H*.

M anchor

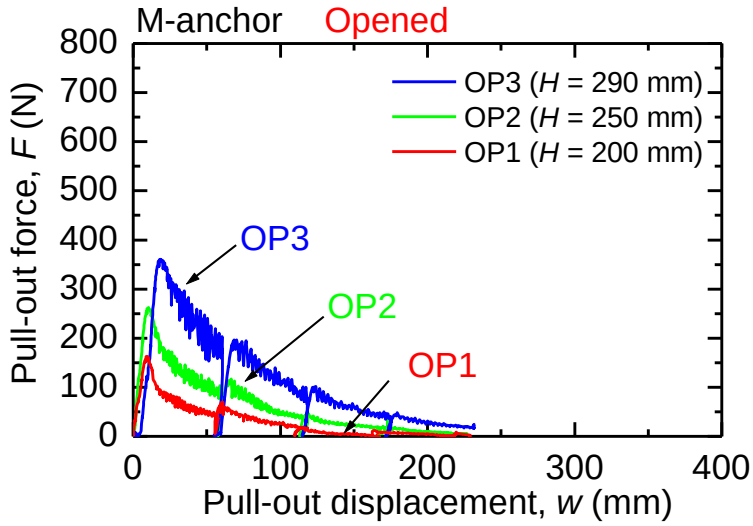

Fig. 3.15. *F* vs. *w* of Opened M anchors at different *H*.

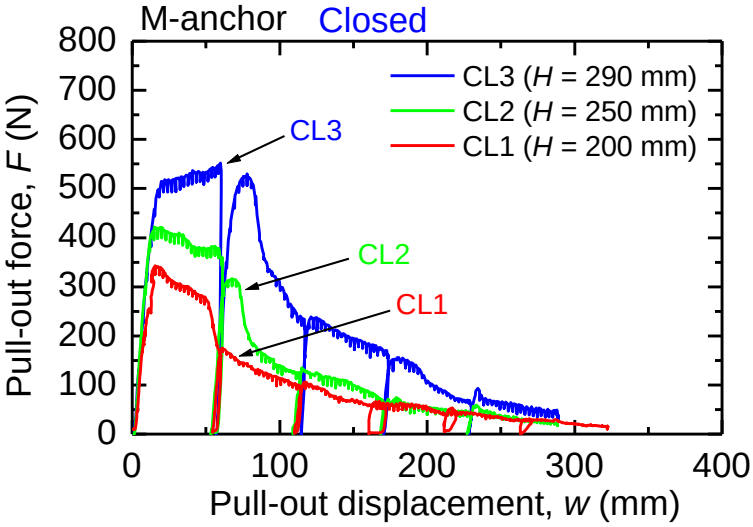

Fig. 3.16. *F* vs. *w* of Closed M anchors at different *H*.

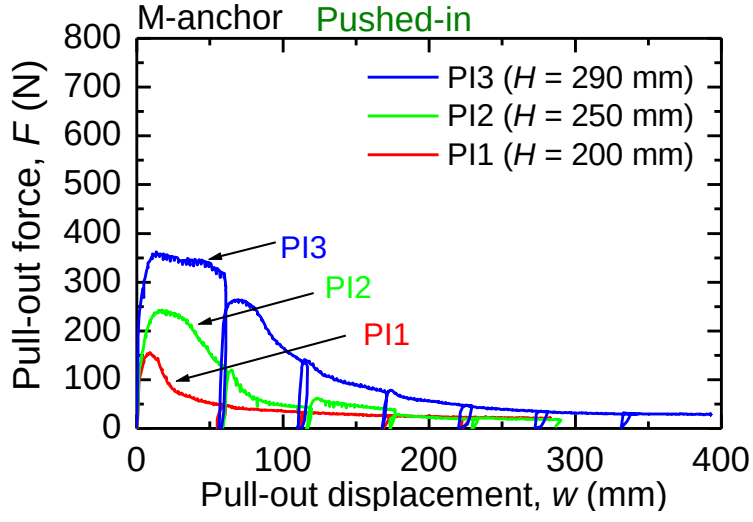

Fig. 3.17. *F* vs. *w* of Pushed-in M anchors at different *H*.

Figure 3.15 shows relationship of F vs w of Opened M anchors at H = 200, 250, 290 mm. Similar to Opened S anchor (Fig. 3.12), F_{max} increased exponentially as H increased. However, unlike Opened S anchor at H = 395 mm, Opened M anchor even at the deepest installation depth of H = 290 mm did not show tenacious pull-out resistance behavior. This could be due to the shallow H for the size of M anchors.

Figure 3.16 shows the same of Closed M anchors. Similar to Closed S anchor (Fig. 3.13), Closed M anchor maintained pull-out resistance tenaciously. This became more pronounced as H increased. Contrary to the expectation, F_{max} of Closed M anchors was larger than Opened M anchors.

Figure 3.17 shows the same of Pushed-in M anchor. F_{max} of Pushed-in M anchors were comparable to Opened M anchor (Fig. 3.15), and about 60% of Closed M anchors. Similar to Closed M anchor (Fig. 3.16), Pushed-in M anchor showed more tenacious resistance than Opened M anchor, and this tendency became more pronounced as H increased. F_{max} of Pushed-in M anchor was comparable to Opened M anchors, and Pushed-in anchors show more tenacious pull-out resistance behavior than Opened anchors.

L anchor

Figure 3.18 shows relationship of F vs w of Opened L anchors installed at H = 200, 250, 290 mm. Similar to Opened S anchor (Fig. 3.12) and Opened M anchor (Fig. 3.15), F_{max} increased exponentially as H increased.

Figure 3.19 shows the same for Closed L anchor. The tendency was similar to that of Closed M anchor (Fig. 3.16) described above.

Figure 3.20 shows the same for Pushed-in L anchors. F_{max} of Pushed-in L anchors were comparable to F_{max} of Opened L anchors, and about 60% of F_{max} of Closed L anchors. Like Closed L anchors, F_{max} lasted longer than Opened L anchors, and the long-lasting resistance increased as H increased.

From the results shown in Figs. 3.15-3.20, A of L anchor was 1.8 times that of M anchor, but F_{max} of L anchors were only about 1.3 times larger than F_{max} of M anchor at most. Hence, F_{max} should be affected by other than overburden pressure related to A. This point will be considered with ground failure model in Chapter 4.

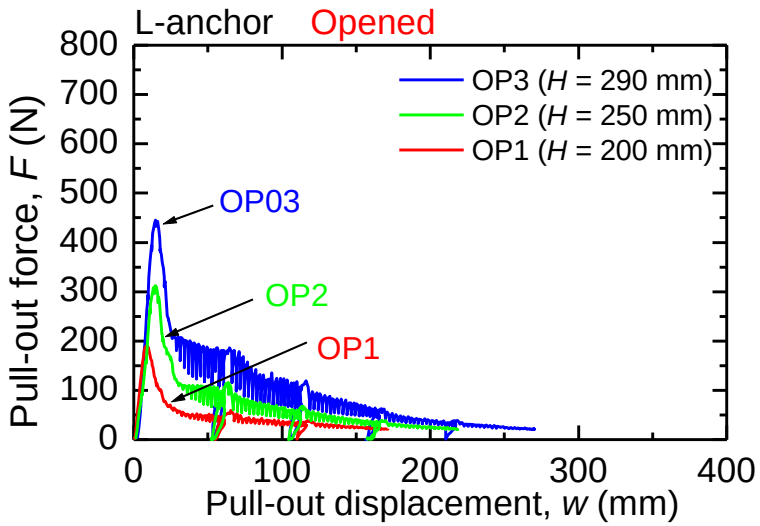

Fig. 3.18. F vs. w of Opened L anchors at different H.

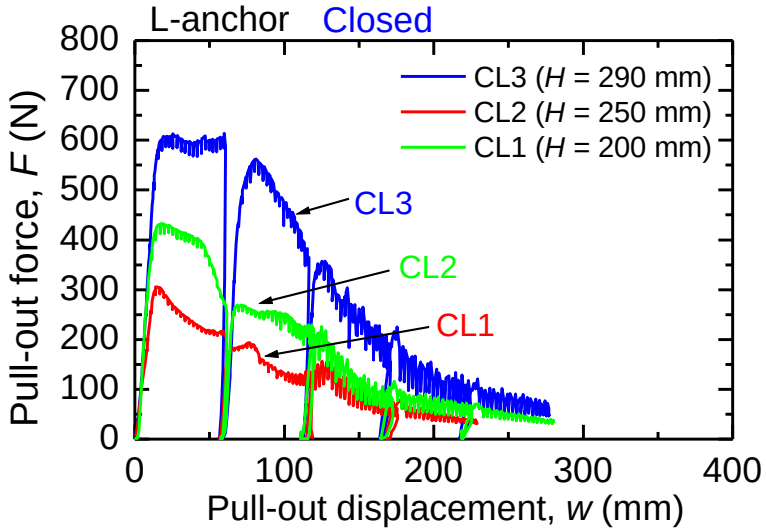

Fig. 3.19. *F* vs. *w* of Closed L anchors at different *H*.

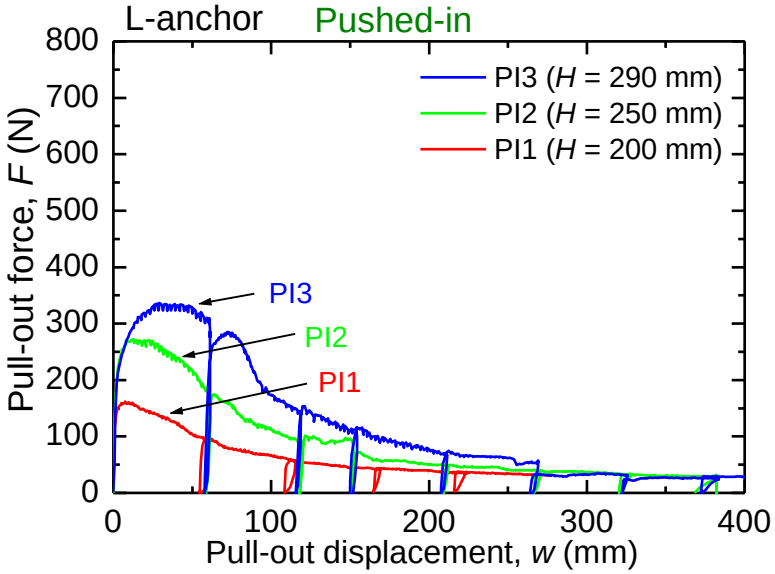

Fig. 3.20. *F* vs. *w* of Pushed-in L anchors at different *H*.

Maximum pull-out resistance F_{max} and maximum pull-out pressure p_{max}

Figures 3.21-3.23 show maximum pull-out resistance F_{max} of each size of anchor for each installation condition, Opened, Closed, and Pushed-in.

Figure 3.21 compares F_{max} of Opened anchor. F_{max} increases exponentially as *H* increases. *A* of L anchor was about 7 times larger than *A* of S anchor, and about 1.8 times *A* of M anchor. However, F_{max} of each anchor was about equivalent. Thus, it can be said that F_{max} of Opened anchors are not proportional to the ratio of *A*.

Figure 3.22 compares F_{max} of Closed anchors. Among Closed anchors, unlike Opened anchors, F_{max} of S anchor was the smallest. Similar to Opened anchors, F_{max} of Closed anchors was not proportional to the ratio of *A*, and increased exponentially as *H* increased.

Figure 3.23 compares F_{max} of Pushed-in anchors. F_{max} of Pushed-in anchors were about 50% of F_{max} of Closed anchors, but had a similar tendency to Closed anchors. F_{max} of Pushed-in M, L

anchors were comparable to F_{max} of Opened M, L anchors. Thus, F_{max} of Pushed-in anchors can be calculated based on the condition of Opened (horizontal plate) anchors.

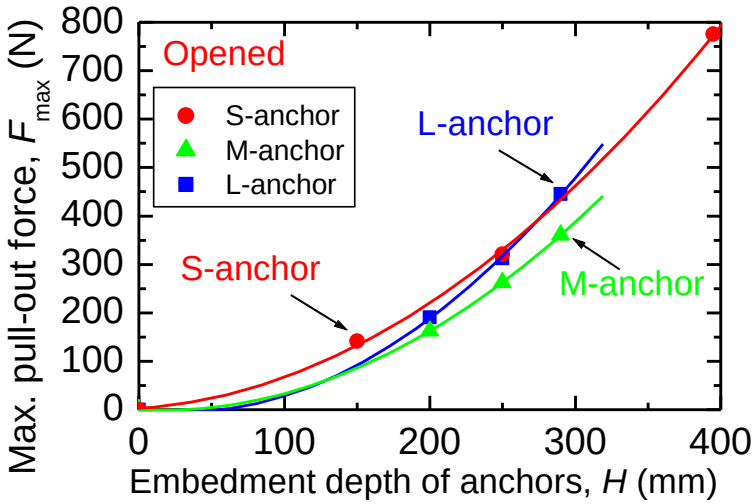

Fig. 3.21. F_{max} of Opened anchors.

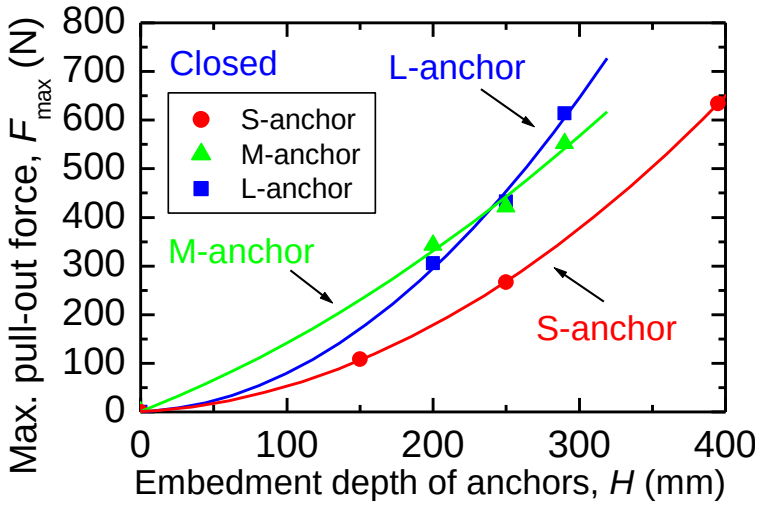

Fig. 3.22. F_{max} of Closed anchors.

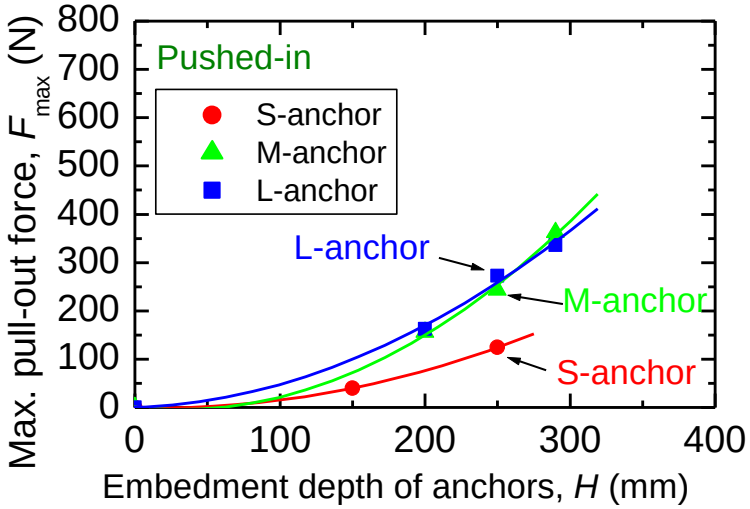

Fig. 3.23. F_{max} of Pushed-in anchors.

F_{max} of Pushed-in anchors were only 50-60% of F_{max} of Closed anchors despite the same state in the ground before being pulled. This can be because that H was too small for the actual anchors, and the influence of the ground destruction while pushing-in process might came out strongly. If there is sufficient H for the actual anchors, F_{max} of Pushed-in anchors would be equivalent to F_{max} of Closed anchors.

Figures 3.24-3.26 show maximum pull-out pressure p_{max} (= F_{max}/A) of each anchor under Opened, Closed, and Pushed-in installation conditions.

Figure 3.24 compares p_{max} of Opened anchors. As H increased, p_{max} of each Opened anchor increased exponentially. p_{max} of S anchor was clearly larger than that of M and L anchors. The smaller the anchor was, the larger p_{max} became. This tendency was the same for anchors with other installation conditions (Figs. 3.25 and 3.26).

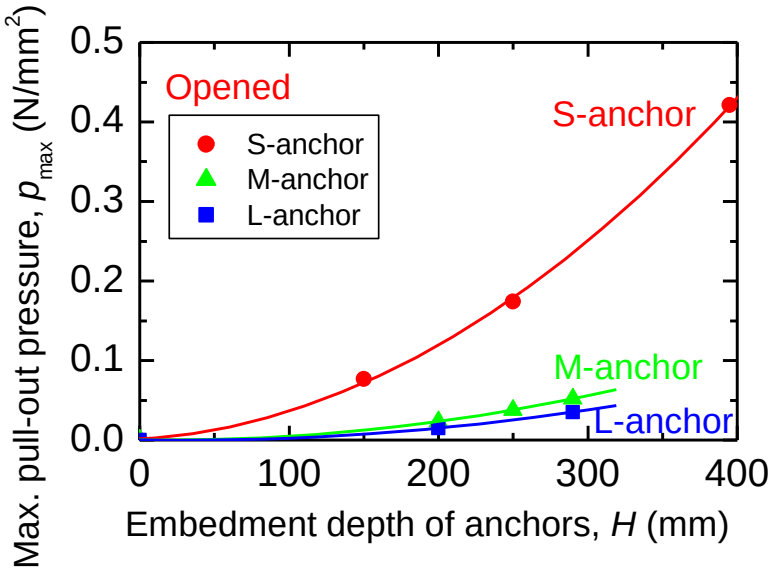

Fig. 3.24. p_{max} of Opened anchors.

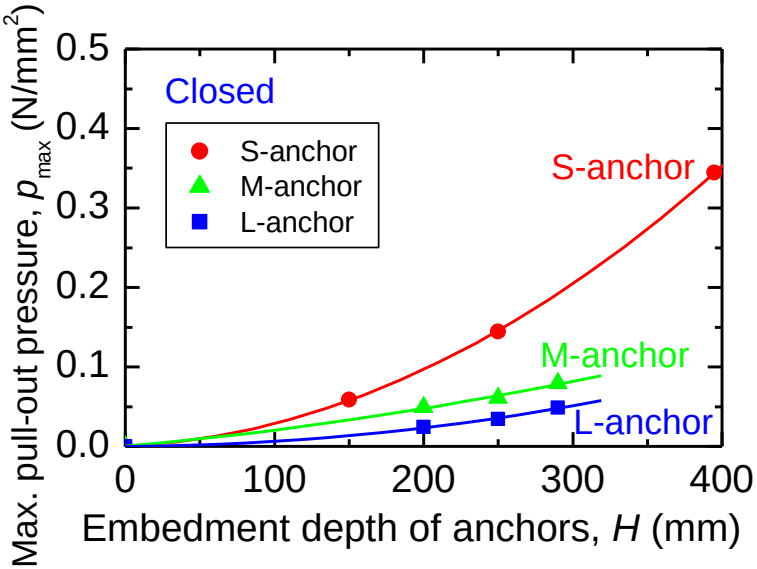

Fig. 3.25. p_{max} of Closed anchors.

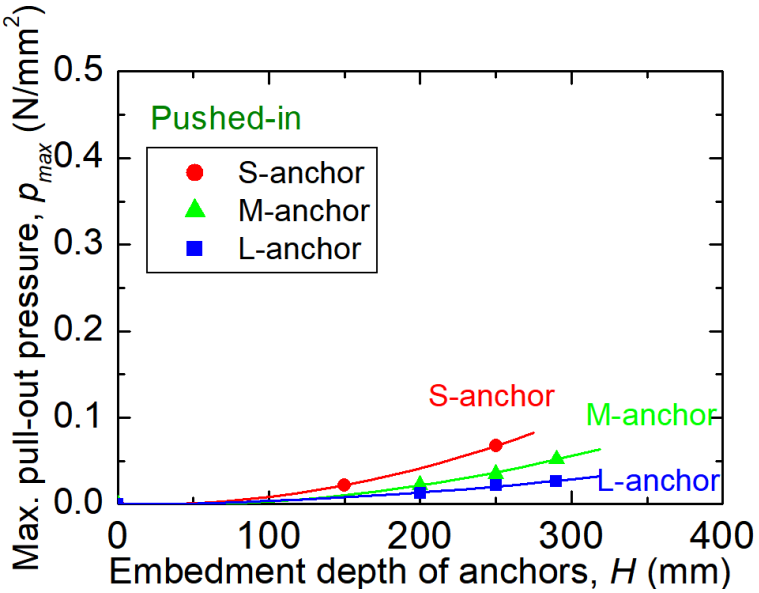

Fig. 3.26. p_{max} of Pushed-in anchors.

These results indicate that p_{max} of the anchors are affected by other than overburden pressure.

Figure 3.27 shows the state of the ground surface after pulling out the Opened L-anchors. The failure area of the ground surface was wider than A. The area seems to become wider as H is larger. This tendency is observed and investigated in a three-dimensional condition in previous studies, such as Baker and Kondner (1966) and Emirler et al. (2016).

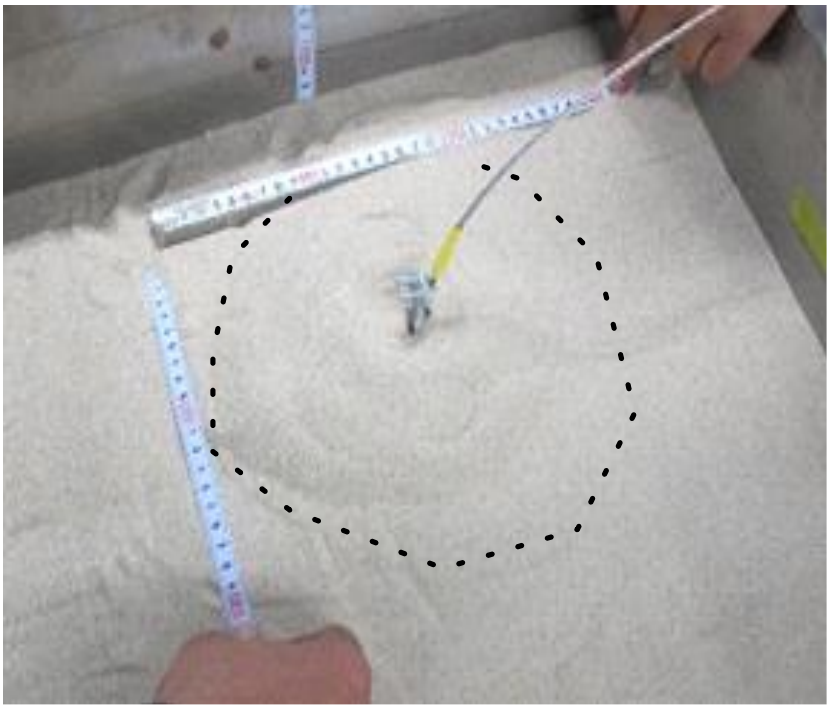

(a) H = 200 mm, diameter = 250 mm

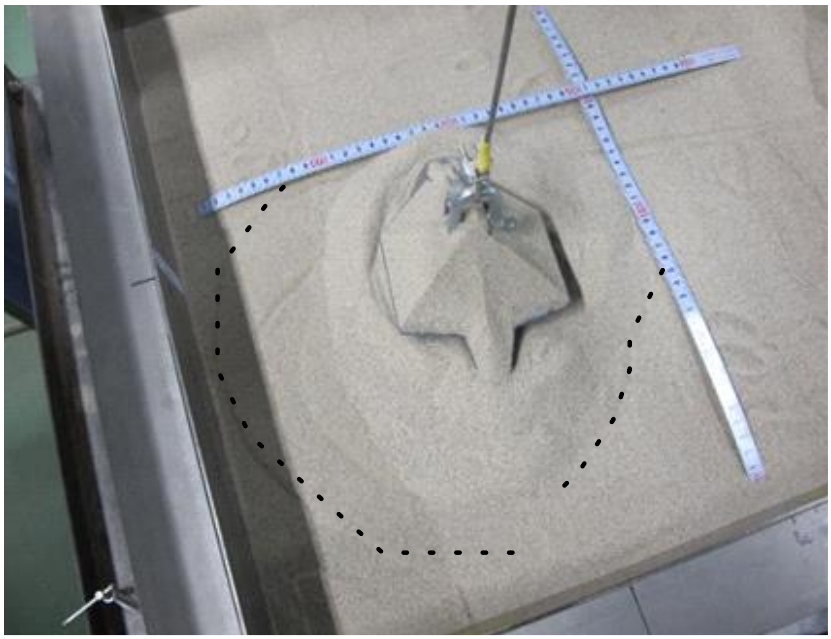

(b) H = 250 mm, diameter = 300 mm

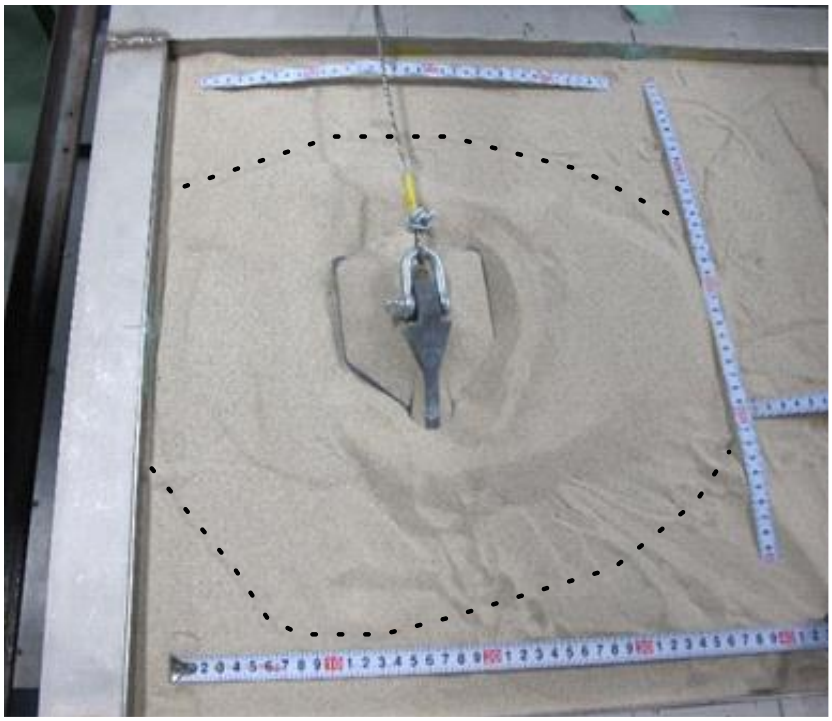

(c) H = 290 mm, diameter = 400 mm

Fig. 3.27. Influenced area of the ground surface when pulling out Opened L anchor.

3.2.4 Discussion of Section 3.2

In this pull-out experiment of actual flip anchors in model sand ground, both expected and unexpected results were obtained. As expected, F_{max} increased as H increased, and an area of the ground surface which was greater than A was influenced by pulling the anchor. As a particularly interesting result,

the larger A was, the larger F_{max} was; whereas the smaller A was, the larger p_{max} (= F_{max}/A) was in any condition.

Some unexpected results were obtained as below.

1) For Opened anchors, there was not much difference in F_{max} of each size of anchors.
2) F_{max} of Opened M & L anchors were smaller than F_{max} of Closed anchors, and F of Opened anchors softened immediately after the peak.
3) F_{max} of Pushed-in anchors was considerably smaller than F_{max} of Closed anchors.

The too small-scale ground for actual flip anchors perhaps caused those unexpected results. (Table 3.3). The embedment ratio H/L was too small especially for M and L anchors. As in Fig. 3.5, actual H/L for Closed and Pushed-in anchors were larger than Opened anchors by L because of the installation conditions. Thus, the results of Opened anchors are thought to be particularly influenced by the small H/L. For Pushed-in anchors, the ground destruction during pushing process affected on F_{max} strongly because of the too small H/L condition.

Table 3.3. Laboratory pull-out experiments using actual flip anchors in the dry sand ground.

	HP25 (S)	H50 (M)	H110 (L)	HG100	HG180	HG320
H (m)	H/L	H/L	H/L	H/L	H/L	H/L
0.15	1.8 (2.8)	-	-	-	-	-
0.20	-	1.3 (2.3)	1.3 (2.3)	-	-	-
0.25	2.9 (3.9)	1.6 (2.6)	1.6 (2.6)	-	-	-
0.29	-	1.8 (2.8)	1.8 (2.8)	-	-	-
0.395	4.6 (5.6)	-	-	-	-	-

( ): actual H/L for Closed & Pushed-in anchors

Because H is limited in the laboratory, these results in a laboratory were examined by conducting full-scale field experiments.

3.3 Field pull-out experiments of flip-type earth anchors embedded or driven in a sand ground

3.3.1 Introduction

In field pull-out experiments, similar to the laboratory experiments, actual flip anchors were installed under the installation conditions: Opened, Closed, or Driven. The above-mentioned results of laboratory experiments were examined by comparing them with the results of field experiments on a full scale (Table 3.4).

Table 3.4. Field pull-out experiments of actual flip anchors in a sand ground.

	HP25 (S)	H50 (M)	H110 (L)	HG100	HG180	HG320
H (m)	*H*/*L*	*H*/*L*	*H*/*L*	*H*/*L*	*H*/*L*	*H*/*L*
1.0	-	6.3	6.3	-	-	-
1.5	-	9.4	9.4	4.4	4.4	-
2.0	-	12.5	12.5	5.9	5.9	-
2.25	-	-	-	6.6	6.6	5.1

3.3.2 Outline of the experiments

A full-scale model sand ground was prepared in a test pit of 4.0 m in length, 4.0 m in width, and 2.5 m in height in a field (Fig. 3.28). Table 3.5 shows physical and mechanical properties of river sand used for the model ground. Internal friction angle of the sand was measured by direct shear tests. The model ground consisting of 10 layers of 0.25 m thick. Each sand layer was compacted using a vibration tamper to have a relative density D_r of around 80% and a dry density p_d of around 1.745 t/m^3.

After the pull-out experiments in the first cases were completed, the ground was recreated and the second cases were conducted. The sand grounds were named "Ground 1" and "Ground 2", respectively.

Fig. 3.28. A model ground for pull-out experiments of actual flip anchors in a field.

Table 3.5. Physical and mechanical properties of river sand used for the model ground.

Density of soil particles, ρ_s (t/m^3)	2.688
Max. dry density, ρ_{dmax} (t/m^3)	1.833
Min. dry density, ρ_{dmin} (t/m^3)	1.463
Max. void ratio, e_{max}	0.837
Min. void ratio, e_{min}	0.466
Int. friction angle at peak strength, ϕ_p (deg)	42
Int. friction angle at residual strength, ϕ_r (deg)	35

Figure 3.29 shows the distribution with a depth of water content w_c of each ground. The w_c of the Ground 1 and the Ground 2 were around 5.5%. Figure 3.30 are distributions of total density ρ_t and dry density ρ_d of each ground. There is not a big difference of the ground conditions between the Ground 1 and the Ground 2.

Portable dynamic cone penetration tests (DCPTs) were conducted in the Ground 1. In the DCPTs, a cone having a diameter of 25 mm was driven with a hammer having a mass of 5 kg and a free-falling height of 500 mm. Figure 3.31 shows N_d-values of the Ground 1. Here, N_d is the blow counts required for the penetration of 100 mm of the cone. Figure 3.32 shows SPT N-values converted from the DCPTs results. DCPTs was not conducted in the Ground 2, because the conditions of the Ground 2 are assumed equivalent to Ground 1 as shown in Figs. 3.29 and 3.30.

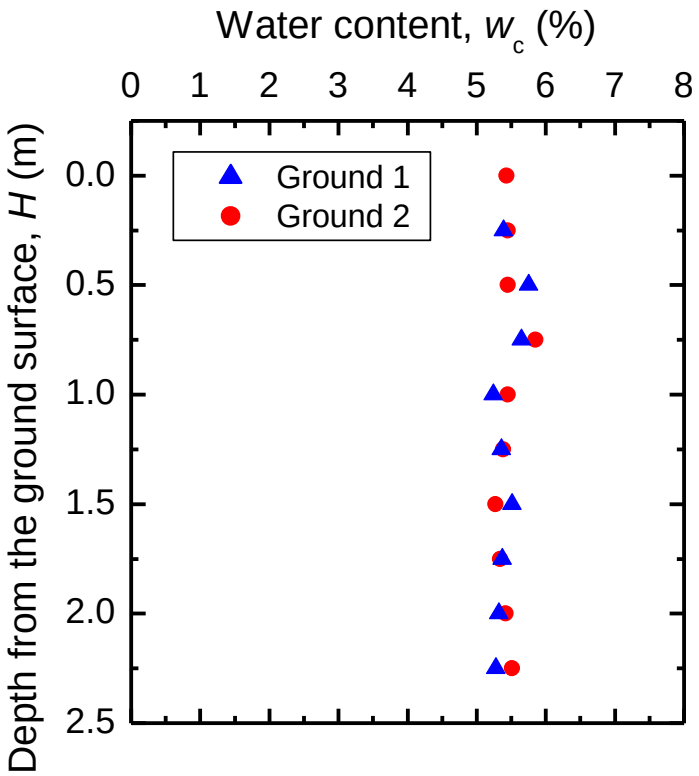

Fig. 3.29. Water content w_c in the Ground 1 and Ground 2.

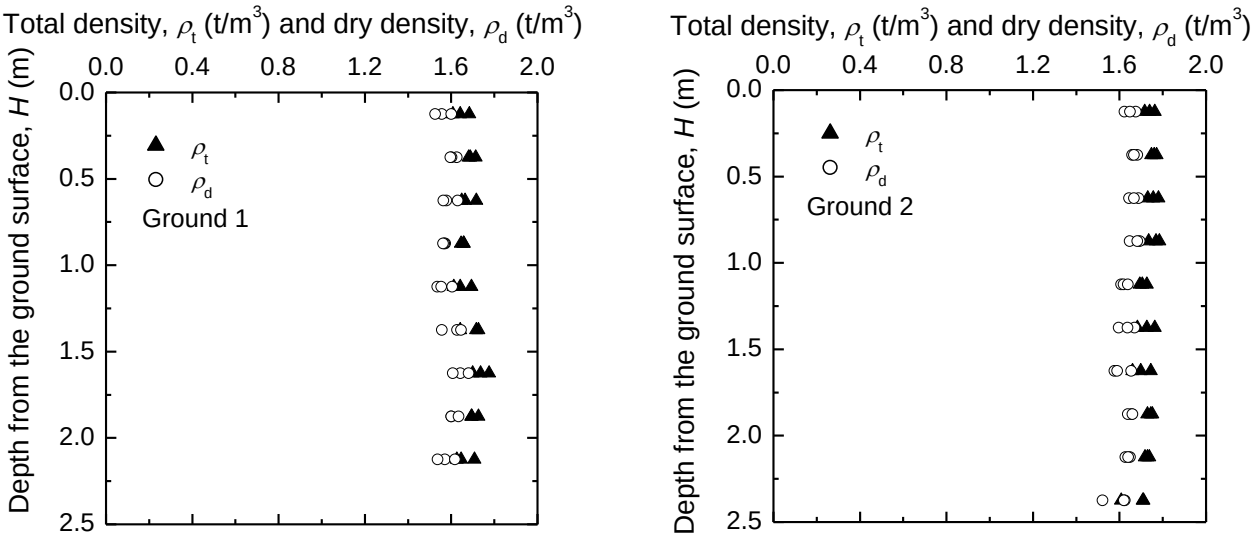

Fig. 3.30. Distribution of soil densities in the Ground 1 and Ground 2.

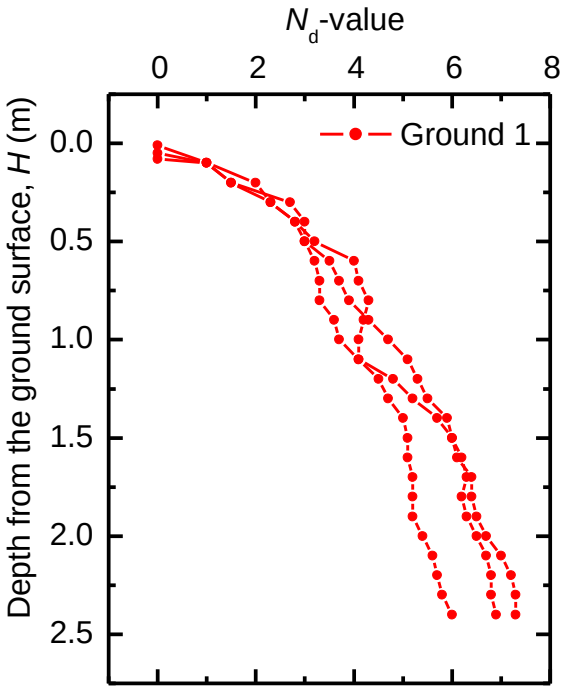

Fig. 3.31. N_d-values in the Ground 1.

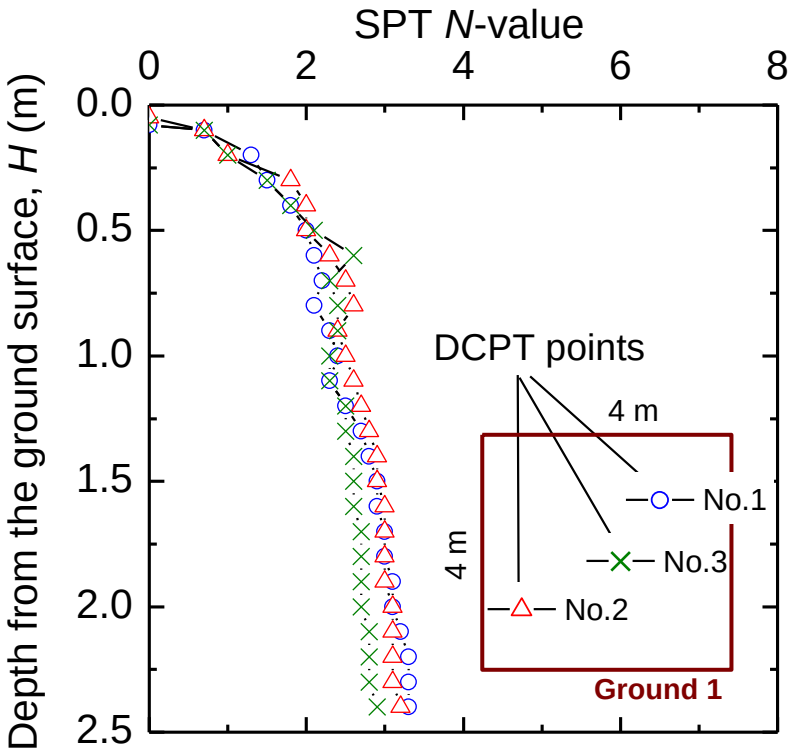

Fig. 3.32. SPT *N*-values in the Ground 1.

Figure 3.33 explains experimental conditions. Table 3.6 and 3.7 lists experimental cases in the Ground 1 and the Ground 2, respectively.

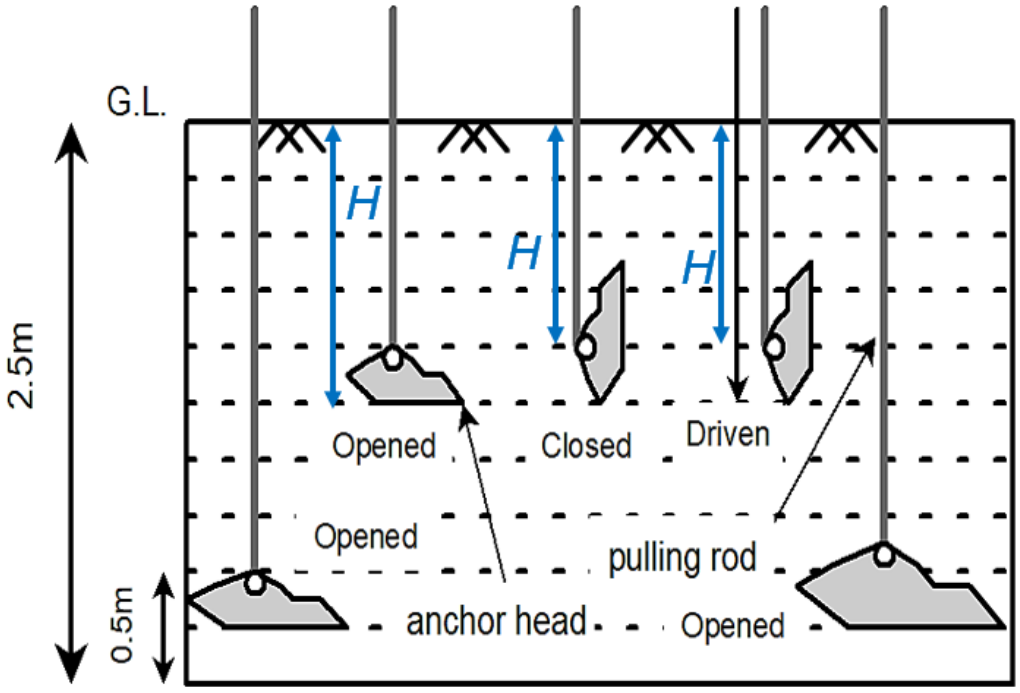

Fig. 3.33. Three installation conditions of actual flip anchors in field pull-out experiments.

Table 3.6. Experimental cases of full-scale pull-out experiments of actual flip anchors in sand (Ground 1).

Case	Anchor	Depth, H (m)	State	Max. force, F_{max} (kN)
G1_C01	HG100	1.5	OP	30.63
G1_C02	H50	2.0	OP	12.28
G1_C03	H110	2.0	OP	20.06
G1_C04	H110	1.5	OP	14.28
G1_C05	H50	1.5	OP	10.31
G1_C06	HG100	2.0	OP	42.88
G1_C07	HG100	2.0	OP	42.88
G1_C08	HG180	2.0	OP	67.39
G1_C09	HG180	1.5	OP	42.88
G1_C10	HG320	1.01	D	18.38
G1_C11	HG180	1.34	D	42.88
G1_C12	HG100	1.33	D	21.44
G1_C13	H110	1.41	D	11.86
G1_C14	H50	1.41	D	9.66

NB: OP: Opened, CL: Closed, D: Driven

Table 3.7. Experimental cases of full-scale pull-out experiments of actual flip anchors in sand (Ground 2).

Case	Anchor	Depth, H (m)	State	Max. force, F_{max} (kN)
G2_C01	H110	1.5	CL	16.34
G2_C02	H110	1.0	OP	8.58
G2_C03	H50	1.0	OP	5.20
G2_C04	H50	1.5	CL	10.86
G2_C05	HG180	2.25	CL	50.20
G2_C06	HG320	2.25	CL	90.30
G2_C07	HG100	2.25	OP	50.20
G2_C08	HG180	2.25	OP	70.10
G2_C09	HG100	2.25	CL	45.00
G2_C10	HG320	2.25	OP	106.50

First, the actual flip anchors (Fig. 3.34) made of ductile iron were buried in the ground at designated H in Opened (OP) or Closed (CL) head conditions while the ground preparation (Figs. 3.35a). In the Ground 1, five sizes of flip anchors were driven into the ground (G1_C10 to C14) (Fig. 3.35b) after the completion of the pull-out experiments of G1_C01 to C09. Figure 3.36 shows a set-up for the pull-out experiments. Each anchor was pulled out with a hydraulic jack, and F and w were measured with a load cell and an encoder.

In the Ground 2, pull-out experiments of the buried anchors (G2_C01 to C10) were conducted.

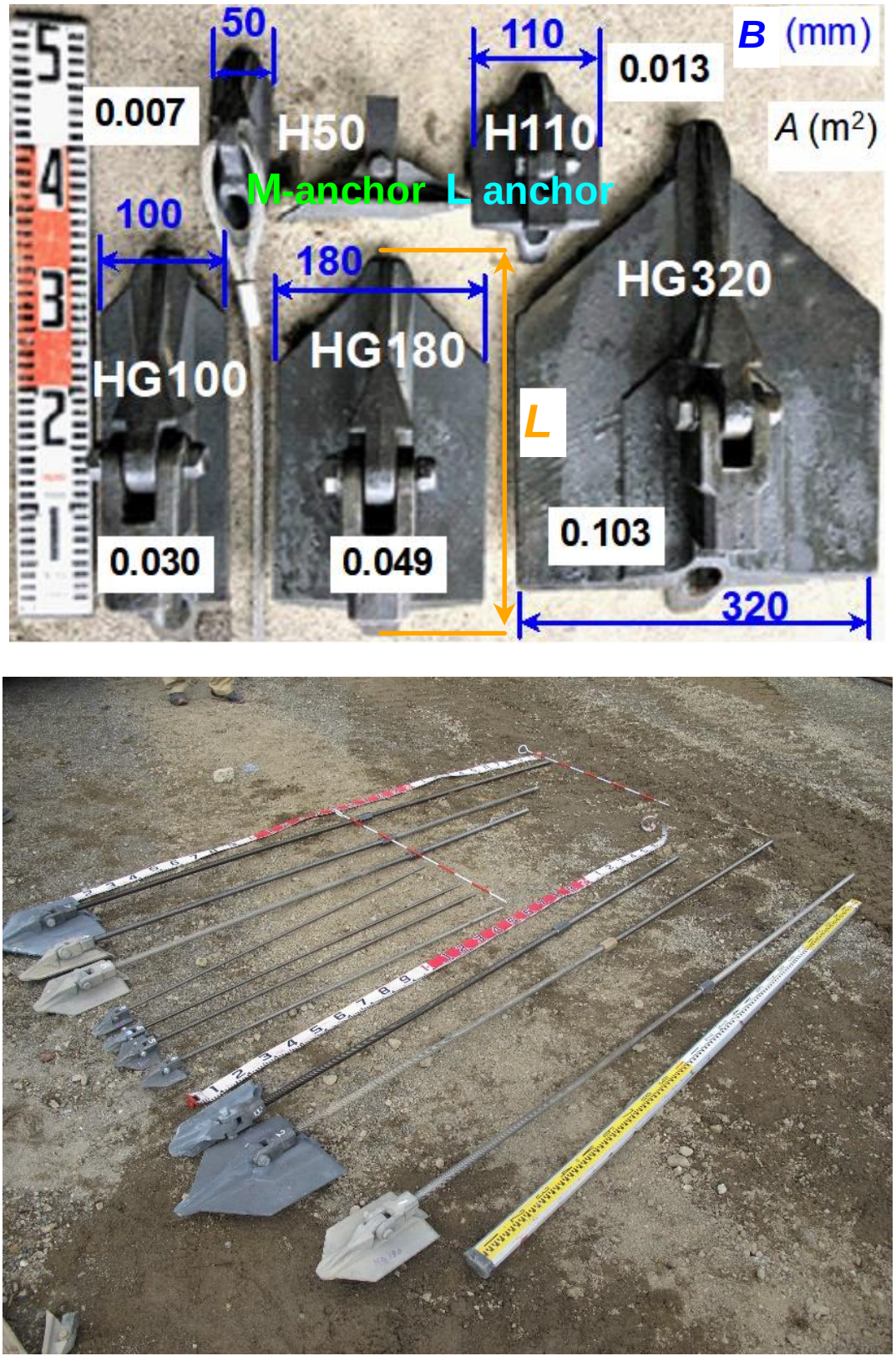

Fig. 3.34. Actual flip anchors used for full-scale pull-out experiments in a field.

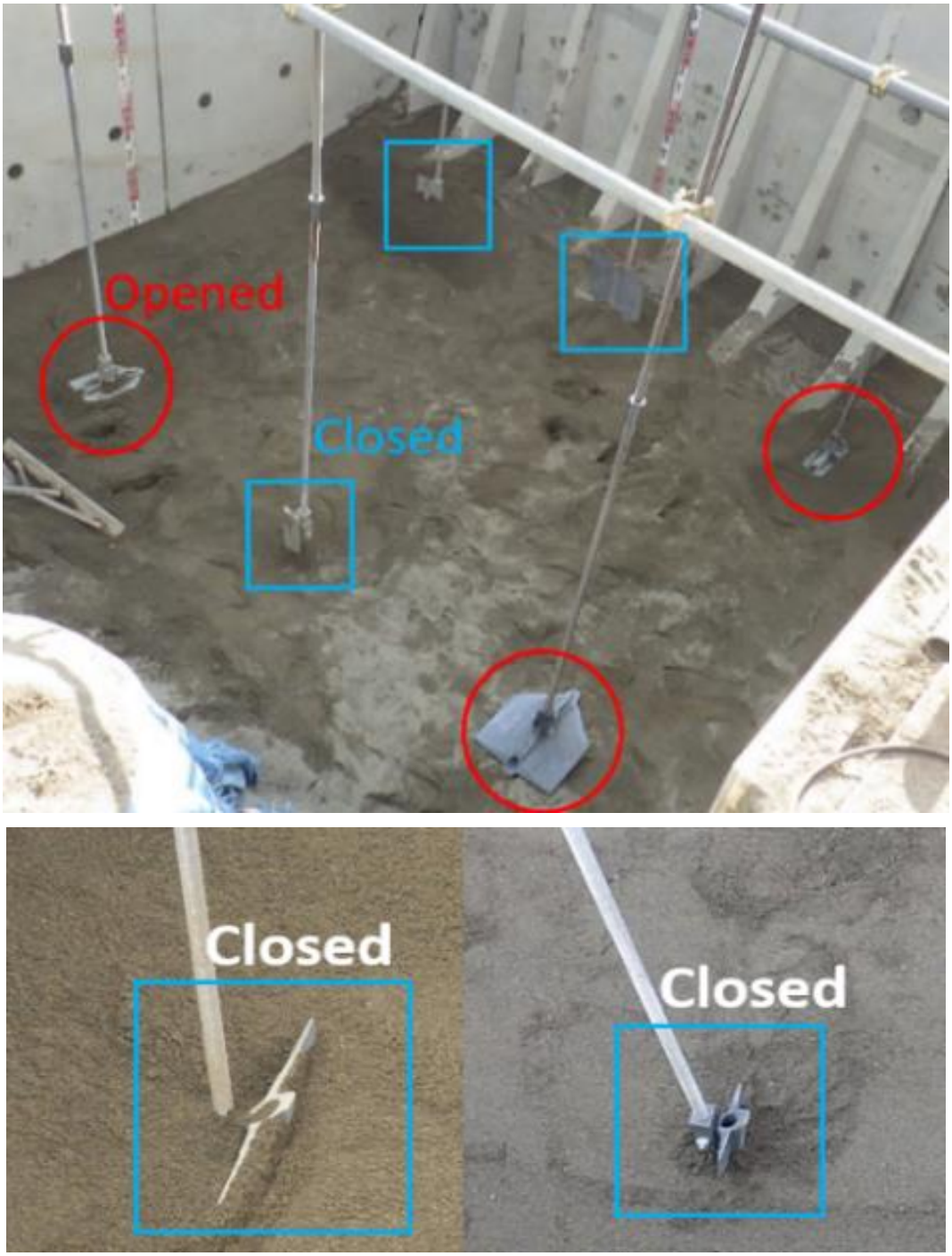

(a) Embedment condition of Opened and Closed anchors

(b) Installation condition of Driven anchors

Fig. 3.35. Installation condition of Opened, Closed, or Driven anchors.

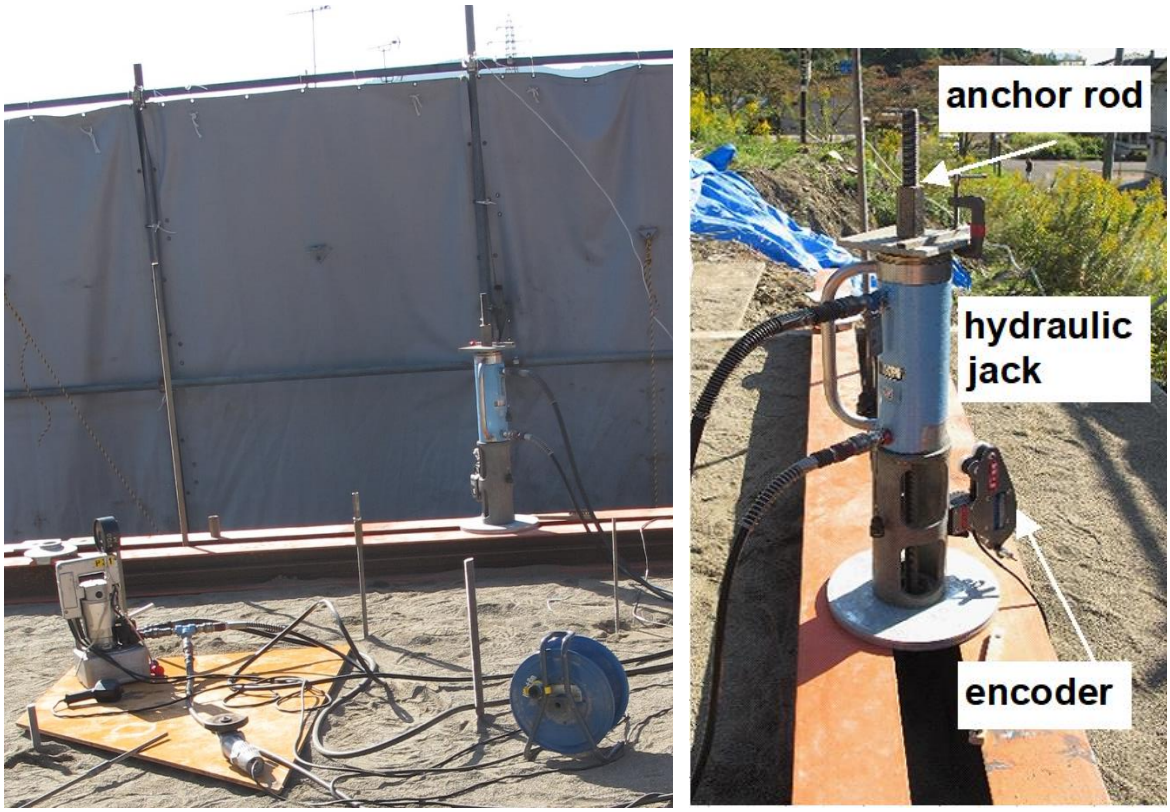

Fig. 3.36. A set-up for pulling-out anchors.

3.3.3 Experimental results

Figures 3.37-3.40 compare *F* vs. *w* by changing *H* of each Opened anchor (excluding HG320).

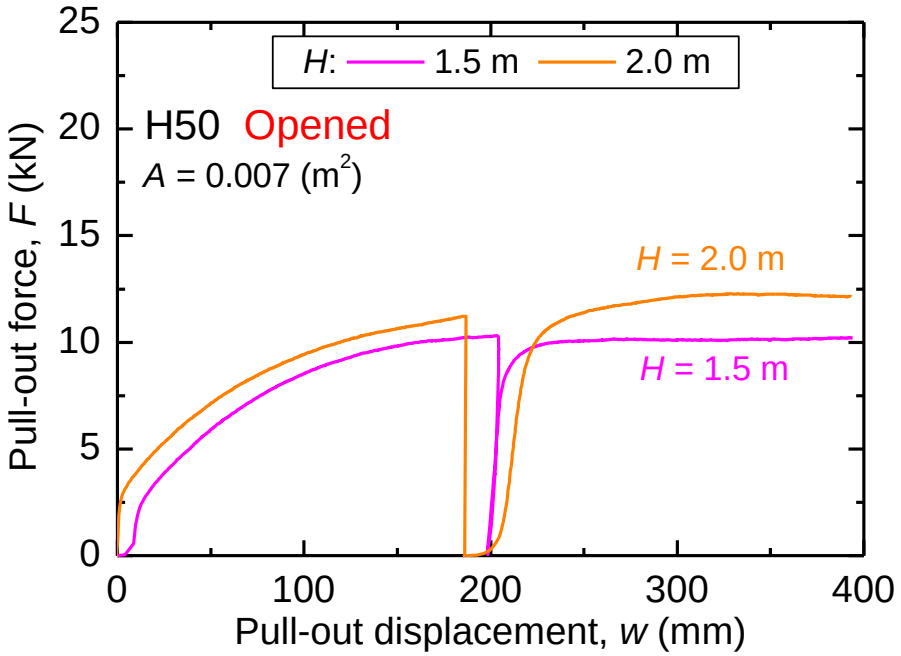

Fig. 3.37. *F* vs. *w* of Opened H50 anchors at different *H*.

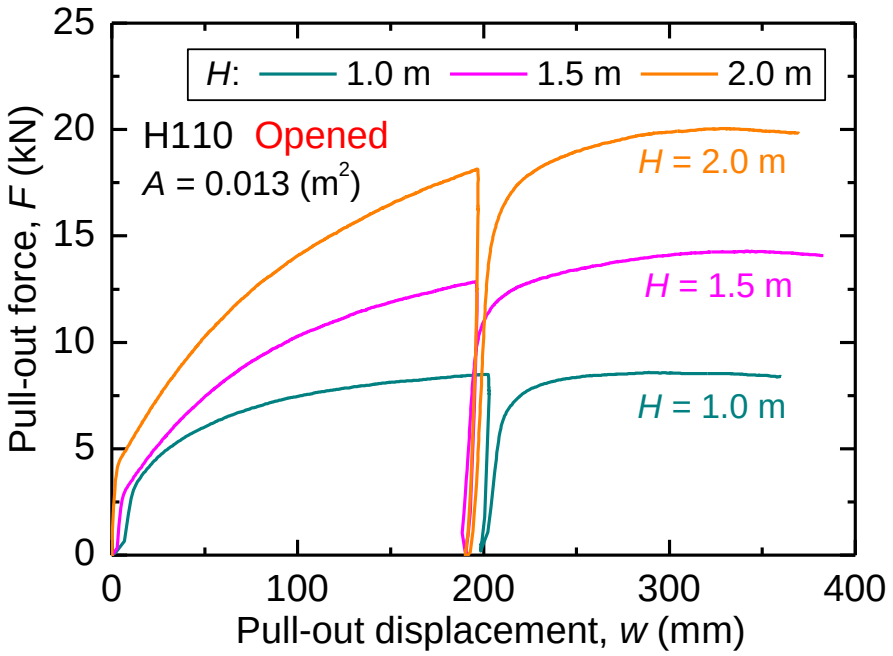

Fig. 3.38. *F* vs. *w* of Opened H110 anchors at different *H*.

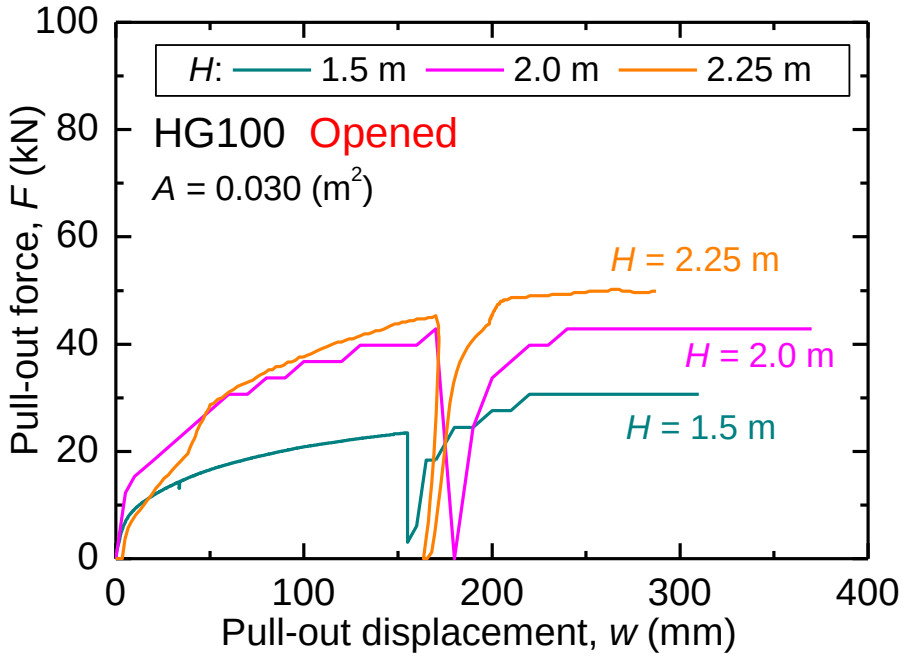

Fig. 3.39. *F* vs. *w* of Opened HG100 anchors at different *H*.

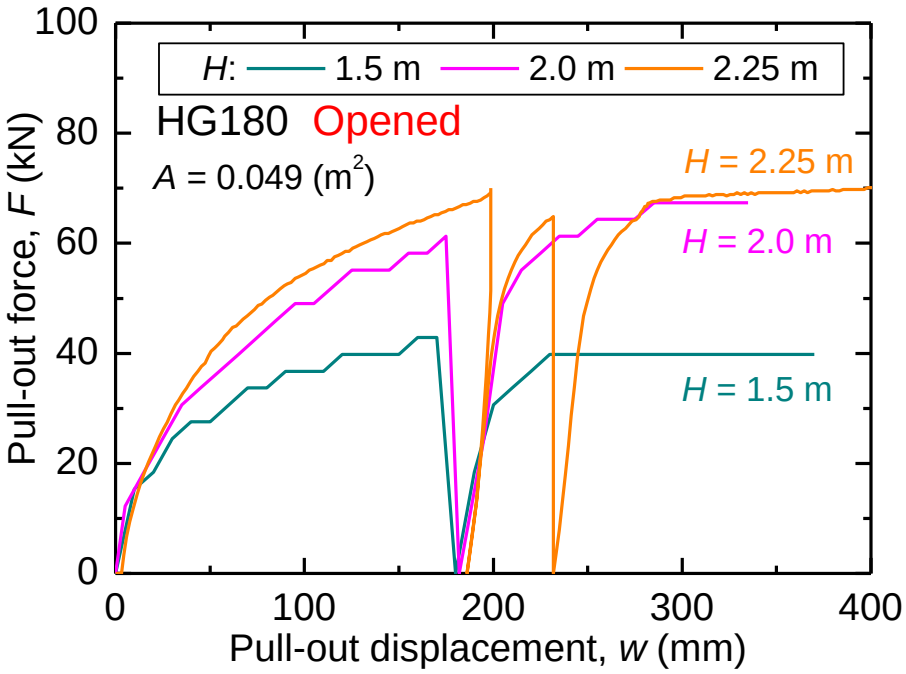

Fig. 3.40. *F* vs. *w* of Opened HG180 anchors at different *H*.

Figure 3.37 shows *F* vs. *w* of H50 anchor at *H* = 1.5 m and *H* = 2.0 m. *F* of H50 anchor at *H* = 2.0 m was larger than *F* at *H* = 1.5 m.

Figure 3.38 shows *F* vs. *w* of H110 anchor at *H* = 1.0 m, 1.5 m, and 2.0 m. As *H* increased, the initial gradient ($\Delta F/\Delta w$) and maximum pull-out force F_{max} increased. F_{max} of H110 anchor at *H* = 1.5 m was about 1.8 times F_{max} at *H* = 1.0 m. F_{max} of H110 anchor at *H* = 2.0 m was about 2.5 times F_{max}

at H = 1.0 m. F_{max} of H110 anchor increased as H increased.

F_{max} of H110 anchor at H = 2.0 m and H = 1.5 m were about 1.7 times and 1.4 times larger than F_{max} of H50, respectively. A of H110 anchor is about 1.9 times A of H50 anchor; however F_{max} did not increase in proportion to A.

Figures 3.39 and 3.40 show F vs. w of HG100 and HG180 anchors at H = 1.5 m, 2.0 m, and 2.25 m. Like H50 and H110 anchors, the larger H became, the larger F_{max} was. A of HG180 anchor is about 1.6 times A of HG100 anchor; however, F_{max} of HG180 anchor was about 1.3 times (H = 1.5 m), about 1.6 times (H = 2.0 m), and about 1.4 times (H = 2.25 m) F_{max} of HG100 anchor. Thus, F_{max} did not increase as much as the ratio of A.

In the laboratory experiments described in Section 3.2, Opened anchors showed softening behavior immediately after reaching F_{max}. In the field experiments, F of any size of Opened anchors did not decrease sharply and maintained values around F_{max} even when w increased further.

Figures 3.41 and 3.42 compare F vs. w of Opened anchors (H = 1.5 m or H = 2.25 m). Figures 3.43 and 3.44 are similar comparisons for Closed anchors. In both anchor condition, F of larger anchors were greater than F of smaller anchors.

The initial gradient of $\Delta F/\Delta w$ of Closed anchors were relatively smaller than the gradient of Opened anchors. For Closed anchors, w of 300 mm was required until F_{max}. It was about 1.5 times w of Opened anchors (w = around 200 mm) at F_{max}.

Comparing H50 vs. H110, and HG100 vs. HG180 having equal L but different B, especially for Closed anchors, the larger B was, the larger the initial gradient ($\Delta F/\Delta w$) was.

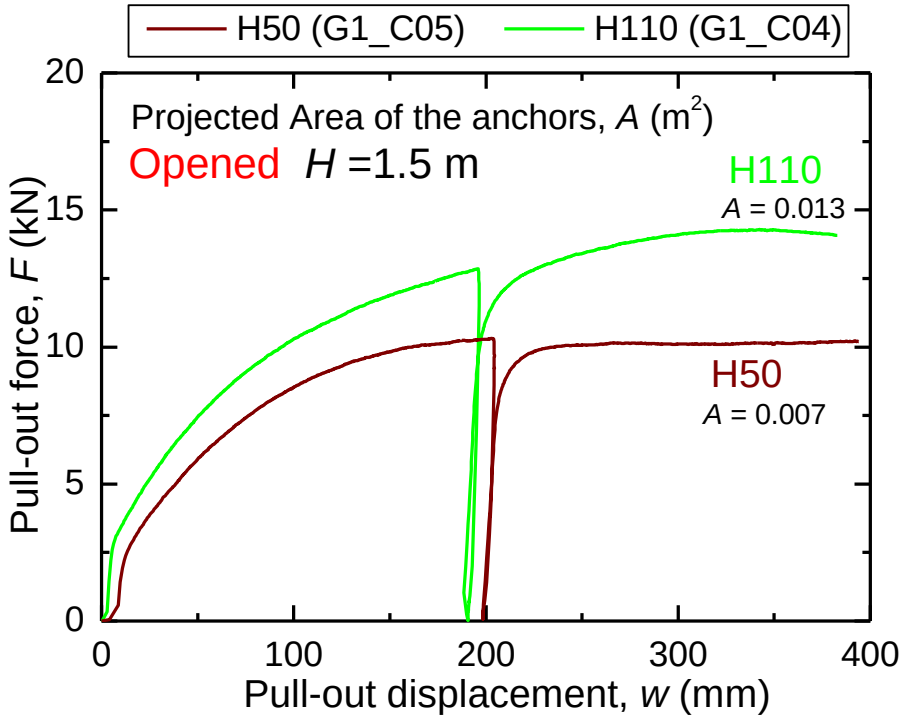

Fig. 3.41. F vs. w of Opened H50 & H110 anchors at H =1.5 m.

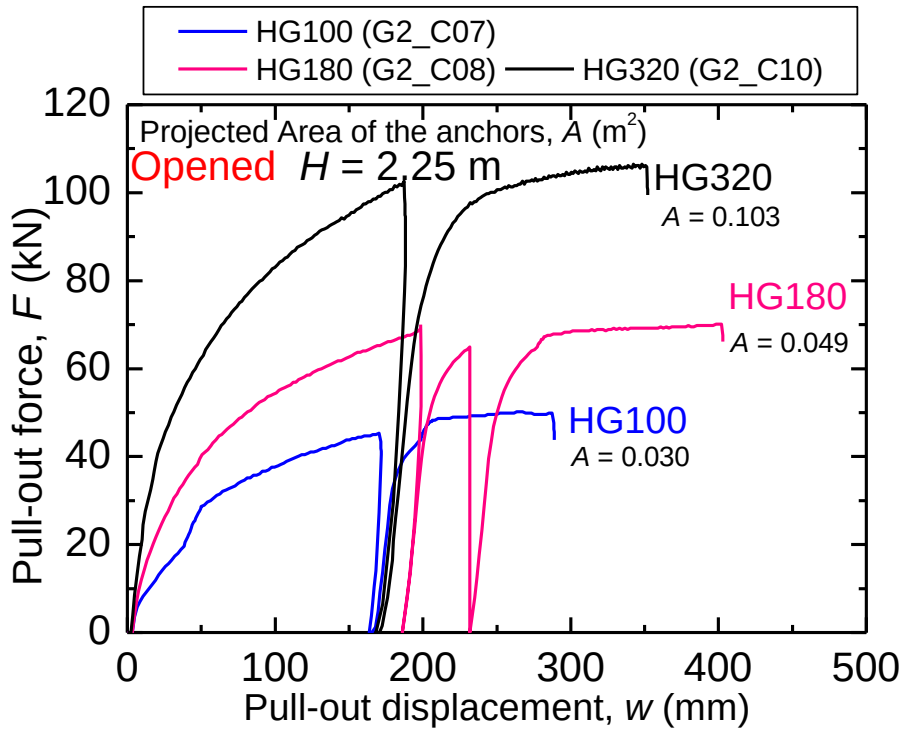

Fig. 3.42. *F* vs. *w* of Opened HG anchors at *H* =2.25 m.

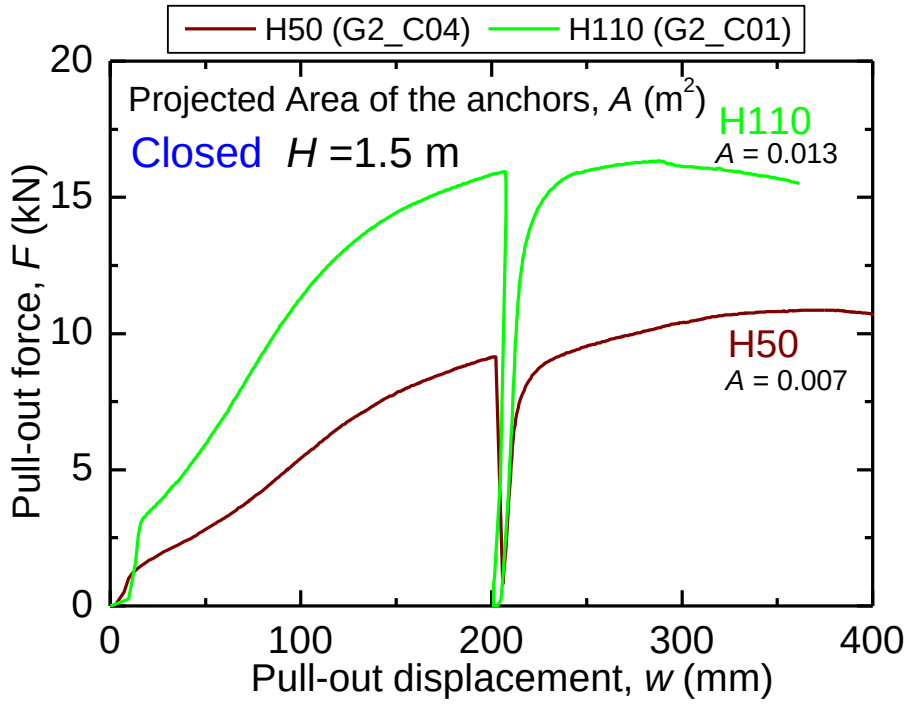

Fig. 3.43. *F* vs. *w* of Closed H50 & H110 anchors at *H* =1.5 m.

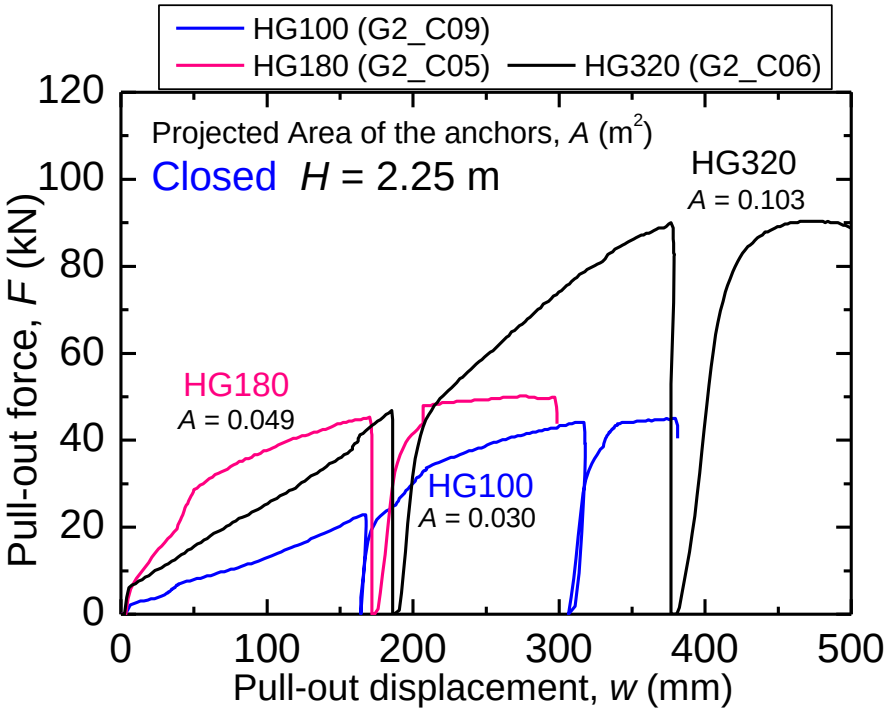

Fig. 3.44. *F* vs. *w* of Opened HG anchors at *H* =2.25 m.

Figures 3.45-3.49 show *F* vs. *w* of Driven and Opened anchors. For both anchors, the larger the *A* was, the larger *F* was. Similar to Closed anchors, the initial gradient ($\Delta F/\Delta w$) of Driven anchors were smaller than Opened anchors. *w* at F_{max} of Driven anchors were about 1.5 times *w* at F_{max} of Opened anchors, and it was equivalent to the amount of *w* of Closed anchors.

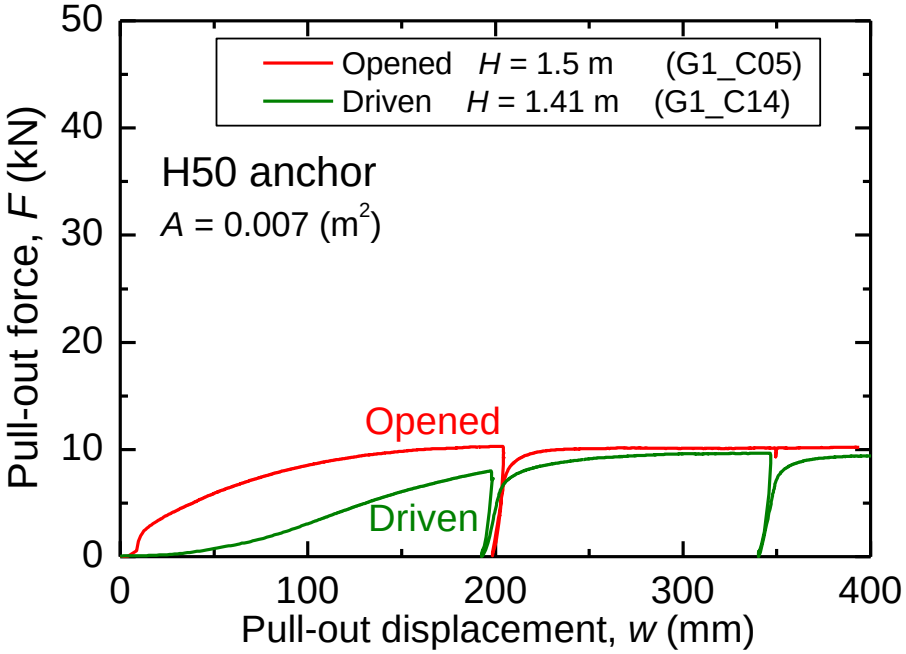

Fig. 3.45. *F* vs. *w* of Opened & Driven H50 anchors.

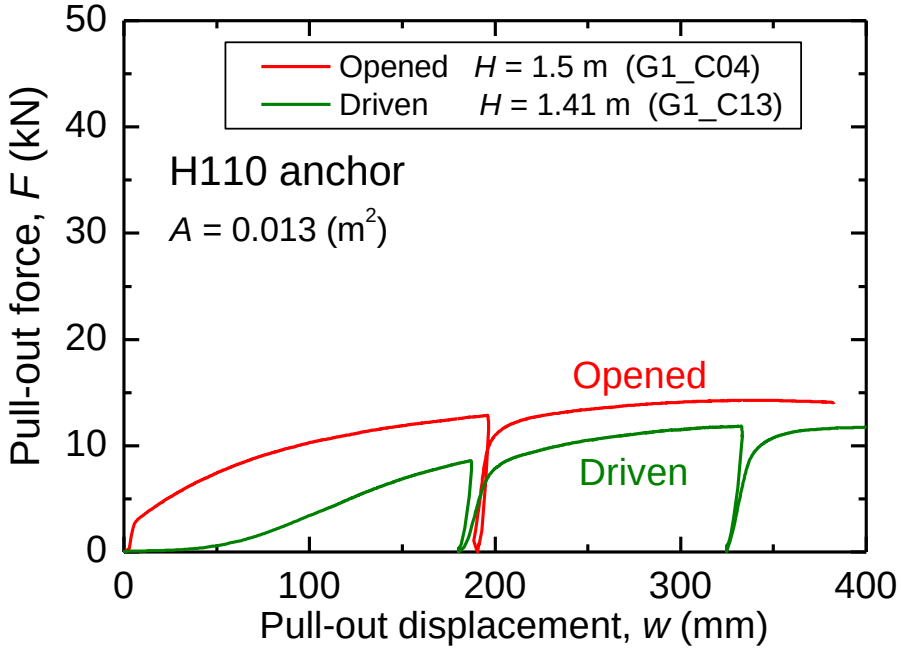

Fig. 3.46. *F* vs. *w* of Opened & Driven H110 anchors.

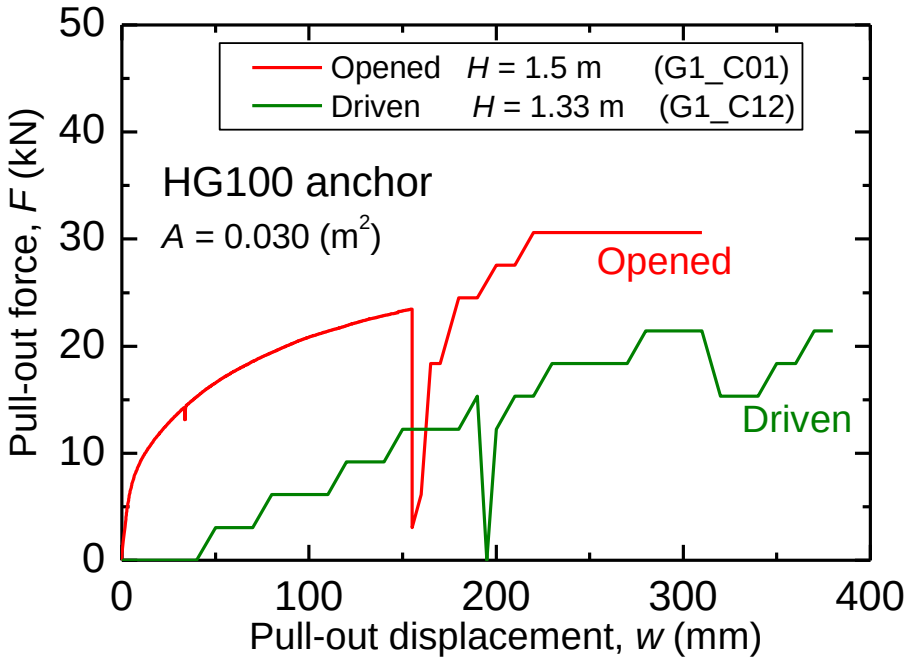

Fig. 3.47. *F* vs. *w* of Opened & Driven HG100 anchors.

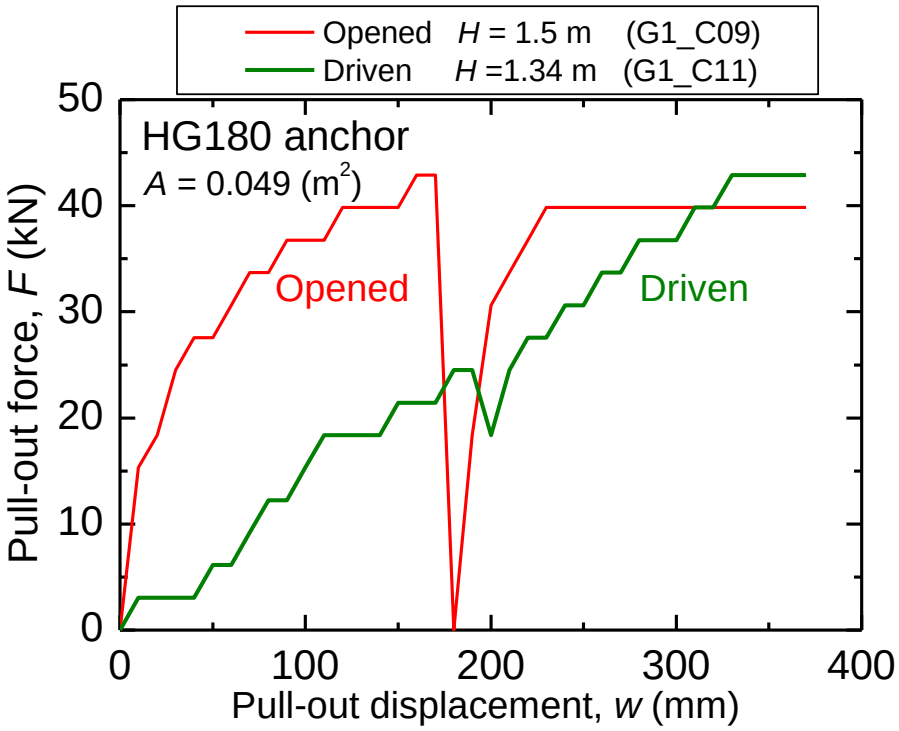

Fig. 3.48. *F* vs. *w* of Opened & Driven HG180 anchors.

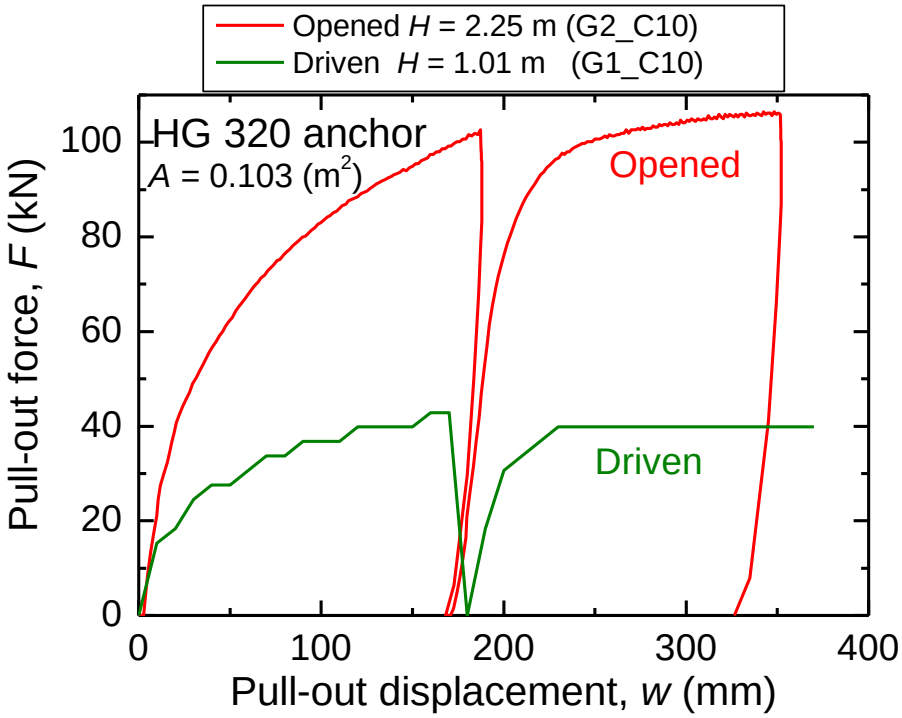

Fig. 3.49. *F* vs. *w* of Opened & Driven HG320 anchors.

F_{max} of Driven anchors whose *H* were slightly smaller than Opened anchors reached about 80% of F_{max} of Opened anchors (Figs. 3.45-3.48). The tendency was similar to Closed anchors. Thus, F_{max} of flip anchors can be expected at least about 80% of F_{max} of Opened anchors (= horizontal plate anchor).

Maximum pull-out force F_{max} and Maximum pull-out pressure p_{max}

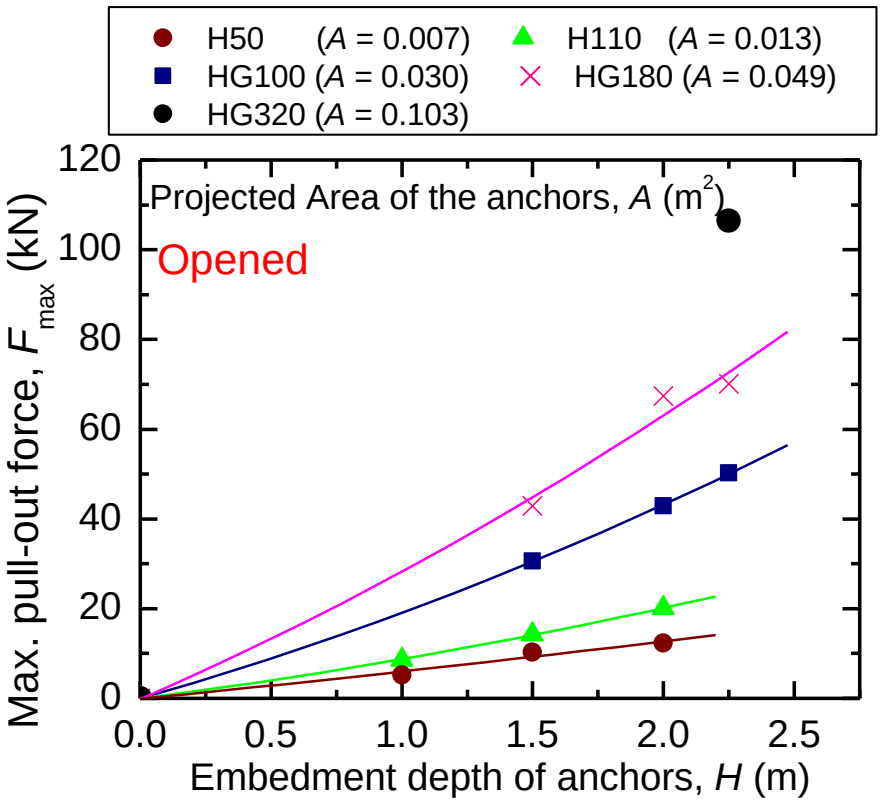

Fig. 3.50. F_{max} of Opened anchors.

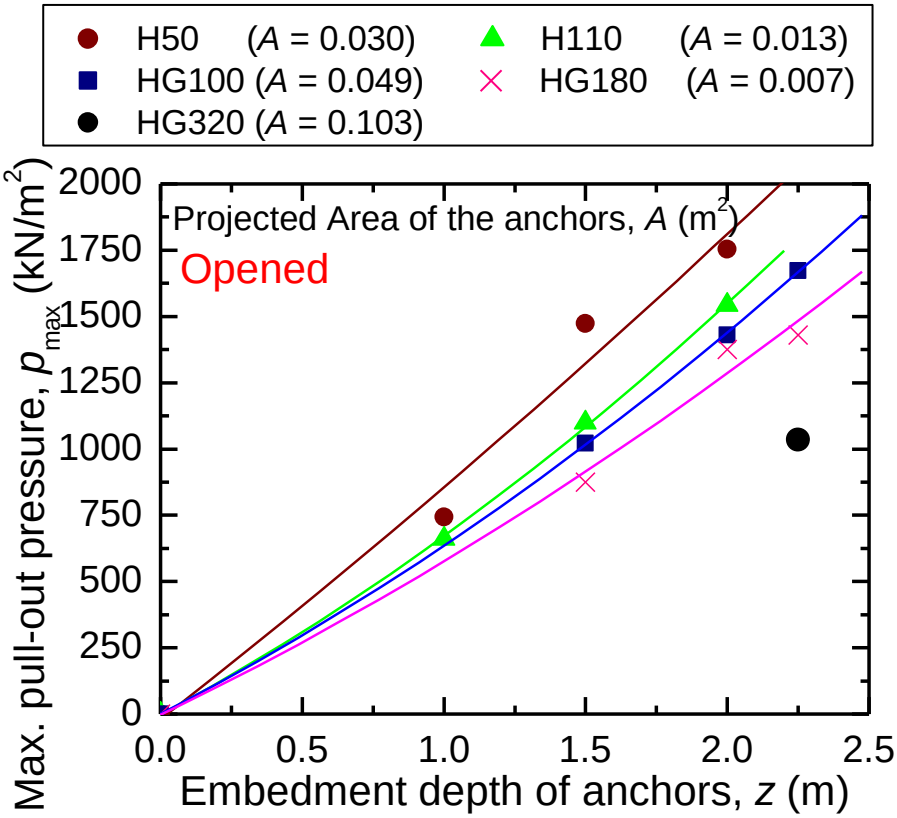

Fig. 3.51. p_{max} of Opened anchors.

Figure 3.50 shows F_{max} of each Opened anchor. As expected, F_{max} of larger anchors were larger, and F_{max} became larger as H increased.

Figure 3.51 shows a comparison of p_{max} acting on each Opened anchor. Contrary to F_{max}, p_{max} of smaller anchors were greater than p_{max} of larger anchors. This agrees with the results of laboratory experiments.

The influenced area of the ground surface (Fig. 3.52) when pulling the anchors was greater than A. This is common to the results in laboratory experiments (Fig. 3.27). This failure pattern of the ground should make p_{max} become larger with a decreasing A. This ground failure pattern accompanied with pull-out of flip anchors will be investigated further in Chapter 4.

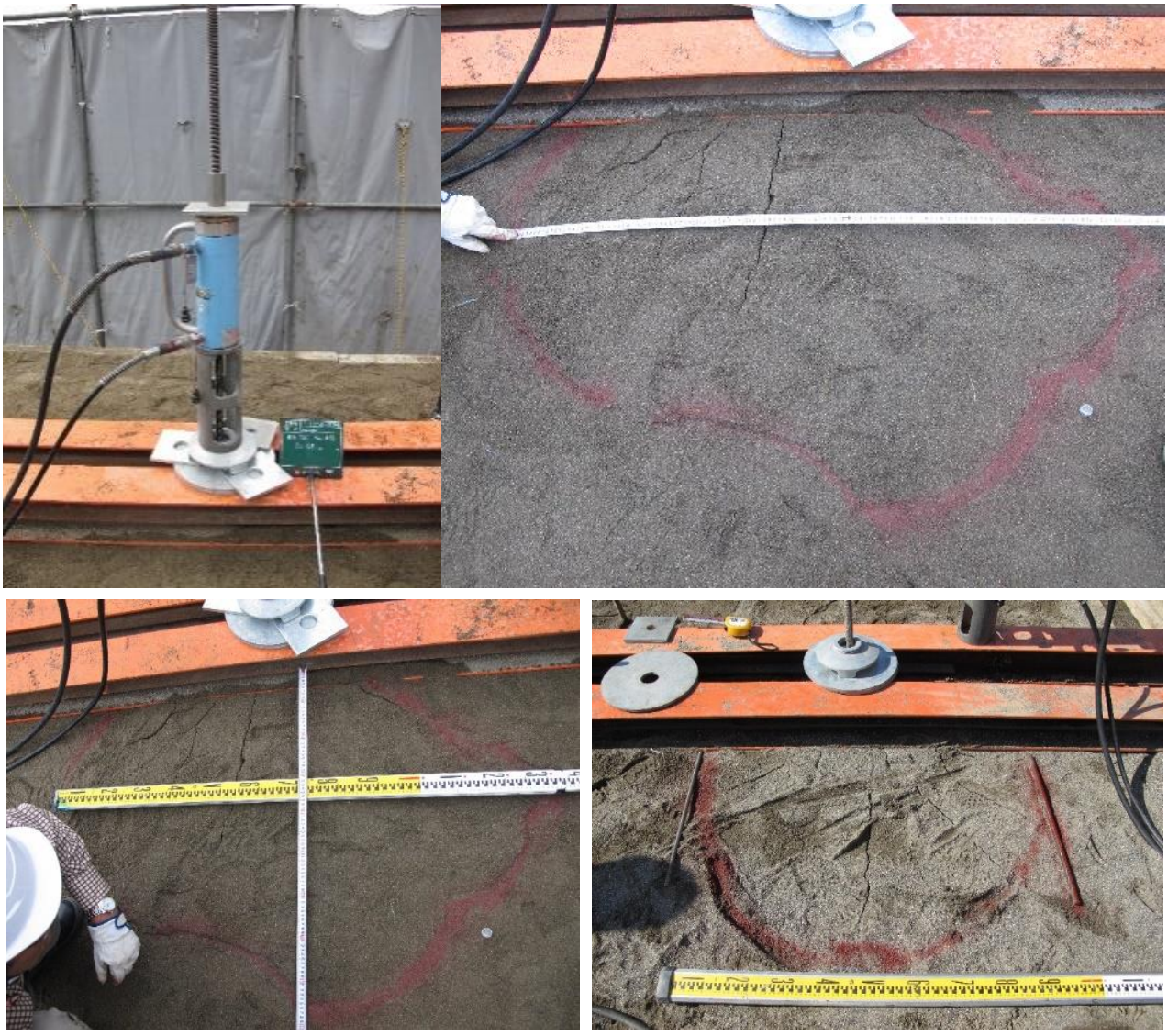

Fig. 3.52. Influenced area of the ground surface by pulling out an anchor (HG320 H = 1.3 m).

State of the anchor during pulled-up

Fig. 3.53 shows states of the flip anchors in the ground after pulled up for about $L/2$ (half the amount of w required for flip anchors to fully open). These anchors were driven to a depth of about 1.3 m.

All the anchors were about half opened because the *w* were smaller than *L*.

(a) HG100 anchor at *w* =180 mm

(b) HG180 anchor at *w* =200 mm

(c) HG320 anchor at *w* =250 mm

Fig. 3.53. State of the anchor heads in the middle of opening in the ground.

3.3.4 Discussion of Section 3.3

Overall, the field experimental results were similar to the experimental results in the laboratory. Unlike the unexpected results of laboratory experiments, the following results were obtained under sufficient H/L conditions in the field.

1) F_{max} of flip anchors increased as A increased.
2) F_{max} of Driven anchors were equivalent to F_{max} of Closed anchors.
3) F_{max} of Driven anchors, which is corresponding to the practical installation condition of flip anchors, reached about 80% of F_{max} of horizontally embedded plate anchors (Opened anchors).
4) F did not soften immediately in any installation condition when H/L is 5 or more.

From the results of field experiment, w required for the flip anchors to open sufficiently in the dense sand could be the same amount as L or about 1.5 times L.

F_{max} of the flip anchors on the sand ground was investigated using the actual anchor both in the laboratory and field. Following the experiments on sand, the behavior of flip anchors in clay was investigated by full-scale pull-out experiments on a clayey ground.

3.4 Field pull-out experiments of flip-type earth anchors driven in a ground consisted of clay and sand layers

3.4.1 Introduction

To investigate behavior including pull-out resistance of flip anchors in clay, pull-out experiments using the actual flip anchors were conducted in a full-scale ground consisted of sand and clay layers. The experimental results in a clay layer were compared with the results in the sand layer or the sand grounds (Chapter 3.3) to examine the difference of behavior of the flip anchors in sand and clay.

Based on the experimental results, an estimation method for pull-out resistance of flip anchors installed in clay ground was proposed.

3.4.2 Outlines of the experiments

The test site was located at Shiga Prefecture, Japan. Figure 3.54 shows installation points of flip anchors, which were set at a position of 2.0 m pitch grids comprising three rows A, B, and C. Basically, nine anchors were installed in each row.

The ground was consisted of a top sand layer overlying a soft clay layer. Portable dynamic cone penetration tests (DCPTs) were conducted at ten locations in the site (Figs. 3.54 and 3.55). It can be seen that the ground shallower than 1.8 m in which the anchors were installed was almost uniform in a plane. The DCPTs device comprised a cone with a diameter of 25 mm, a drop hammer mass of 5 kg, and a hammer drop height of 500 mm. The converted SPT N-values (Fig. 3.56) were empirically estimated from the DCPTs results. The converted SPT N-value to a depth of 2.0 m within the top sand layer and the underlying clay layer was around 5, and increased to around 15 in the bottom sand layer.

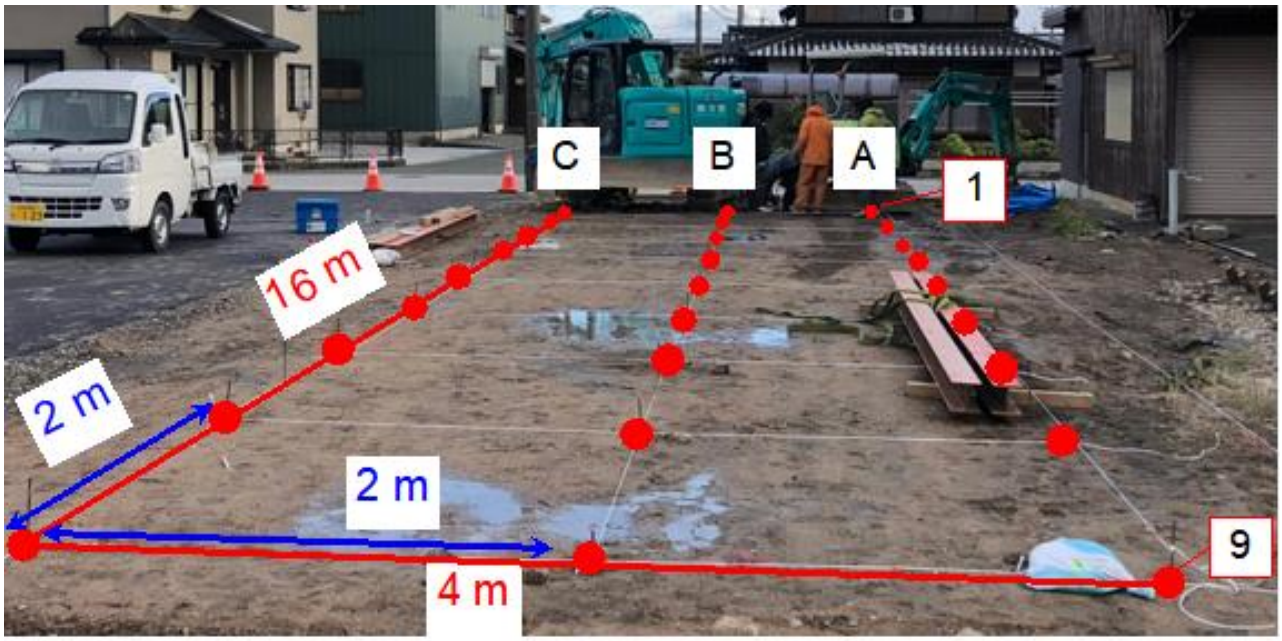

Fig. 3.54. A test site for the full-0scale pull-out experiments in a clayey ground.

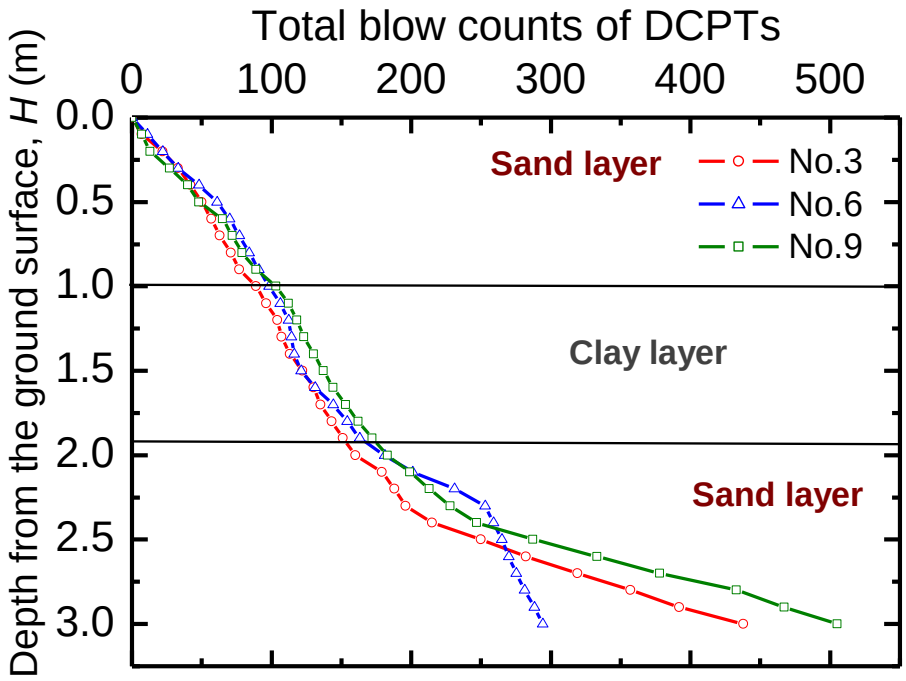

Fig. 3.55. Total blow counts of DCPTs.

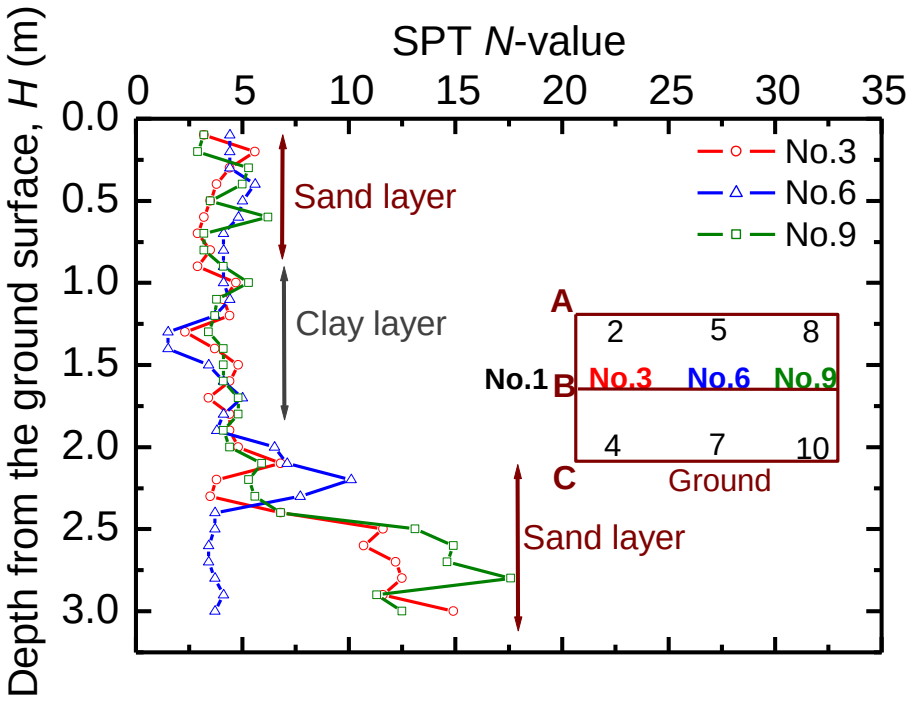

Fig. 3.56. SPT *N*-value converted from the result of DCPTs.

From Fig. 3.57, the approximate thickness of the clay layer can be estimated. Figure 3.57 shows the (a) driving rod, (b) anchor rods, and (c) anchor heads, for the anchors installed at H = 1.8 m in the clay layer. After pulled-out, the traces of clay left on the driving and anchor rods. From the traces, it is expected that the clay layer exists from the depth about 1.8 m to 1.0 m. This is consistent with the range of the clay layer assumed from the DCPT results.

(a) Clay left on a driving rod.

(b) Clay left on anchor rods.

(c) Clay left on anchor heads.

Fig. 3.57. Clay left on the anchor material after the pull-out experiments.

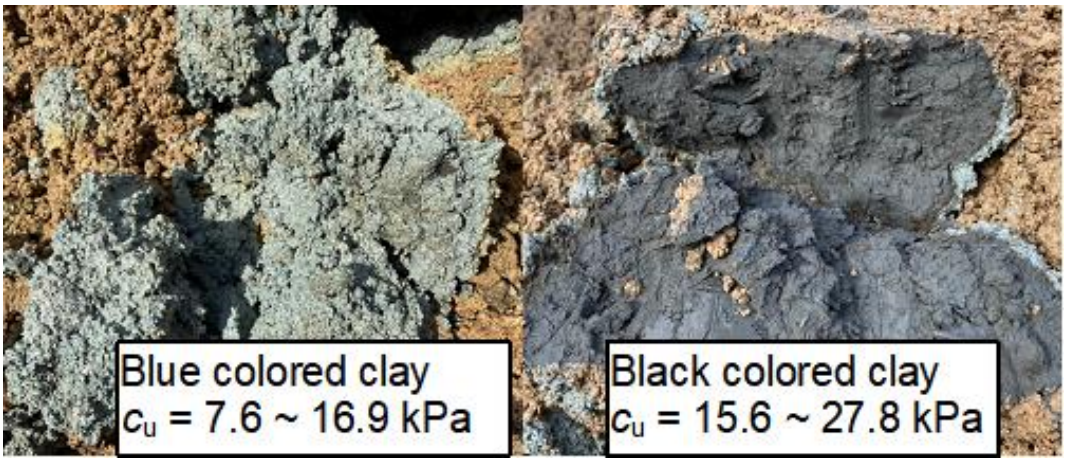

Fig. 3.58. Two types of clay in the ground.

Furthermore, the ground was excavated at two locations for observing the soil directly. The top sand layer was 1.0 m deep, followed by the clay layer to a depth of 1.8 m. As shown in Fig. 3.58, the clay layer comprised two types of clay. The blue-colored clay contained a small amount of sand particles while the black-colored clay was pure sticky clay. The former was located in between the sand layer and the black-colored clay. Vane shear tests were conducted in the clay layer to measure the undrained shear strength c_u. The black-colored clay had a relatively larger c_u than the blue-colored clay.

Figure 3.59 shows the water content w_c of the ground. The w_c of the black-colored clay was nearly 3 times w_c of the blue-colored clay. No significant difference was observed in w_c at each location.

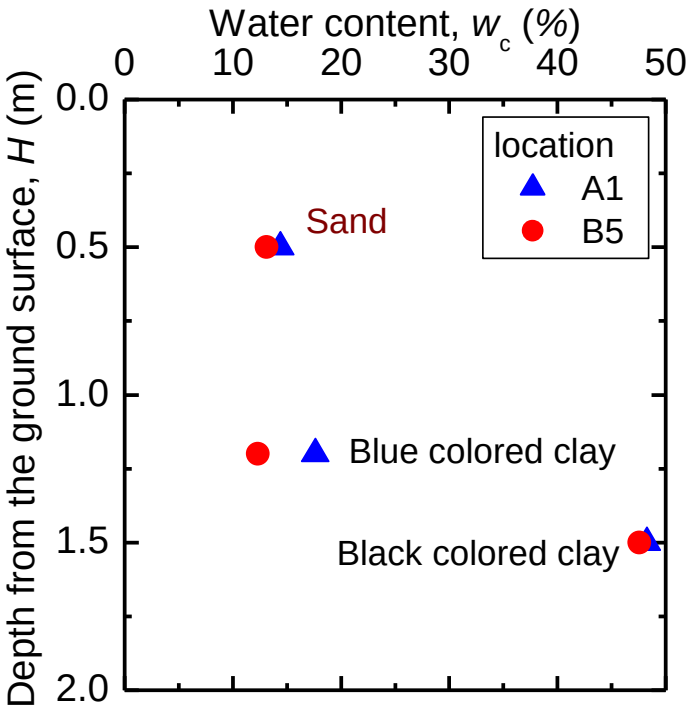

Fig. 3.59. Distribution of water content w_c in the ground.

As shown in Figure 3.34, the five types of flip anchors were used in the experiments. The smaller anchors were called as H series, and the larger ones are called as HG series. The numbers after H and HG denote a width of an anchor B. A length of the anchor L is 160 mm for H50 and H110, 340 mm for HG100 and HG180, and 440 mm for HG320. The projected area of the anchor A is also indicated in the figure.

As listed in Table 3.8, a total of 26 cases of pull-out experiments were conducted. H denotes the installation depth from an apex of the closed anchor plate to the ground surface. Anchors were driven into the ground with a percussion device and pulled out with a hydraulic jack (Fig. 3.60). F and w were measured while pulling out the anchors.

Table 3.8. Experimental cases and results of full-scale pull-out experiments of actual flip anchors in the ground consisted of sand and clay layers.

Case	Anchor	Depth, H (m)	Soil	Max. force, F_{max} (kN)
A1	HG320	1.8	Clay	*37.3
A2	HG320	1.2	Sand	35.8
A3	HG180	1.2	Sand	51.1
A4	HG100	1.2	Sand	45.9
A5	HG320	1.8	Clay	*16.2
A6	H110	1.0	Sand	26.0
A7	H50	1.0	Sand	14.0
A9	HG320	1.8	Clay	*13.1
B1	HG100	1.8	Clay	-
B2	HG100	1.8	Clay	*7.9
B3	H50x2	1.0	Sand	16.2
B4	H110	1.0	Sand	20.5
B5	HG100	1.8	Clay	*12.5
B6	H110	1.8	Clay	*6.1
B7	H110	1.8	Clay	*8.5
B8	H50	1.8	Clay	*4.5
B9	HG100	1.8	Clay	*8.8
C1	HG180	1.8	Clay	*17.1
C2	HG320	1.2	Sand	66.1
C3	HG180	1.2	Sand	64.3
C4	HG100	1.2	Sand	62.7
C5	HG180	1.8	Clay	*17.7
C6	H110	1.0	Sand	37.6
C8	H50	1.0	Sand	22.3
C9	HG180	1.8	Clay	*12.5
BC2.5	H50	1.0	Sand	10.7

Note: * F_{max} between the depths of 1.8 and 1.3 m.

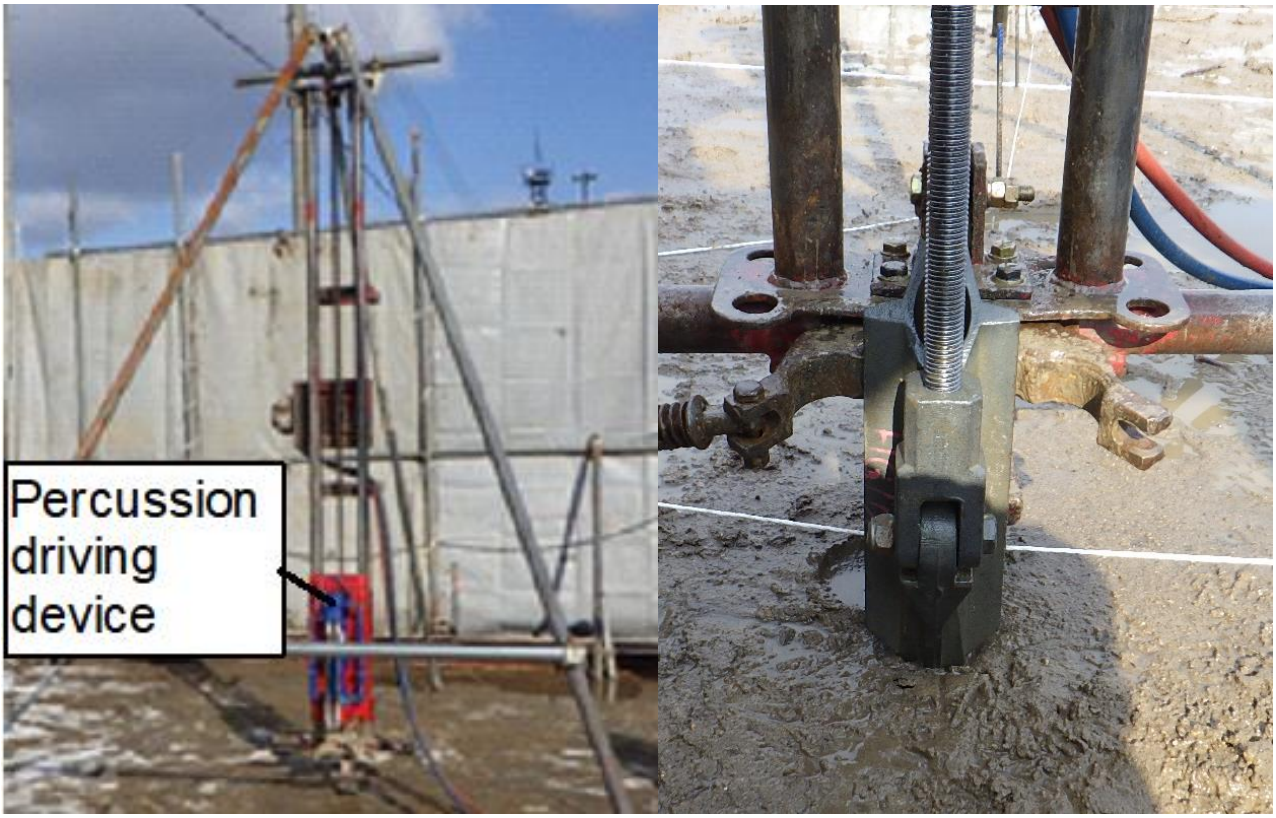

(a) Driving device of flip anchors

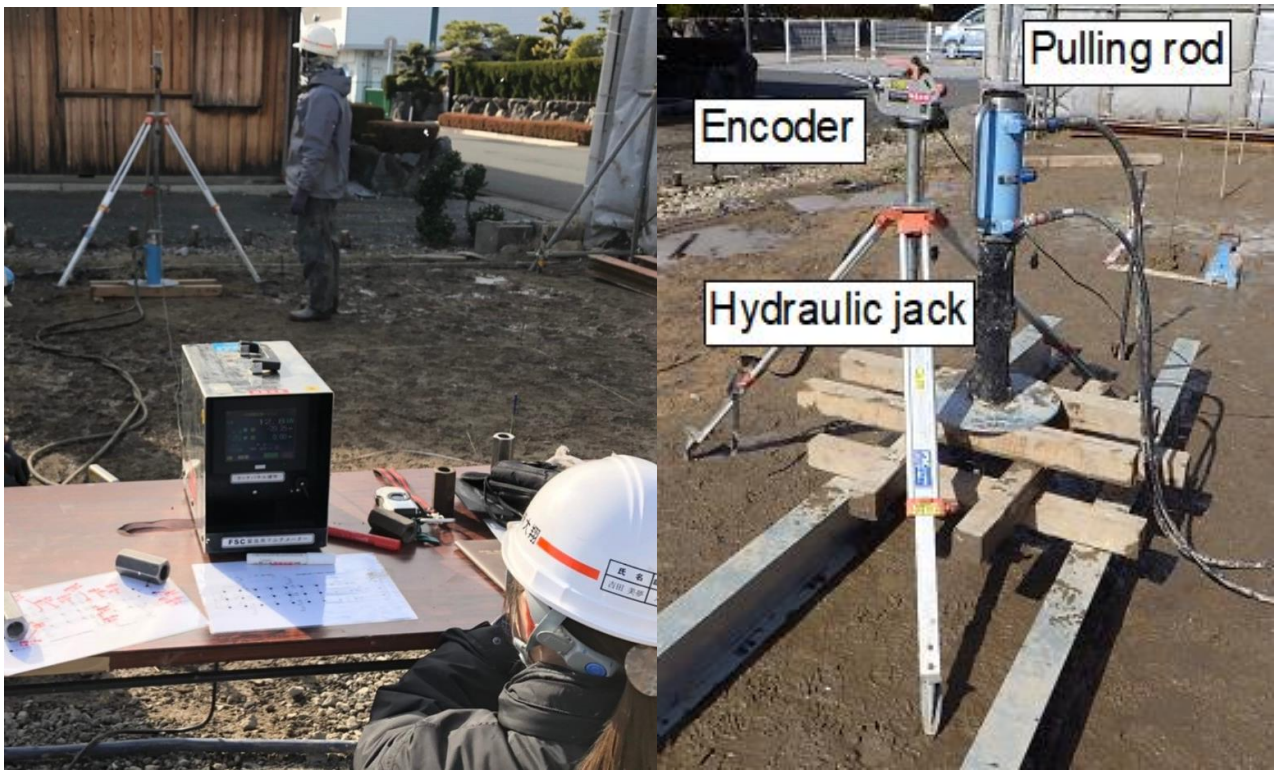

(b) Pull-out device of flip anchors

Fig. 3.60. Device for the full-scale pull-out experiments of actual flip anchors in the ground consisted of sand and clay layers.

3.4.3 Experimental results

Pull-out force F vs. pull-out displacement w

Figures 3.61-3.65 compare *F* vs. *w* of the anchors installed in the sand or the clay layer. The sand and the clay layers were separated at about a depth of 1.0 m (Figs. 3.56).

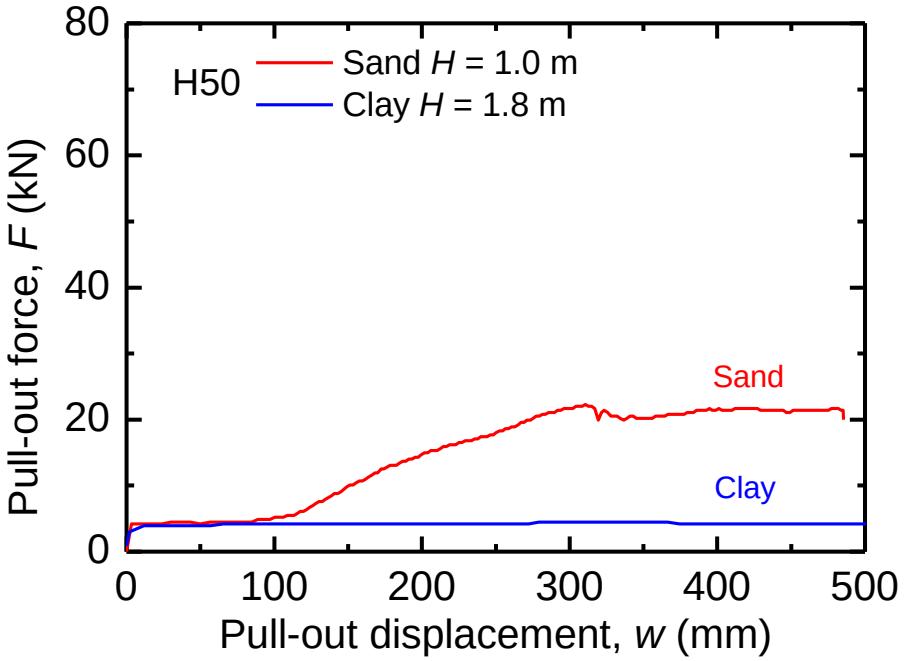

Fig. 3.61. *F* vs. *w* of H50 anchors installed in the sand or the clay layer.

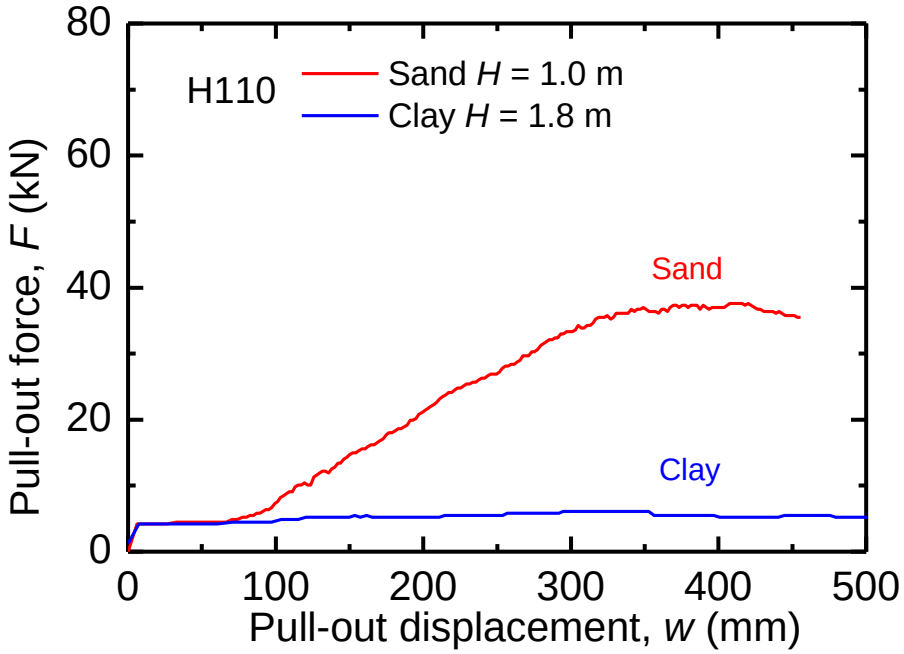

Fig. 3.62. *F* vs. *w* of H110 anchors installed in the sand or the clay layer.

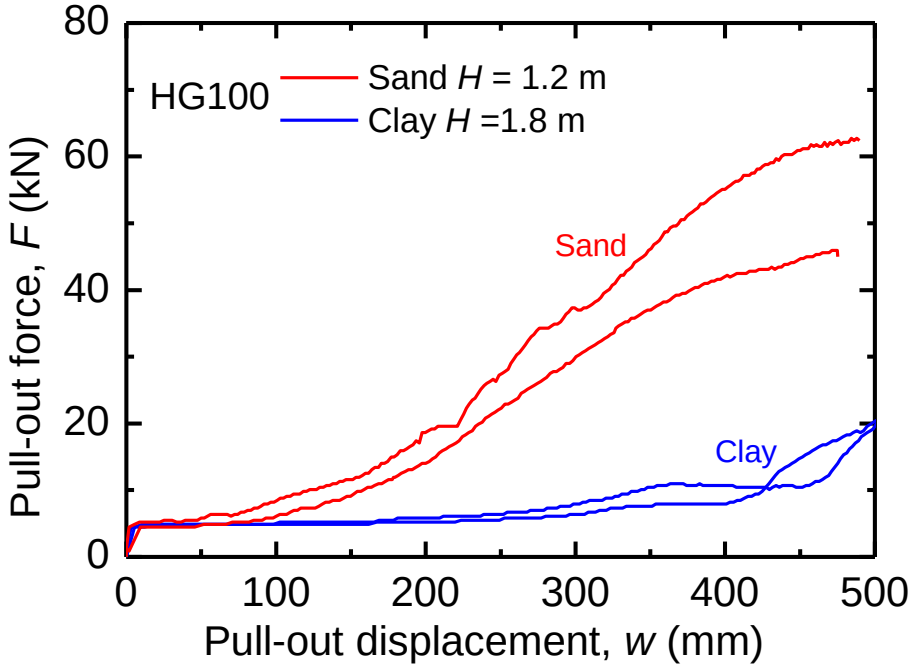

Fig. 3.63. *F* vs. *w* of HG100 anchors installed in the sand or the clay layer.

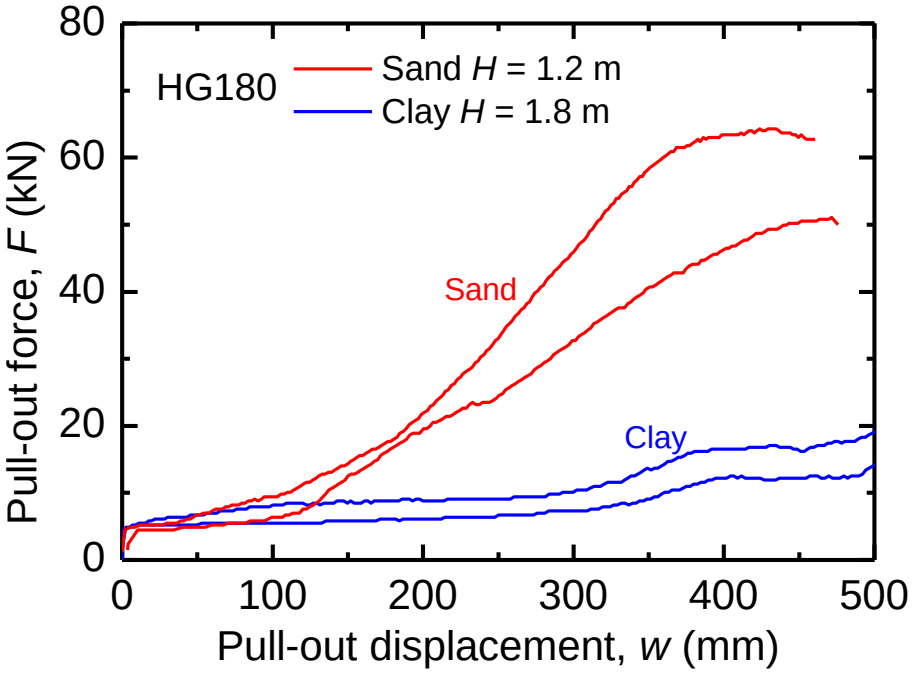

Fig. 3.64. *F* vs. *w* of HG180 anchors installed in the sand or the clay layer.

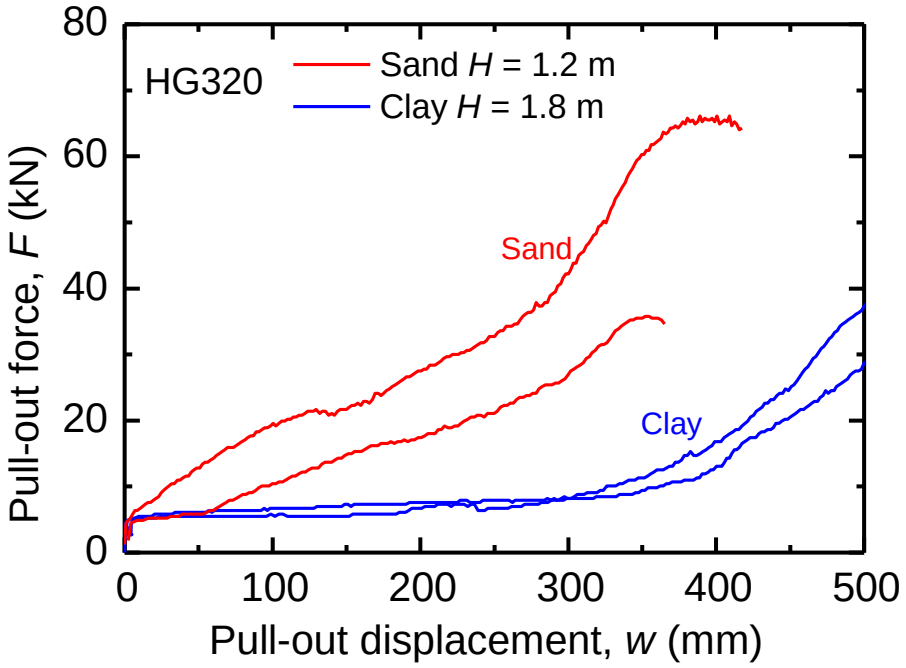

Fig. 3.65. *F* vs. *w* of HG320 anchors installed in the sand or the clay layer.

In the initial stages of pull-out, the behaviors of most of the anchors showed similar trends. For the anchors in the sand layer, except HG320, *F* was mobilized very quickly with a small *w* and then leveled off until *w* reached about 100 mm. *F* began to increase again after this plateau and attained F_{max} at *w* of 400-500 mm.

By comparing Figures 3.64 and 3.65, *F* of the 440 mm-long HG320 anchor began to increase at about 50% of *w* of the 340 mm-long HG180. Because the apex levels of HG anchors were equal at *H* = 1.2 m, 200 mm-section of the anchor head were embedded in the clay layer. That is, the section length of HG100 and HG180 in the sand layer was 140 mm, while that of HG320 was 240 mm at the start of the pull-out tests. Hence, it is reasonable that pull-out resistance of HG320 was promptly mobilized by smaller *w*, compared with that of HG180.

In the clay layer, the anchors maintained the plateau from the initial stage to *w* larger than 500 mm, as shown in Figs. 3.61 and 3.62 in which small-sized anchors were tested. As shown in Figures 3.63 and 3.64, HG100 and HG180 anchors (*L* = 340 mm) required *w* equal to *L* until *F* began to increase again, and reached their peak values in the clay layer at an additional Δw of around 100 mm. The anchors seemed to be fully opened at this stage.

As shown in Figs 3.61-3.65, the anchors in the sand layer had significantly greater *F* than the anchors in the clay layer. However, overburden pressures in the sand layer were smaller than those in the clay layer. Therefore, if the anchors are installed in the clay layer below the sand layer, the effects of the top sand layer could be ignored in design of pull-out resistance when the anchors do not reach the sand layer. In Stewart (1985), when buried at the same depth, pull-out resistance of plate anchors were greater when there was a sand layer above it. Pull-out resistance of plate anchors in layered soil was well investigated by Stewart (1985).

Figures 3.66-3.68 shows F vs. w of the flip anchors installed at H = 1.8 m in clay. The anchors were pulled out to the sand layer through the clay layer.

When the anchors were pulled in the clay layer, F was not affected much by the overlying sand layer until w = 400 mm. At around w = 400 mm, F seemed to begin to be affected by the overlying sand layer. F began to increase rapidly when the anchors reached the sand layer. In the sand layer, basically, the larger A was, the greater F was.

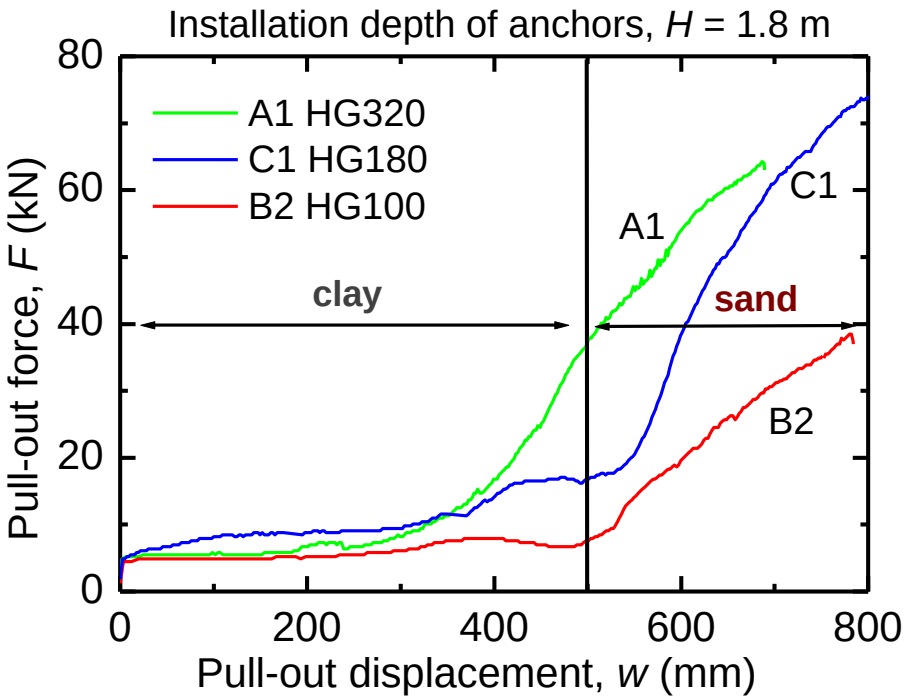

Fig. 3.66. F vs. w of HG anchors installed in the clay layer through the overlying sand layer.

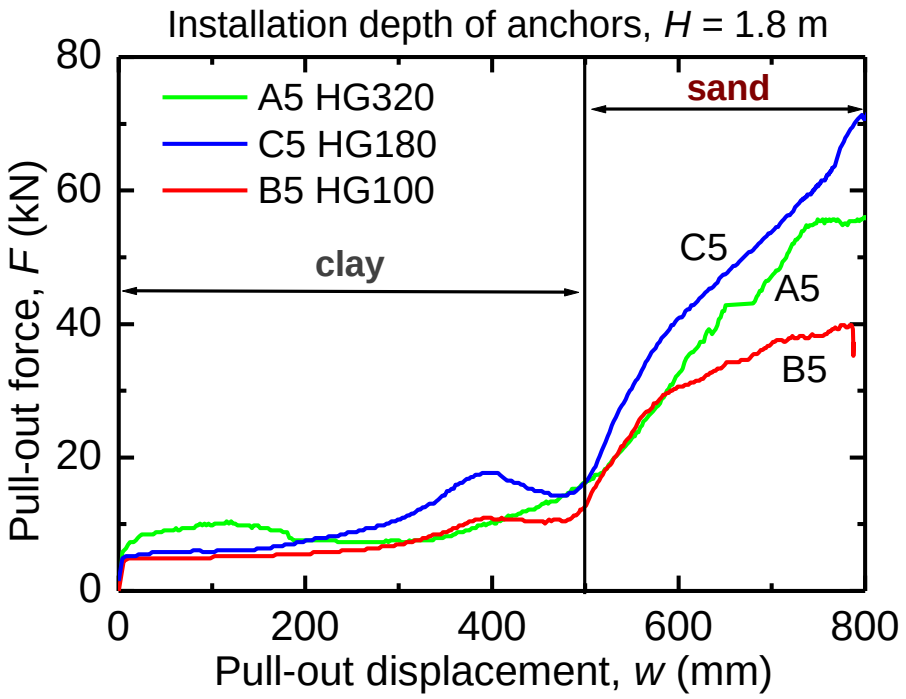

Fig. 3.67. F vs. w of HG anchors installed in the clay layer through the overlying sand layer.

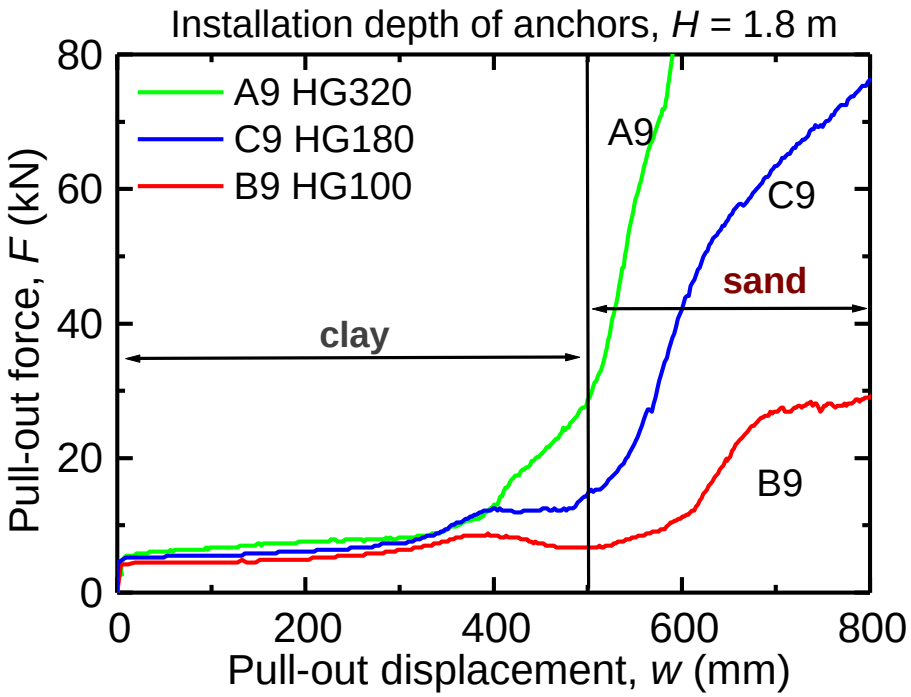

Fig. 3.68. *F* vs. *w* of HG anchors installed in the clay layer through the overlying sand layer.

Figures 3.69-3.71 shows the results above (Figs. 3.66-3.68) in terms of *p* vs. *w*. *p* of each anchor was almost constant while being pulled in the clay layer. *p* of HG320 (L = 440 mm) were the smallest among *p* of HG100 and HG180 (L = 340 mm) in the clay layer during w < 400 mm. It is because that L of HG320 is 1.3 times larger than L of HG100 and HG180, so HG320 requires at least w of 440 mm to open sufficiently. In this experiments, HG320 seemed to be affected by the overlying sand layer before completely opened. As a result, *p* of HG320 in the clay were relatively smaller than *p* of HG100 and HG180.

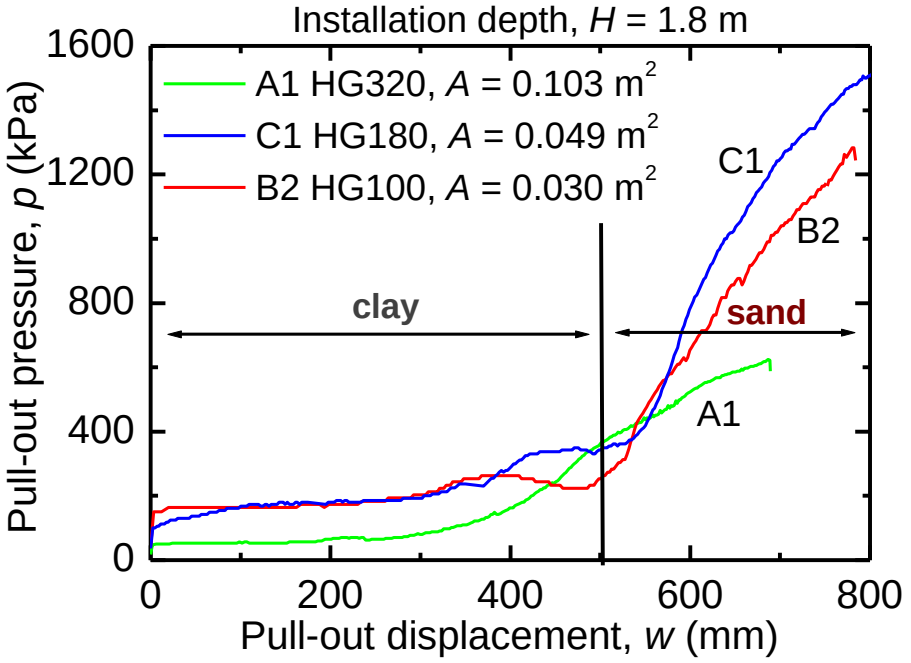

Fig. 3.69. *p* vs. *w* of HG anchors installed in the clay layer through the overlying sand layer.

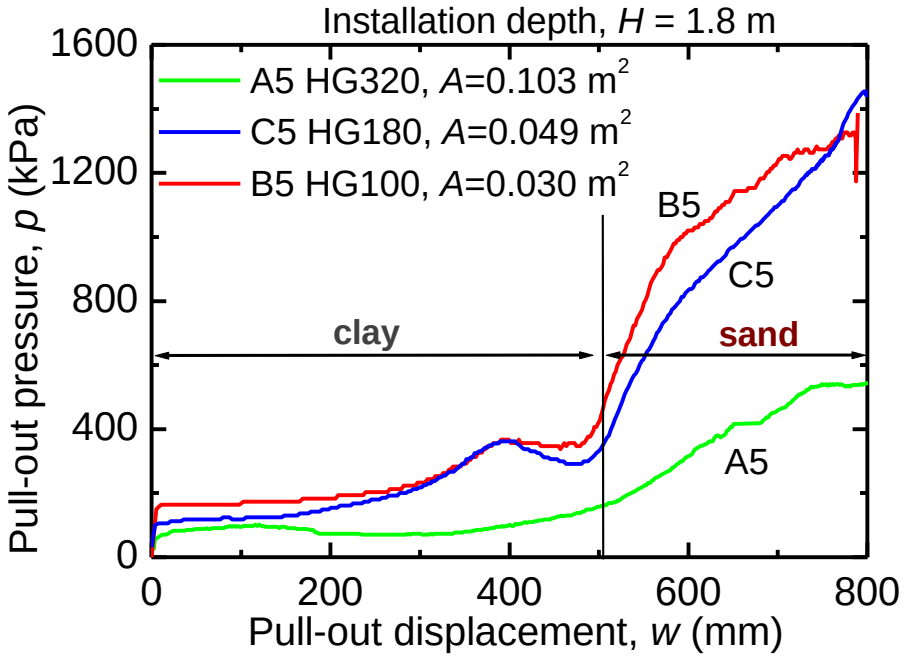

Fig. 3.70. *p* vs. *w* of HG anchors installed in the clay layer through the overlying sand layer.

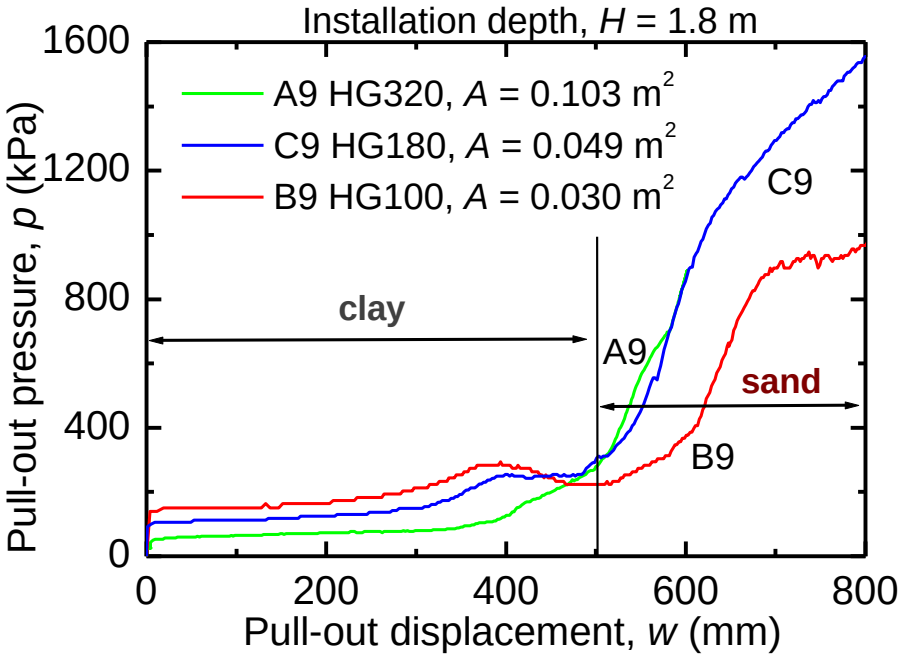

Fig. 3.71. *p* vs. *w* of HG anchors installed in the clay layer through the overlying sand layer.

Except for the case where there was an extreme difference in *F*, *p* became smaller with an increasing *A* in the sand layer, as in the above-mentioned experimental results. The tendency of *p* in the clay layer and the sand layer was clearly different. In clay, the values of *p* were almost equivalent regardless of *A*. Thus in the clay layer, *p* of sufficiently opened anchors should be equal regardless of *A*.

State of the anchors after pulled-up in the ground

Fig. 3.72 shows states of the flip anchors in the ground after pulled up for about (a) 650 mm and (b) 700 mm. Because w were much greater than L, the both anchors were completely opened in the ground.

(a) HG180 at A3, H = 1.2 m at w = 650 mm

(b) HG320 at A1, H = 1.8 m at w = 700 mm

Fig. 3.72. State of the flip anchors after pull-out experiments.

3.4.4 A calculation method of F_{max} of plate anchors in clay

Das (1980) presented a procedure for estimation of the ultimate uplift capacity of shallow and deep anchors in clay as Eq. (3.1).

$$Q_0 = BL(\beta F_c^* c_u + \gamma H) \tag{3.1}$$

where Q_0 is net ultimate capacity, B is a width of an anchor plate, L is a length of an anchor plate, $\beta = F_c/F_c^*$, F_c is breakout factor for a shallow anchor [$H/B < (H/B)_{cr}$], F_c^* is breakout factor for

a deep anchor [$H/B \geq (H/B)_{cr}$], c_u (kPa) is undrained shear strength of soil, γ is effective unit weight of soil, H is embedment depth of the anchor.

In this procedure, once c_u is given, critical embedment ratio $(H/B)_{cr}$ can be calculated using Eq. (3.2) or Eq. (3.3) for a square and circular anchor $(H/B)_{cr(S)}$, or a rectangular anchor $(H/B)_{cr(R)}$, respectively (Das, 1980).

$$(H/B)_{cr(S)} = 0.107c_u + 2.5 \leq 7 \tag{3.2}$$

$$(H/B)_{cr(R)} = (H/B)_{cr(S)} \{0.73 + 0.27\,(L/B)\} \tag{3.3}$$

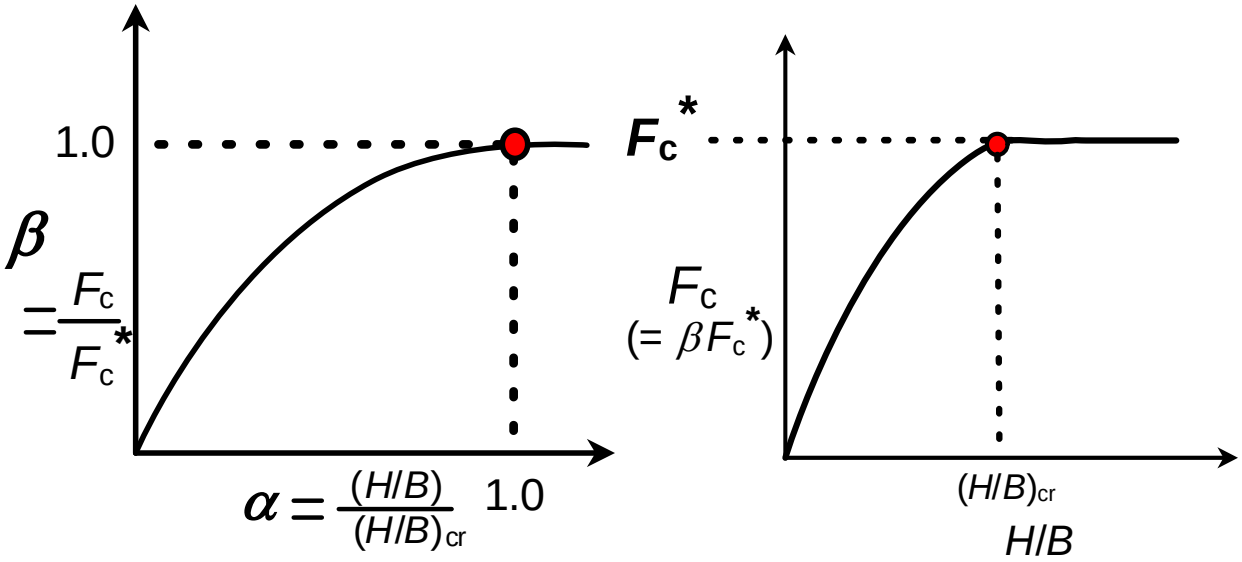

(a) (b)

Fig. 3.73. Plots of (a) α vs. β, and (b) F_c vs. H/B (Das, 1980).

Using the value of $(H/B)_{cr}$, α [= $(H/B)/(H/B)_{cr}$] can be estimated. Then, β can be estimated from the value of α (Fig. 3.73a). F_c increases with increasing H/B, then levels off at $(H/B)_{cr}$ as the maximum value (= F_c^*) (Fig. 3.73b). That is, β functions as a reduction coefficient for F_c^* for a shallow anchor.

Value of F_c^* is usually considered as F_c^* for a square or circular anchor (= $F_{c(S)}^* \simeq 9$).

For a rectangular anchor, $F_{c(R)}^*$ is estimated by Eq. (3.4) reflecting shape factor s (Das 1978).

$$F_{c(R)}^* = F_{c(S)}^* s \tag{3.4}$$

where $F_{c(R)}^*$ is breakout factor of a rectangular deep anchor, $F_{c(S)}^*$ is breakout factor of a square deep anchor, and s is shape factor of an anchor [$s = 0.84 + 0.16\,(B/L)$].

When all the parameters are determined according to these procedures, Q_0 can be finally calculated using Eq. (3.1).

3.4.5 A calculation method of F_{max} of flip anchors in clay

In a field, c_u of the ground usually is not uniform, and $(H/B)_{cr}$ and F_c^* vary with c_u. And because the shape of flip anchors are neither square nor rectangular, s and $F_{c\,(R\ or\ S)}^*$ cannot be directly applied to flip anchors. Moreover, as a certain amount of w is necessary for flip anchors to attain F_{max}, $(H/B)/(H/B)_{cr}$ for flip anchor cannot be estimated accurately. Thus, an alternative procedure was proposed for estimating F_{max} of flip anchors installed in clay ground.

As an estimation method of F_{max} of flip anchors in clay, an interpretation method for T-bar penetration test is invoked. It is because pulling a flip anchor throughout clay is just reverse way of pushing T-bar into the clay. In the T-bar test, c_u value is estimated using Eq. (3.5) (Almeida et al. 2013) with the measured value of p on the T-bar:

$$c_u = p/N_b \tag{3.5}$$

where N_b is the bearing factor of T-bar. N_b depends on the surface roughness of the bar, varying between 9.1 and 11.9 (Almeida et al., 2013). An average value of $N_b = 10.5$ is recommended for a deep penetration condition (Randolph, 2004). N_b of 12 is suggested in Low et al. (2010).

In this field experiment, the range of c_u of the clay was measured by vane shear tests, as mentioned earlier. Even when estimating c_u from soil tests other than the T-bar test, it is assumed that the pressure of the anchor p can be estimated using Eq. (3.6):

$$p = N_b\, c_u \tag{3.6}$$

Figures 3.74-3.76 show measured p vs. calculated p from Eq. (3.6). It is seen that the range of the calculated p reasonably agreed with the measured p.

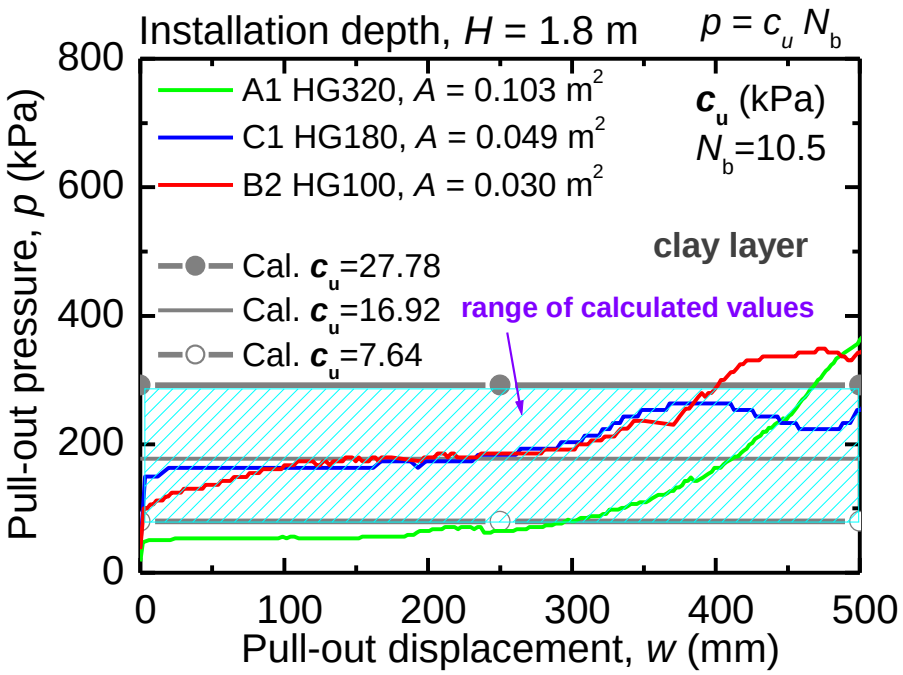

Fig. 3.74. Calculated p vs. measured p in clay.

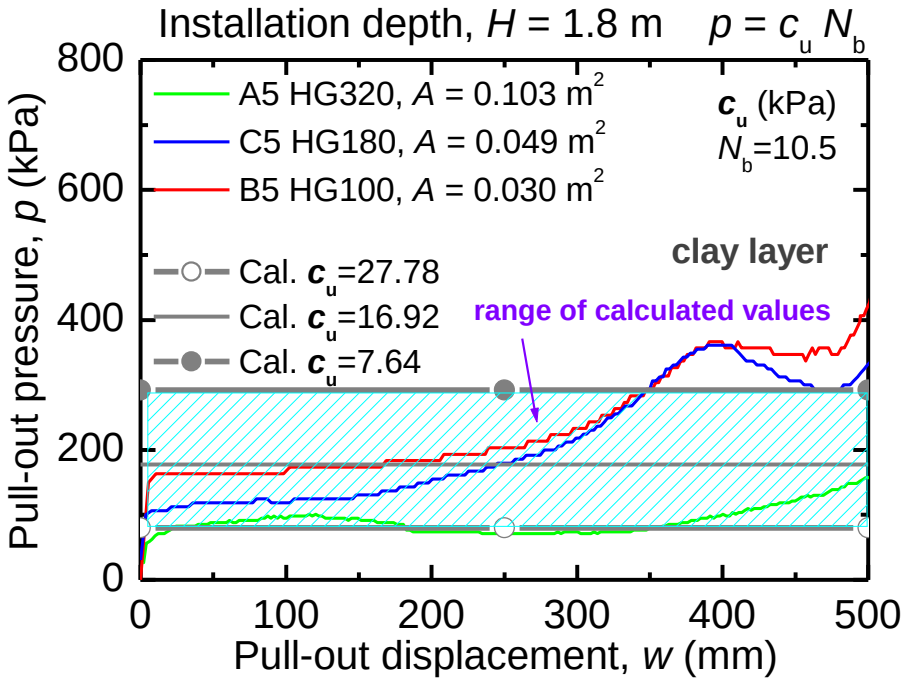

Fig. 3.75. Calculated p vs. measured p in clay.

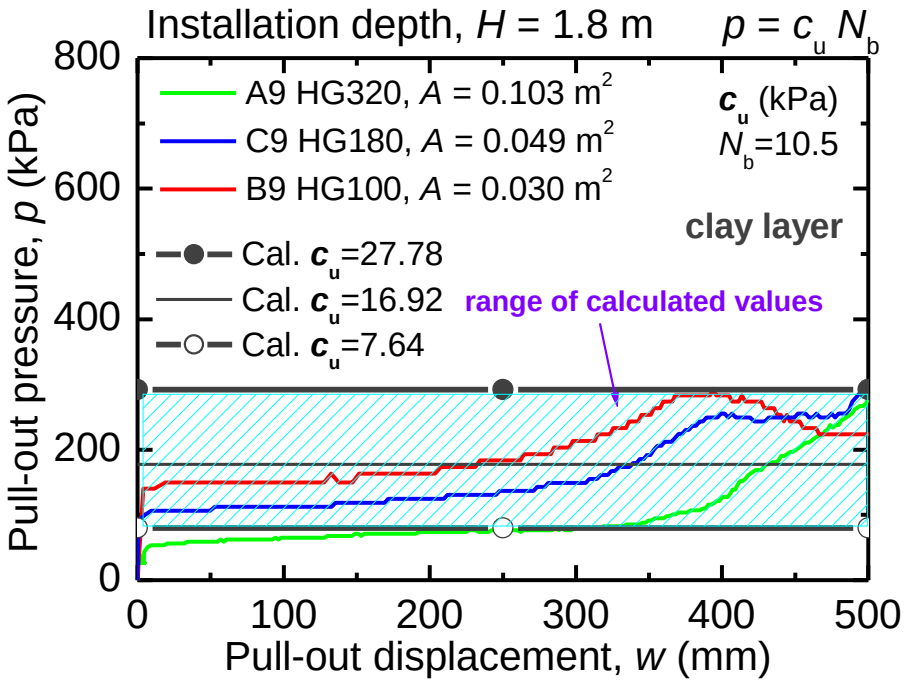

Fig. 3.76. Calculated p vs. measured p in clay.

When performing the T-bar penetration test on site, p from the T-bar test can be directly used in Eq. (3.7) to estimate pull-out resistance of a flip anchor.

$$F = pA \tag{3.7}$$

Currently, the T-bar penetration test is rarely used for site investigations in Japan. In practice, c_u are empirically estimated from SPT-N values, VSTs, pressure-meter test, or unconfined compression test. If c_u is obtained, p on the anchor can be estimated using Eq. (3.6).

3.4.6 Discussion of Section 3.4

In this section, to investigate the behavior and pull-out resistance of flip anchors in clay, the field pull-out experiments of flip anchors were conducted in the ground where a top sand layer covered a clay layer.

Main findings from the experiments are summarized as:

1) Pull-out behavior of flip anchors in clay was quite different from that in sand.
2) As for the anchors pulled out in clay, F was not as strongly affected by the overburden pressure as the anchors installed in sand.
3) In clay, F_{max} is proportional to A. In other words, p acting on the anchor head was constant regardless of A.
4) The predicted p range estimated from c_u from the VSTs and bearing factor of T-bar N_b of 10.5 agreed well with the measured p range.
5) The estimation method based on the interpretation of T-bar penetration test can be a promising way to estimate pull-out resistance of flip anchors in clay ground.

3.5 Conclusions of Chapter 3

In sand

The main findings on the behavior and pull-out resistance F_{max} of flip anchors in sand are the below.

1) F_{max} of flip anchors increased as A or H increased.
2) F_{max} of Driven anchors were equivalent to F_{max} of Closed anchors.
3) F_{max} of flip (Driven) anchors can reach at least about 80% of F_{max} of horizontal pre-embedded plate anchors (Opened anchors).
4) Pull-out resistance did not soften immediately in any installation condition when H/L is 5 or more.
5) The area of the ground surface greater than A was influenced by pull-out of the anchor.
6) The larger A was, the larger F_{max} was; whereas the smaller A was, the larger p_{max} (= F_{max}/A) was in any condition.
7) w required for a flip anchor to open sufficiently is the same as L or about 1.5 times L

In clay

Pull-out behavior of flip anchors in clay is quite different from that in sand. In clay, F_{max} is proportional to A because p acting on the anchor head is equal regardless of A. In clay, the overburden pressure does not directly affect the pull-out resistance as in the sand; however a flip anchor should

be installed deeper than $(H/L)_{cr}$ to apply the maximum value of breakout factor N_b = 10.5. c_u tends to be larger at deeper points in the ground, so it is desirable to install the anchors deeper in consideration of the balance with workability. The estimation method invoked form the interpretation of T-bar penetration test can be a promising way to estimate F_{max} of flip anchors in clay. In that case, H/L should be based on Fig. 3.77 as that in sand, considering w required for a flip anchor to open sufficiently.

Premise for the calculation of pull-out resistance

Because F_{max} of Driven anchors are equivalent to F_{max} of Opened anchors, F_{max} of flip anchors can be designed based on F_{max} of pre-embedded plate anchors. Pull-out displacement w can be the same amount as L or about 1.5 times L from the results of the experiments. Thus as in Fig. 3.77, H at least from a tail of a flip anchor to the ground surface should be regarded as equivalent H for plate (Opened) anchor at the same H.

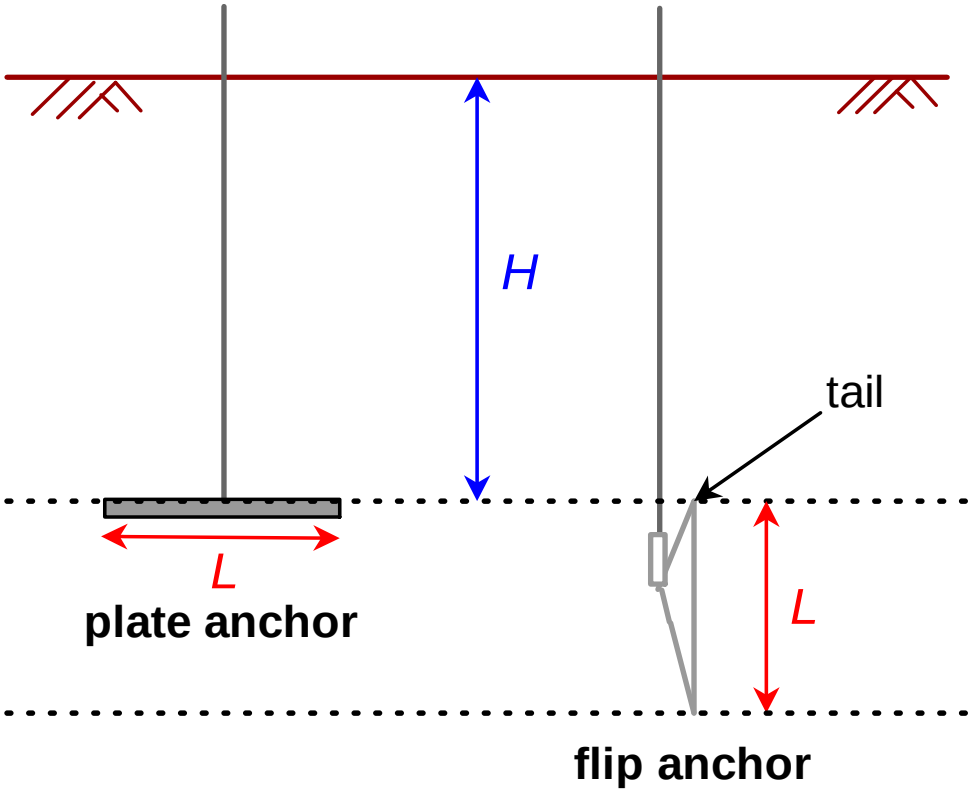

Fig. 3.77. H for flip anchors when estimating F_{max} compared with plate anchors.

As previously studied in many research, pull-out resistance of a plate anchor in sand largely depends on the shape of the ground failure pattern by the pulling of the anchor. The same would be applied to flip anchors because similar trends of deformation of the ground surface was observed during the pull-out experiments. The reason why p_{max} (= F_{max}/A) increases as A decreases should be due to the ground failure pattern.

Thus, in the next Chapter 4, ground failure pattern was observed in a plane strain condition.

References in Chapter 3

Almeida M.S.S., Oliveira J.R.M.S., Rammah K.I., and Trejo P.C. (2013). Investigation of bearing capacity factor of T-bar penetrometer at shallow depths in clayey soils. Journal of Geo Engineering Sciences, 1, pp. 1-12.

Baker W. H., and Kondner R. L. (1966). Pullout load capacity of a circular earth anchor buried in sand. Highway Research Record, 108, pp. 1-10.

Das B.M. (1978). Model tests for uplift capacity of foundations in clay. Soils and Foundations, 18(2), pp. 17-24.

Das B.M. (1980). A procedure for estimation of ultimate uplift capacity of foundations in clay. Soils and Foundations, 20(1), pp.77-82.

Emirler B., Tolun M., and Laman M. (2016). Experimental investigation of the uplift capacity of group anchor plates embedded in sand. Geomechanics and Engineering, 11(5), pp. 691-711.

Low H. E., Lunne T., Andersen K.H., Sjursen M.A., Li X., and Randolph M. F. (2010). Estimation of intact and remoulded undrained shear strengths from penetration tests in soft clays. Géotechnique, 60(11), pp. 843-859.

Niroumand H., and Kassim K. A. (2013). Pullout capacity of irregular shape anchor in sand. Measurement, 46(10), pp. 3876-3882.

Randolph M. (2004). Characterisation of soft sediments for offshore applications. Proc. Geotechnical and Geophysical Site Characterization, Millpress, Rotterdam, pp. 209-232.

Stewart W. (1985). Uplift capacity of circular plate anchors in layered soil. Canadian Geotechnical Journal. 22(4), pp. 589-592.

Chapter 4
Experimental studies on the pull-out resistance of flip-type earth anchor using the model anchors

4.1 Introduction

In the pull-out experiments using the actual flip anchors in Chapter 3, not only the pull-out resistance of flip anchors in sand or clay, the differences on the development of pull-out resistance of flip anchors and plate anchors were investigated. The pull-out resistance of flip and plate anchors in sand largely depends on the shape of the ground failure pattern when the anchor is pulled. In the pull-out experiments using actual anchors, the deformed area of the ground surface when pulling the flip anchor was larger than *A*. That causes a flip or plate anchor with smaller *A* has larger p_{max} than a larger anchor does.

Thus in this chapter, the ground failure pattern was observed during pull-out experiments in a plane strain condition. Pull-out experiments using model plate or model flip anchors in a plane strain condition were conducted. Firstly, push-up experiments of a model horizontal plate anchor (trap door) were conducted (Section 4.2). Subsequently, vertical and diagonal pull-out experiments of model flip anchors were conducted (Section 4.3). In both experiments, the soil box was made of transparent acrylic plates, so that the ground failure patterns could be observed well.

In the pull-out experiment, the mechanism of a flip anchor that rotates and opens in the ground was simulated by embedding a rotable model flip anchor in the "Closed" state in the ground. Furthermore, by embedding the anchors under “Opened” condition, which is equivalent condition to a horizontal plate anchor, those results of the Closed anchor as a model flip anchor were able to be compared with the performance of general plate anchors.

Based on the results of the experiments, the ground failure pattern for flip anchors in sandy ground was simply modeled. Based on the 2D model, an estimation method of pull-out resistance of flip anchors was proposed. The 2D model was verified by comparing the calculated values based on the model with the measured values of the experiments in this chapter.

4.2 Push-up experiments of a trap door simulating a plate anchor in a model sand ground

4.2.1 Introduction

Before investigating on flip anchors, to investigate pull-out resistance and ground failure patterns of horizontal plate (Opened) anchors in detail, push-up experiments of a trap door simulating a horizontal plate anchor were conducted.

4.2.2 Outline of the experiments

Figure. 4.1 shows an experimental setup for push-up experiments of a trap door (horizontal plate anchor). A model box (length 800 mm, height 500 mm, width 98 mm) is made of transparent acrylic plates. The transparent soil box makes particle image velocimetry (PIV) analysis possible to observe the ground failure pattern. Photos were taken from the front side of the box at an interval of 2 seconds to observe the behavior of the sand particles. The photos were processed using a software named Trackpy (Trackpy Contributors, 2019) to obtain the traces of the soil particles during the push-up experiments.

A model horizontal plate anchor (length 80 mm, made of Teflon) was set on the bottom of the model box. The model anchor lifted 50 mm of the ground with a loading jack. This experiment was referred to Tanaka and Sakai, 1987.

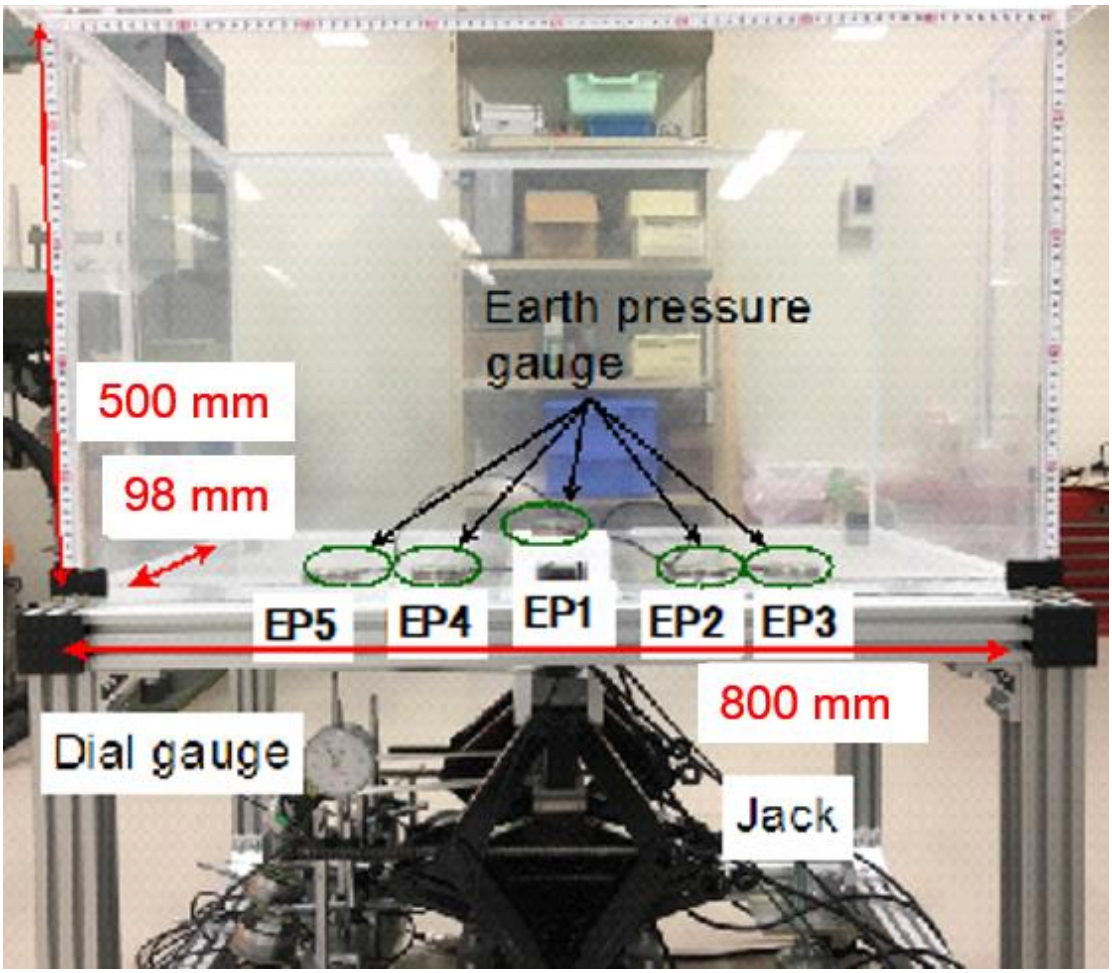

Fig. 4.1. A setup for push-up experiment of a model plate anchor (trap door).

Push-up force and push-up displacement in this experiments are synonymous with pull-out force F and pull-out displacement w. F and w were measured by a load cell and a dial gauge respectively. The trap door was pushed up at a rate of about 0.1 mm/s. Sampling frequency of the data was 2 Hz.

The model ground was made of dry silica sand #3. The physical properties of the silica sand are listed in Table 4.1. The model ground consisted of 50 mm layers. Firstly, the silica sand of 50 mm height was put in the soil box. Then, the sand layer was tapped to adjust the ground to a predetermined dry density of ρ_d = 1.512 g/cm^3 (relative density D_r = 80%).

Table 4.1. Physical and mechanical properties of the silica sand #3.

Density of soil particles, ρ_s (g/cm^3)	2.632
Max. dry density, ρ_{dmax} (g/cm^3)	1.567
Min. dry density, ρ_{dmin} (g/cm^3)	1.325
Max. void ratio, e_{max}	0.987
Min. void ratio, e_{min}	0.679
Int. friction angle at peak strength, ϕ_p (deg)	42
Int. friction angle at residual strength, ϕ_r (deg)	35

A total of four cases of the experiments were conducted with different H of 200, 300, 400, and 450 mm (Fig. 4.2). Fig. 4.3 is an example of the model ground with H of 200 mm.

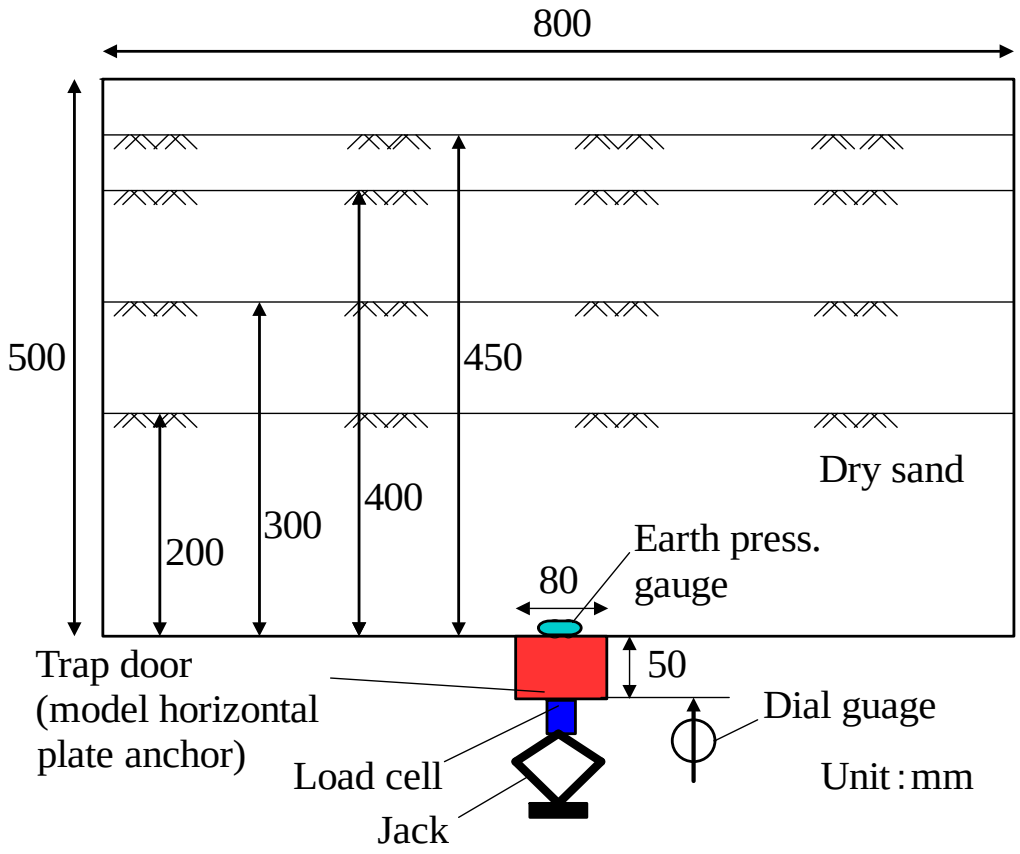

Fig. 4.2. A diagram of a setup for push-up experiment of the model plate anchor (trap door).

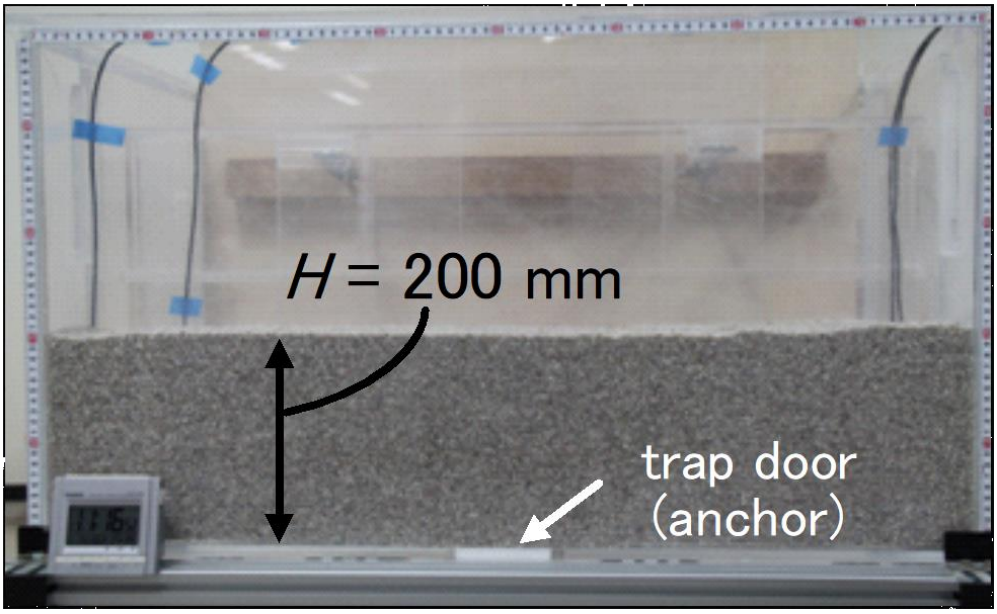

Fig. 4.3. An example of the model ground in a transparent soil box (H = 200 mm).

4.2.3 Results of the experiments

Fig. 4.4 shows the relationship between push-up force F acting on the trap door and push-up displacement w. F increased as the depth of the anchor H increased. It is interesting that w at maximum push-up force F_{max} increased as H increased.

Fig. 4.5 shows F_{max} vs. H. F_{max} increased exponentially as H increased.

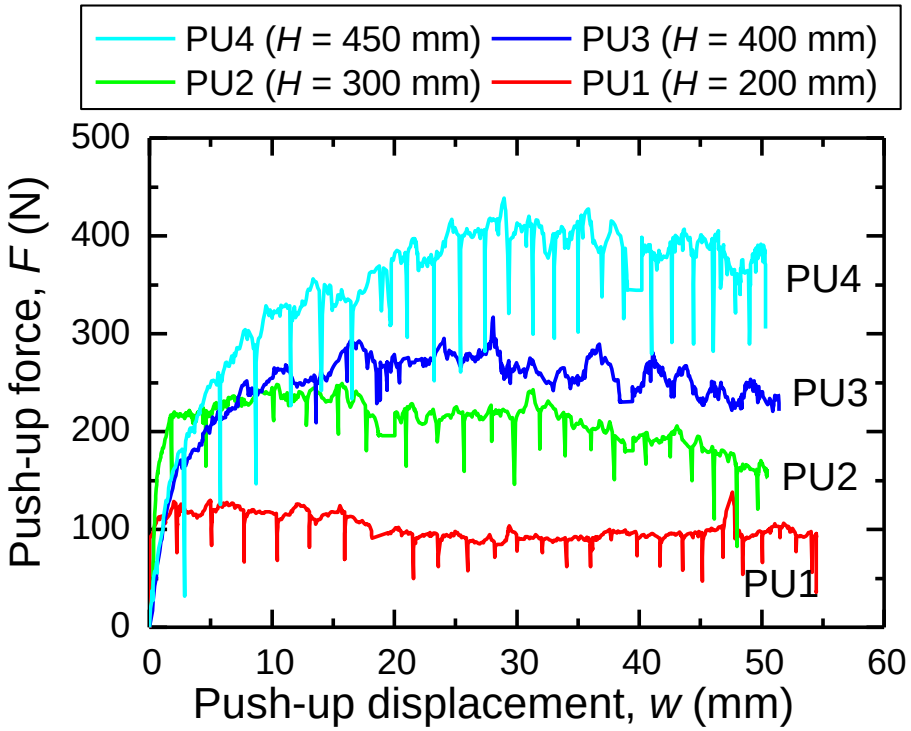

Fig. 4.4. Relationship between F and w.

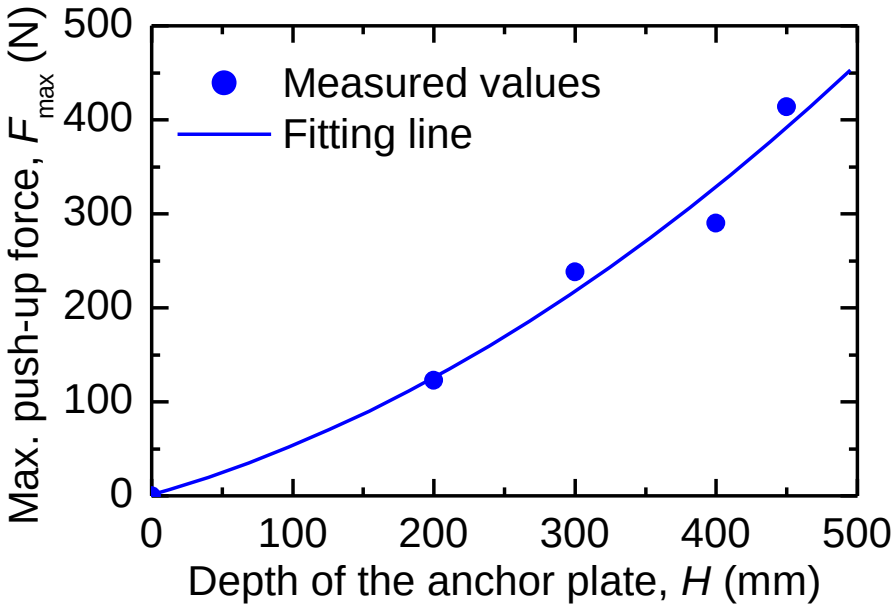

Fig. 4.5. Relationship between F_{max} and H.

4.2.4 Modelling of ground failure

Fig. 4.6 shows the traces of the soil particles obtained in all the experiments until the anchor (trap door) was pushed up for 50 mm. The clear distinct movements of the soil particles can be found, so that the slip (failure) lines were identified visually. Large amounts of the movements of the soil particles are detected inside the slip lines, while almost no movements of the soil particles are found outside the slip lines. The slip line extended from both edges of the anchor to the ground surface in an arc shape. The angles between the slip lines at the edge of the anchor from the vertical direction θ were around 20 degrees in all the cases regardless of H.

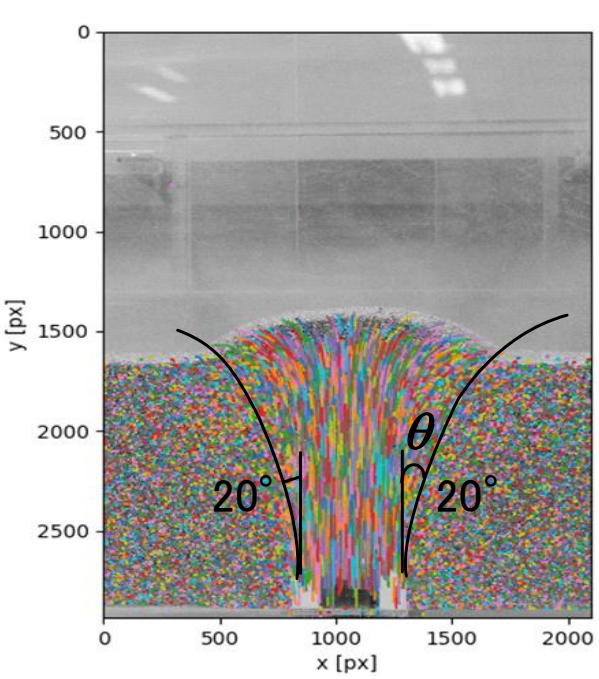

(a) H = 200 mm

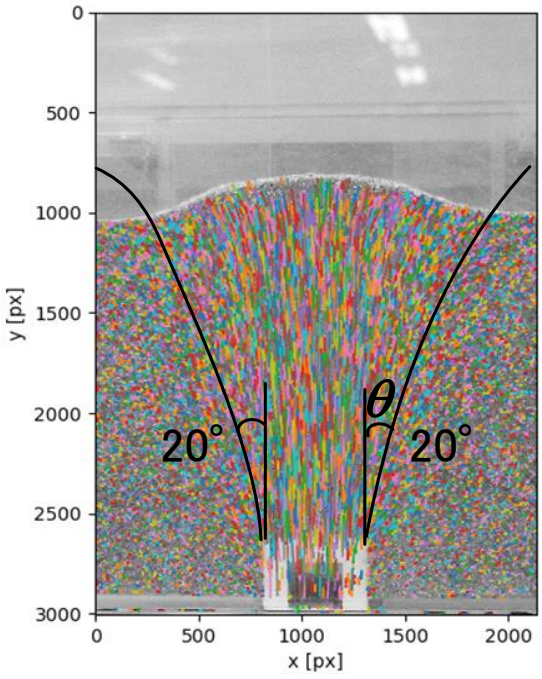

(b) H = 300 mm

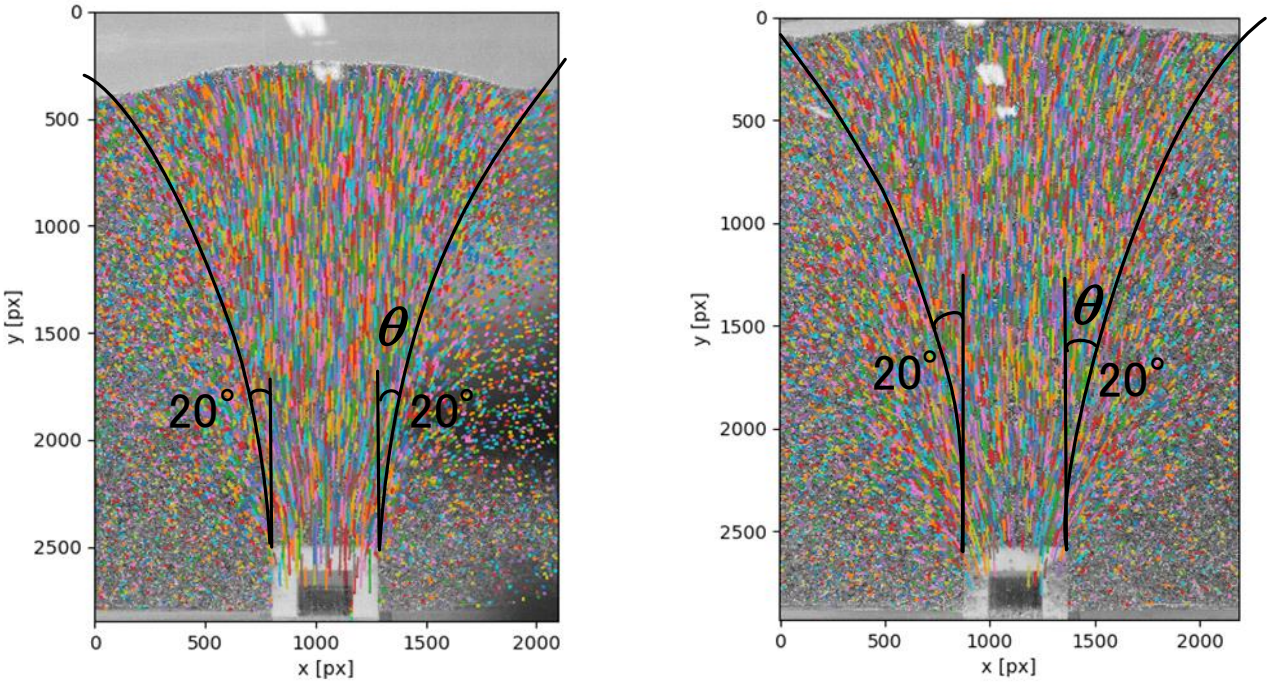

(c) H = 400 mm (d) H = 450 mm

Fig. 4.6. Ground failure pattern observed by image analysis.

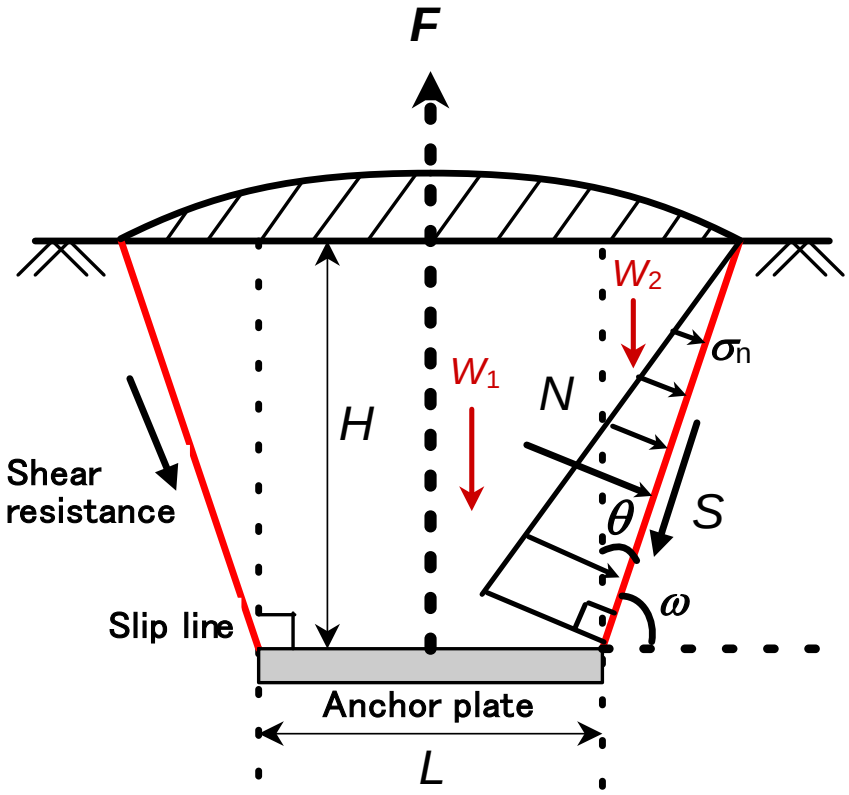

Fig. 4.7. A simplified 2D ground failure model caused by pull-out of a flip anchor.

As shown in Fig. 4.7, a failure pattern of the ground was simply modelled from the ground behavior obtained by the image analysis; where H is an embedment depth of an anchor, γ is a unit weight of the soil, W_1 is a weight of the rectangular soil mass, $W_1 = L/2 \times H \times B \times \gamma$, W_2 is a weight of the triangular soil mass, $W_2 = H \times H \tan\theta \times 1/2 \times B \times \gamma$, L is a length of an anchor plate, B is a breadth of an anchor, θ is an angle of slip line from a vertical direction, N is normal force acting on a failure plane, S is shear resistance acting along failure plane ($S = N \tan\phi$), f is pull-out resistance acting on the half of anchor ($f = W_1 + W_2 + S \cos\theta$), σ_n is effective vertical stress on a failure plane $[(1 + K_0)(\sigma_v / 2) + (1 - K_0)(\sigma_v / 2) \cos 2\omega]$, σ_v is effective earth pressure, K_0 is coefficient of lateral earth pressure at rest.

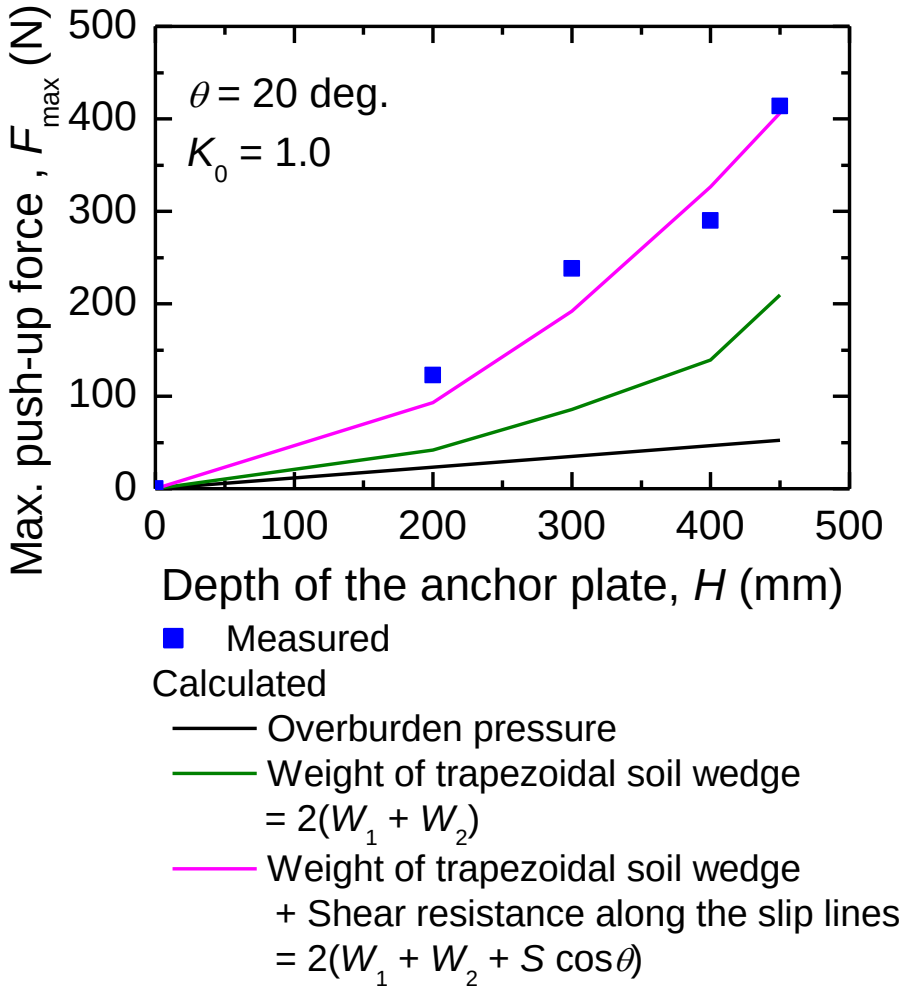

Fig. 4.8. Calculated F_{max} vs. Measured F_{max} based on the 2D ground failure model.

Fig. 4.8 shows comparisons of calculated F_{max} vs. measured F_{max}. Considering the ground was made by tapping, the value of K_0 was set to 1.0 for the calculation. The measured F_{max} are square plots (■). The black line is the calculated F_{max} from the dead weight of the rectangular soil only above the anchor (= $2W_1$). The green line is the calculated F_{max} from the dead weight of the inverted trapezoidal soil wedge above the anchor [= $2(W_1 + W_2)$]. The purple line is the calculated F_{max} from the sum of the dead weight of the inverted trapezoidal soil wedge above the anchor and the vertical components of the shear resistance along the slip lines [= $2(W_1 + W_2 + S \cos\theta)$]. Fig. 4.8 shows that the calculated values (purple line) agree with the experimental values (■) qualitatively and quantitatively.

4.2.5 Discussion of Section 4.2

Push-up experiments of a model horizontal plate anchor were conducted to investigate pull-out resistance and ground failure patterns of plate anchors in a plane strain condition. Based on the observations of the ground failure, the 2D ground failure pattern of a horizontal plate anchor was simply modelled. The model is an inverted trapezoidal soil wedge above the anchor with θ was about 20 degrees (= ϕ/2). Pull-out resistance of horizontal plate anchors were calculated by the calculation method based on the 2D model.

Considering the weight of the soil wedge and vertical component of shear resistance of the slip lines, calculated F_{max} based on the model were agreed well with the measured values.

Some models consider only the weight of the soil were proposed in previous studies, such as Mors (1959); however, as shown in Fig. 4.8, the vertical component of the shear resistance on the slip lines need to be taken into consideration in the calculation. This failure mechanism of the ground explains why a smaller anchor has larger p_{max} than a larger anchor.

The authors are aware that the push-up experiments using the trap door do not perfectly reproduce behaviors of the pull-out of a horizontal plate anchor because soil particles were not allowed to move into a cavity under the anchor. Thus, pull-out experiments of model flip anchors were conducted subsequently.

4.3 Vertical and diagonal pull-out experiments of model flip-type earth anchors embedded in a model sand ground in a plane-strain condition

4.3.1 Introduction

In the push-up experiments of a horizontal model plate anchor, the inverted trapezoidal-shaped ground failure pattern was observed. Subsequently in this section, vertical and diagonal pull-out experiments using model flip anchors in a plane-strain condition were conducted to investigate the same for flip anchors. Similar to the experiments in Chapter 3, “Opened” or “Closed” embedment conditions were prepared for model flip anchors.

The failure shape of the ground caused by a model flip anchor was compared whether it is similar to that of a plate anchor (Section 4.2). Furthermore, by pulling the flip anchors vertically or diagonally, the differences in the pull-out resistance or ground failure pattern depending on the pull-out direction or plate angles were also examined.

4.3.2 Outline of the experiments

A transparent acrylic box with a length of 800 mm, a height of 500 mm and a width of 98 mm was used for a model ground (Fig. 4.9). It is the same box used in the experiment using a trap door. Dry silica sand #3 was used for the model ground. Physical properties of the sand are listed in Table 4.1 in Section 4.2. The model ground was prepared in 10 layers of 50 mm thick. Relative density D_r of the model ground was adjusted to be about 80% (dry density ρ_d = 1.512 ton/m^3) by tapping each layer. Internal friction angle ϕ = 42° was obtained from direct shear tests of the sand with D_r = 80%.

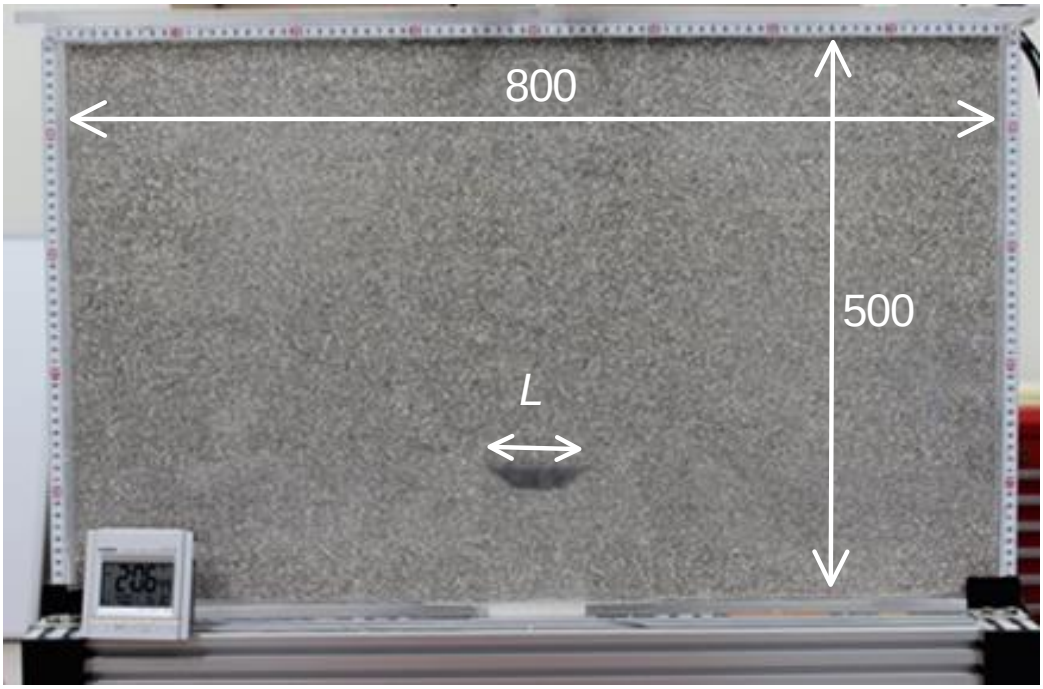

Fig. 4.9. A model ground in a transparent soil box for vertical or diagonal pull-out experiments.

Model flip anchors used for the experiment is shown in Fig. 4.10. A steel plate having a length *L* of 48 or 80 mm, a width *B* of 97 mm and a thickness of 5 mm. For pulling the anchor, wire ropes are attached to eye bolts on the anchor. The wires can move on the ring of the eye bolt freely, so that the anchor can rotate to open as a flip anchor when being pulled.

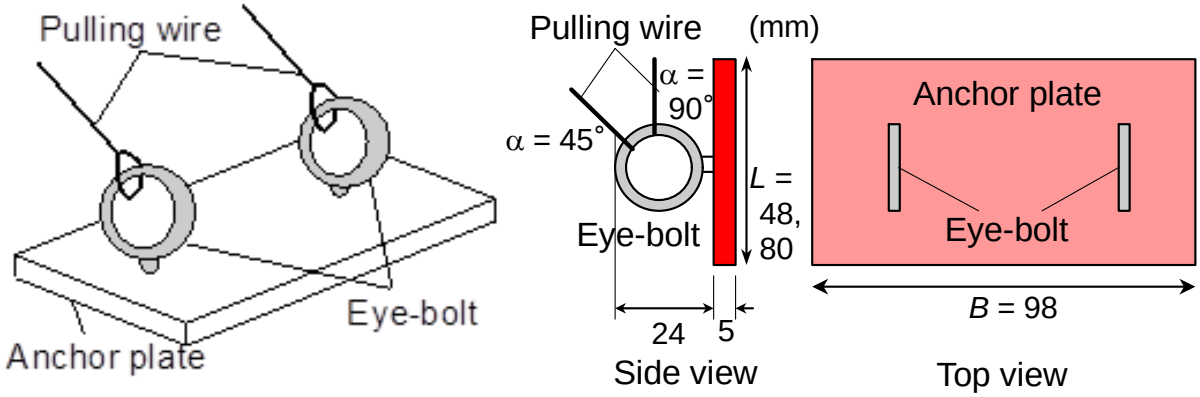

Fig. 4.10. Dimensions of model flip anchors (*L* = 48 or 80 mm).

Figure 4.11 shows a set-up for the pull-out experiments. The model flip anchor with pulling wires was embedded at a given embedment depth *H* during the preparation of the ground. A winch for pulling the wires was set on a loading frame. A load cell (LC) for measuring pull-out force *F* was set between a winch and the pulling wires. Pull-out displacement *w* was measured with an encoder (ENC). Five earth pressure gages (EP) were attached to a side wall of the box to measure lateral earth pressures.

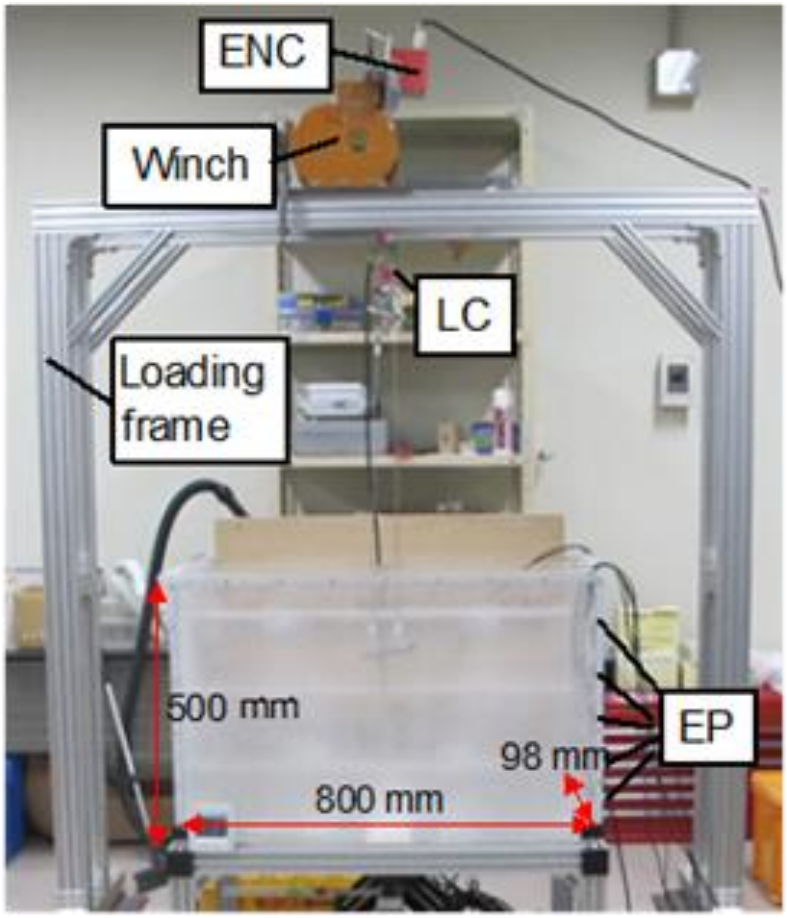

Fig. 4.11. A setup for vertical or diagonal pull-out experiments of the model flip anchors.

To observe the ground during the pull-out experiments, PIV analysis was conducted in the same manner as Section 4.2.4.

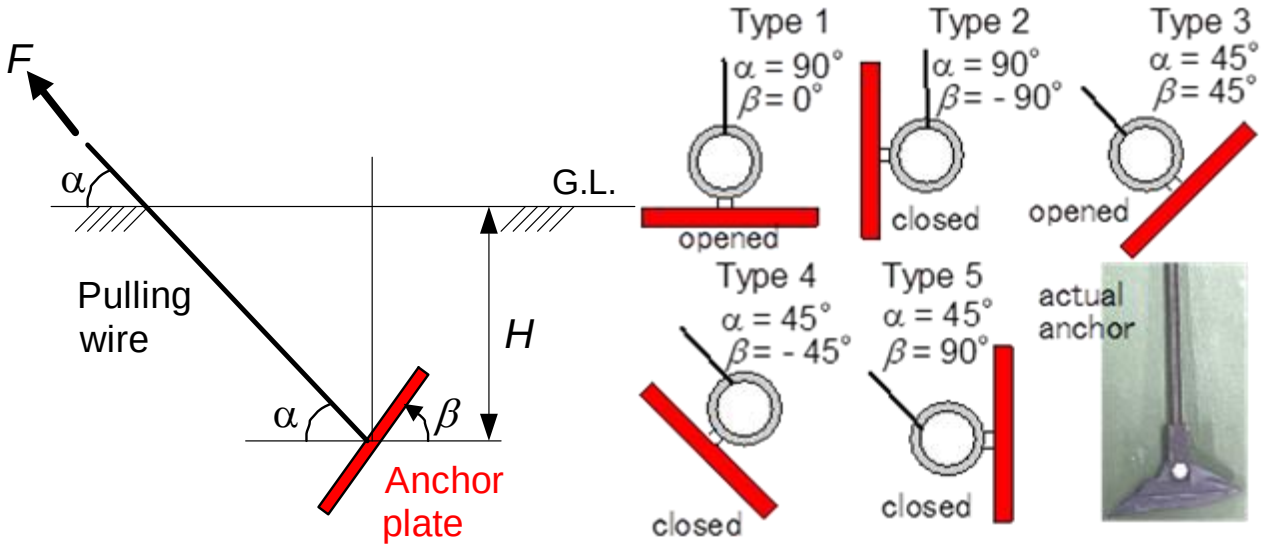

Fig. 4.12. Experimental conditions of vertical or diagonal pull-out experiments of model flip anchors.

Figs. 4.12 shows variety of conditions of pull-out experiments. H was varied as 100, 200, 300 and 400 mm, and L was 48 or 80 mm. Pull-out angles α was set at 45 or 90 degrees. Under a condition of $\alpha = 90°$, the anchor was pulled out vertically, and at $\alpha = 45°$, the anchor was pulled out diagonally.

Some diagonal or horizontal pull-out experiments of plate anchors were previously conducted by, such as Harvey and Burley (1973), Das and Seeley (1975), Ghaly and Clemence (1998), Hannna et al. (2015), and Yue et al. (2020). β is an angle of the embedded anchor plate. There were five types of pull-out conditions with different combinations of α and β, as shown in Figs. 4.12. The conditions can be broadly divided into vertical or diagonal pull-out, and Opened or Closed conditions of the anchor plate to the pull-out direction.

Table 4.2 lists all the cases of pull-out experiments.

Table 4.2. Experimental cases of vertical and diagonal pull-out experiments of model flip anchors.

Case	L (mm)	Opened or Closed	H (mm)	α (deg)	β (deg)
01	48	Opened	400	90	0
02	48	Closed	400	90	-90
03	48	Opened	400	90	0
04	48	Opened	300	90	0
05	48	Opened	200	90	0
06	48	Opened	100	90	0
13	80	Opened	100	90	0
14	80	Opened	200	90	0
15	80	Opened	300	90	0
16	80	Opened	400	90	0
17	48	Closed	400	90	-90
18	48	Closed	300	90	-90
19	48	Closed	200	90	-90
20	48	Closed	100	90	-90
21	48	Closed	100	90	-90
22	48	Closed	200	90	-90
23	48	Closed	300	90	-90
24	48	Closed	400	90	-90
25	48	Opened	100	45	45
26	48	Opened	200	45	45
27	48	Opened	300	45	45
28	48	Opened	400	45	45
29	48	Closed	100	45	-45
30	48	Closed	200	45	-45
31	48	Closed	300	45	-45
32	48	Closed	400	45	-45
33	48	Closed	100	45	90
34	48	Closed	200	45	90
35	48	Closed	300	45	90
36	48	Closed	400	45	90

4.3.3 Experimental results

Pull-out force F vs. pull-out displacement w

Figures 4.13 & 4.14 show comparisons of relationships between F and w of Opened (β = 0°) anchors under different H. As expected, F became larger with an increasing H. F of the larger anchor (L = 80 mm) was larger than F of the smaller anchor (L = 48 mm) at the same H.

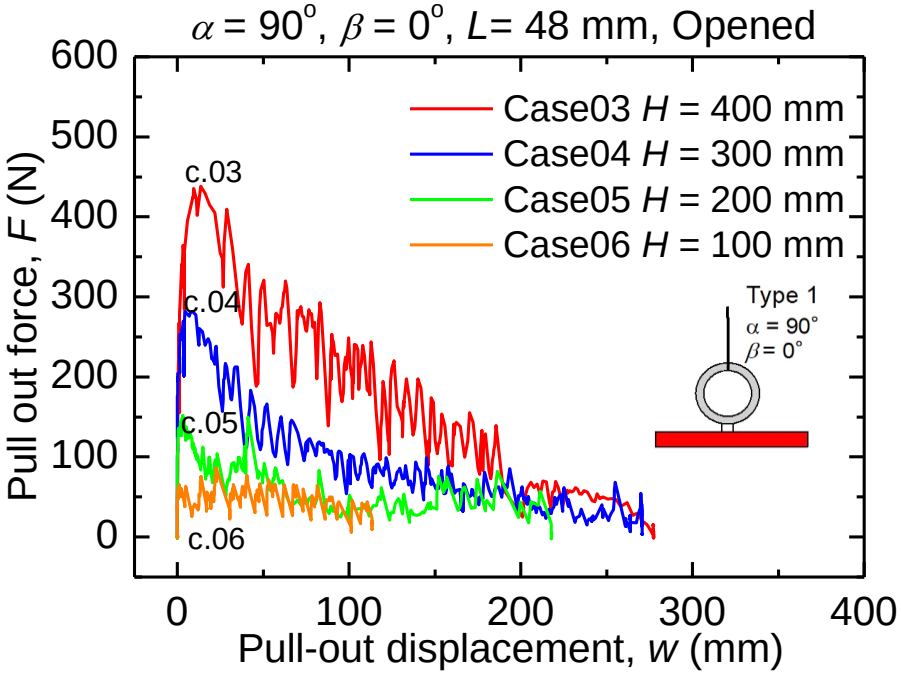

Fig. 4.13. F vs. w of the Type 1 anchor at different H (L = 48 mm).

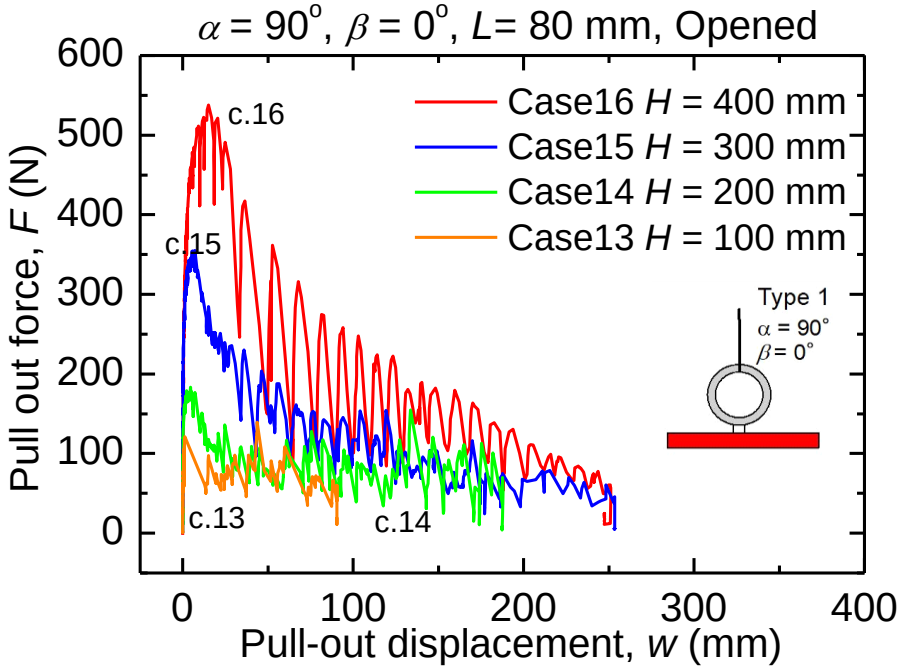

Fig. 4.14. F vs. w of the Type 1 at different H (L = 80 mm).

Figure 4.15 is the comparison of maximum pull-out resistance F_{max} of each Opened anchor when pulled vertically ($\alpha = 90°$). F_{max} of both anchors increased with an increasing H. F_{max} of the larger anchor was larger than F_{max} of the smaller anchor at any H. The projected area A of the larger anchor was about 1.7 times A of the smaller anchor. However, F of the larger anchor at every H was about only 1.3 times larger than F of the smaller anchor. That is, F_{max} did not increases as much as the ratio of A.

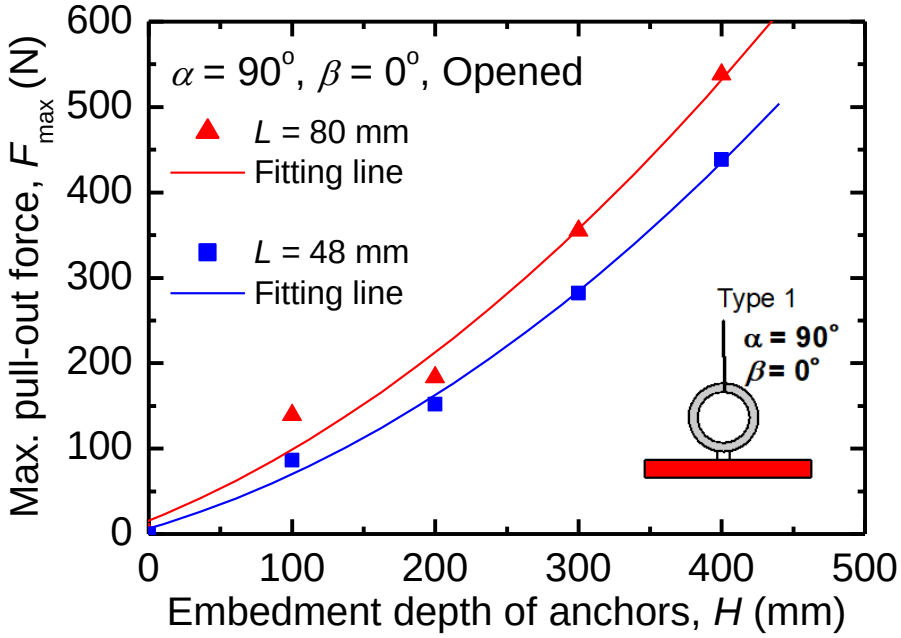

Fig. 4.15. F_{max} vs. H of the Type 1 anchors (L = 48 or 80 mm).

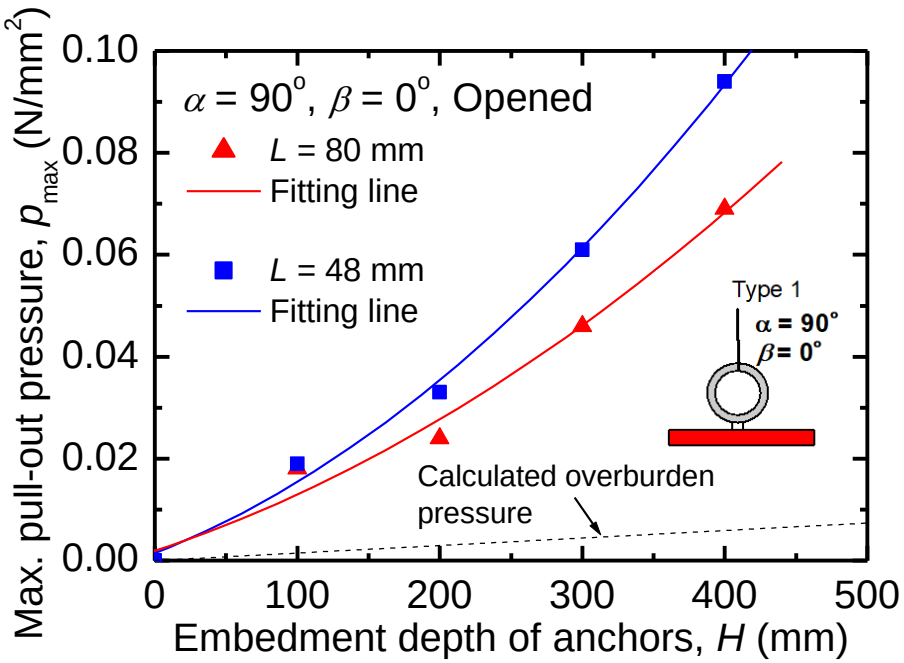

Fig. 4.16. p_{max} vs. H of the Type 1 anchors (L = 48 or 80 mm).

Figure 4.16 shows the comparison of maximum pull-out pressure p_{max} (= F_{max}/A) of each anchor. Contrary to F_{max}, p_{max} became larger as A became smaller. This tendency is common to the experiments using the actual flip anchors or the model plate anchor. It can be said that again that p_{max} is affected by other factors besides overburden pressure.

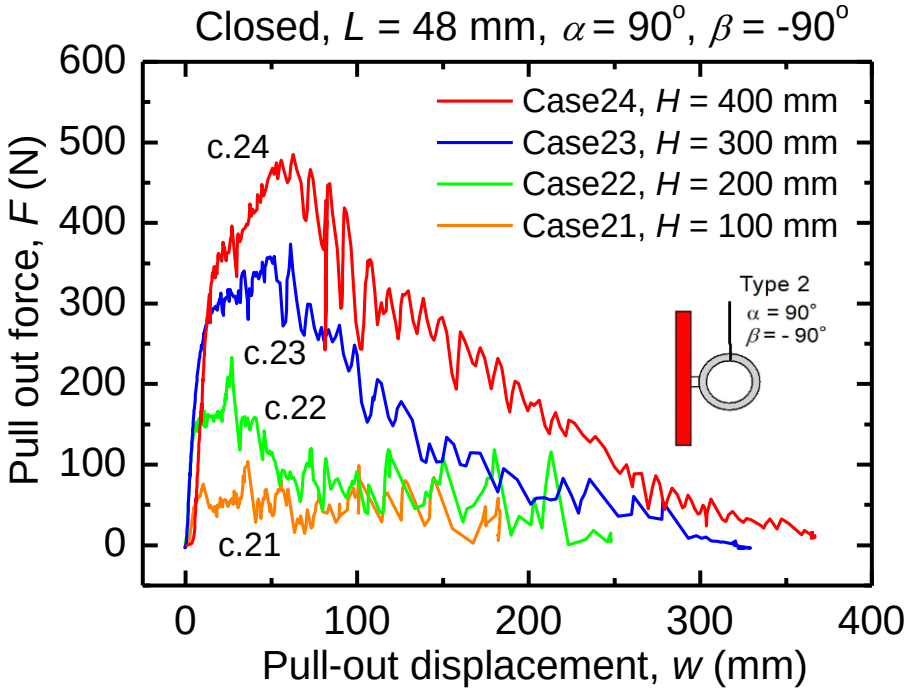

Fig. 4.17. *F* vs. *w* of the Type 2 anchor at different *H*.

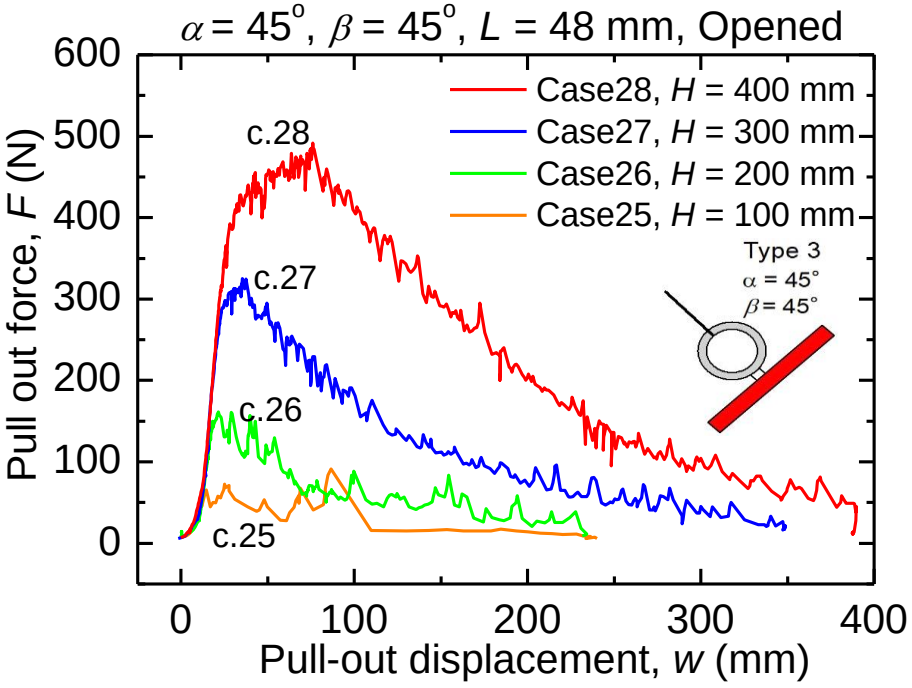

Fig. 4.18. *F* vs. *w* of the Type 3 at different *H*.

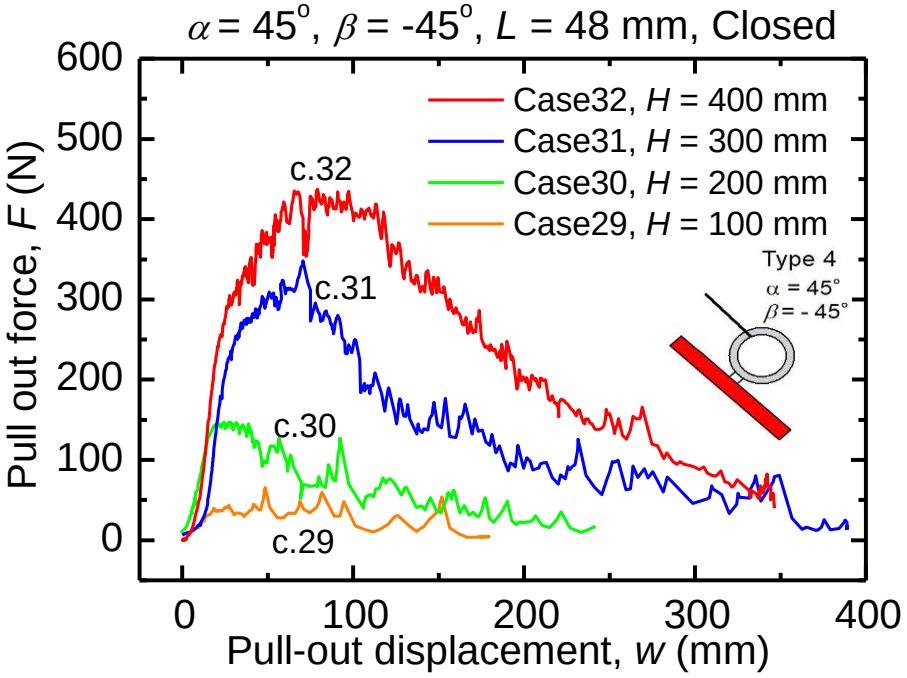

Fig. 4.19. *F* vs. *w* of the Type 4 at different *H*.

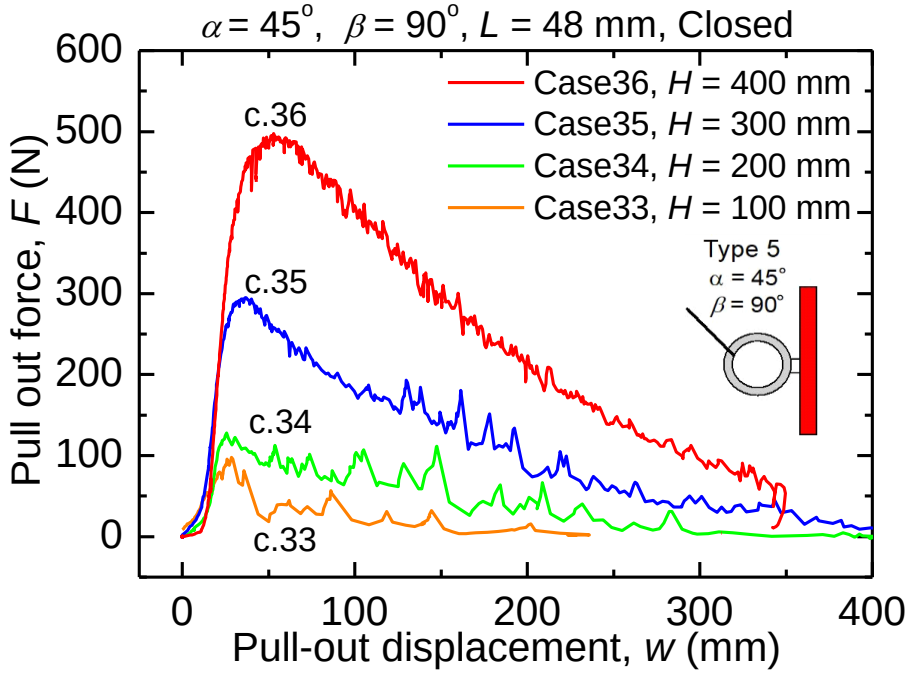

Fig. 4.20. *F* vs. *w* of the Type 5 at different *H*.

Figures 4.17-4.20 show comparisons of *F* vs. *w* of Opened (β = 0°) and Closed (β = -90°) anchors under different *H*. Regardless of pull-out angle α and anchor plate angle β, F_{max} became larger with an increasing *H*. *F* vs. *w* of the anchors (Types 2 to 5) showed almost similar tendency to that of Type 1 anchor (Fig. 4.13).

Figure 4.21 shows the relationships between F and w of Opened and Closed anchors pulled out vertically (α = 90°, H = 400 mm). F_{max} of Closed anchor (Type 2) was larger than F_{max} of Opened anchor (Type 1). Closed anchor requires a larger w to attain F_{max}.

Figure 4.22 shows F vs. w of the anchors with different β pulled out diagonally (α = 45°, H = 400 mm). F_{max} of Type 5 was almost equal to F_{max} of Type 3. F_{max} of Type 4 was about 80% of F_{max} of Type 3. There were some differences in the amount of w at F_{max}. For example, w of Types 3 and 4 at F_{max} were larger than w of Type 5. Overall, β had little effect on F_{max}.

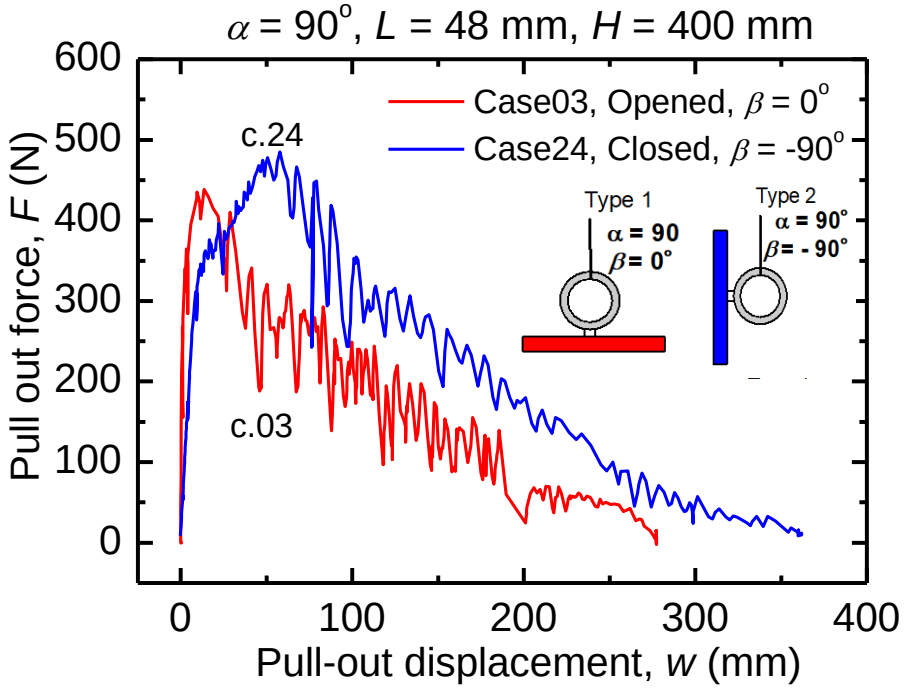

Fig. 4.21. F vs. w of the Type 1 and Type 2 anchors with α = 90° at H = 400 mm.

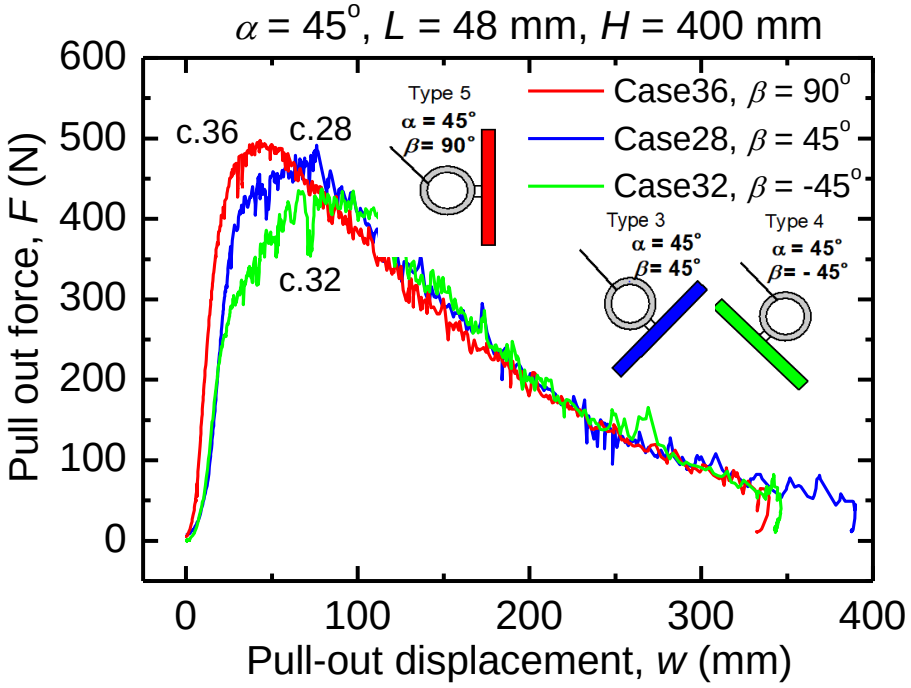

Fig. 4.22. F vs. w of the Types 3, 4 and 5 anchors with α = 45° at H = 400 mm.

Figure 4.23 shows F vs. w of Opened anchors pulled out vertically or diagonally (α = 90° or 45°). It was found again that α, as well as β, did not significantly affect F_{max}.

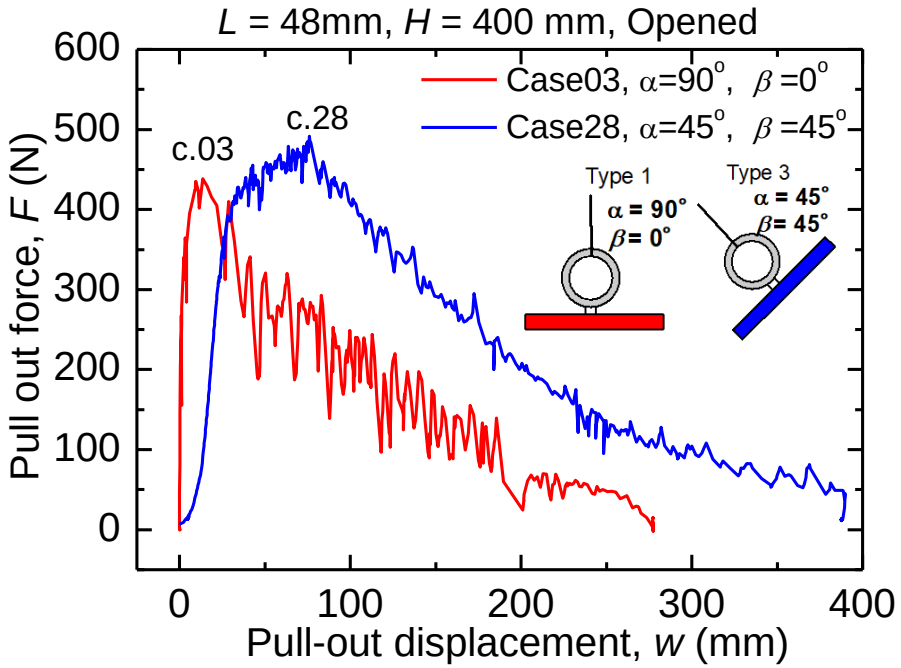

Fig. 4.23. F vs. w of the Type 1 (α = 90°, β = 0°) and Type 3 (α = 45°, β = 45°) anchors at H = 400 mm.

Figure 4.24 is a similar comparison of Fig. 4.23 for Closed anchors. Same as Opened anchors, α as well as β, did not significantly affect F_{max}.

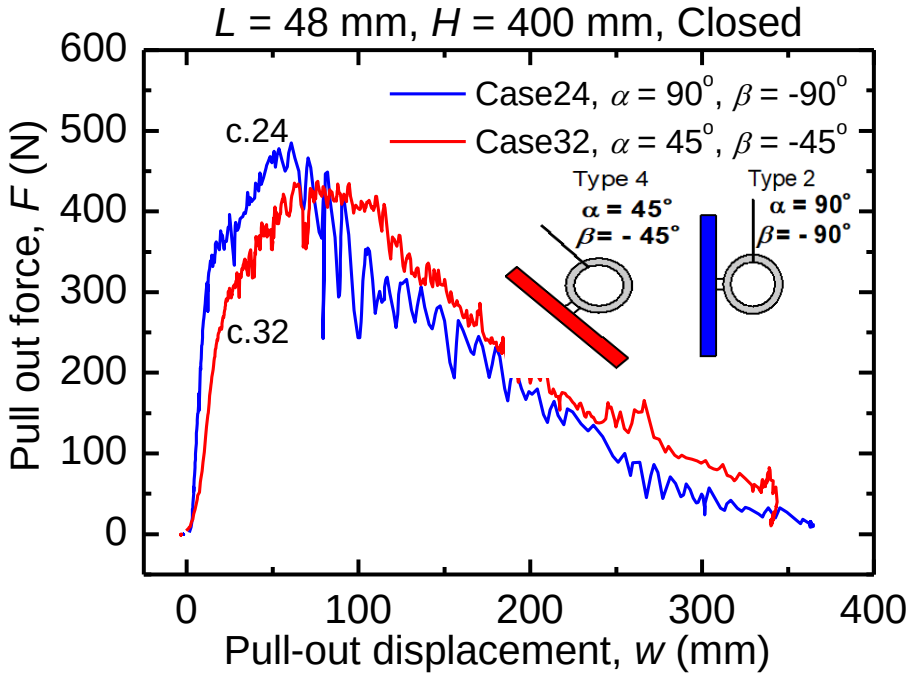

Fig. 4.24. F vs. w of Type 2 (α = 45°, β = -45°) and Type 4 (α = 90°, β = -90°) anchors at H = 400 mm.

Based on the results of Figs 4.21-4.24, it can be concluded that F_{max} on any pull-out condition was comparable to F_{max} of Type 1 (Opened anchor pulled vertically). Thus, because F_{max} largely depends on the shape of the ground failure pattern, the ground failure pattern in Type 1 can be used for calculating F_{max} of a flip anchor embedded and pulled in any condition.

4.3.4 Modelling of ground failure

In this research, the PIV analysis was also conducted. Figure 4.25a shows a photo of the ground deformation with displacement vectors. Fig. 4.25b shows a zoom-up of the traces of the sand particles until w reached 15.1 mm at F_{max} = 538 N (Case 16).

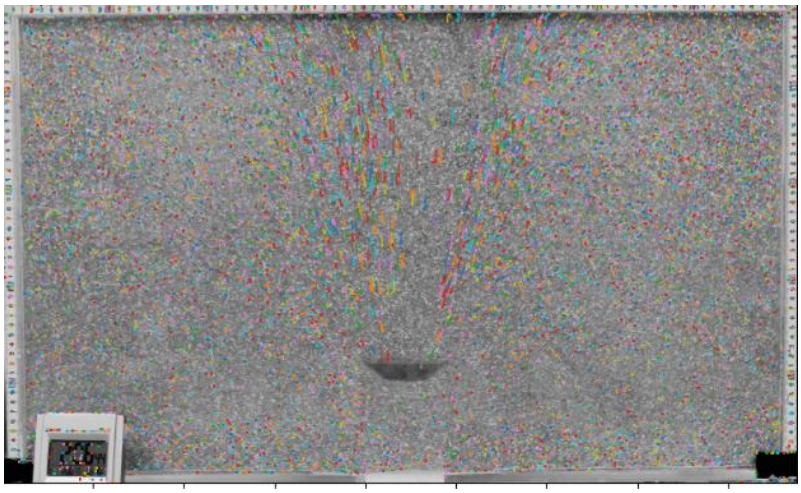

(a) Photo of the ground deformation with displacement vectors

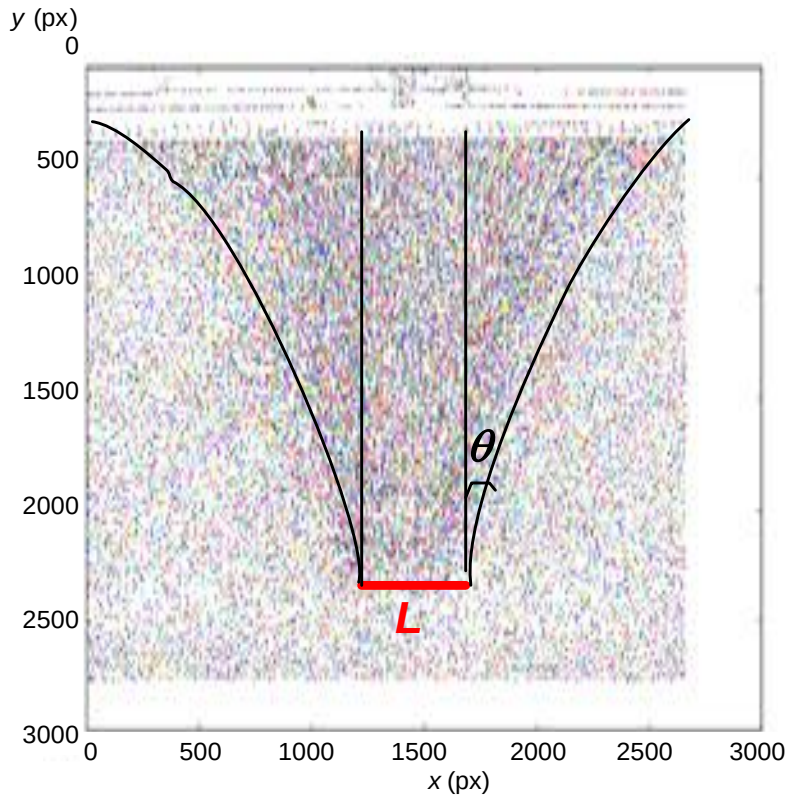

(b) Displacement vectors of the ground (Enlarged)

Fig. 4.25. Ground deformation and displacement vectors at F_{max}(Case 16: L = 80 mm, H/L = 5).

An inverted trapezoidal ground failure pattern was clearly observed. This kind of ground failure patterns are also observed in previous studies on plate anchors, such as Baker and Kondner (1966), Dickin (1988), Tanaka and Sakai (1993), Merifield and Sloan (2006), Liu et al. (2012), Niroumand et. al (2013), Yang et. al (2020).

Figure 4.26 shows similar results of the PIV analysis of Case 1 (w = 13.0 mm at F_{max} = 438 N). An inverted trapezoidal failure pattern was also clearly observed.

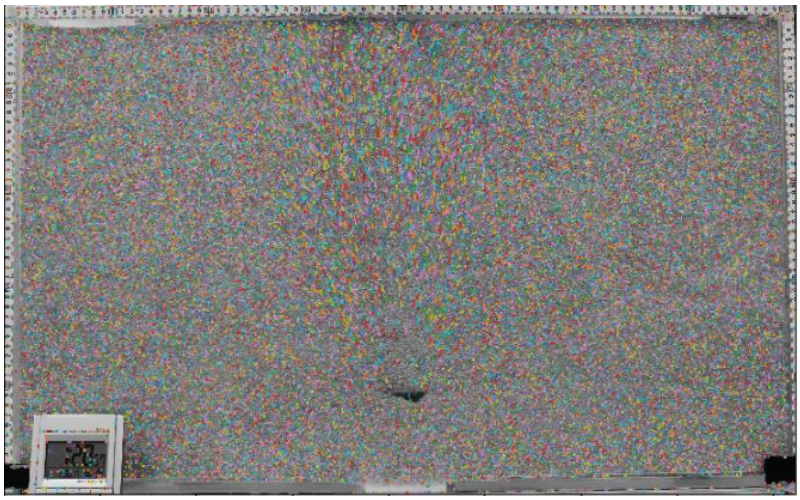

(a) Photo of ground deformation with displacement vectors

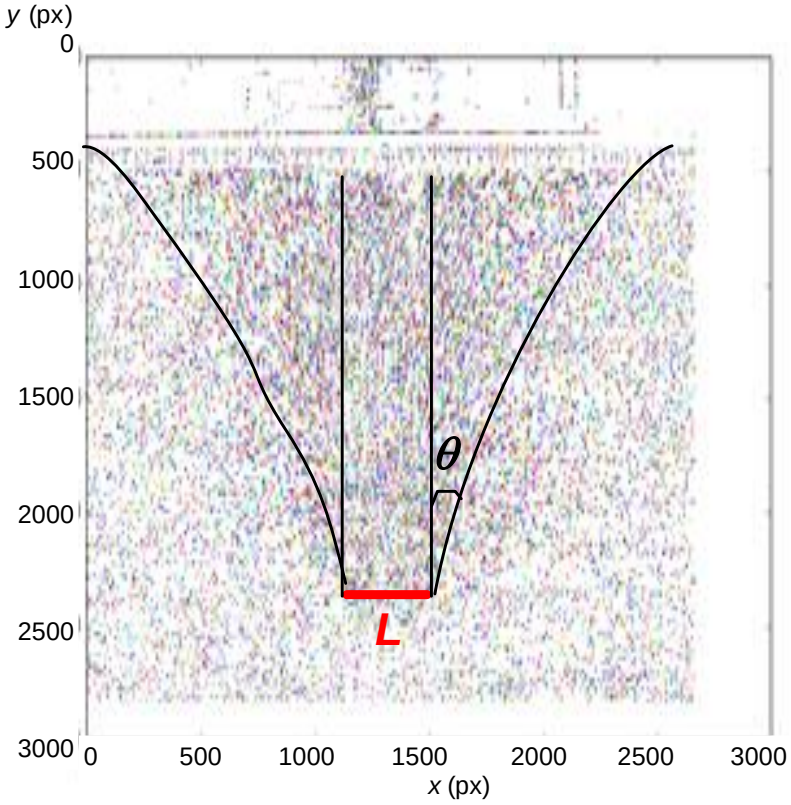

(b) Displacement vectors of the ground (Enlarged)

Fig. 4.26. Ground of ground deformation and displacement vectors at F_{max} (Case 1: L = 48 mm, H/L=8.3).

It is seen from Figs. 4.25 & 4.26 that the ground failure patterns were similar regardless of L. θ observed in all the vertical pull-out experiments ranged from approximately 20° to 22°. The average was $\theta = 21°$.

The ground failure patterns of the model flip anchors observed in this experiment was similar to that observed in the experiments of the model plate anchor (Section 4.2). Thus, ground failure pattern of flip anchors also can be simply modelled as Figure 4.7. The shape is similar to Mors' model (Fig. 2.2), in which θ is assumed to be $\phi/2$.

In Mors' model, the pull-out resistance F_{max} is calculated from only the weight of the soil W of the inverted truncated cone above the anchor plate; whereas, in the two-dimensional model proposed in this study (Fig. 4.7), F_{max} is calculated from the W of the inverted trapezoidal soil wedge and the vertical component of S acting along the slip lines.

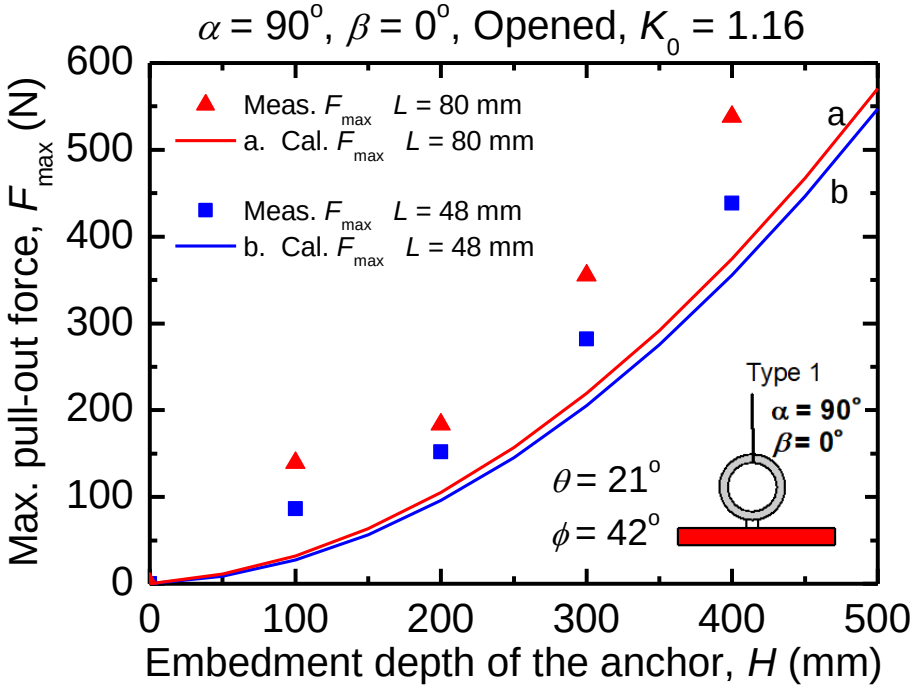

Fig. 4.27. Calculated F_{max} vs. measured F_{max} based on the model.

As shown in Fig. 4.27, measured and calculated F_{max} were both increase exponentially with an increasing H. Calculated values are qualitatively agreed well with the measured values. From a quantitative point of view, calculated F_{max} were 50% - 70% of measured values. Because the values were qualitatively captured, the quantitative difference may be caused by the frictional force between the sand and the acrylic plate generated on the side surface that was not considered in the calculation.

4.3.5 Discussion of Section 4.3

In this section, pull-out experiments of model flip anchors in sand grounds under a plane strain condition were conducted. Main experimental parameters were an embedment depth H, a length of an anchor plate L, pull-out angle α, and embedment angle of anchor plate β (Opened or Closed).

In this experimental conditions, α and β did not significantly affect F_{max}. Thus, F_{max} of flip

anchors under any pull-out condition can be calculated based on the ground failure model of horizontal plate anchor pulled vertically.

There was no difference in the ground failure patterns between the horizontal model plate anchor (Section 4.2) and the model flip anchors. Thus F_{max} of flip anchors can be calculated based on the same ground failure model as the plate anchor.

4.4 Conclusions of Chapter 4

In this chapter, following the pull-out experiments using actual flip anchors in a three-dimensional conditions, the pull-out experiments using model plate or model flip anchors in a two-dimensional condition were conducted to investigate ground failure pattern in addition to pull-out resistance. Because F_{max} of plate and flip anchors largely depend on the ground failure pattern, F_{max} of plate and flip anchors can be calculated based on the ground failure models.

In the push-up experiment of the horizontal model plate anchor, the ground failure pattern same as previous studies on plate anchors was observed. Subsequently, in a pull-out experiment of model flip anchors, the ground failure pattern similar to that of the plate anchors was observed.

Main findings from the experiments are summarized as;

1) F_{max} of flip anchors increased exponentially as H increased.
2) F_{max} became larger as A became larger; whereas p_{max} (= F_{max}/A) became larger as A became smaller.
3) α, as well as β, do not significantly affect the value of F_{max}.
4) F_{max} of flip anchors with any α and β can be approximated by F_{max} of a horizontal plate anchor pulled vertically.
5) F_{max} calculated from the proposed 2D ground failure model, which is similar to that of a horizontal plate anchor, agreed well with measured F_{max} of flip anchors of any pull-out condition.

As Balla (1961) proposed, the slip lines observed in the experiments were generated in an arc shape. In this study, because it does not cause a serious error, the slip lines are approximated by straight lines (Fig. 4.7) to simplify the calculation. Even with that model, the calculation results were in good agreement with the measured values as mentioned above.

The tendency of F_{max} and p_{max} of the model flip anchors under a plane-strain condition was consistent with the tendency of the actual flip anchors in three-dimensional condition. Thus, the proposed two-dimensional ground failure model can be extended to three-dimensional conditions.

In the next chapter, the 2D model will be extended to the 3D model to calculate F_{max} of flip anchors under a three-dimensional condition.

References in Chapter 4

Baker W. H., and Kondner R. L. (1966). Pullout load capacity of a circular earth anchor buried in sand. Highway Research Record, 108, pp. 1-10.

Das B. M., and Seeley G. R. (1975). Inclined load resistance of anchors in sand. Journal of Geotechnical and Geoenvironmental Engineering, 101(GT9), pp. 995-998.

Dickin E.A. (1988). Uplift behavior of horizontal anchor plates in sand. Journal of Geotechnical Engineering, 114(11), pp. 1300-1317.

Ghaly A. M., and Clemence S. P. (1998). Pullout performance of inclined helical screw anchors in sand. Journal of Geotechnical and Geoenvironmental Engineering, 124(7), pp. 617- 627.

Hannna A., Foriero A., and Ayadat T. (2015). Pullout capacity of inclined shallow single anchor plate in sand. Indian Geotechnical Journal, 45(1), pp. 110-120.

Harvey R. C., and Burley E. (1973). Behaviour of shallow inclined anchorages in cohesionless sand. Ground Engineering, 6(5), pp. 48-55.

Liu J., Liu M., and Zhu Z. (2012). Sand deformation around an uplift plate anchor. Journal of Geotechnical and Geoenvironmental Engineering, 138(6), pp. 728-737.

Merifield R.S., and Sloan S.W. (2006). The ultimate pullout capacity of anchors in frictional soils. Canadian Geotechnical Journal, 43(8), pp. 852-868.

Niroumand H., Kassim K. A., and Nazir R. (2013). The influence of soil reinforcement on the uplift response of symmetrical anchor plate embedded in sand. Measurement, 46(8), pp. 2608–2629.

Tanaka T., and Sakai T. (1987). A trap-door problem in granular materials: Model test and finite element analyses. Journal of Irrigation Engineering and Rural Planning, 11, pp 8-23.

Tanaka T., and Sakai T. (1993). Progressive failure and scale effect of trap-door problems with granular materials. Soils and Foundations, 33(1), pp. 11-22.

Trackpy Contributors. (2019). https://soft-matter.github.io/trackpy/v0.3.2/

Yang M., Ai Z., and Deng B. (2020). Experimental and analytical study on uplift loading capacity of strip plate anchors near sand slope. International Journal of Geomechanics, 20(1), pp. 1-13.

Yue H., Zhuang P., Zhang H., and Song X. (2020). Failure and deformation mechanisms of vertical plate anchors subjected to lateral loading in sand. International Journal of Geomechanics, 20(11), pp. 1-13.

Chapter 5
Calculation methods for maximum pull-out resistance of flip-type earth anchors by LEM and FEM

5.1 Introduction

In the pull-out experiments on sand, not only pull-out resistance and behavior of flip anchors, but also correlations between flip anchors and plate anchors were investigated. And ground failure patterns caused by pull-out of a flip anchor were also observed and modelled. In the pull-out experiments of the model flip anchors under a plane strain condition, the inverted trapezoidal soil wedge was lifted by a flip anchor. The failure pattern explains well why a flip anchor with smaller A has larger p_{max}. In Chapter 4, the calculation method of pull-out resistance F_{max} of flip anchors was proposed based on the 2D ground failure model.

In this Chapter 5, the 2D model was extended to 3D models to calculate pull-out resistance of actual flip anchors, Based on the proposed 3D model, F_{max} of flip anchors was calculated by limit equilibrium method (LEM). And F_{max} of flip anchors was also calculated by empirical theory of breakout factor f_q in previous studies for plate anchors.

Furthermore, as an alternative solution, F_{max} of flip anchors was also calculated using finite element method (FEM). In the FEM analysis, the ground failure patterns at different embedment ratio H/L were investigated as well as the relationship between F vs w.

Comparing the calculated and measured values (Section 3.3), the effectiveness of proposed calculation estimation methods of F_{max} of flip anchors in sandy grounds were demonstrated.

5.2 Calculations of F_{max} of flip anchors by Limit equilibrium method (LEM)

5.2.1 Three-dimensional ground failure models

To estimate pull-out resistance of actual flip anchors, the 2D model (see Fig. 4.7) need to be extended to 3D models. For plate anchors, as shown in Fig. 5.1, the ground failure models have been considered as “Shallow depth” model or “Great (Deep) depth” model separately according to H/L (= D/B in Fig. 5.1). It is because the slip lines extend from the anchor plate do not reach the ground surface when the anchor is installed deeper than a certain value of H/L. That critical depth H_{cr} at that time is different depending on the size of anchors. The value of H/L is usually expressed as critical embedment ratio $(H/L)_{cr}$, which is expressed as $(H/h)_{cr}$ in Das et al. (1977); where H is an installation depth of an anchor, and L is a length of an anchor plate, h is a height of a vertical anchor plate.

If H/L is smaller than $(H/L)_{cr}$, the failure pattern appears as a "Shallow anchor" model, and if H/L is equal or greater than $(H/L)_{cr}$, the pattern appears as a "Deep anchor" model. When calculating F_{max} of the deep anchor using the shallow anchor model, the F_{max} will be excessive. Thus, Fig. 4.7 can be regarded as a 2D model only for the "Shallow anchor". Technically, there is a transition failure pattern between the "Shallow anchor" and the "Deep anchor" patterns (Ghaly et al., 1991, Lin et al., 2015); however it is sufficient to consider only the shallow or deep anchor model to calculate F_{max}.

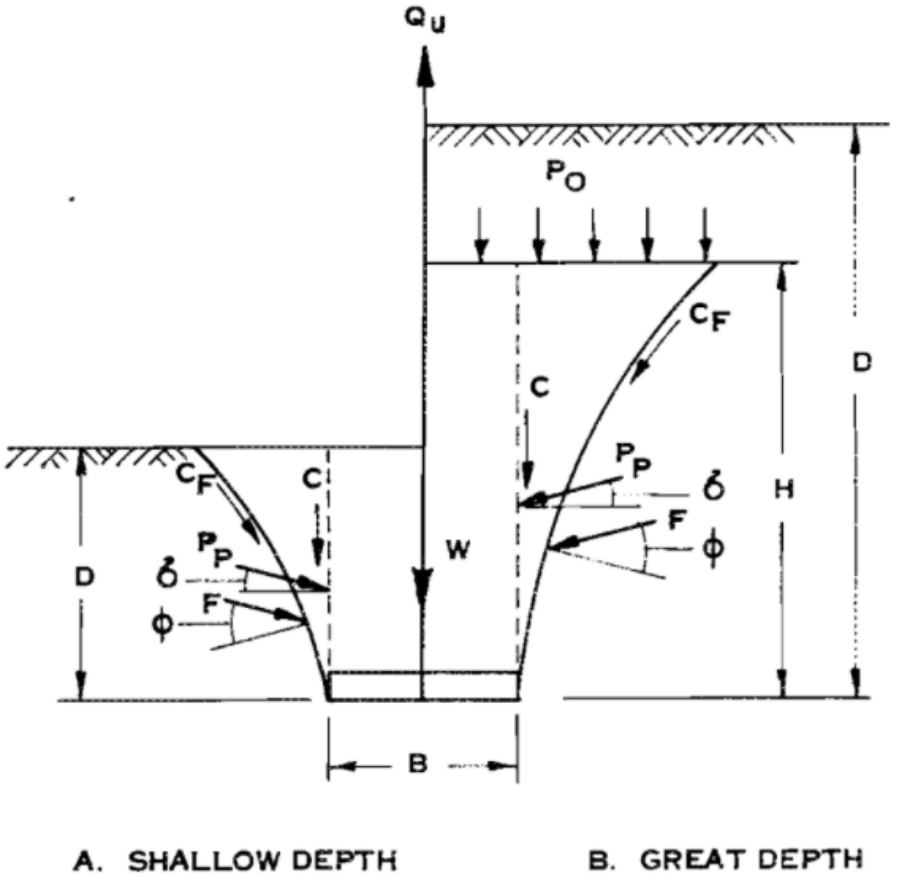

Fig. 5.1. Failure of soil above a strip footing (plate anchor) under uplift load (Meyerhof and Adams, 1968).

Some 3D ground failure models for plate anchors are presented in previous studies, such as Zhao et al. (2011). In this study, with reference to Fig. 4.7 and Fig. 5.1, 3D shallow and deep anchor models are proposed as shown in Fig. 5.2 to calculate F_{max} of flip anchors. F_{max} is calculated considering the weight of the soil lifted by an anchor and vertical component of shearing resistance of failure plane of the 3D models.

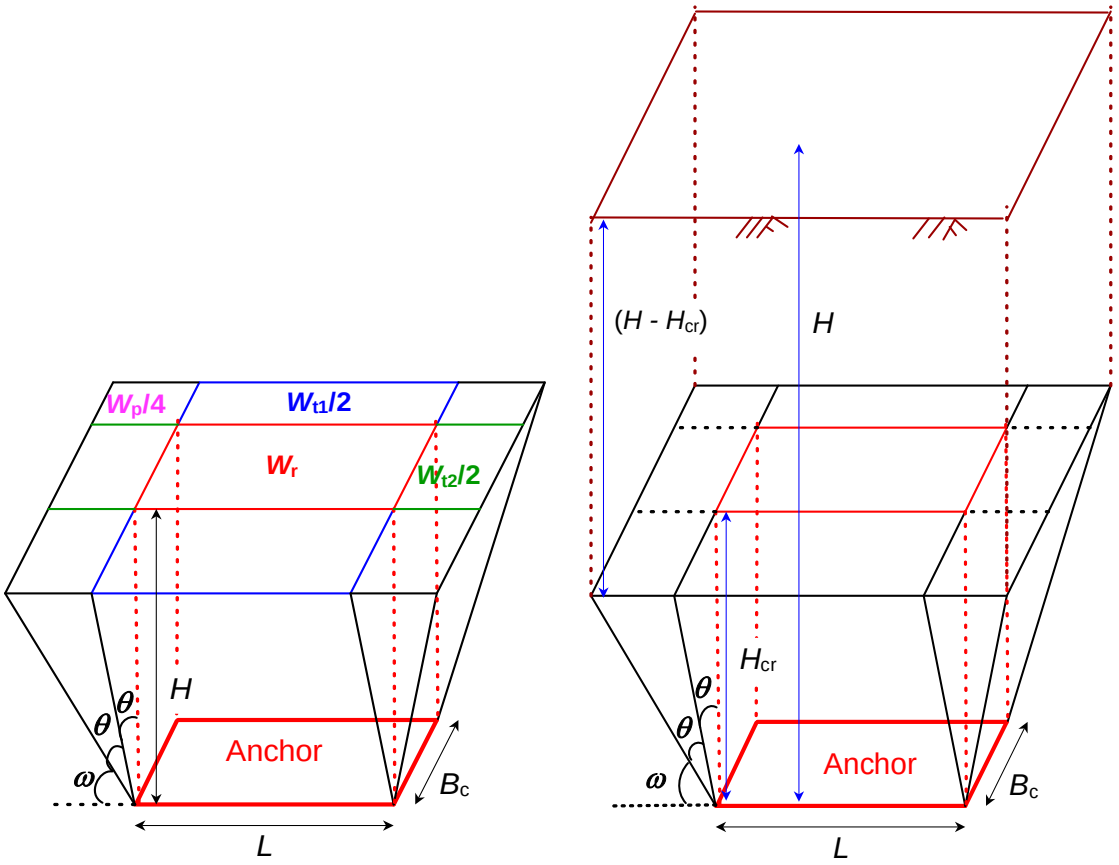

(a) Shallow anchor model (b) Deep anchor model

Fig. 5.2. 3D ground failure models above a flip (plate) anchor under uplift load.

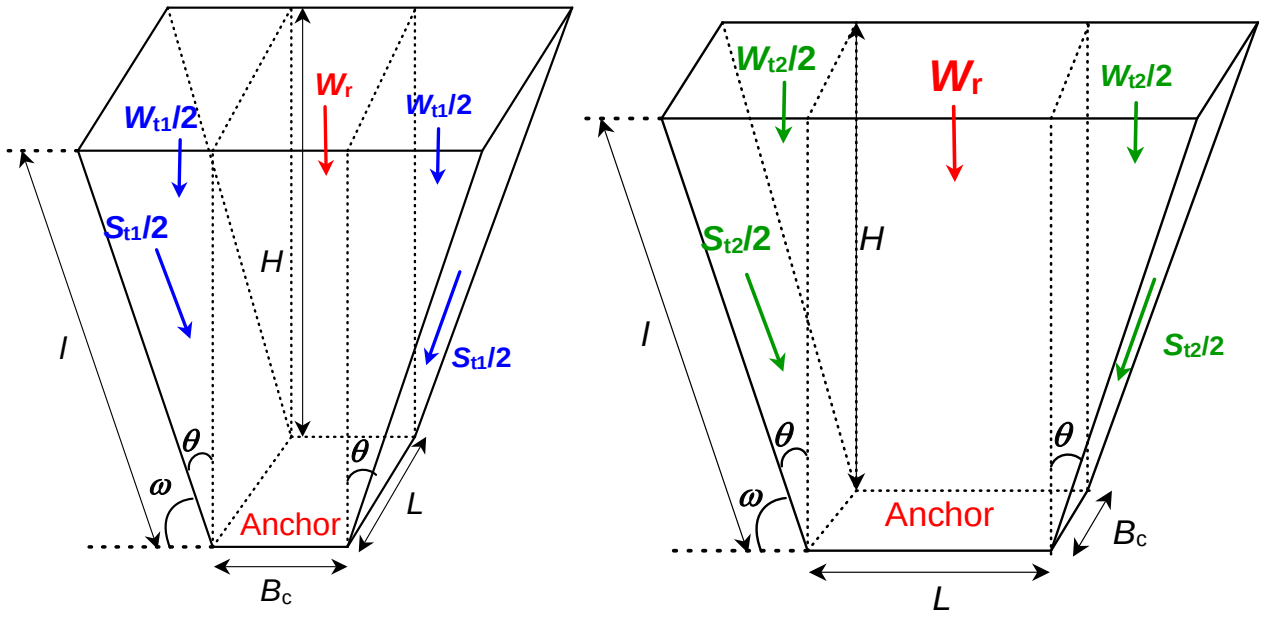

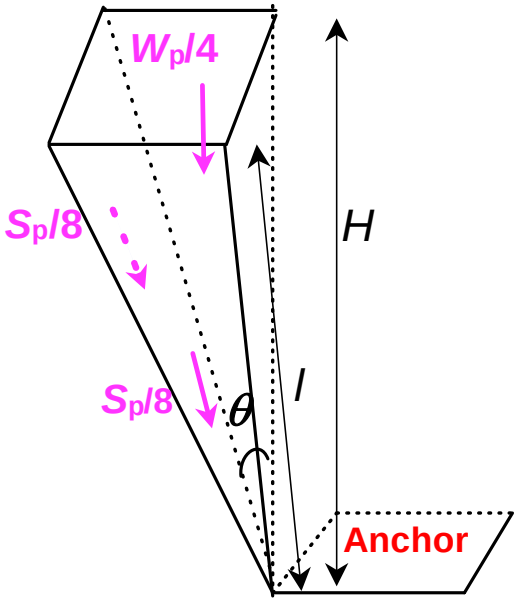

Fig. 5.3. 3D ground failure models divided into several components for the calculation of F_{max} of a flip anchor.

In Figs. 5.2 and 5.3, H is an embedment depth of an anchor, γ is the unit weight of the soil, W_r is a weight of the rectangular soil mass, $W_r = (L \times B_c \times H \times \gamma)$, W_{t1} is a weight of the triangular soil mass having a length of L, $W_{t1} = 2(H \tan\theta \times H/2 \times L \times \gamma)$, W_{t2} is a weight of the triangular soil mass having a length of B, $W_{t2} = 2(H \tan\theta \times H/2 \times B_c \times \gamma)$, W_p is a weight of the triangular soil mass at four corners, $W_p = 4\{(H \tan\theta)^2 \times H/3 \times \gamma\}$, θ is an angle of slip line from a vertical direction, N (N/m) is normal force acting on a failure plane, $N = \sigma_n \times l /2$, S_{t1} is shear force acting along failure plane having a length of L, $S_{t1} = 2(N \tan\phi \times L)$, S_{t2} is shear force acting along failure plane having a length of B, $S_{t2} = 2(N \tan\phi \times B_c)$, S_p is shear force acting along failure plane at four corners, $S_p = 8\{N \tan\phi \times (H \tan\theta) / 2\}$, L is a length of an anchor plate, σ_n is effective vertical stress on a failure plane, $(1 + K_0)\ \sigma_v / 2 + (1 - K_0)(\sigma_v / 2) \cos 2\omega$, ω is an angle of slip line from horizontal direction, σ_v is effective earth pressure, K_0 is coefficient of lateral earth pressure at rest.

For the calculation, because the flip anchor has a unique shape, the shape is approximated to a rectangle having the same A by adjusting B as B_c (Table 5.1 and Fig. 5.4).

Table 5.1. Dimensions of approximated rectangular shapes of flip anchors for the calculation.

	L (m)	*B_c (m)	B (m)	A (m^2)
H25	0.085	0.022	0.025	0.002
H50	0.160	0.043	0.050	0.007
H110	0.160	0.079	0.110	0.013
HG100	0.340	0.088	0.100	0.030
HG180	0.340	0.143	0.180	0.049
HG320	0.440	0.235	0.320	0.103

* B_c = approximated breadth of a flip anchor for calculation

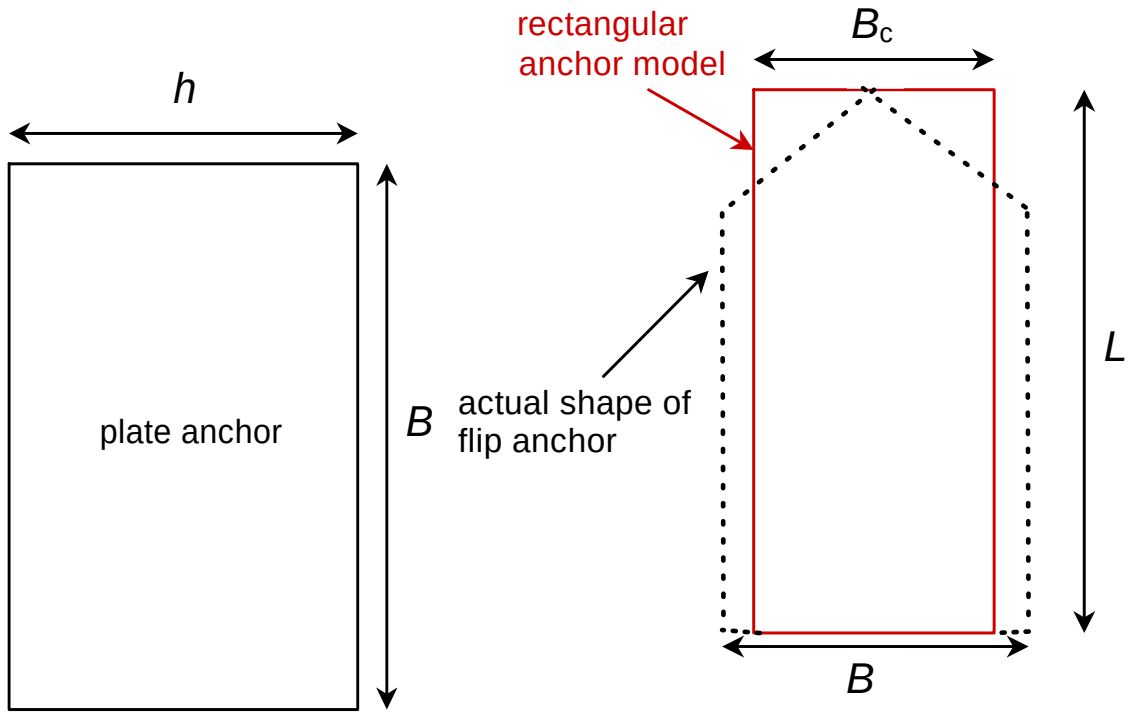

Fig. 5.4. A concept of an approximated rectangular shape of a flip anchor for the calculation.

Angle of the slip line θ

F_{max} of flip anchors largely depends on the shape of the ground failure models. And the scale of the model largely depends on θ. θ is expressed as 90° - ω; where ω is an angle of the slip line from a horizontal direction. When the slip line reaches the ground surface, the line should intersect the ground surface at an angle of 45° - 1/2 ϕ as Balla (1961) proposed. If the slip line is extended from the end of the anchor so that it intersects the ground surface at 45°- 1/2 ϕ, θ becomes too large. If the slip lines are in an arc shape, the lines extend close to vertical near the edges of the anchor, and intersect the ground surface in an angel of close to 45° - 1/2 ϕ. As observed in the 2D laboratory experiments and as proposed by Balla (1961), the slip lines actually extend in an arc shape.

According to Liu et. al (2012), the value of θ is affected by the density of the ground. On loose sand grounds, θ is smaller than θ on dense sand grounds. In practice, θ can be regarded as a function of internal friction angle of soil ϕ. According to Meyerhof and Adams (1968), θ is in the range from 1/3 ϕ to 2/3 ϕ, and the average is 1/2 ϕ. In design guidelines of the general grouted ground anchors, θ is 30° or 45° (Littlejohn and Bruce, 1977), or 2/3 ϕ (Habib, 1989) in case of sandy ground. In the experiments conducted on the ground composed of sand with ϕ = 42 degrees, θ = 21 degrees was measured from the image analysis. Thus, it is certainly reasonable to adopt the range of θ as proposed by Meyerhof and Adams (1968).

In practice, ϕ can be converted from SPT-N values measured on site such as $\phi = \sqrt{15N} + 15$. When designing with an emphasis on safety, θ can be calculated using θ = 1/3 ϕ. In this study, θ = 1/2 or 2/3 ϕ is applied to the 3D models of flip anchors to calculate F_{max}.

Critical embedment ratio $(H/L)_{cr}$

$(H/L)_{cr}$ can be found from the observation of the ground failure pattern at F_{max} in a plane strain condition. In the case of H/L when the slip lines do not extend to the ground surface, the H/L at that time can be regarded as $(H/L)_{cr}$.

In a three dimensional condition, $(H/L)_{cr}$ can be found by observing the ground surface at F_{max}. If the ground surface is deformed at F_{max}, such as heaving or cracking, H/L at that time is thought to be smaller than $(H/L)_{cr}$. If not, it should be equal or greater than $(H/L)_{cr}$. Liu et. al (2012) shows that $(H/L)_{cr}$ is affected by the density of the ground. On loose sand grounds, $(H/L)_{cr}$ seems to be smaller than that on dense sand. In practice, Meyerhof and Adams (1968) proposed values of $(H/L)_{cr}$ in relation to ϕ (Table 5.2 and Fig. 5.5) according to the results of pull-out experiments.

Table 5.2. $(H/L)_{cr}$ depending on ϕ (Meyerhof and Adams, 1968).

ϕ	20°	25°	30°	35°	40°	45°	48°
$(H/L)_{cr}$	2.5	3	4	5	7	9	11

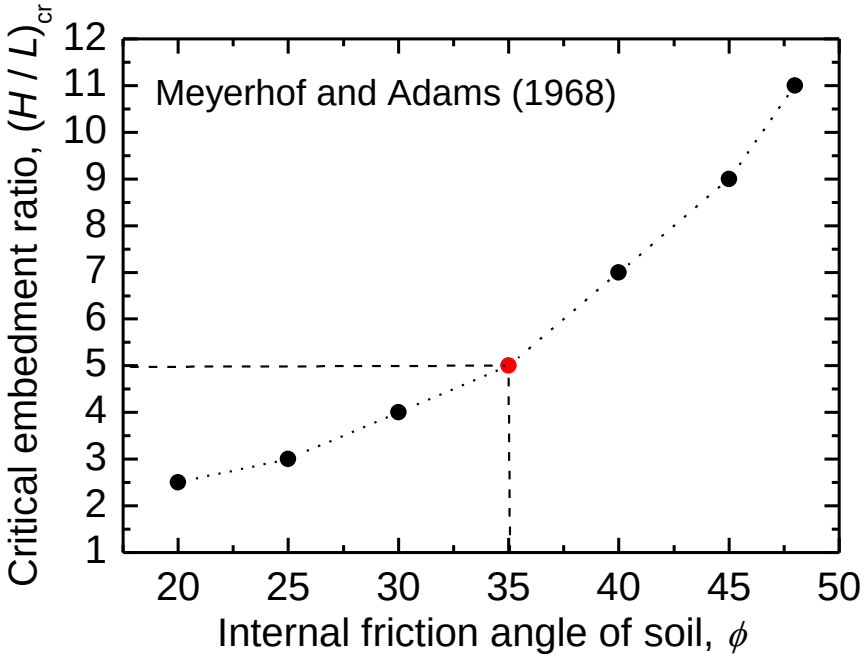

Fig. 5.5. ($H/L)_{cr}$ vs. ϕ (Meyerhof and Adams, 1968).

5.2.2 Calculation of F_{max} of flip anchors from the 3D ground failure models

Once θ and $(H/L)_{cr}$ are set, the shape of the 3D ground failure model (Fig. 5.2) is fixed. Now F_{max} of flip anchors can be calculated based on the model.

For "shallow anchor", $F_{max(s)}$ can be calculated by Eq. 5.1.

$$F_{max(s)} = (W_r + W_{t1} + W_{t2} + W_p) + (S_{t1}\cos\theta + S_{t2}\cos\theta + S_p\cos\theta) \quad (5.1)$$

where $F_{max(s)}$ is F_{max} for "shallow anchor".

For “deep anchor”, $F_{max(d)}$ can be estimated by Eq. 5.2. $F_{max(d)}$ increases linearly in proportion to the increase of (H - H_{cr}).

$$F_{max(d)} = F_{max(s)} + [\{L + 2(H_{cr} \tan\theta)\}\{B + 2(H_{cr} \tan\theta)\} (H - H_{cr})] \times \gamma \quad (5.2)$$

where $F_{max(d)}$ is F_{max} for “deep anchor”, H is embedment depth of an anchor, H_{cr} is critical embedment depth of an anchor.

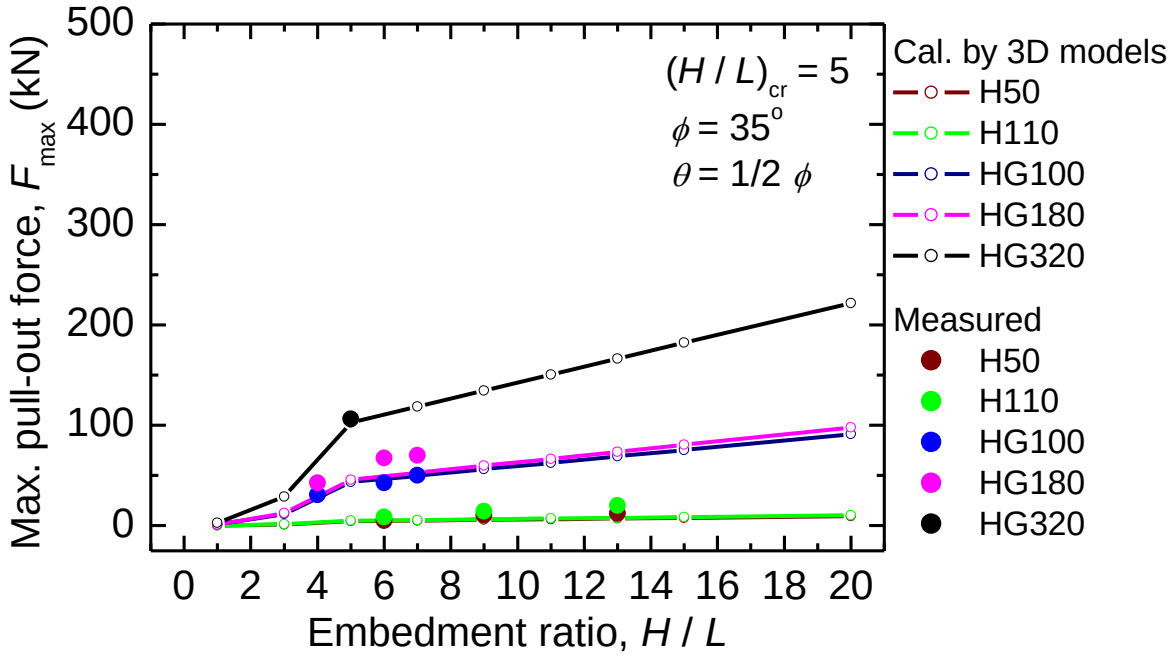

Fig. 5.6. Measured F_{max} (Section 3.3) vs. calculated F_{max} (by 3D models, θ = 1/2 ϕ).

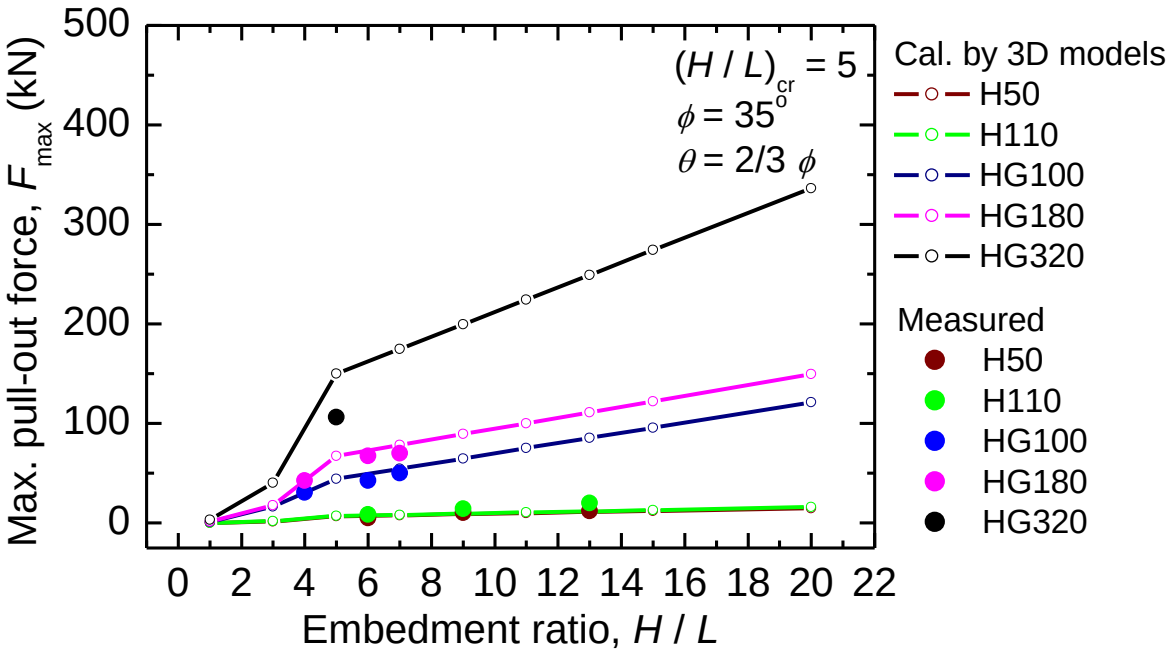

Fig. 5.7. Measured F_{max} (Section 3.3) vs. calculated F_{max} (by 3D models, θ = 2/3 ϕ).

Figure 5.6 shows calculated F_{max} based on the 3D models ($\theta = \phi/2$) vs. measured F_{max} (Chapter 3.3) of actual flip anchors. Figure 5.7 shows the same in the case of $\theta = 2/3\ \phi$. Both calculated results agreed with measured values. The difference between calculated F_{max} of HG100 (blue line) and HG180 (purple line) having same L but different B, was more apparent in the condition of $\theta = 2/3\ \phi$.

5.2.3 Calculation of F_{max} of flip anchors using breakout factor f_q

Estimation of breakout factor f_q for flip anchors

A dimensionless breakout factor f_q (= $F_{max}/\gamma AH$) is often used for estimating F_{max} of plate anchors; where F_{max} is maximum pull-out resistance, γ is unit weight of the soil, A is projected area of an anchor.

f_q of rectangular plate anchor can be calculated by Eq. 5.3 (Das and Seeley, 1975).

$$f_q = 1 + [\{1 + 2m\,(H/h)\}(h/B) + 1](H/h)\,K_u \tan\phi \qquad (5.3)$$

where h is a breadth of an anchor, B is a length of an anchor, m is a coefficient related to shape factor which is a function of ϕ (Table. 5.3), K_u is a nominal uplift coefficient (Fig. 5.8), and K_{pv} (= $K_u \tan\phi$)is a vertical component of the passive earth pressure K_p based on curved failure surface (Caquot & Kérisel, 1949).

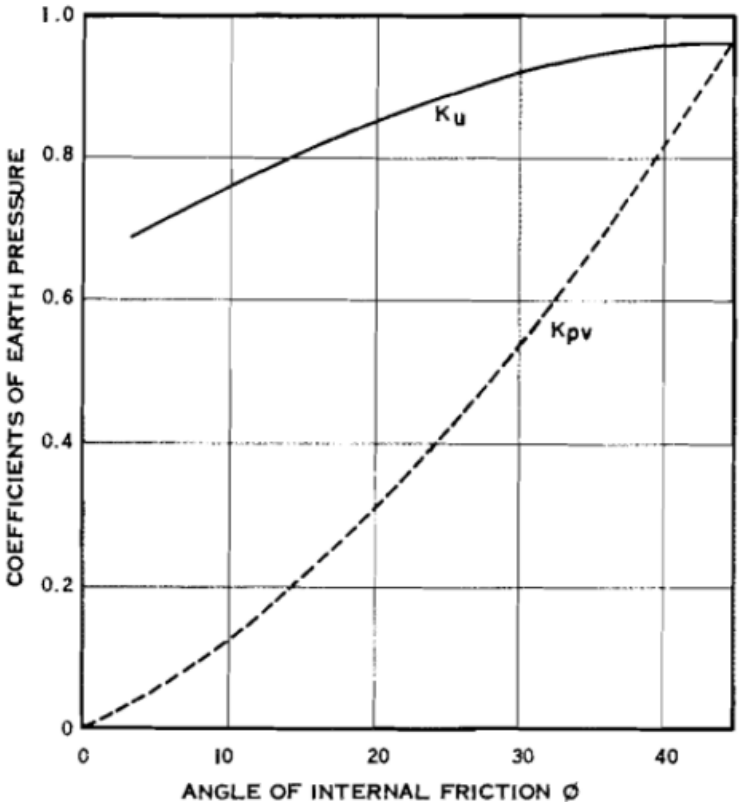

Fig. 5.8 Theoretical uplift coefficients of earth pressure for strip footing (Meyerhof and Adams, 1968)

Table 5.3. Variation of m depending on ϕ (Meyerhof and Adams, 1968).

ϕ	20°	25°	30°	35°	40°	45°	48°
m	0.05	0.1	0.15	0.25	0.35	0.5	0.6

When f_q is invoked for the calculation of F_{max} of flip anchors, the shape of a flip anchor need to be approximated to a rectangle having the same A by fixing L (Table 5.1). Thus Eq.5.3 can be rewritten as Eq.5.4 for a flip anchor. When designing installation depth for flip anchors, using H/L is convenient rather than using H/B because the anchor is driven into the ground in closed state having the L in the driving direction. Thus, it is recommended to use Eq.5.5 for flip anchors. Whether calculated with Eq. 5.4 or Eq. 5.5, the calculated values will be the same, so which equation is used will not affect the result.

When the shape of a flip anchor is approximated square ($B = L$), the value of f_q will be a little smaller than f_q for a rectangle; however, the difference is only an insignificant amount. Thus the shape of the flip anchors can be approximated by a rectangle having same L with an actual anchor.

$$f_q = 1 + [\{1 + 2m\,(H/B)\}(B/L) + 1](H/B)\,K_u \tan\phi \tag{5.4}$$

$$f_q = 1 + [\{1 + 2m\,(H/L)\}(L/B) + 1](H/L)\,K_u \tan\phi \tag{5.5}$$

f_q of the flip anchors in the experiments in Chapter 3 can be back calculated using measured F_{max}. $(H/L)_{cr} = 5$ was assumed from Table 5.2 because the value of ϕ_p was 42° and ϕ_r was 35° (Table 3.3).

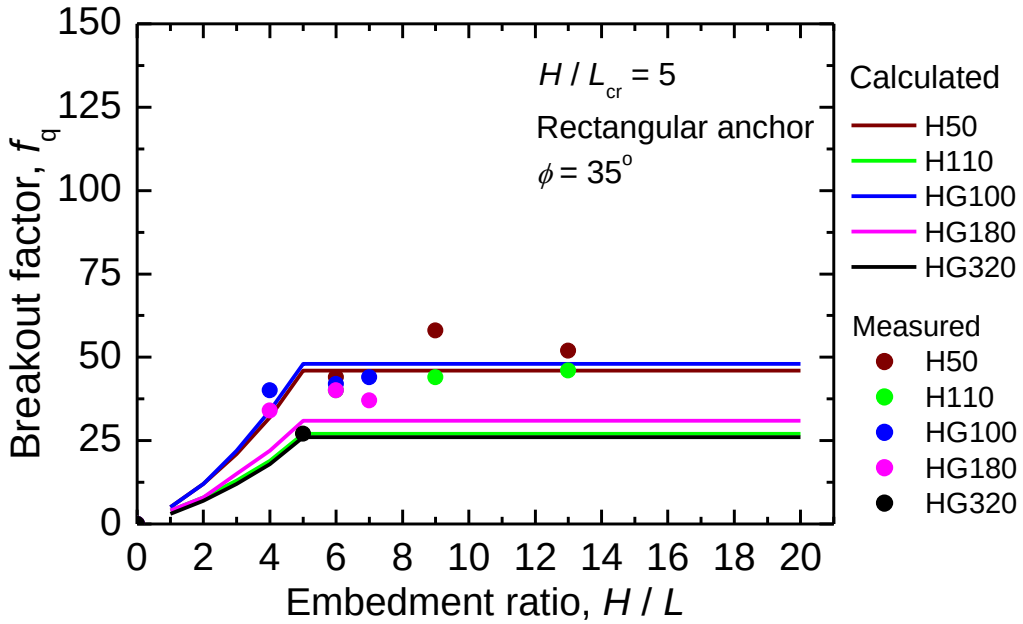

Fig. 5.9. Measured f_q (= $F_{max}/\gamma AH$) in Section 3.3 vs. calculated f_q (by Eq. 5.5).

Calculated f_q and measured f_q (= $F_{max}/\gamma AH$) (in Section 3.3) were compared in Fig. 5.9. Calculated values and measured values were qualitatively agreed well.

Generally, f_q increases as H/L increases up to $(H/L)_{cr}$, then becomes constant after that. Thus,

the f_q at $(H/L)_{cr}$ is maximum f_q, which is expressed as f_q^*. Calculated f_q from Eq. 5.5 were constant as f_q^* when $H/L \geq (H/L)_{cr} = 5$. Although there are not sufficient numbers of measured values at $H / L < (H/L)_{cr}$ in the field experiments in Section 3.3, similar to the calculated values, measured f_q seems to become constant at $H/L \geq (H/L)_{cr}$. If f_q at $H/L < (H/L)_{cr}$ were measured, the values perhaps increase exponentially as H/L increases until $(H/L)_{cr}$.

f_q calculated by calculated F_{max} based on the 3D models

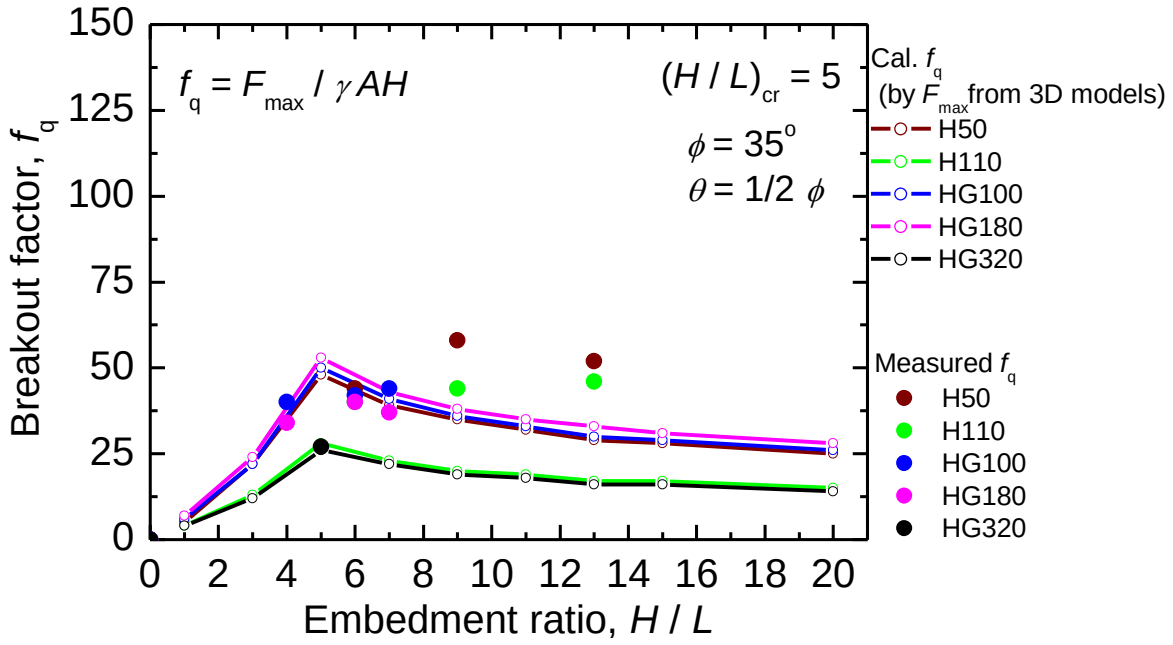

Fig. 5.10. Measured f_q (in Section 3.3) vs. calculated f_q (= $F_{max}/\gamma AH$) using F_{max} from the 3D models with $\theta = 1/2\ \phi$.

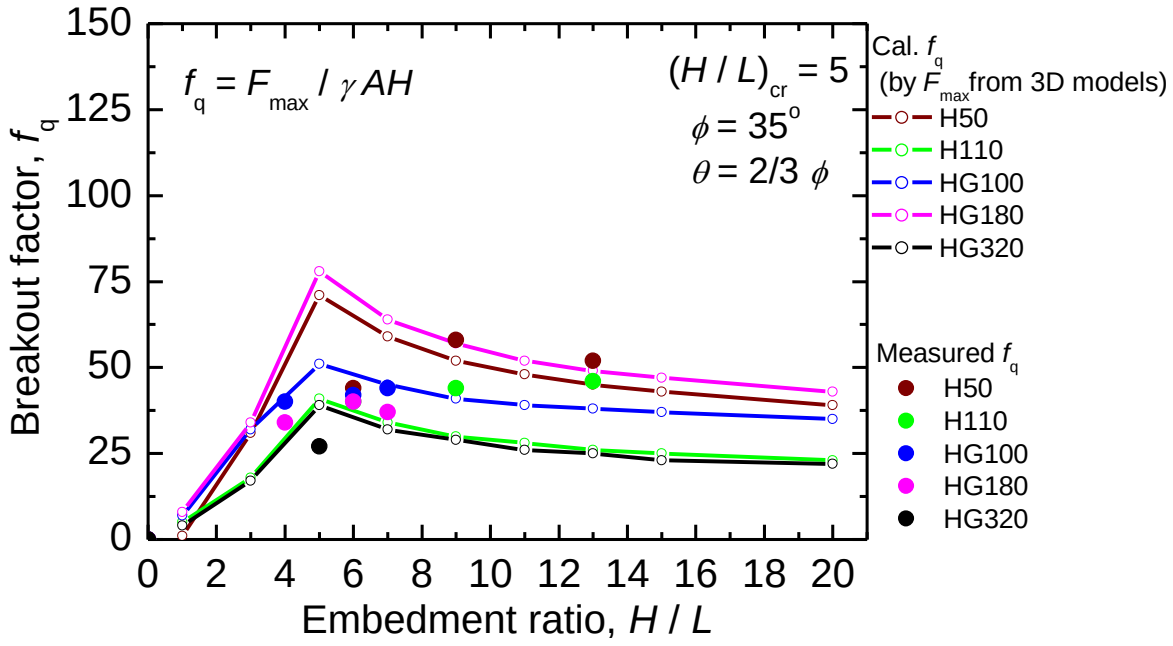

Fig. 5.11. Measured f_q (in Section 3.3) vs. calculated f_q (= $F_{max}/\gamma AH$) using F_{max} from the 3D models with $\theta = 2/3\ \phi$.

Figures 5.10 and 5.11 show the comparisons between measured f_q and calculated f_q from the F_{max} calculated using the 3D models (Fig. 5.2). Same as the theory, f_q became peak at $(H/L)_{cr}$. Then, f_q became almost constant while decreasing a little from the peak value. Although not in perfect agreement quantitatively, the overall trend of value range agreed well.

Estimation methods of F_{max} of flip anchors using f_q

For plate anchors, gross ultimate pull-out resistance $Q_{u(g)}$ is ordinary calculated by substituting f_q into following equations Eqs. 5.6 & 5.7 for Shallow anchor and Deep anchor, respectively (Das and Shukla, 2013).

For shallow anchor;

$$Q_{u(g)} = f_q \gamma A H + W_a \tag{5.6}$$

For deep anchor;

$$Q_{u(g)} = f_q^* \gamma A H + K_0 p (H - H_{cr}) \bar{\sigma}'_0 \tan\phi + W_a \tag{5.7}$$

where f_q is breakout factor for shallow anchor, γ is unit weight of a soil, A is projected area of an anchor, H is an embedment depth of anchor, W_a is a weight of an anchor, f_q^* is maximum breakout factor, K_0 is coefficient of earth pressure at rest, p is perimeter of an anchor shaft (rod), $\bar{\sigma}_0'$ is average effective stress between $(H - H_{cr})$, that is, $\bar{\sigma}'_0 = 1/2\gamma(H - H_{cr})$.

If the weight of an anchor and the frictional resistance of the shaft are neglected, Eqs. 5.6 & 5.7 can be simplified for F_{max} as Eq. 5.8 & Eq. 5.9.

$$F_{max} = f_q \gamma A H \quad [\, H/L > (H/L)_{cr} \,] \tag{5.8}$$

$$F_{max} = f_q^* \gamma A H \quad [\, (H/L)_{cr} \leq H/L \,] \tag{5.9}$$

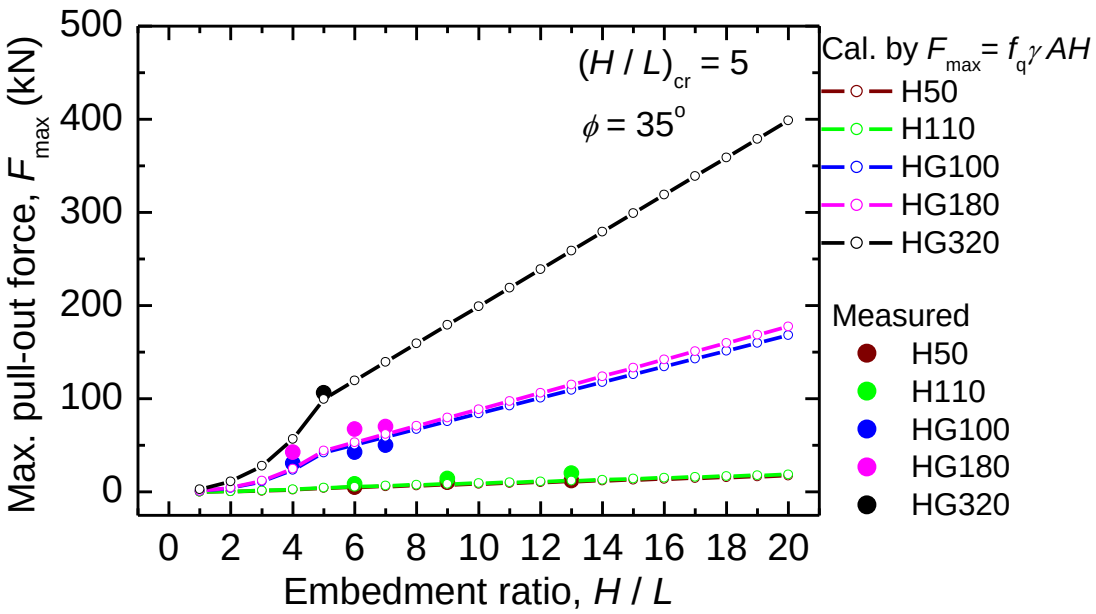

Fig. 5.12. Measured F_{max} (in Section 3.3) vs. calculated F_{max} (by Eq. 5.8 & 5.9) using f_q from Eq. 5.5.

Fig. 5.12 shows relationships between calculated F_{max} by Eq. 5.8 & Eq. 5.9 and measured F_{max}.

Calculated and measured values agreed well. Calculated F_{max} increase exponentially as H/L increase until $(H/L)_{cr}$. After passing $(H/L)_{cr}$, calculated F_{max} increase linearly. The tendency seems to be similar to measured F_{max}. For anchors having the same L, there is not much difference in calculated F_{max} even if B are different.

5.2.3 Discussion of Section 5.2

In this section, F_{max} of flip anchors were calculated by LEM based on 3D models and breakout factor f_q. The 3D models were made from the 2D model (Fig. 4.7, Fig. 5.1), assuming the flip anchor as a rectangle shape (Fig.5.4). Calculating F_{max} based on the 3D models, it is necessary to calculate the "Shallow anchor" and "Deep anchor" models separately. $(H/L)_{cr}$ is the boundary between "Shallow anchor" and "Deep anchor". The value of $(H/L)_{cr}$ depends on ϕ. In this study, $(H/L)_{cr}$ was set according to Meyerhof and Adams (1968).

Both methods using the 3D models and f_q can be promising ways to estimate F_{max} of flip anchors in sandy grounds. From the results, $(H/L)_{cr}$ can be reasonably determined according to the empirical values of Meyerhof and Adams (1968).

The calculated F_{max} using f_q is smaller, safer in other words, than F_{max} based on the 3D model until the H/L is about 10 or less. To reflect the difference of anchors having same L but different B on F_{max}, the method using the 3D models is more effective.

θ greatly affect the magnitude of F_{max}. Usually, $\theta = 2/3\ \phi$ are applied for the design of ordinary grouted ground anchors in sandy grounds. From the results of the field experiments, $\theta = 2/3\ \phi$ is reasonable for estimating F_{max} of flip anchors as well. And $\theta = 1/2\ \phi$, which is an average value by Meyerhof and Adams (1968), is safe for designing but might be too conservative, especially in deep anchor condition. In any case, when using the 3D models, the calculated F_{max} can be adjusted by the value of θ.

5.3 Calculations of F_{max} of flip anchors by Numerical analysis (FEM)

5.3.1 Introduction

Using finite element method (FEM), not only F_{max}, but also the relationships between F and w can be obtained. Furthermore, the 3D ground failure pattern also can be observed. Looking at those FEM analytical results comprehensively, an alternative estimation method of F_{max} for flip anchors using FEM are considered in this section.

5.3.2 Modelling of the ground and plate anchors

The field pull-out experiment (Section 3.3) was simulated by FEM analysis to examine the effectiveness of FEM analysis. A FEM analysis software Plaxis 3D was used for the FEM analysis.

As shown in Fig. 5.13, the ground with a length of 4.0 m, a width of 2.0 m, and a depth of more than H/L = 20 was modelled for each anchor used in the field experiments. For simplicity, the model was split in half, where the anchor plate was halved ($B_c/2$). (Table. 5.1). As the displacement boundary conditions, the horizontal displacement of the side surface and the vertical displacement of the bottom

surface were fixed. The Mohr-Coulomb model was applied to the soil constitutive law.

Table 5.4 shows parameters of the ground based on the ground conditions of the field experiments in Section 3.3 (see Table 3.4). Residual internal friction angle ϕ_r was adopted in the FEM analysis. Modulus of elasticity E' was empirically calculated by $E' = 2700\,N$ (kPa) based on measured N-values of the ground (Fig. 3.32). Table 5.5 shows parameters of an anchor plate based on the actual flip anchors used in the experiments (Fig. 3.34). Interfaces were made between below the anchor plate and sand.

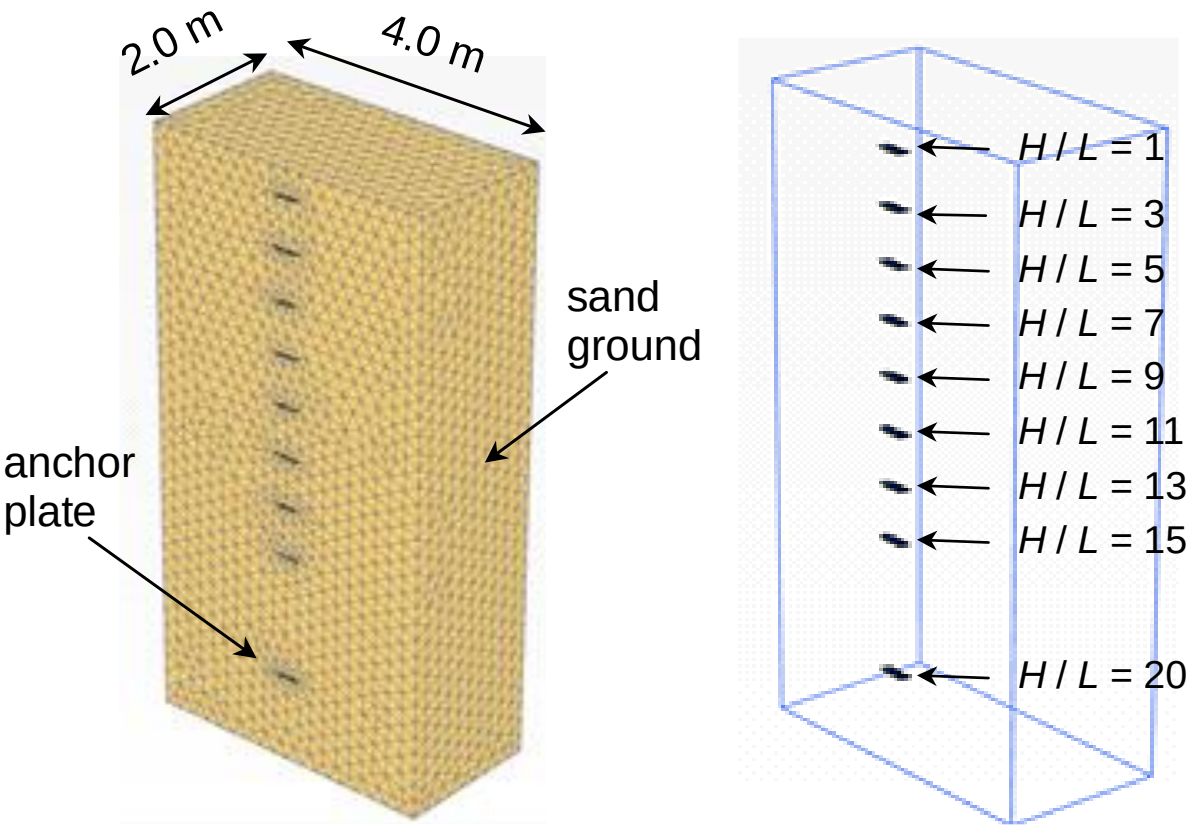

Fig. 5.13. Modelling of the ground and plate anchors for FEM analysis.

Table 5.4. Parameters of the sand ground for FEM analysis.

Item	Value
Unit weight of the unsaturated soil, γ_{unsat} (kN/m^3)	17.101
Initial void ratio, e_{init}	0.540
Modulus of elasticity, E' (kPa)	8400
Poisson's ratio, ν	0.30
Cohesion, c (kPa)	0.0
Int. friction angle, ϕ (deg)	35
Dilatancy angle, ψ (deg)	0.0
The earth pressure coefficient at rest, K_0	0.43

Table 5.5. Parameters of the anchor plates for FEM analysis.

Item	Value
Unit weight, γ (kN/m^3)	71.54
Thickness, d (mm)	50.0
Young's modulus, E (GPa)	176.0
Poisson's ratio, ν	0.27

The following procedure were applied to simulate the pull-out experiment (Section 3.3).
a) Initial phase: K_0 self-weight analysis on horizontal ground was performed with $K_0 = 1 - \sin\phi$.
b) Pull-out phase: An anchor plate was set and vertical upward prescribe displacement that is equal to L was applied to the anchor plates.

5.3.3 Calculation of F_{max} of flip anchors by FEM

Pull-out force F vs. pull-out displacement w

Figures 5.14-5.18 show the relationships of F vs. w for each H/L. F becomes larger with an increasing H/L. The tendency of the relationship changes with increasing H/L. When $H/L \leq 5$, F_{max} was clearly appeared; whereas when $H/L > 5$, F_{max} cannot be defined because F kept increasing. The tendency of the relationship of F vs. w seems to shift from general shear failure to local shear failure with increasing H/L. And $(H/L)_{cr}$ is regarded as a turning point of switching the tendency. In these cases (Figs. 5.14-5.18), $(H/L)_{cr}$ should be between 5 and 7.

Thus for Deep anchors [$(H/L)_{cr} \leq H/L$], maximum allowable w is need to be defined to determine F_{max}. Some references (Das and Puri, 1989) regard the point of w where the gradient ($\Delta F/\Delta w$) changes to the minimum as the maximum w at F_{max}. For flip anchors in this study, the amount of maximum allowable w for Deep anchor is defined as $L/2$.

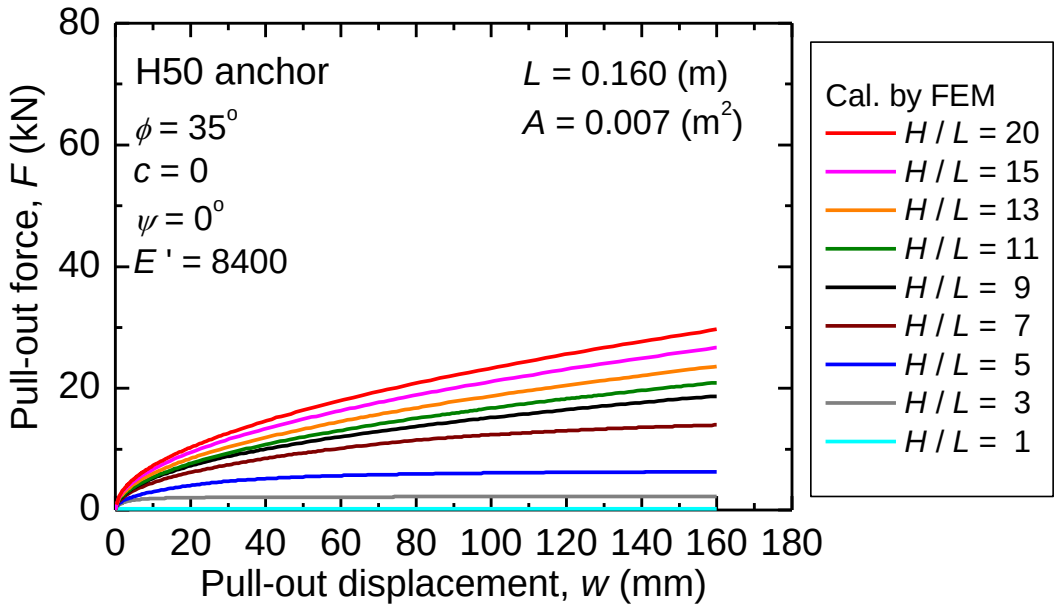

Fig. 5.14. F vs. w by FEM simulations for H50 anchor.

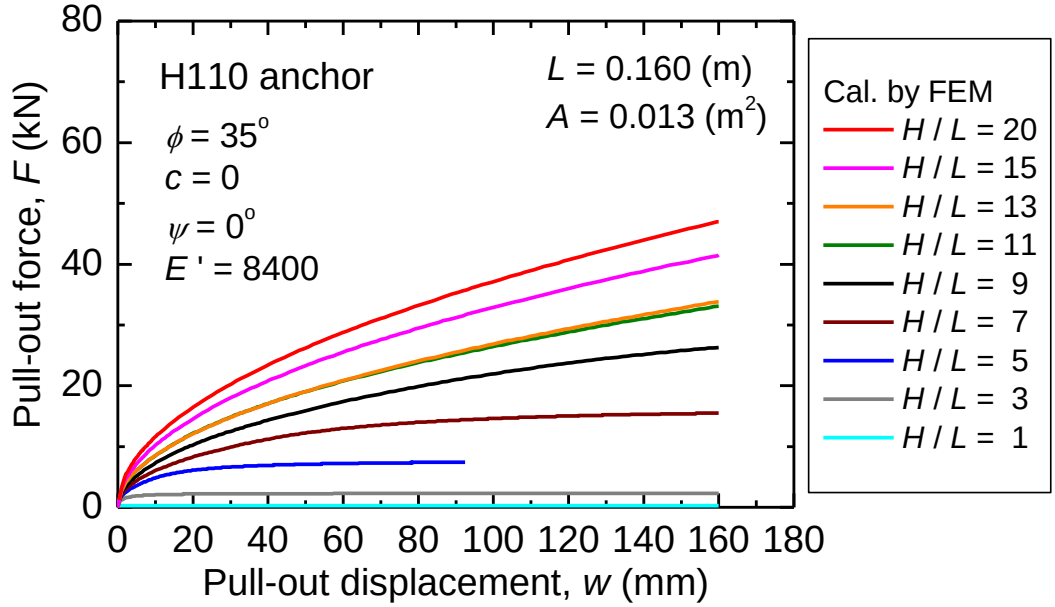

Fig. 5.15. *F* vs. *w* by FEM simulations for H110 anchor.

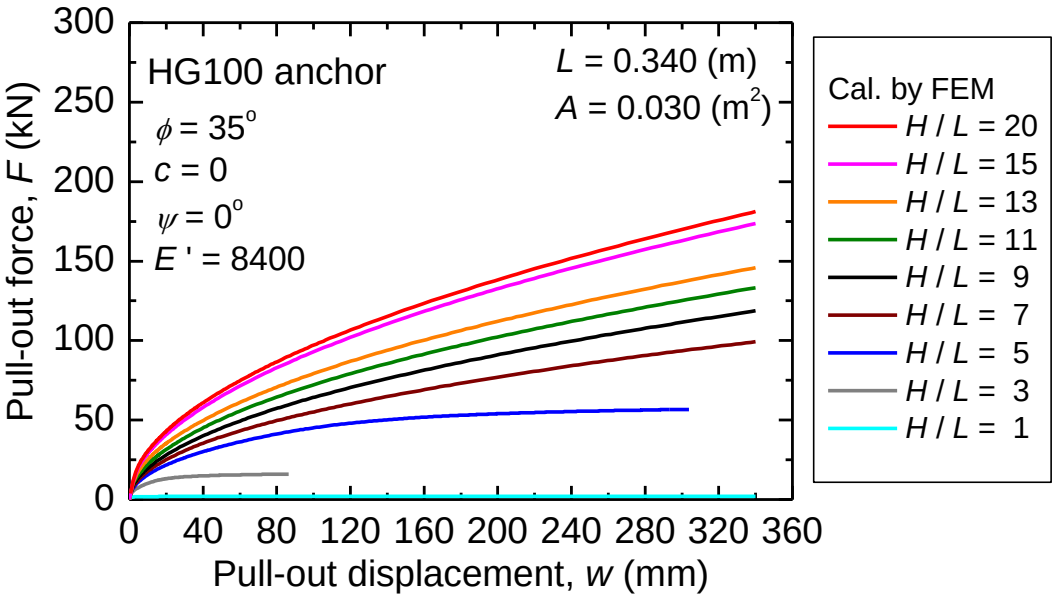

Fig. 5.16. *F* vs. *w* by FEM simulations for HG100 anchor.

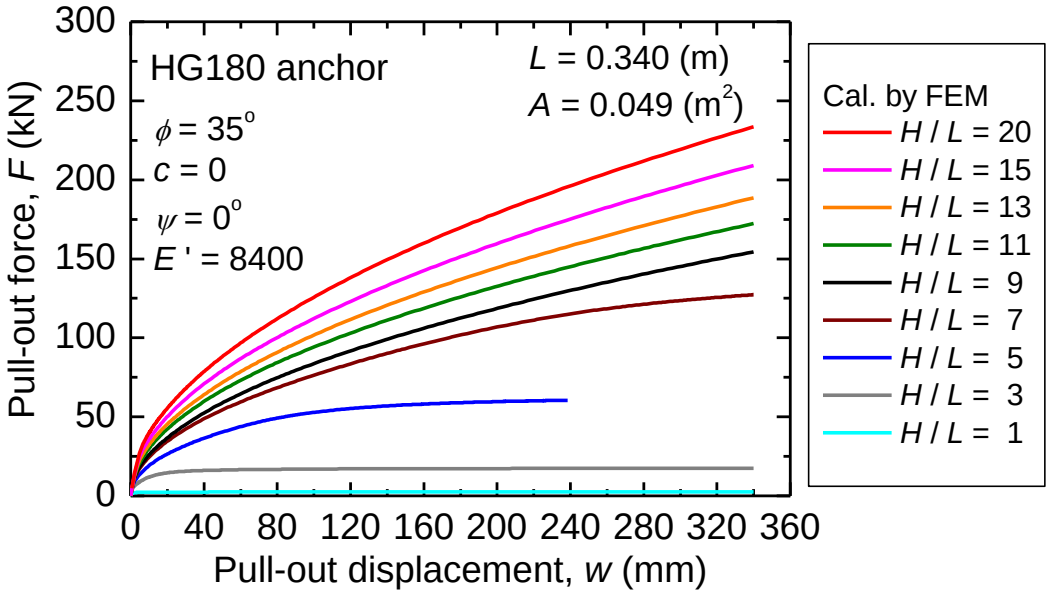

Fig. 5.17. *F* vs. *w* by FEM simulations for HG180 anchor.

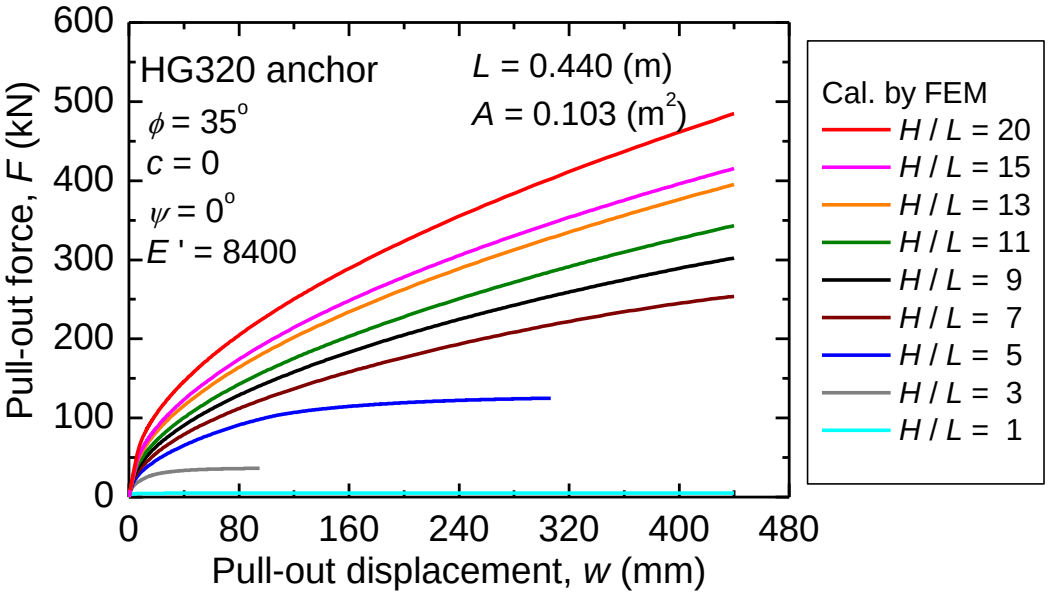

Fig. 5.18. *F* vs. *w* by FEM simulations for HG320 anchor.

Figure 5.19 shows F_{max} calculated by FEM vs. measured F_{max} (Section 3.3). The calculated and measured values are in good agreement. F_{max} of each anchors in deep anchor condition were got from F at $w = L/2$. F_{max} become larger with increasing A or H/L. The increasing tendency of F_{max} changes from an exponential increase tendency to a linear increasing tendency at $(H/L)_{cr}$ as the boundary. That linear increasing tendency with increasing H is a reason why f_q for a deep anchor becomes constant value.

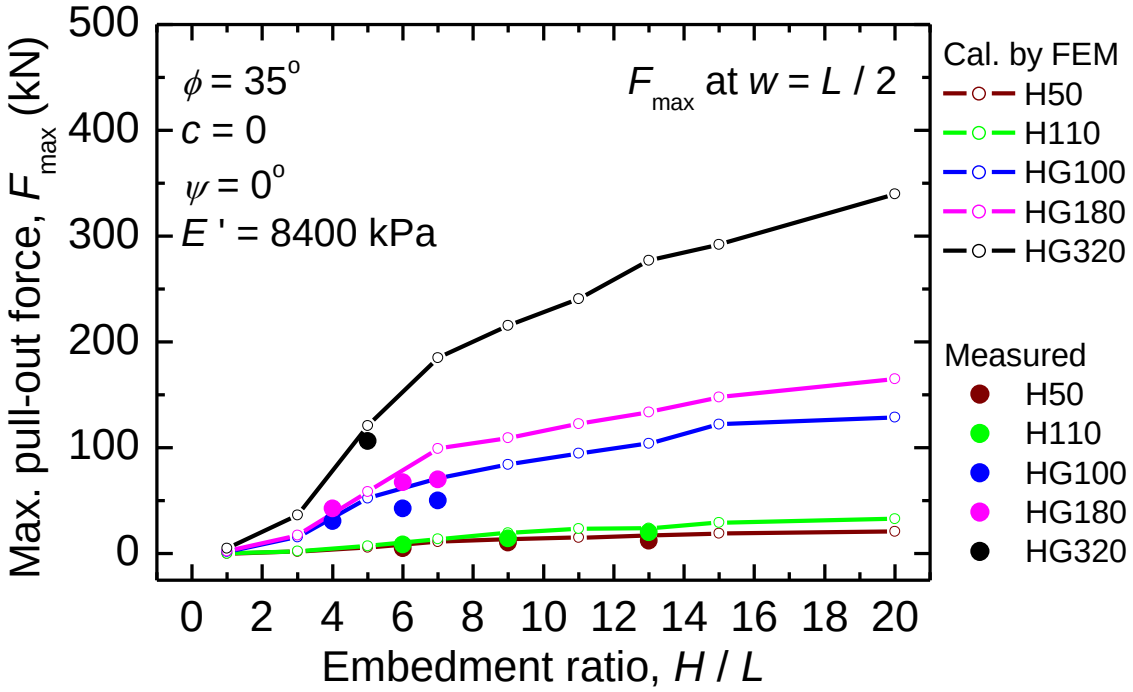

Fig. 5.19. Measured F_{max} (in Section 3.3) vs. calculated F_{max} (by FEM).

Break-out factor f_q vs. Embedment ratio H/L

Figure 5.20 is a re-expression of the above FEM analysis results (Fig. 5.19) in terms of the relationship between f_q and H/L. As well in LEM based on the 3D models (Figs. 5.11 & 5.12), f_q became almost constant while decreasing a little after $(H/L)_{cr}$. From the values of f_q, $(H/L)_{cr}$ can be assumed certainly around 5 to 7.

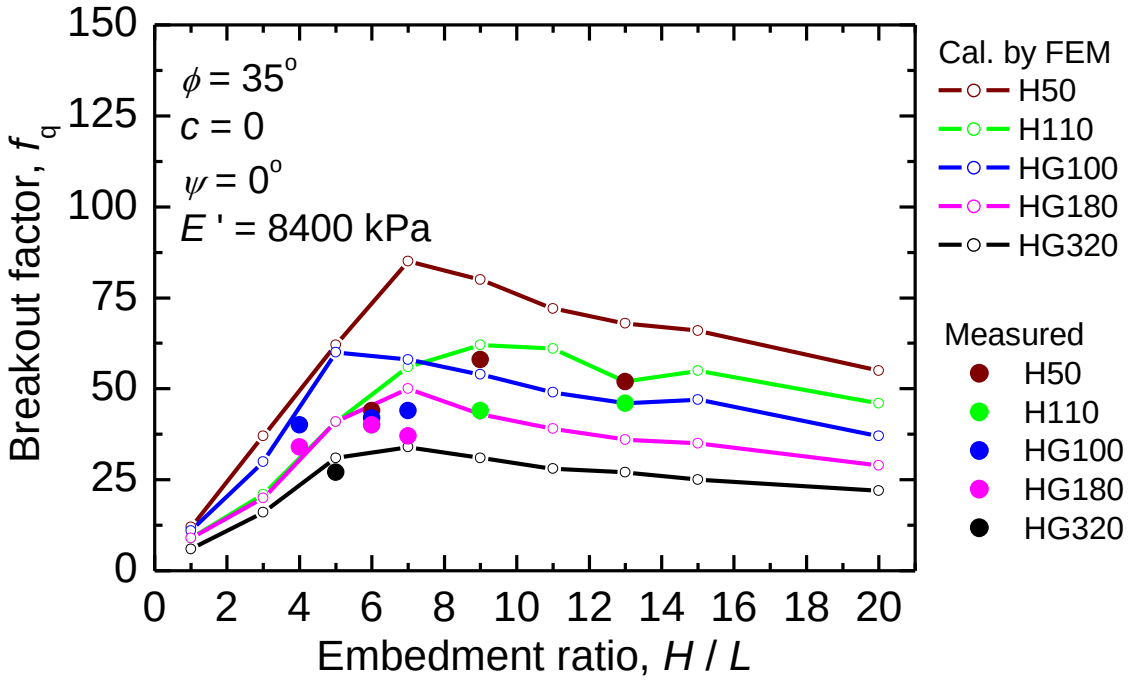

Fig. 5.20. Measured f_q (in Section 3.3) vs. calculated f_q (= $F_{max}/\gamma AH$) by FEM.

Displacement of the ground analysed by FEM

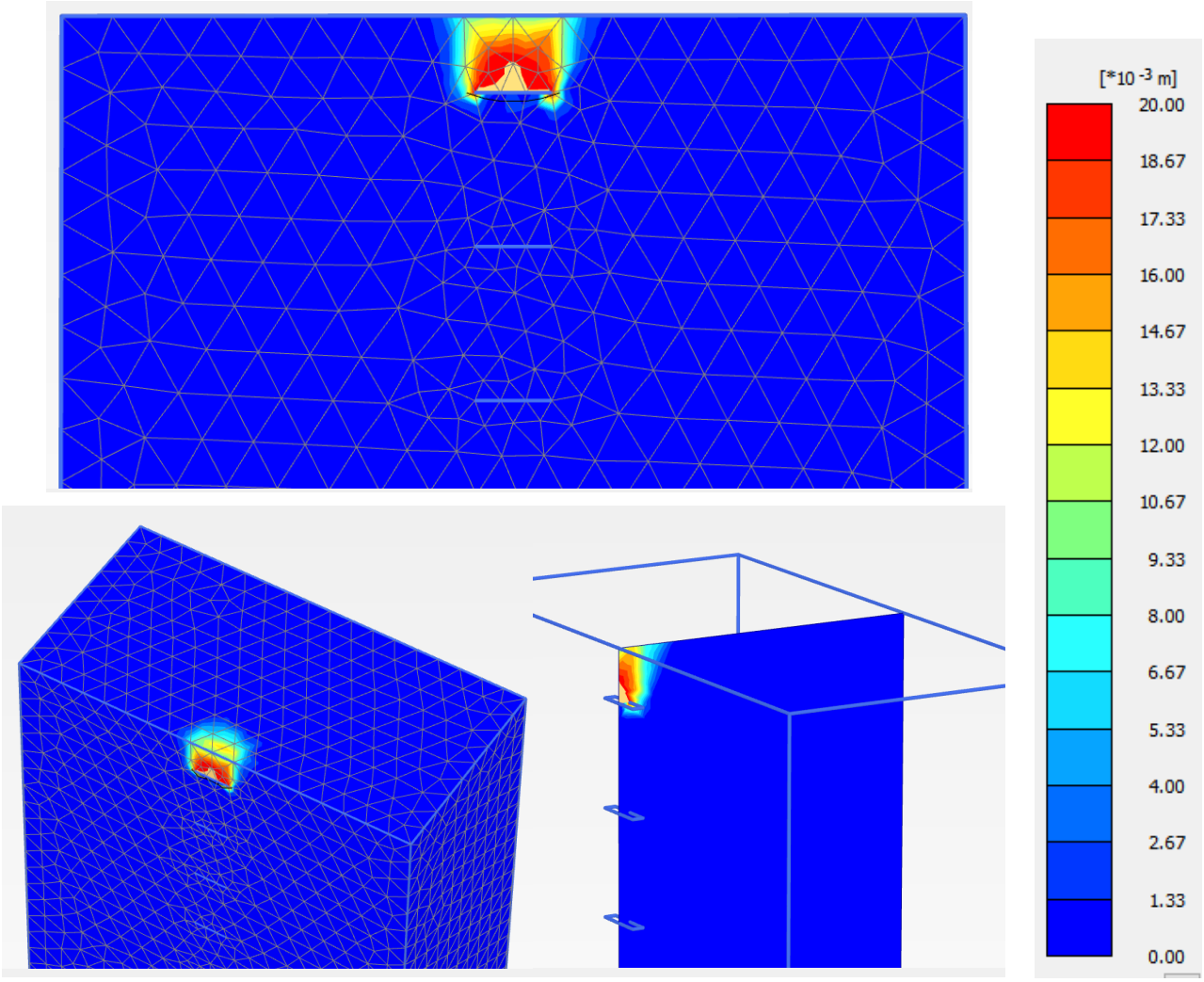

(a) Total displacement of the ground (@ w = 20 mm)

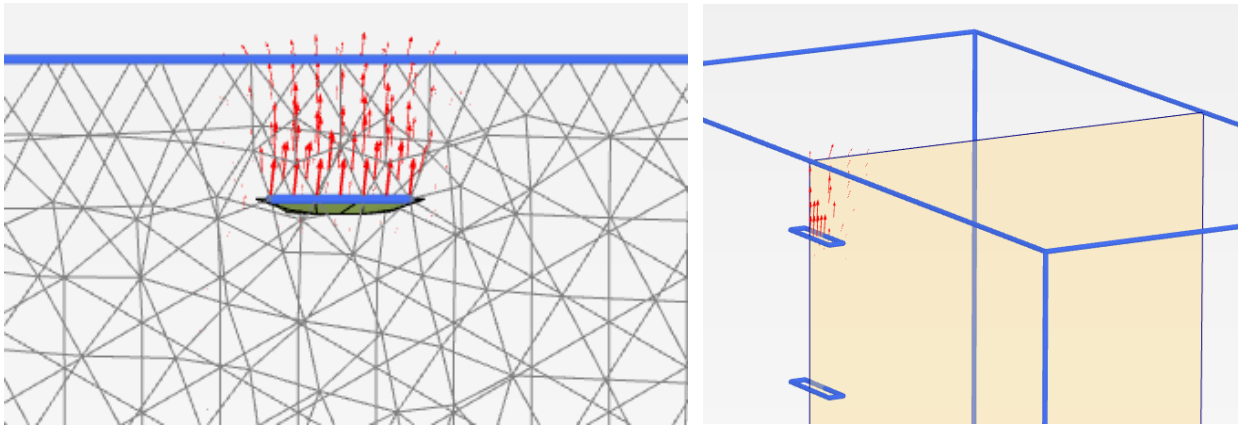

(b) Displacement vector (@ w = 20 mm, scaled up 5 times)

Fig. 5.21. Displacement (failure) of the ground observed by FEM (HG180, H/L = 1).

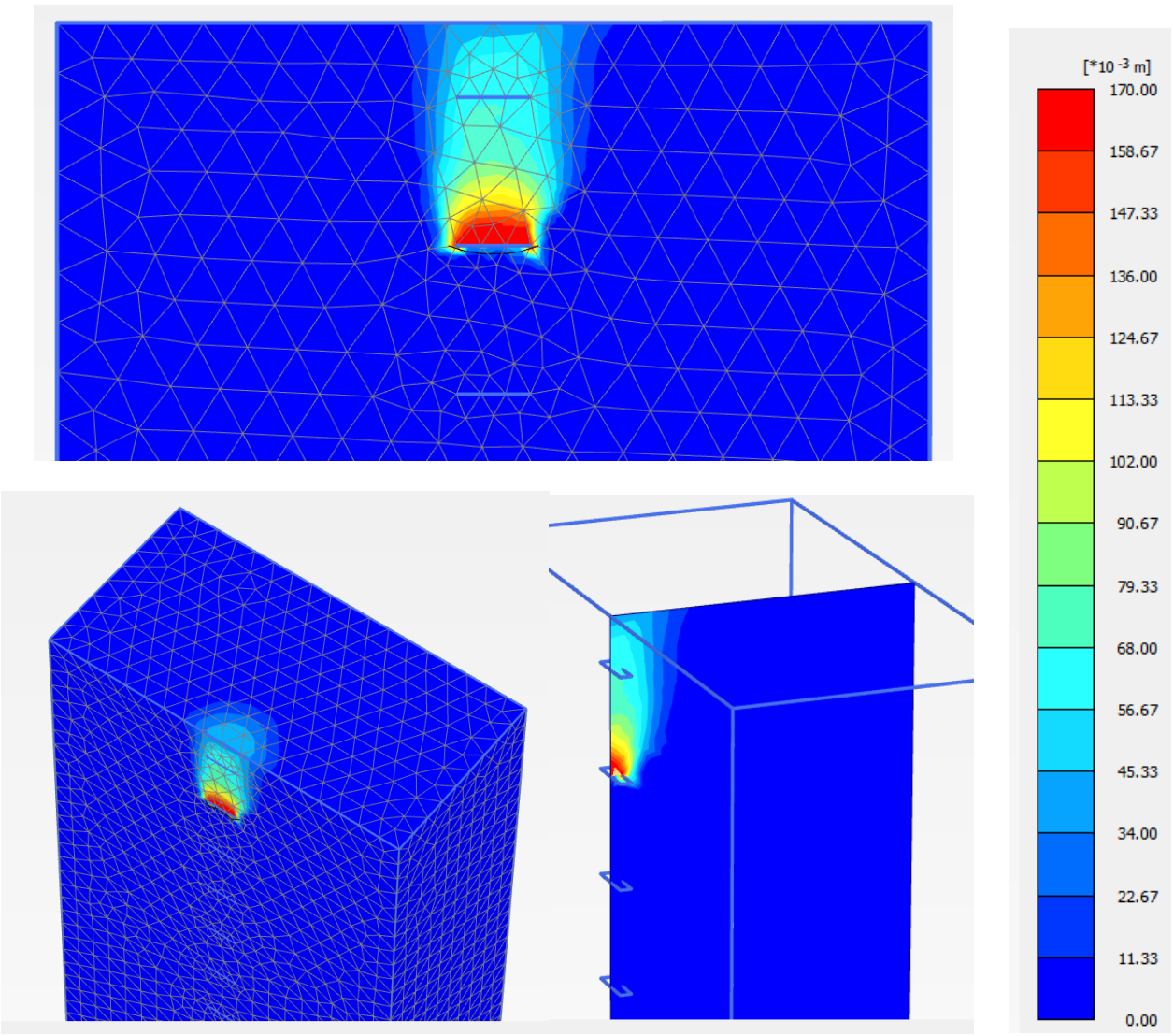

(a) Total displacement of the ground (@ w = 170 mm)

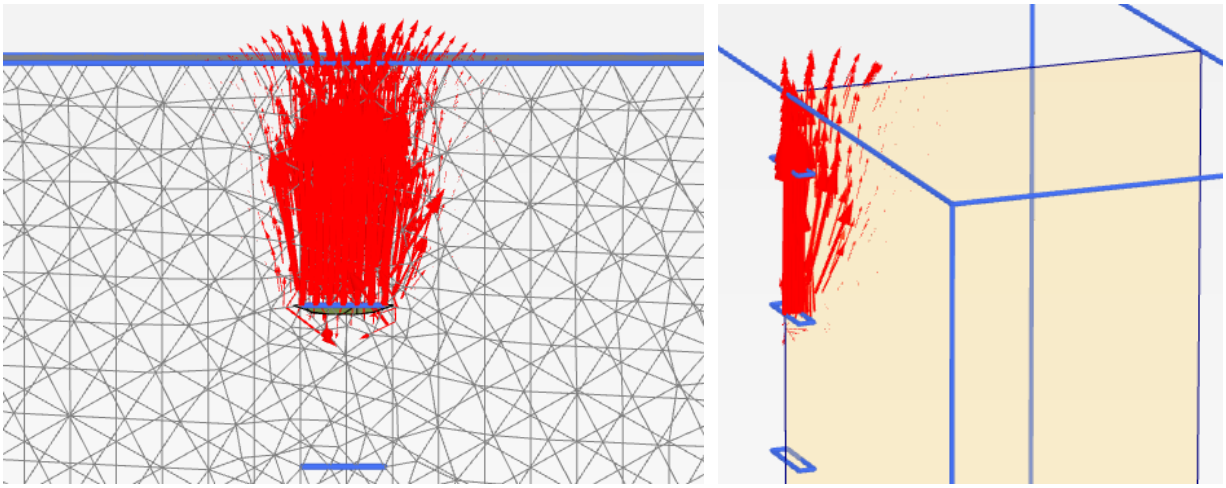

(b) Displacement vector (@ w = 170 mm, scaled up 5 times)

Fig. 5.22. Displacement of the ground observed by FEM (HG180, H/L = 3).

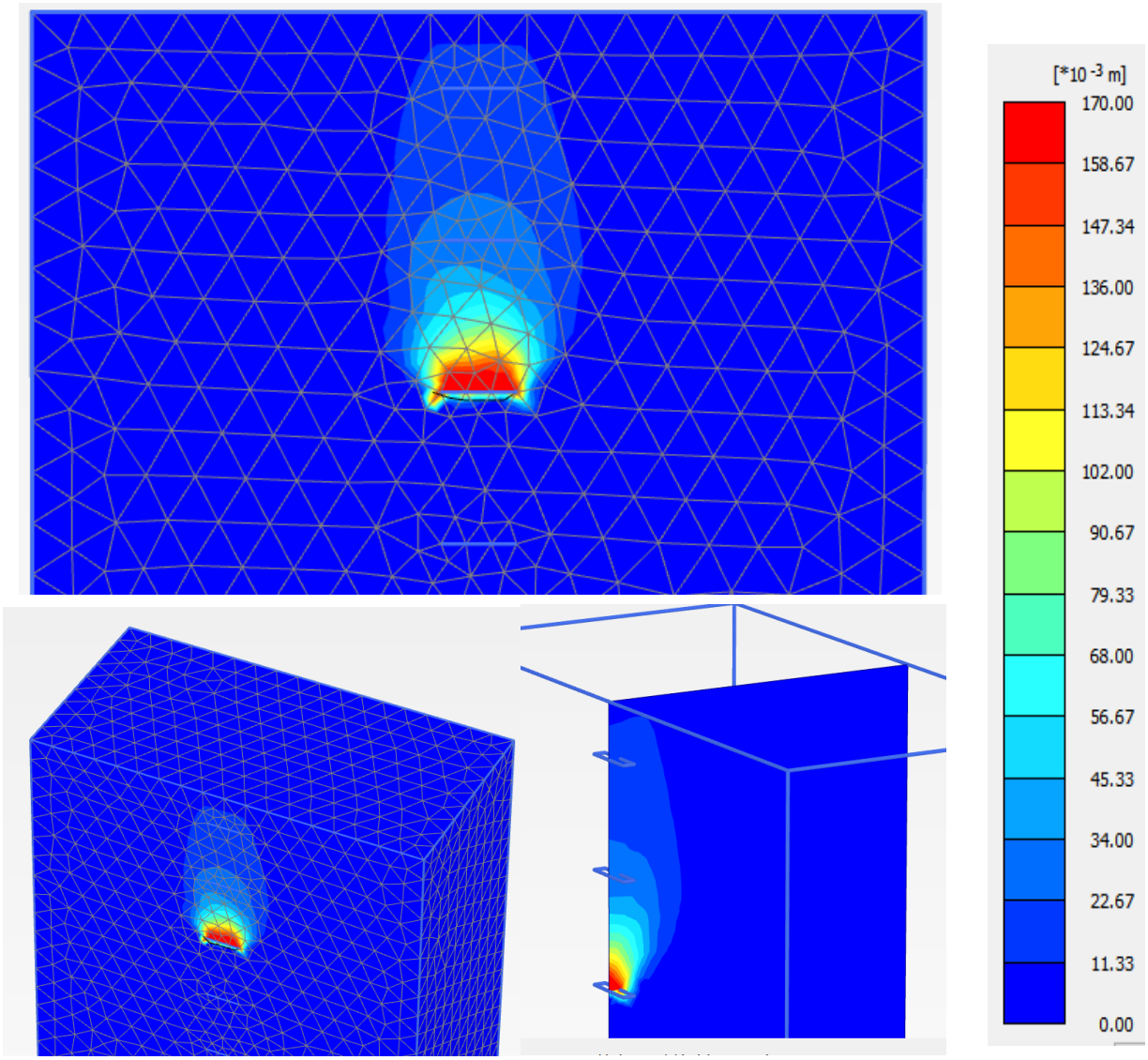

(a) Total displacement of the ground (@ w = 170 mm)

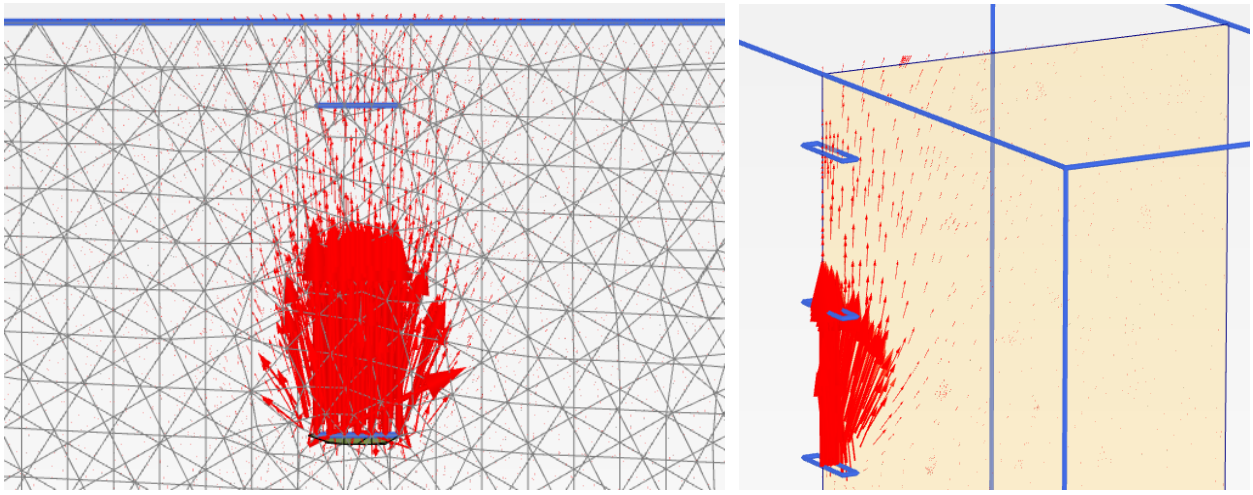

(b) Displacement vector (@ w = 170 mm, scaled up 5 times)

Fig. 5.23. Displacement (failure) of the ground observed by FEM (HG180, H/L = 5).

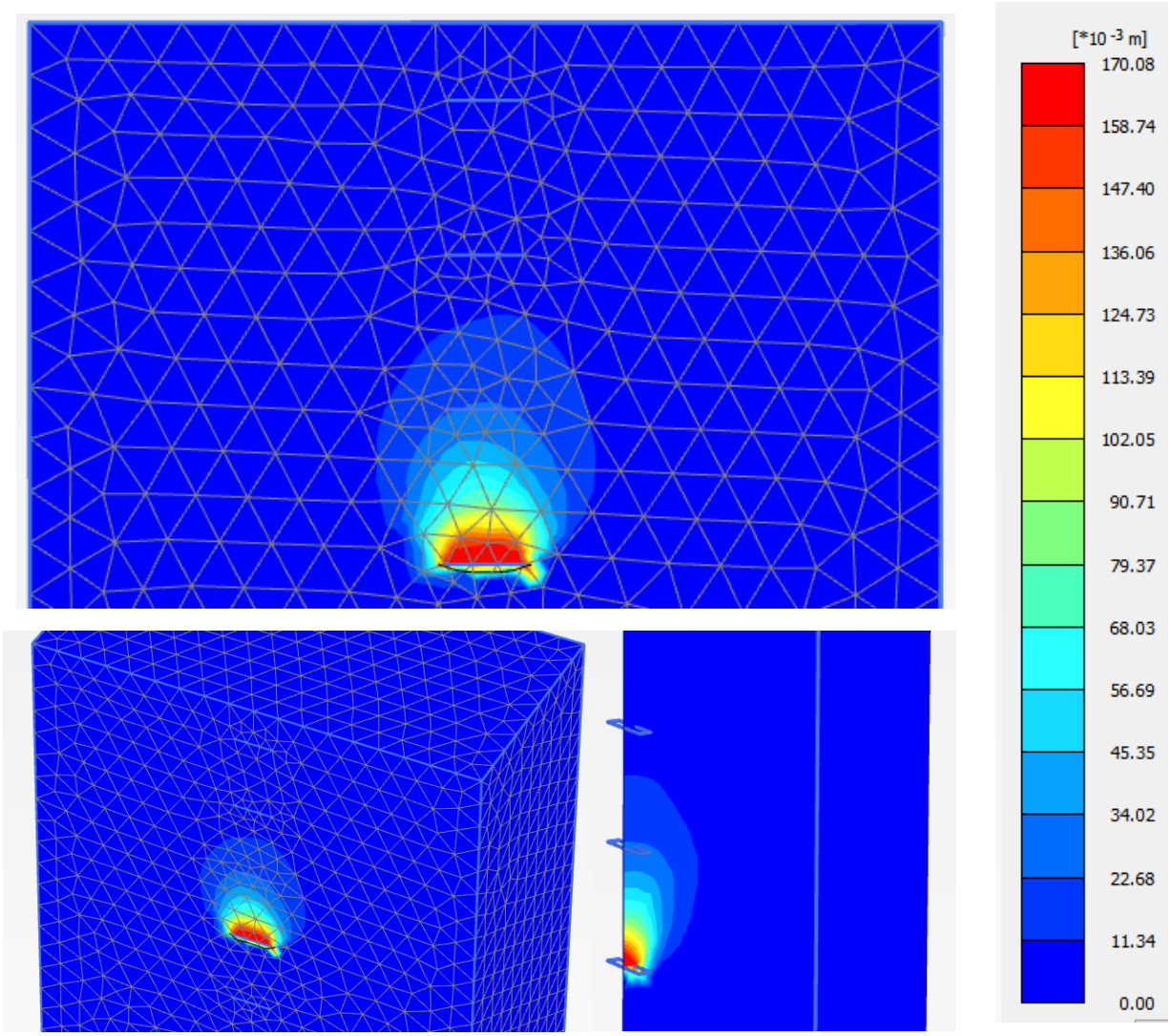

(a) Total displacement of the ground (@ w = 170 mm)

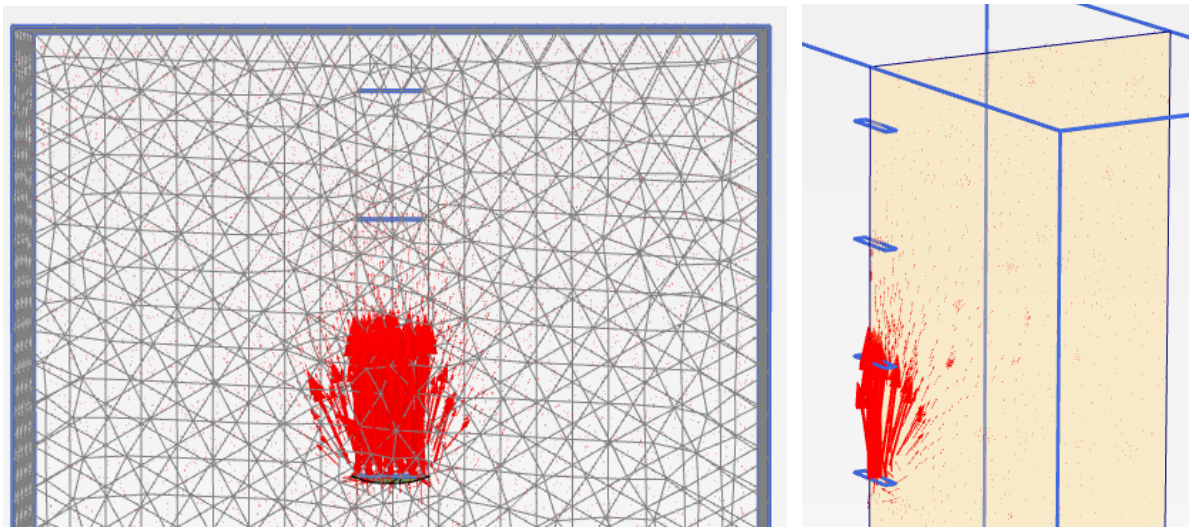

(b) Displacement vector (@ w = 170 mm, scaled up 5 times)

Fig. 5.24. Displacement (failure) of the ground observed by FEM (HG180, H/L = 7).

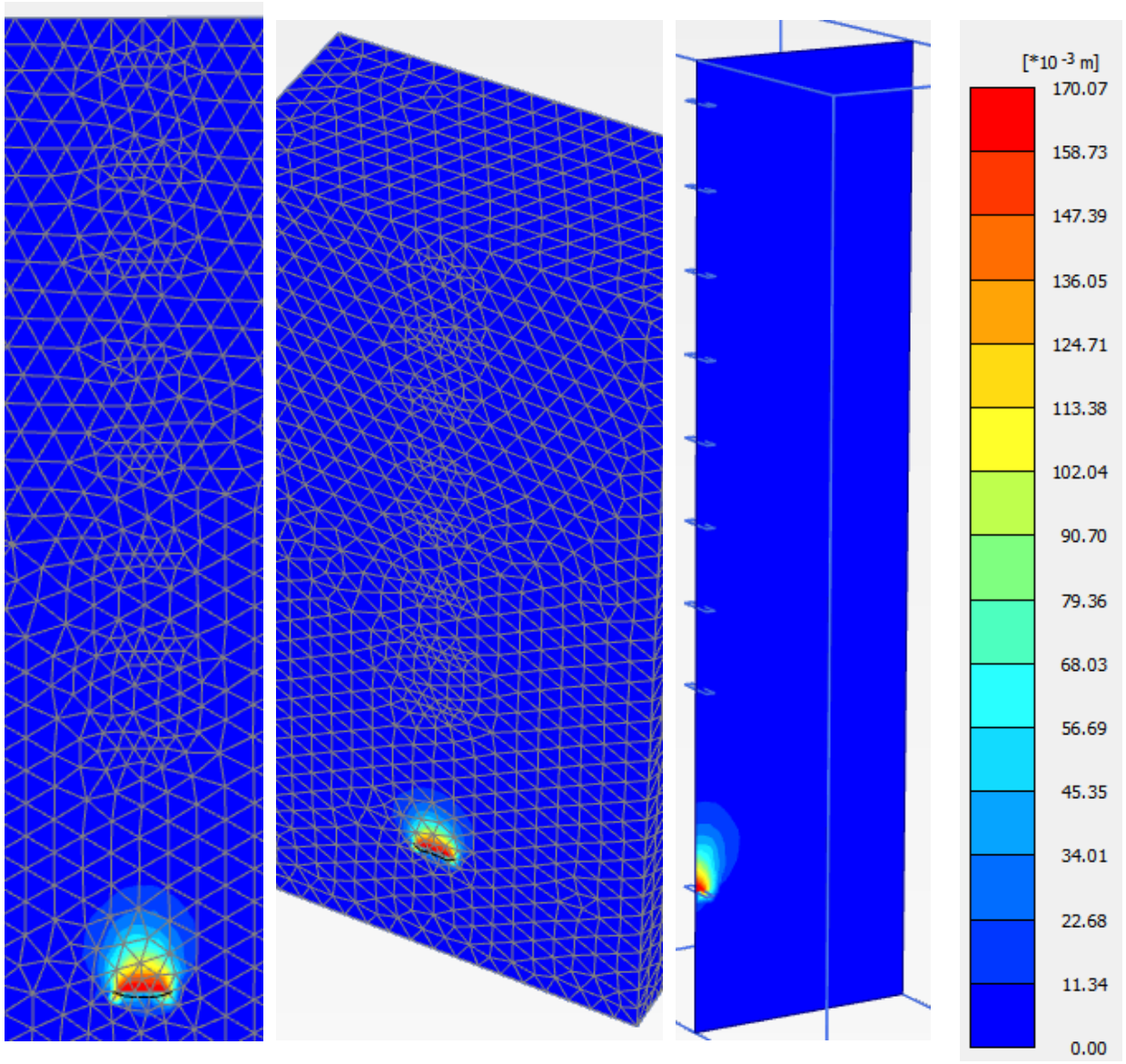

(a) Total displacement of the ground (@ w = 170 mm)

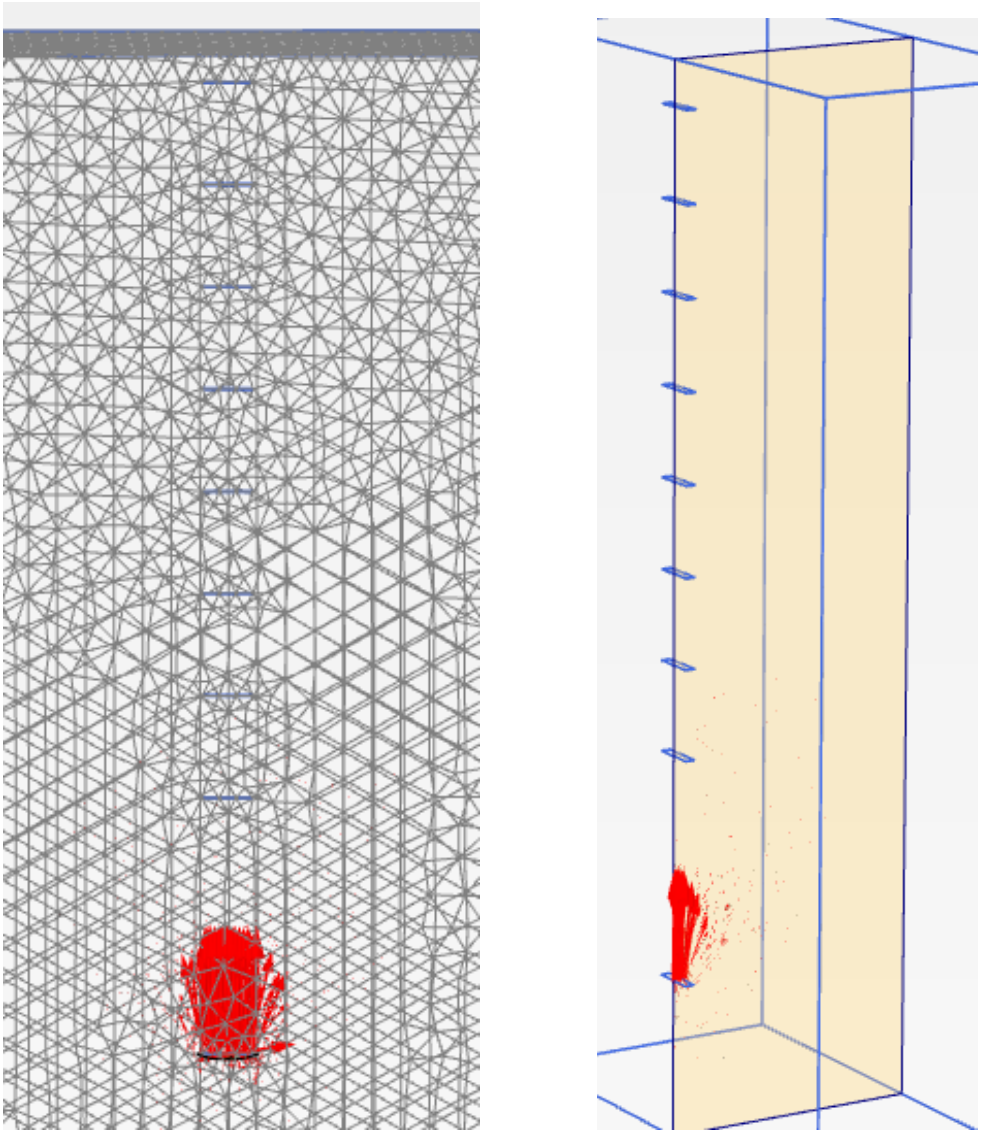

(b) Displacement vector (@ w = 170 mm, scaled up 5 times)

Fig. 5.25. Displacement of the ground observed by FEM (HG180, H/L = 20).

Figures 5.21-5.25 show the results of FEM analysis on displacement of the soil when the HG180 anchor was pulled until the w at F_{max}. The displacement affected the ground surface when H/L = 1, 3; however when H/L = 5 or more, the displacement did not affect the ground surface. From these results, H/L = 5 can be regarded as $(H/L)_{cr}$. 3D truncated-cone-shaped ground failure patterns were observed by FEM analysis.

5.3.4 Calculation of F_{max} of flip anchors by FEM for different pull-out conditions

Vertical pull-out vs. diagonal pull-out

Subsequently, pull-out resistance of a flip anchor pulled-out diagonally was calculated by FEM and compared with that of pulled vertically. Fig. 5.26 shows that the tendency of F vs. w of the anchor pulled diagonally were similar to that of pulled vertically.

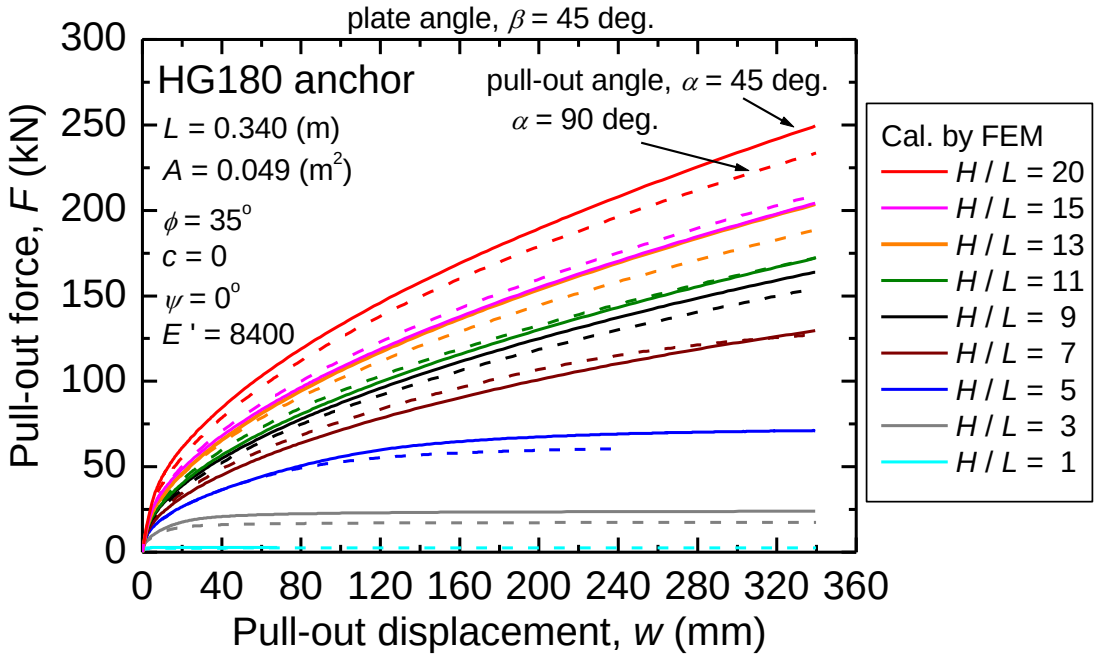

Fig. 5.26. F vs. w by FEM simulations for HG180 anchor pulled diagonally (α = 45°) or vertically (α = 90°).

Fig. 5.27 shows a comparison of measured F_{max} (Section 3.3), and calculated F_{max} of the anchor pulled diagonally or vertically. When F_{max} was plotted at $w = L/2$ where $(H/L)_{cr} \geq 5$, F_{max} of the anchors pulled vertically or diagonally were equivalent. This is similar to the results of the two-dimensional experiments in Section 4.3. As shown in Fig. 5.27, F_{max} of flip anchors pulled diagonally can be relatively larger than F_{max} of the anchor pulled vertically. The smaller the pull-out angle, the larger F_{max} is observed in Hanna et al. (2015). Thus, because it is easy and safer when designing, F_{max} of flip anchors pulled at any angle could be calculated based on the horizontal model pulled vertically (Section 5.2).

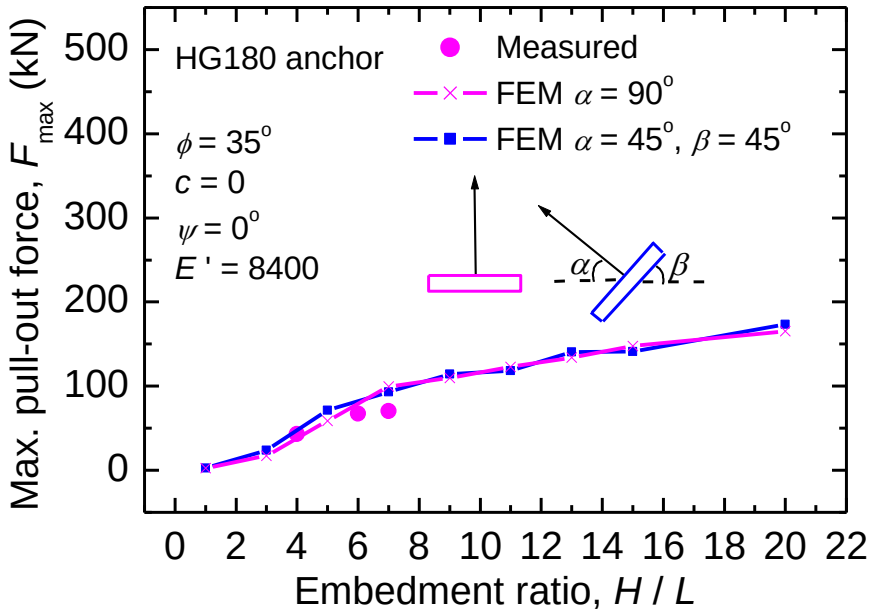

Fig. 5.27. Measured F_{max} of HG180 anchor pulled vertically in Section 3.3 vs. calculated F_{max} of HG180 anchor pulled vertically (α = 90°) or diagonally (α = 45°) by FEM.

As shown in Fig. 5.28 (a), when $(H/L)_{cr} < 5$, the displacement of the ground lifted by the anchor pulled diagonally reached the ground surface. As shown in Figs. 5.28 (b), (c) and (d), when $(H/L)_{cr} \geq 5$, the shapes of the ground failure were like a tilted vertical pattern by α.

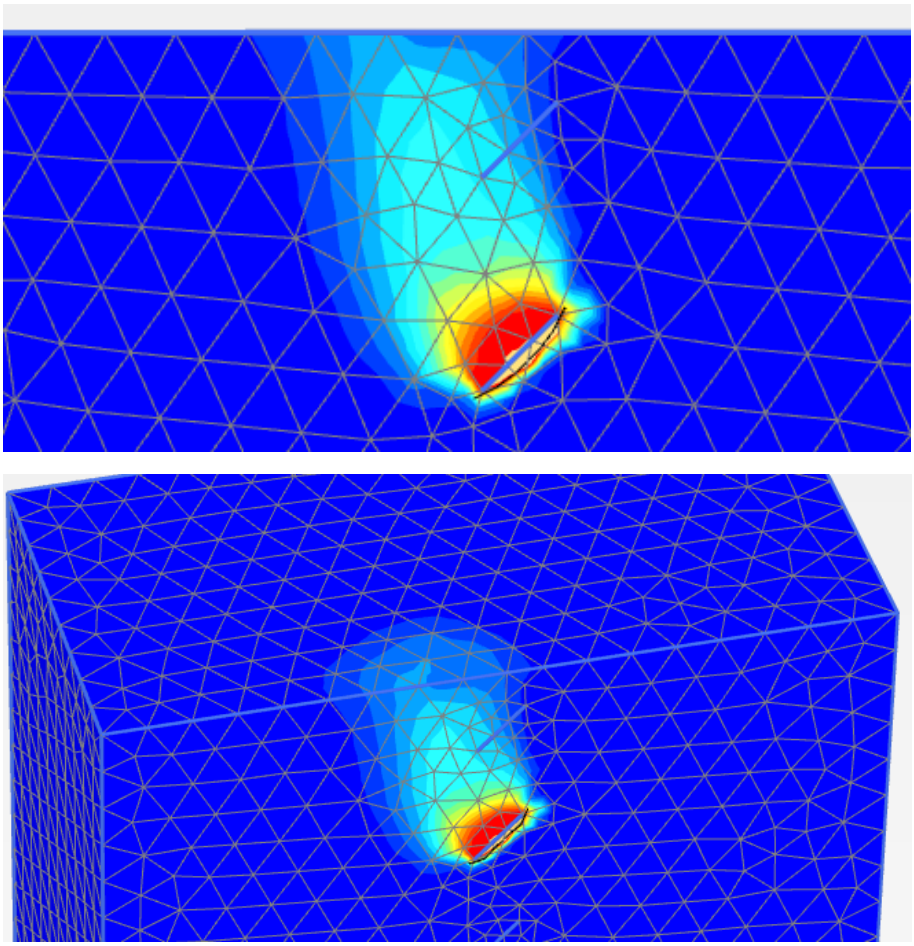

(a) $H/L = 3$

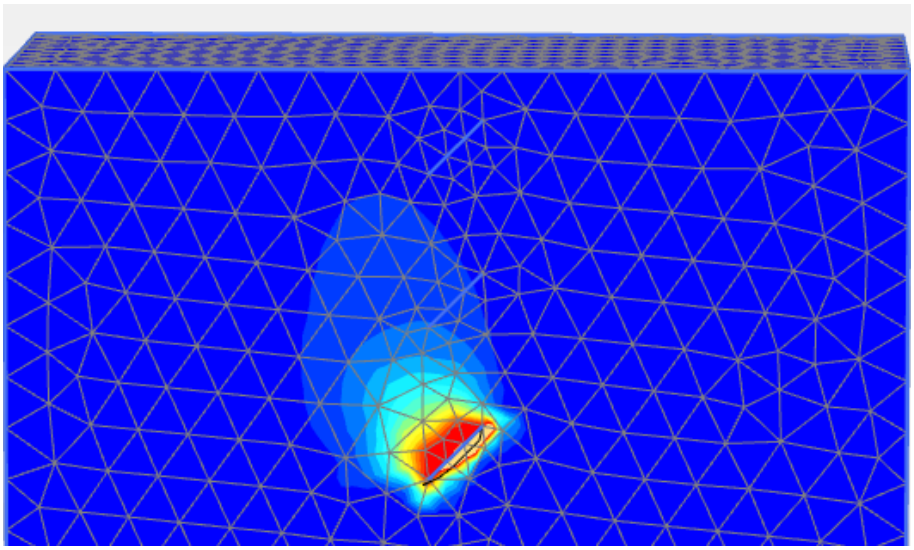

(b) $H/L = 5$

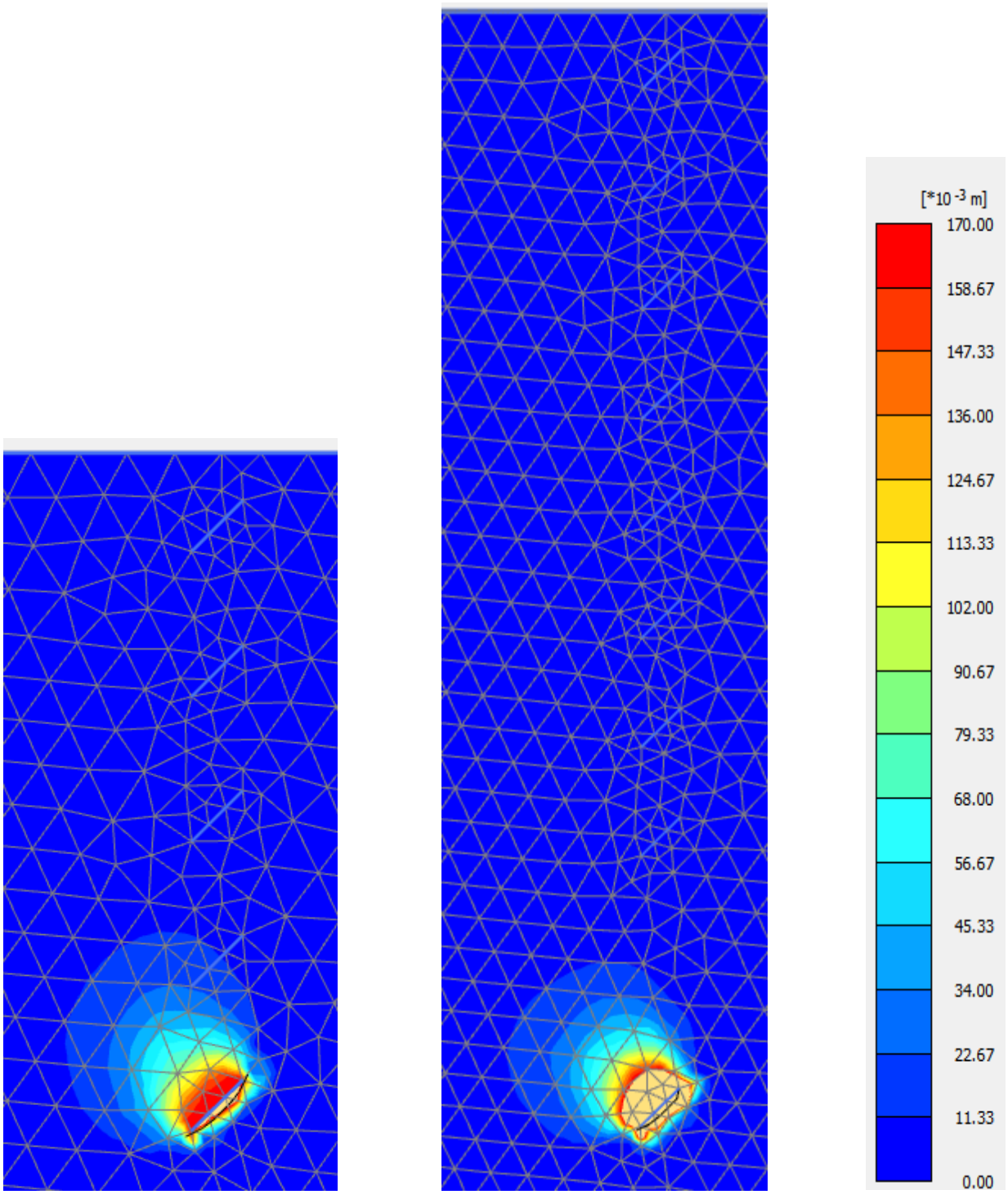

(c) H/L = 9 (d) H/L = 20

Fig. 5.28. Displacement of the ground observed by FEM (at w = 170 mm, α = 45°, β = 45°, HG180).

Fig. 5.29 shows the comparison of F vs. w of horizontal (β = 0°) and inclined (β = 45°) anchors pulled vertically (α = 90°). The inclined anchor imitates the anchor in the middle of opening or the anchor half opened (such as Fig. 3.53). As shown in Fig. 5.29, if the anchor half opened, F tend to be smaller than F of the horizontal (completely opened) anchor.

As shown in Fig. 5.30, F_{max} of the half opened anchor was about 2/3 of F_{max} of the anchor completely opened.

Pull-out of Full-opened anchor vs. half opened anchor

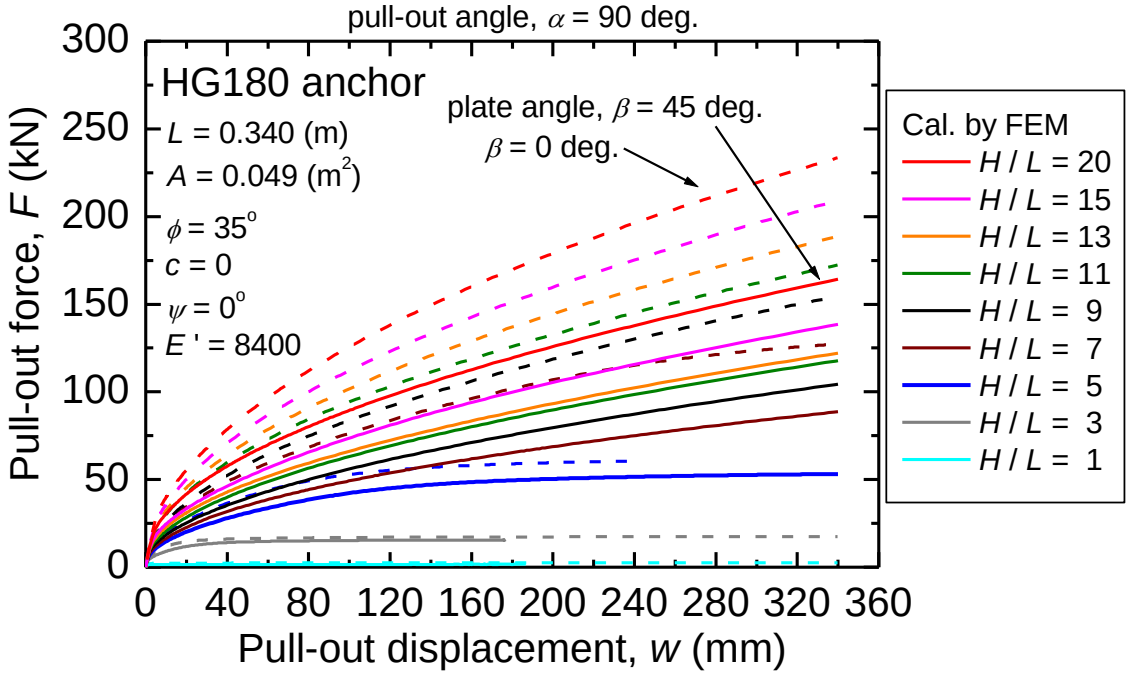

Fig. 5.29. F vs. w by FEM simulations for HG180 anchor embedded horizontally ($\beta = 0°$) or to be inclined at $\beta = 45°$.

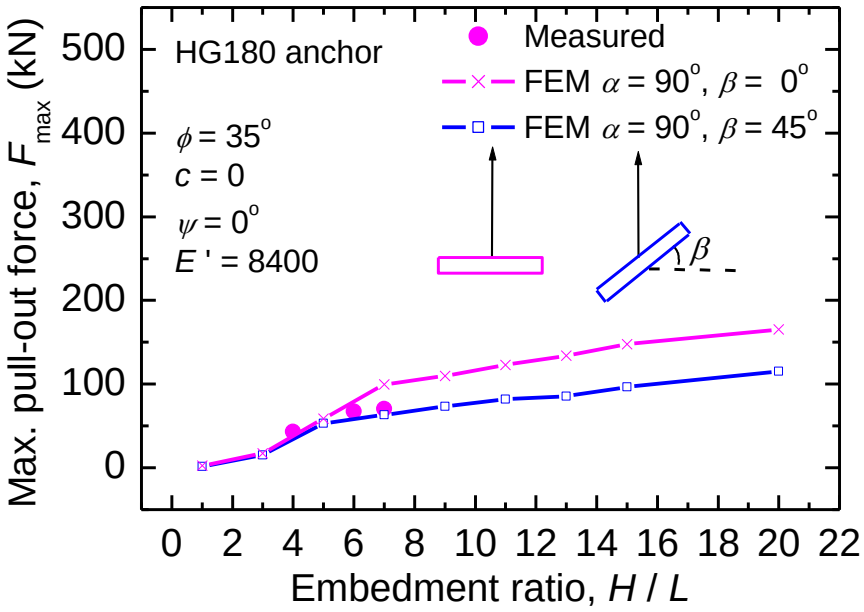

Fig. 5.30. Measured F_{max} of HG180 anchor pulled vertically in Section 3.3 vs. calculated F_{max} of HG180 anchor installed at $\beta = 45°$ and pulled vertically ($\alpha = 90°$) by FEM.

Fig. 5.31 shows the results of FEM analysis on displacement of the ground when pulling the inclined (half opened) anchor vertically. Although the basic tendency is not so different from that of

fully opened anchor, the displacement area seems to be distorted and slightly smaller. That might be the reason for the smaller F_{max}. Thus, in practice, it is particularly important to ensure that the anchor can be fully opened to be perpendicular to the pull-out direction. Conversely, when the anchor plate is half opened, it reaches 70% of F_{max} fully opened anchor.

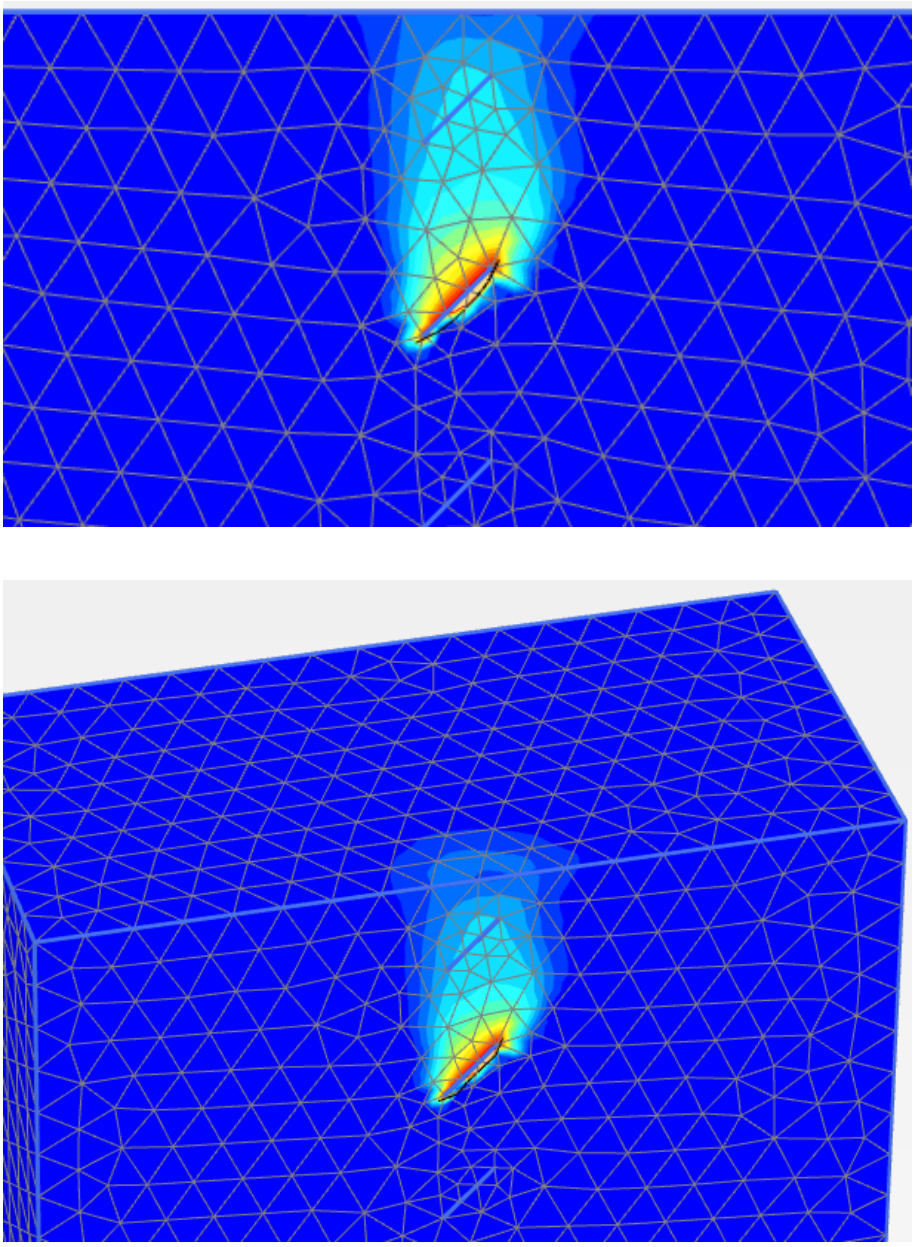

(a) H/L = 3

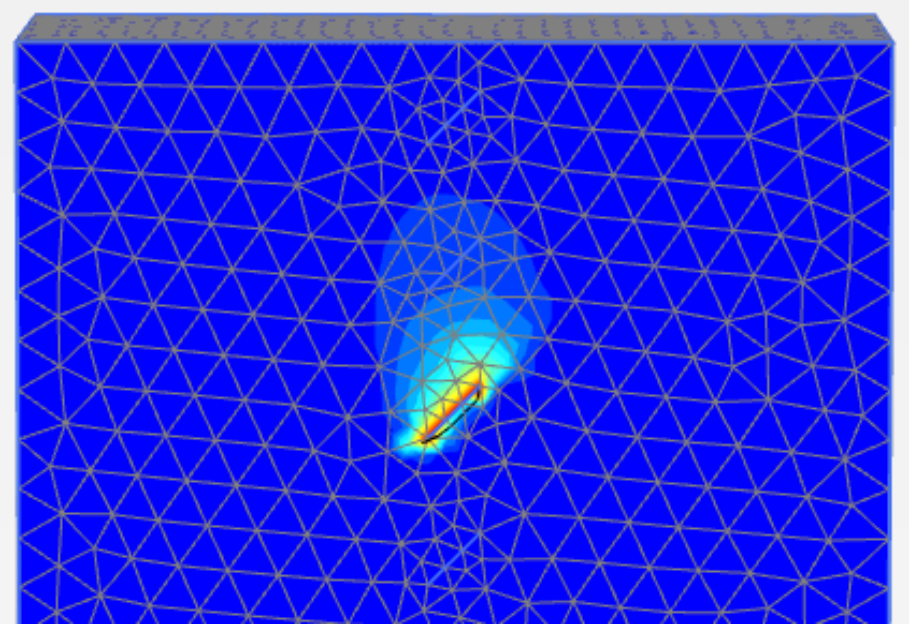

(b) H/L = 5

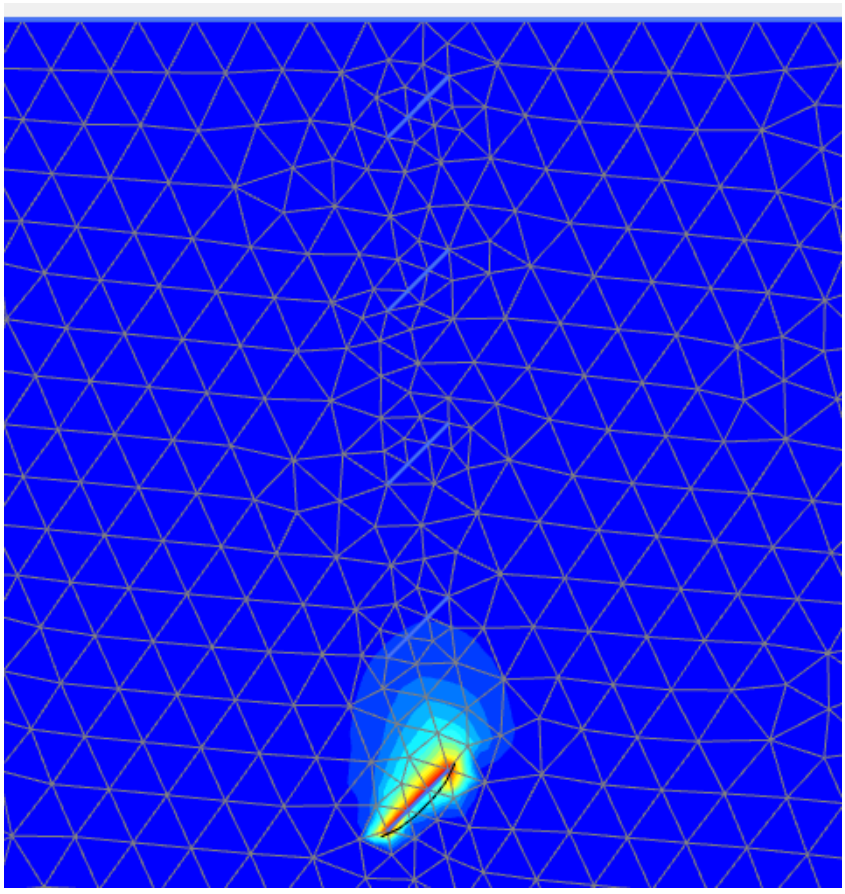

(c) H/L = 9

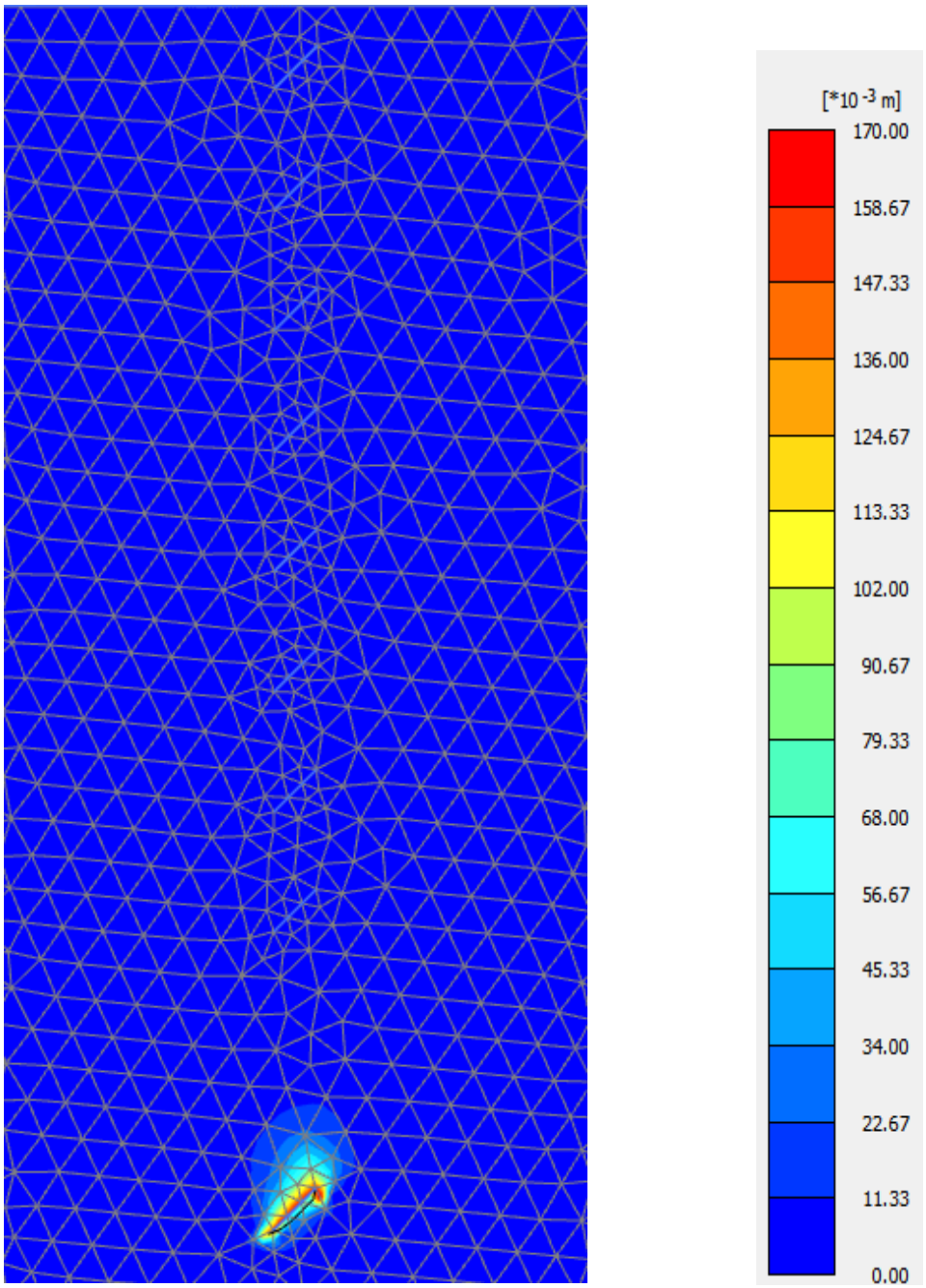

(d) H/L = 20

Fig. 5.31. Displacement of the ground observed by FEM (at w = 170 mm α = 90°, β = 45°, HG180).

5.3.5 Discussion of Section 5.3

In FEM analysis, the tendency of F vs. w in each H/L condition were observed. Because an apparent F_{max} did not appear when $(H/L)_{cr} \leq H/L$, F at $w = L/2$ was defined as F_{max}.

The calculated F_{max} by FEM agreed with the measured F_{max}. And the ground failure patterns observed by FEM analysis certainly changes from "Shallow anchor" to "Deep anchor" at $(H/L)_{cr}$ = 5, which was in common with the value assumed empirically.

5.4 Conclusion of Chapter 5

As shown in Figs. 5.32, calculated F_{max} of flip anchors by the above 3 methods using: 3D models, f_q, and FEM, agree well with each other overall.

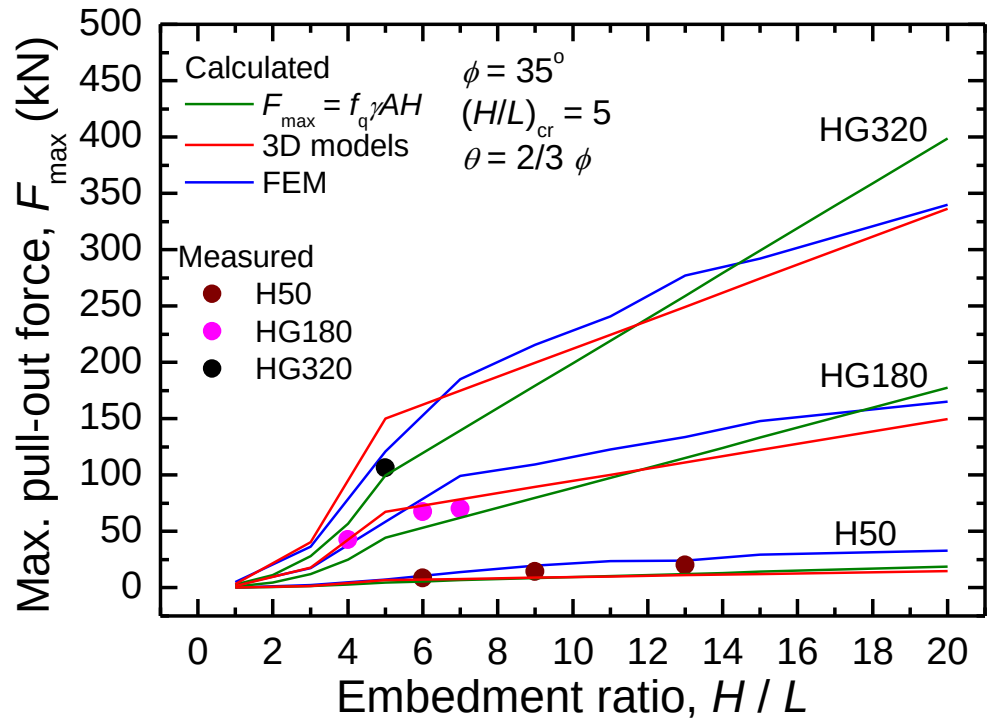

(a) $\theta = 2/3\ \phi$ for the 3D model

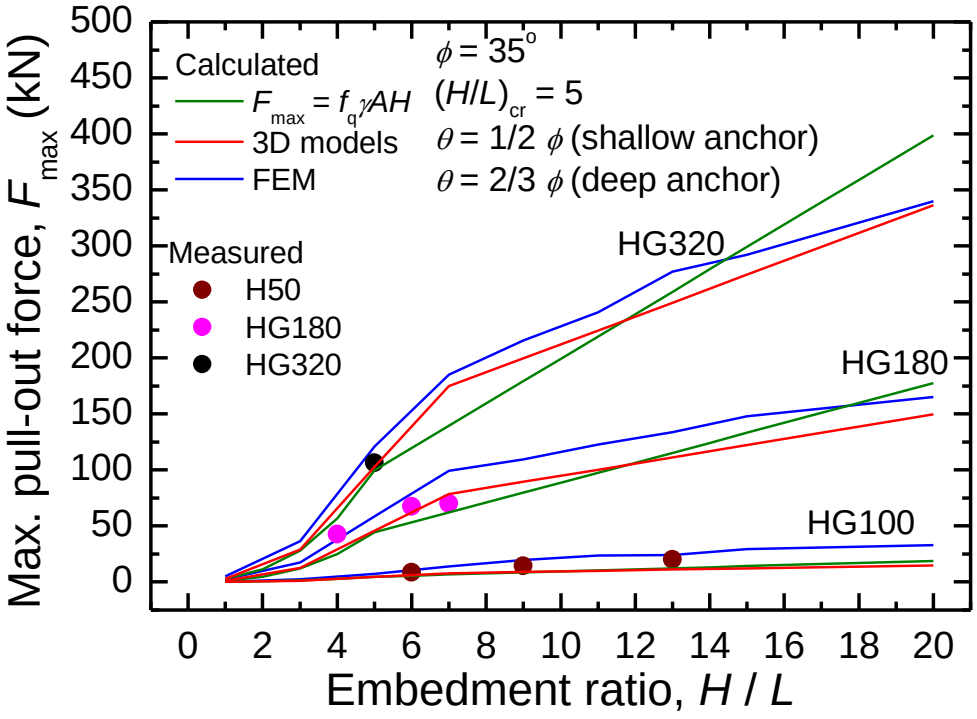

(b) $\theta = 1/2\ \phi$ (for shallow anchor) and $\theta = 2/3\ \phi$ (for deep anchor) for the 3D model

Fig. 5.32. Comparison of calculated F_{max} by each estimation method vs. measured F_{max}.

Calculated F_{max} by the 3D models with $\theta = 2/3\ \phi$ (Fig. 5.32a) agree well with measured values, but might be slightly overestimated for the largest anchor HG320 when $H/L < (H/L)_{cr}$. When $\theta = 1/3\ \phi$ for shallow anchor (Fig. 5.32b), calculated F_{max} by 3D models agreed better with the measured values for HG320. Thus, it seems safer to apply $\theta = 1/3\ \phi$ for shallow anchor, but F_{max} of deep anchor, $(H/L)_{cr} \leq H/L$, are tended to be underestimated with $\theta = 1/3\ \phi$. Thus, in Fig. 5.32b, calculated F_{max} based on the 3D models by applying θ properly to shallow ($\theta = 1/3\ \phi$) and deep anchor ($\theta = 2/3\ \phi$). If $\theta = 1/2\ \phi$ is applied when $H / L < (H/L)_{cr}$, and $\theta = 2/3\phi$ is applied when $(H/L)_{cr} \leq H/L$, the accuracy of the results was improved. By adjusting θ from $1/3\ \phi$ to $2/3\ \phi$, it is possible to design properly in consideration of economic and safety aspects.

The estimation method using f_q tends to underestimate F_{max} where practical anchor installation depths. In Fig. 5.32b, although the FEM slightly overestimates, the results using FEM agreed well with the results using 3D models.

These calculation results agreed well with measured F_{max} of flip anchors, but all the methods do not take into consideration the unique mechanism for flip anchor that rotate and open in the ground after being driven in closed state. The pull-out experiments (Chapter 3, 4) have shown that flip anchors can be attain about 80% or more of F_{max} of horizontal plate anchors having same A. In addition, the ground failure pattern at F_{max} is similar even if the anchors pulled out from opened from closed state.

Thus, if the amount of w required for flip anchors to open sufficiently is taken into considerations as Fig. 3.77, F_{max} of flip anchors can be reasonably estimated based on the above three methods. Looking back on the results of the experiment, the flip anchors (Closed, Driven) require w equal to L or up to 1.5 times L until the anchors sufficiently open. As a result, compared to horizontal plate anchors at same H, flip anchors should be installed (Driven) deeper by L. If the anchor plate is not fully opened, F_{max} will be about 70% as shown in Fig. 5.30. It is necessary to estimate F_{max} with such possibility in mind.

Furthermore, because the pull-out angle does not significantly affect F_{max}, and F_{max} tends to be larger in the diagonal pull-out as in Fig. 5.27, or Hannna (2015), it is thought to be safe to use the vertical pull-out model for any condition.

Studies on F_{max} of plate anchors have been conducted for more than half a century. Those studies and theories on plates anchors support this study for flip anchors. Not only that, the calculation results can be complemented by using numerical analysis as well as limit equilibrium method on plate anchors such as ones using f_q.

References in Chapter 5

Balla A. (1961). The resistance to breaking-out of mushroom foundations for pylons. Proceedings of the 5th international conference on Soil Mechanics and Foundation Engineering, 1, pp. 569-576.

Caquot A., and Kérisel J. (1949). Traité de mécanique des sols, Paris Gauthier-Villars.

Das B. M., and Seeley G. R. (1975). Breakout resistance of shallow horizontal anchors. Journal of the Geotechnical Engineering Division, 101(9), pp. 999-1003.

Das B. M, Seely G. R., and Das S. C. (1977). Ultimate resistance of deep vertical anchor in sand. Soils and Foundations, 17(2), pp.52-56.

Das B.M. and Puri V. K. (1989). Load displacement relationship for horizontal rectangular anchors in sand. Proc. 4th Int. Conf. Civil Struct. Eng. Computing, London, Civil-Comp Press, 2, pp. 207–212.

Das B. M., and Shukla S. K. (2013). Earth Anchors 2nd edition. J. Ross Publishing, Inc.

Ghaly A., Hanna A, and Hanna M. (1991). Uplift behavior of screw anchors in sand. I: Dry Sand. Journal of Geotechnical Engineering, 117(5), pp. 773-793.

Habib P. (1989). Recommendations for The Design, Calculation, Construction and Monitoring of Ground Anchorages. CRC Press, 136 pp.

Hannna A., Foriero A., and Ayadat T. (2015). Pullout capacity of inclined shallow single anchor plate in sand. Indian Geotechnical Journal, 45(1), pp. 110-120.

Lin J. G., Hsu S. Y., and Lin S. S. (2015). The new method to evaluate the uplift capacity of belled piles in sandy soil. Journal of Marine Science and Technology, 23(4), pp. 523-533.

Littlejohn G. S., and Bruce D. A. (1977). Rock anchors - state of the art. FOUNDATION PUBLICATIONS LTD.

Liu J., Liu M., and Zhu Z. (2012). Sand deformation around an uplift plate anchor. Journal of Geotechnical and Geoenvironmental Engineering, 138(6), pp. 728-737.

Meyerhof G. G., and Adams J. I. (1968). The ultimate uplift capacity of foundations. Canadian Geotechnical Journal, 5(4), pp. 225-244.

Zhao L., Li L., Yang F., and Liu X. (2011). Joined influences of nonlinearity and dilation on the ultimate pullout capacity of horizontal shallow plate anchors by energy dissipation method. International Journal of Geomechanics, 11(3), pp. 195-201.

Chapter 6
Loading experiments on the shoulder of a slope reinforced by plate anchors or flip-type earth anchors

6.1 Introduction

Flip anchors are expected to be applied to slope stability like grouted ground anchors and soil nails. For ground anchors and soil nails, pull-out resistance that contributes to slope reinforcement is usually designed with frictional resistance on the peripheral surface between grout and the ground. In case of flip anchors, pull-out resistance is expected by the bearing resistance of the anchor plate. Some softwares such as “Slides 2” (Rocscience Inc., 2021) allows the design of flip anchors for slope stabilizations as “End Anchored support” (Fig. 6.1).

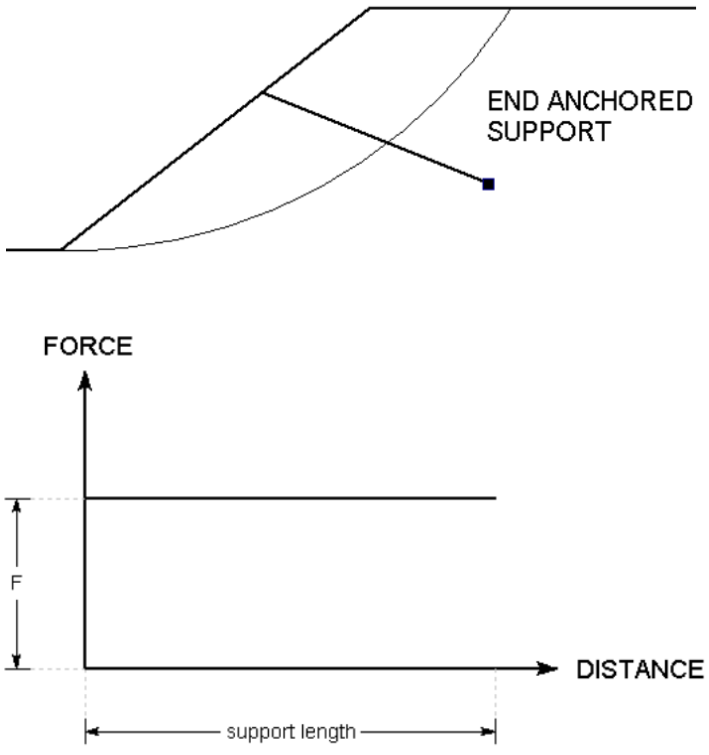

Fig. 6.1. Image and force diagram of end anchored support (Rocscience Inc., 2021).

To examine the applicability of flip anchors to slope stability, loading experiments on a shoulder of a model slope ground reinforced by model plate anchors or small actual flip anchors were conducted in a laboratory. The experiments using model plate anchors were conducted in a plane

strain condition to investigate reinforcement effect and to observe slope failure. Subsequently, the experiment using small actual flip anchors were conducted in a three-dimensional condition to investigate the same on flip anchors.

The slope reinforcement effect of the flip anchor was investigated by applying an external force to the unreinforced slope or reinforced slope with the anchors. Furthermore, the experiment was simulated by numerical analysis (FEM) as well.

6.2 Experimental studies

6.2.1 Outline of the experiments

As shown in Fig. 6.2, the model slope ground with slope angle of 35°, a length of 800 mm, a height of 470 mm, and a width of 98 mm was made in a transparent acrylic soil box having a length of 800 mm, a height of 500 mm and a width of 98 mm. Model ground was prepared in 10 layers of basically 50 mm thick by compacting.

An experimental setup is shown in Fig. 6.3. A loading plate having a length of 100 mm and a width of 97 mm was set on the shoulder of the slope. The loading plate applied vertical load P to the shoulder while the subsidence displacement w was controlled by a jack. P was measured by a load cell (LC) and w was measured by an encoder (ENC) and a dial gauge (DG). When installing the anchors, three anchors were set while ground preparation. Lateral earth pressure was measured by 5 earth pressure gauges (EP) on the side wall at intervals of 80 mm in the height direction (Fig. 6.4).

Similar to the other 2D experiments (Chapter 4), the movement of soil particle in the transparent soil box was observed by photos. Dry silica sand #3 was used for the model ground. Physical and mechanical properties of the sand are listed in Table 6.1. Relative density D_r of the model ground was adjusted to be about 80% (dry density ρ_d = 1.512 ton/m^3) by tapping the sand of each layer. Internal friction angle ϕ = 42° was obtained from direct shear tests of the sand with D_r = 80%.

Table 6.1. Physical and mechanical properties of silica sand #3.

Density of soil particles, ρ_s (g/cm^3)	2.632
Max.dry density, ρ_{dmax} (g/cm^3)	1.567
Min.dry density, ρ_{dmin} (g/cm^3)	1.325
Max. void ratio, e_{max}	0.987
Min. void ratio, e_{min}	0.679
Int. friction angle at peak strength, ϕ_p (deg)	42
Int. friction angle at residual strength, ϕ_r (deg)	35

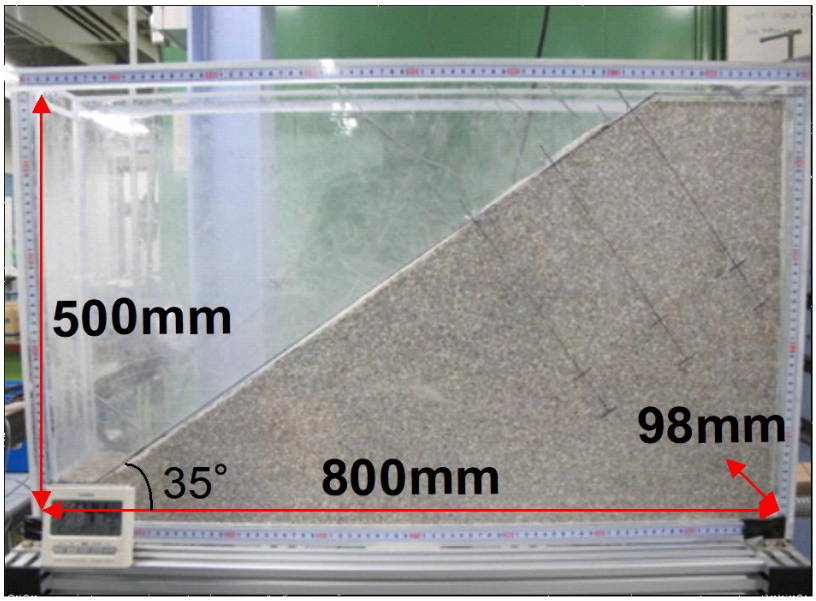

Fig. 6.2. A model slope ground in the transparent soil box.

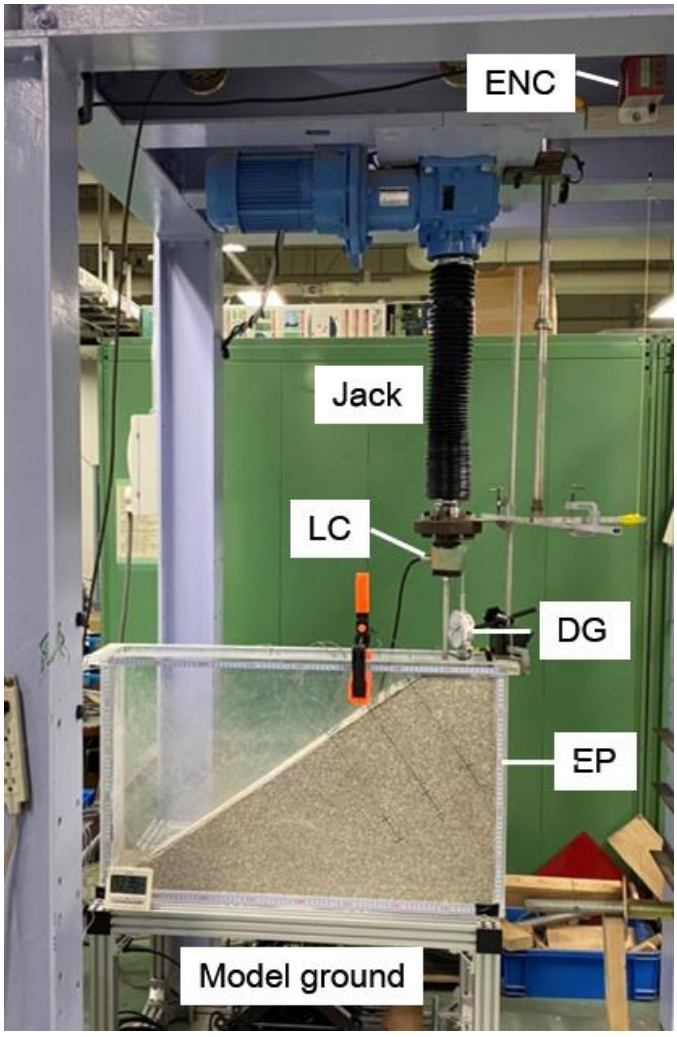

Fig. 6.3. A setup for loading experiments on the slope.

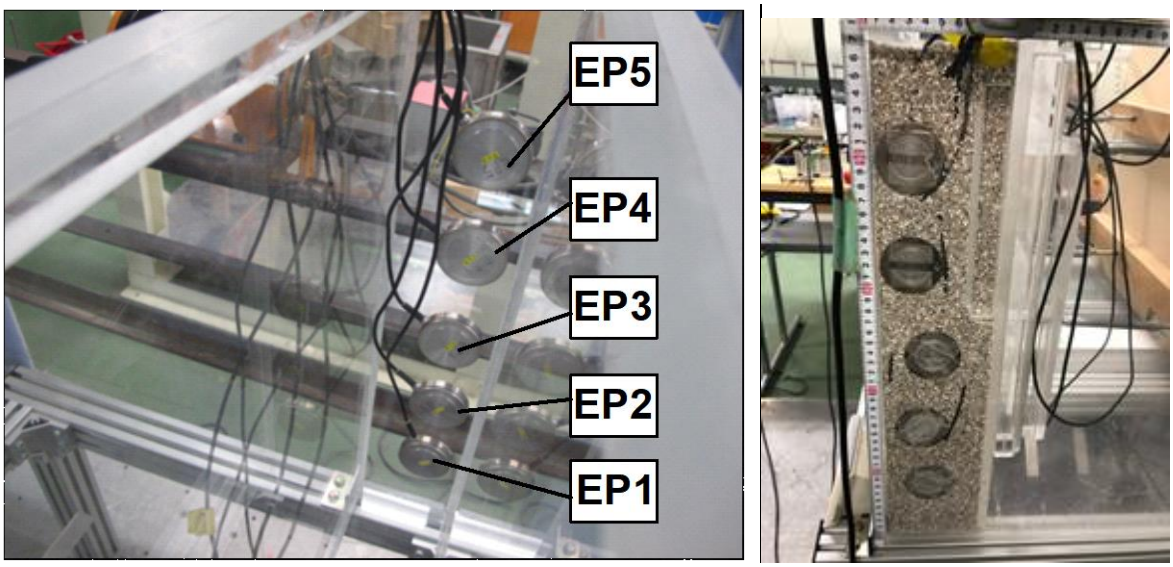

Fig. 6.4. Earth pressure gauges (EP) on a side wall of the soil box.

Loading experiments in a plane strain condition with plate anchors were conducted. Figure 6.5 shows a model anchor which has an almost same width with the ground. Steel rods having a diameter of 2.8 mm were used as anchor rods. To measure the tensile force *T* acting on the anchor rods, two strain gauges were attached at 35 mm away from the bearing plate for each rod.

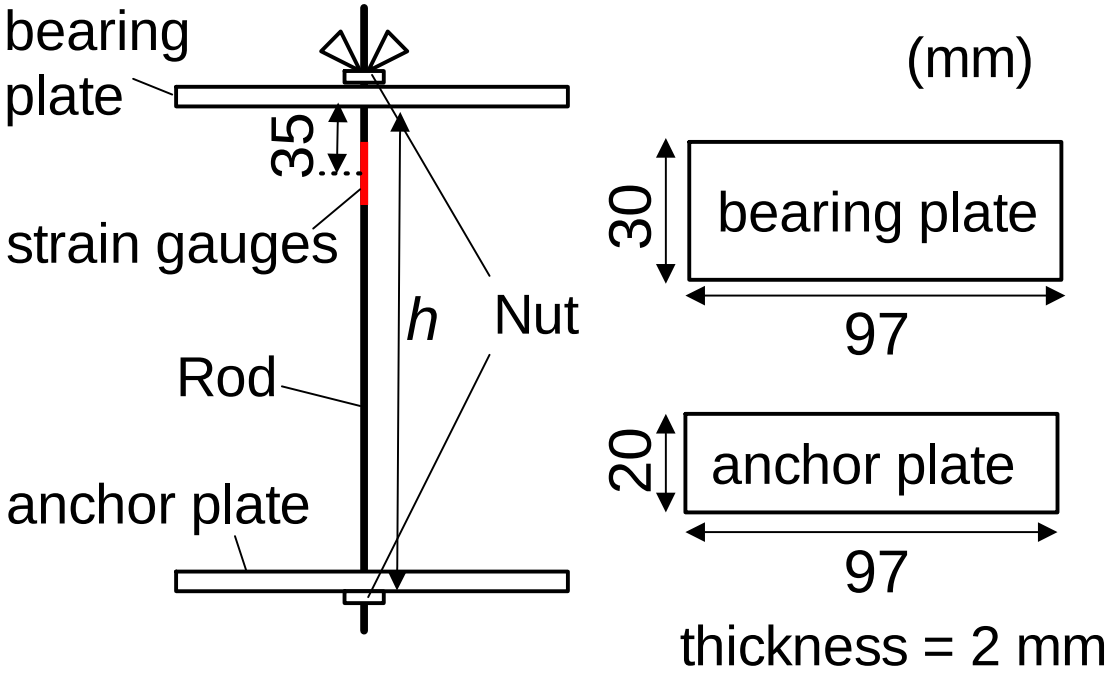

Fig. 6.5. Diagrams of model plate anchors.

Subsequently, loading experiments in a 3D condition using actual flip anchors with wire ropes having a diameter of 3.0 mm were conducted (Figure 6.6). The width *B* of the actual flip anchor was 25 mm; whereas the width of the ground was 98 mm. When setting the anchors, the central axis of the anchor was aligned with the center line in the width direction of the ground. In Opened case, the anchor head was installed facing the shoulder of the slope.

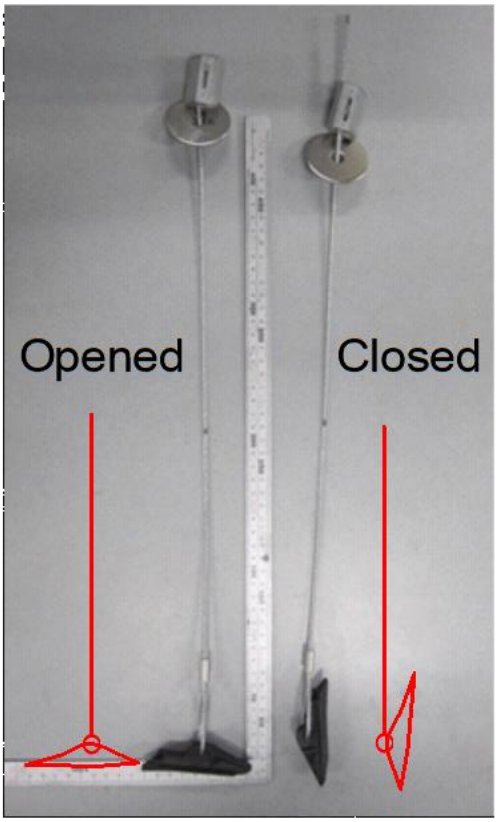

Fig. 6.6. Actual flip anchors (HP25) used for the experiment.

Figure 6.7a shows the experiment on unreinforced slope of Case 06. In Case 07 and 09, a length of an anchor *h* was 200 mm (Fig. 6.7b) or 250 mm (Fig. 6.7c). The 2D model anchors were set as Anchor 1, Anchor 2, and Anchor 3 as illustrated.

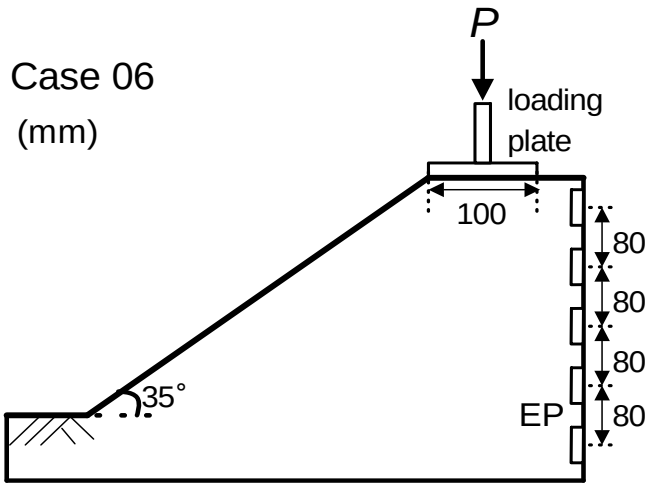

(a) Case 06

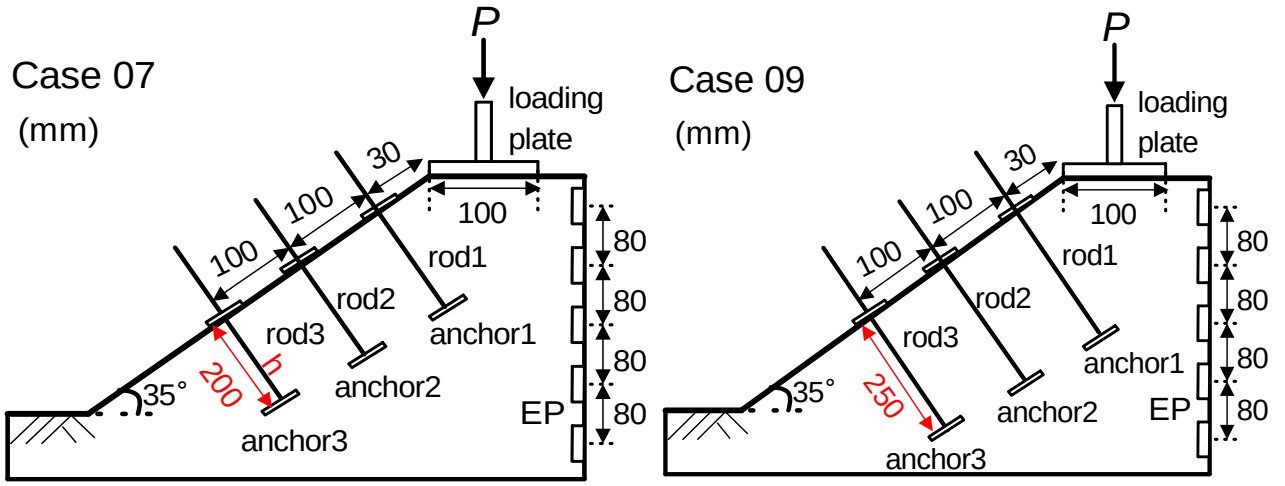

(b) Case 07 (c) Case 09

Fig. 6.7. Experimental conditions with or without model anchors.

The actual flip anchors were set at 80 mm away from the shoulder of the slope, and was set at same position of Anchor 3. The actual anchors were embedded under Opened (Fig. 6.8a) or Closed (Fig. 6.8b) conditions.

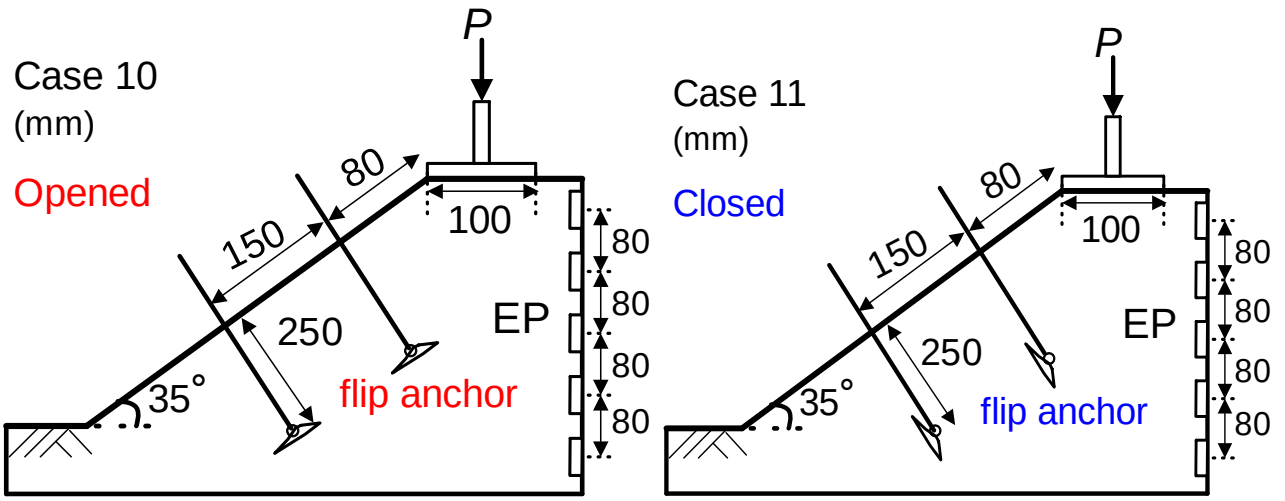

(a) Case 10 (b) Case 11

Fig. 6.8. Experimental conditions with actual anchors.

Preliminary experiments of Case 01-05 were conducted to define the optimum slope angle, slope shape, and *h* for the experiments. Finally, a total of 5 cases of experiments were conducted as listed in Table 6.2. Case08 is omitted because the experimental equipment was broken due to the too much load *P* in the experiment.

Table 6.2. Experimental cases of loading experiments on a shoulder of a slope.

Case	Slope angle (deg.)	Number of anchors	Anchor length *h* (mm)	Anchor type	Opened or Closed
06	35	0	N/A	w/o anchor	Opened
07	35	3	200	Model plate anchor	Opened
09	35	3	250	Model plate anchor	Opened
10	35	2	250	Flip anchor	Opened
11	35	2	250	Flip anchor	Closed

The experimental procedures were as follows.

1) The loading plate was loaded by a screw jack at a displacement rate of 0.2 mm/s.
2) The signals of each sensor were measured at a sampling frequency of 5 Hz, and the ground behavior was photographed at every 2 second.
3) To follow the movement of sand particles during the loading, the photos were analyzed in a same manner as in Chapter 4.

6.2.2 Results of the experiments

Experiments using model plate anchors in a plane strain condition

Figure 6.9 shows *P* vs. *w*. In Case 06 (without an anchor), maximum vertical load P_{max} was 3000 N. In Case 07 and Case 09 (reinforced with 3 anchors), even when 6000 N was applied, P_{max} did not appear. In these experiments, considering the risk of destruction of the soil box, loading was stopped at about 6000 N.

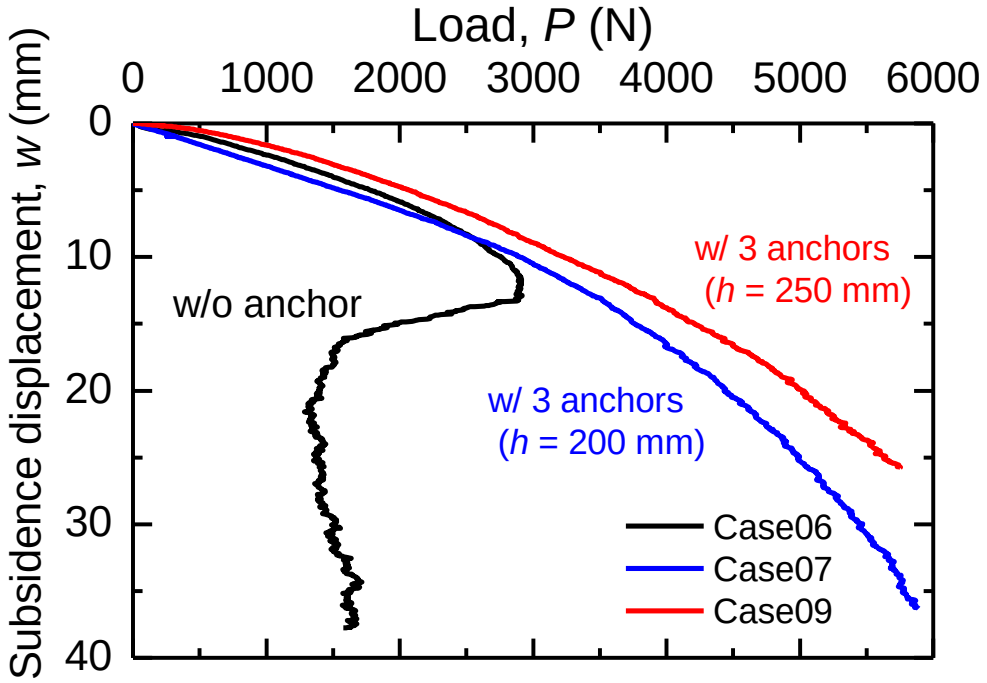

Fig. 6.9. *P* vs. *w* in Case 06 (w/o anchor), Case 07 (w/3 anchors, *h* = 200 mm) and Case 09 (w/3 anchors, *h* = 250 mm).

P in Case 06 rapidly decreased after P_{max}. In contrast, in Case 07 and 09, the softening behavior did not appear during the experiments up to 6000 N. In reinforced cases, *P* could likely to increase further if loaded further.

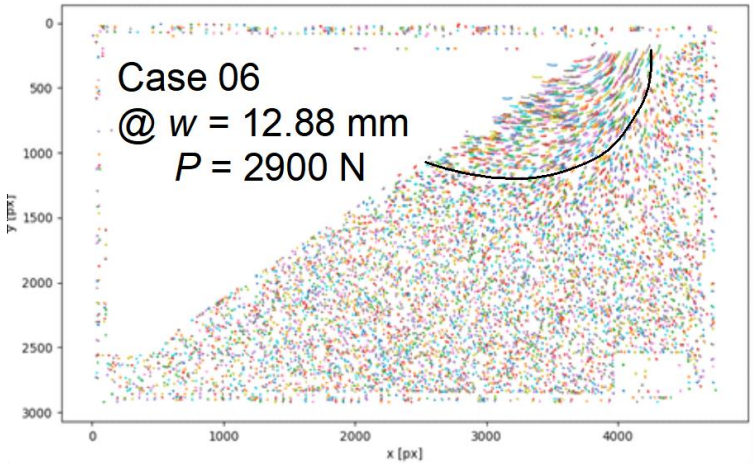

(a) Case 06: without anchor

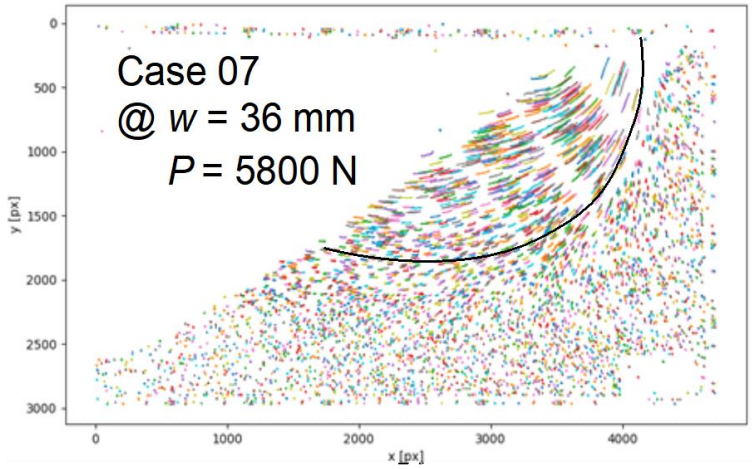

(b) Case 07: with 3 anchors, *h* = 200 mm

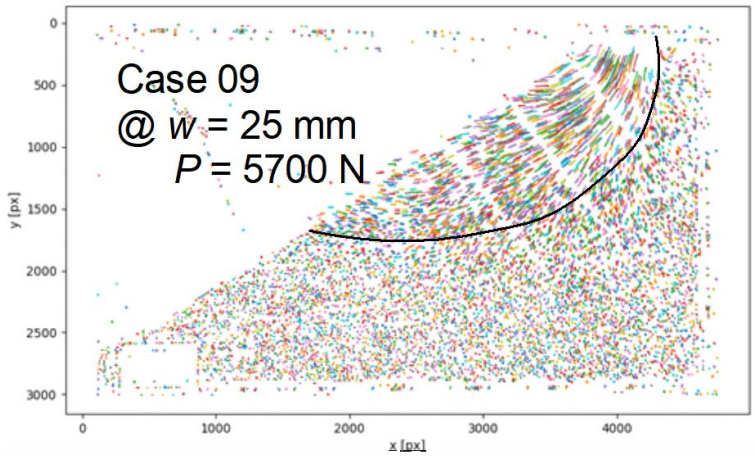

(c) Case09: with 3 anchors, *h* = 250 mm

Fig. 6.10. Displacement vector (slip lines) of soil particles observed in the experiments.

From these results, plate anchors can be considered as an effective means for reinforcing slopes against slope failure. Comparing the reinforcement effects by different h, the anchor having h = 250 mm had a smaller gradient ($\Delta w/\Delta P$) than the anchor having h = 200 mm. That is, an amount of w of the slope reinforced by 250 mm anchors was less than w of the slope reinforced by 200 mm anchors at the same P. If the loading was continued up to P_{max}, the greater reinforcement effect by larger h could be observed more clearly.

Figures 6.10a shows the displacement vector of soil particle at P_{max} of Case 06. Figure 6.10b & 6.10c show the same for Case 07 and 09, respectively. The slip lines of (b) and (c) were generated deeper than that of (a). The resistance against slope failure of (b) and (c) were larger than that of (a). In (b) and (c), although h was different, the shape of the slip lines was not much different perhaps because they were not loaded up to P_{max}.

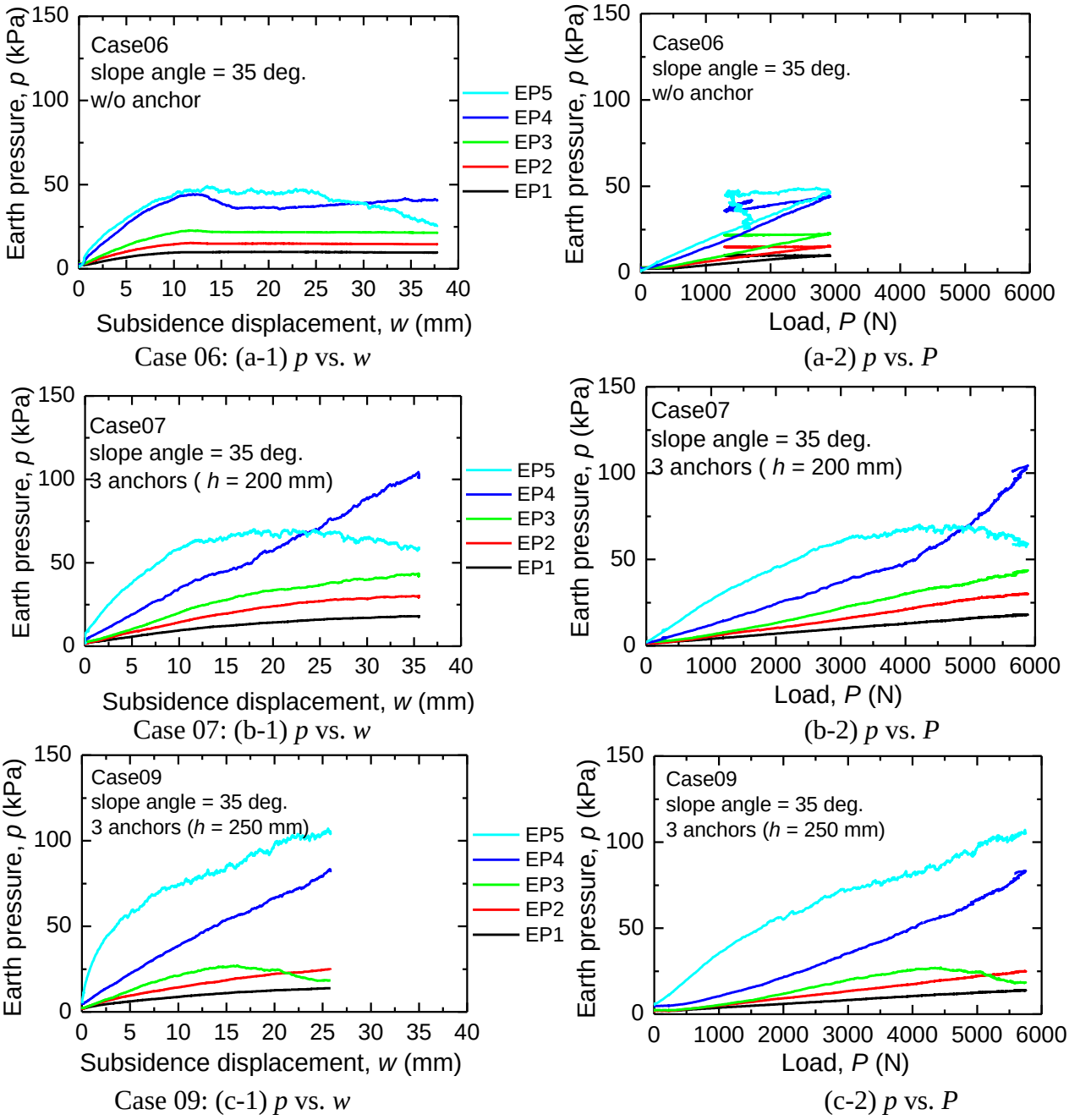

Case 06: (a-1) p vs. w (a-2) p vs. P

Case 07: (b-1) p vs. w (b-2) p vs. P

Case 09: (c-1) p vs. w (c-2) p vs. P

Fig. 6.11. Lateral earth pressure p vs. w or P.

Figure 6.11 shows lateral earth pressure p vs. w (a-1, b-1, c-1) or P (a-2, b-2, c-2) for Case06, 07, and 09, respectively. In Case06 (unreinforced), p at any point increased with increasing w (or P) until w = 13 mm at P_{max} (a-2). After that, EP4 decreased related to ground failure, and EP5 also gradually decreased.

In Case 07, only EP5 decreased. In Case09, only EP3 decreased. The other EPs kept increasing in reinforced cases. The magnitude of p was larger overall in Case 07 & 09 than in Case 06.

From these results, it can be confirmed that the slopes were reinforced by the anchors, and the ground maintains its stability even with larger P.

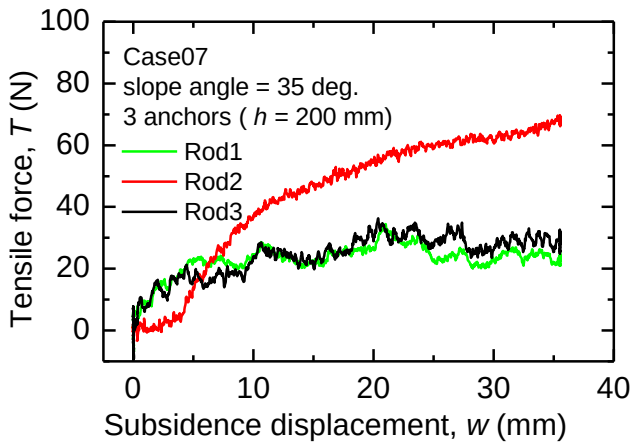

Case 07: (a-1) T vs. w

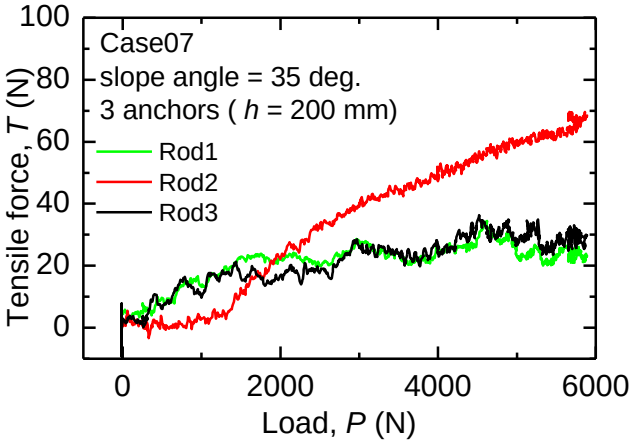

(a-2) T vs. P

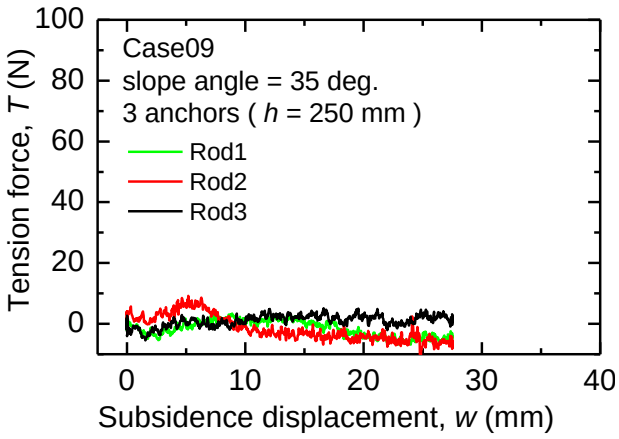

Case 09: (b-1) T vs. w

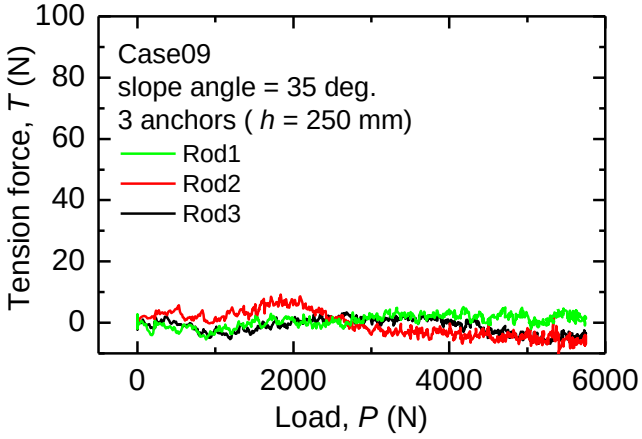

(b-2) T vs. P

Fig. 6.12. Tensile force T vs. w or P.

Figure 6.12 shows relationships between T vs. w (a-1, b-1) or P (a-2, b-2) in Case 07 & 09. In Case 07, although compressive force initially appear on Rod 2, T gradually increased as P loaded. In contrast, T appeared on Rod 1 and Rod 3 from the beginning. After w = 5 mm, T on Rod 2 became the largest.

Looking at Fig. 6.10b, sand particles were moving significantly around Rod 2. The largest T is thought to act on the anchor rod which was installed at the deeper in a failure plane. And the influence of the dilatancy is greater where the thickness of the moving soil is larger. The dilatancy

of the sand greatly affect *T* due to the activation mechanism of pull-out resistance of flip anchors. And the ground in this experiment was compacted well, the influence of dilatancy was more likely to appear.

In Case 09 (Fig. 6.12b-1, b-2), *T* was failed to be measured. In this experiment, it was difficult to accurately measure *T* because two very small strain gauges were attached symmetrically to a thin rod with a diameter of 2.8 mm. Thus, *T* on the rod will be investigate later also in the FEM analysis.

Experiments using flip anchors in a three-dimensional condition

The experimental results using actual flip anchors are shown in Figs. 6.13-15. Figure 6.13 shows *P* vs. *w* in Case 06, 10, and 11. Case 10 (Opened) and Case 11 (Closed) showed similar trends up to P_{max} in Case 06. When *P* exceeded 3000 N, the gradient ($\Delta P/\Delta w$) in Case 10 (Opened) was smaller than that in Case 11 (Closed). In Case 10, P_{max} appeared at around 5000 N, and levelled off without immediately softening. In contrast, in Case 11, *P* kept increasing even *w* passed 40 mm. And *P* in Case 11 finally approached P_{max} in Case 10.

After the experiments, in Case 11, the Closed anchor remained almost closed state in the ground. This is probably because *w* was not enough to push the bearing plates and open the anchors. Thus, when an external force is applied to a reinforced slope with Closed anchors, the ground could gradually displace until the anchors are fully opened. As *w* increases, reinforcement effects of Closed anchors would be more effective and approach that of Opened anchors.

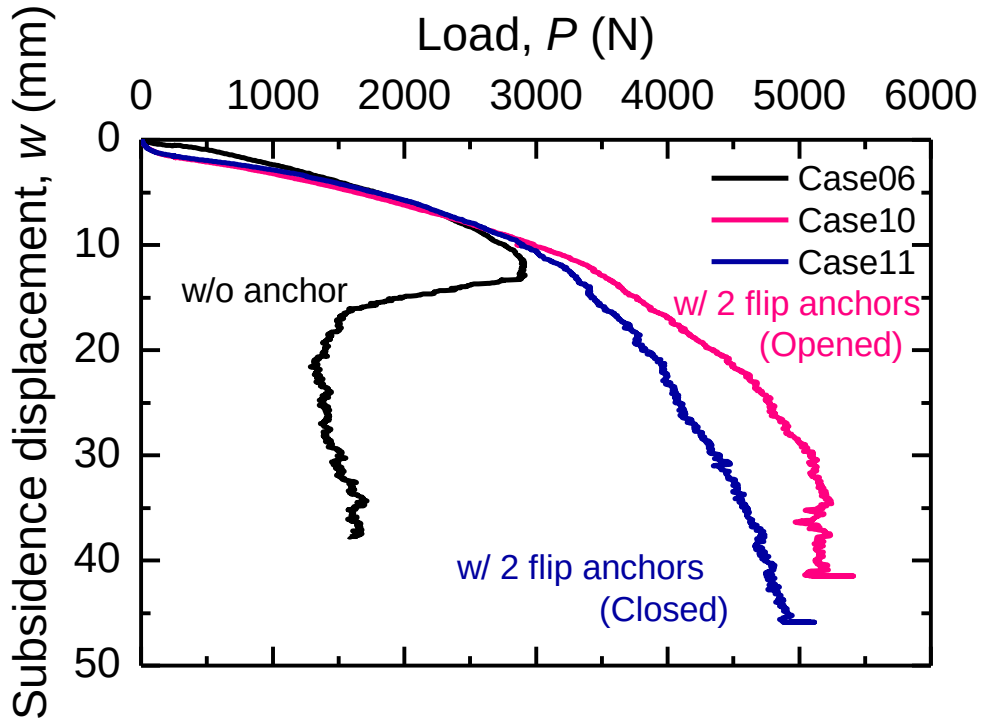

Fig. 6.13. *P* vs. *w* in Case 06 (w/o anchor), Case 10 (w/2 flip anchors, Opened) and Case 11 (w/2 flip anchors, Closed).

Figure 6.14 shows displacement vector of sand particles analysed with photos during the experiments. No notable difference in the shape of slip lines was seen between Case 10 and Case 11.

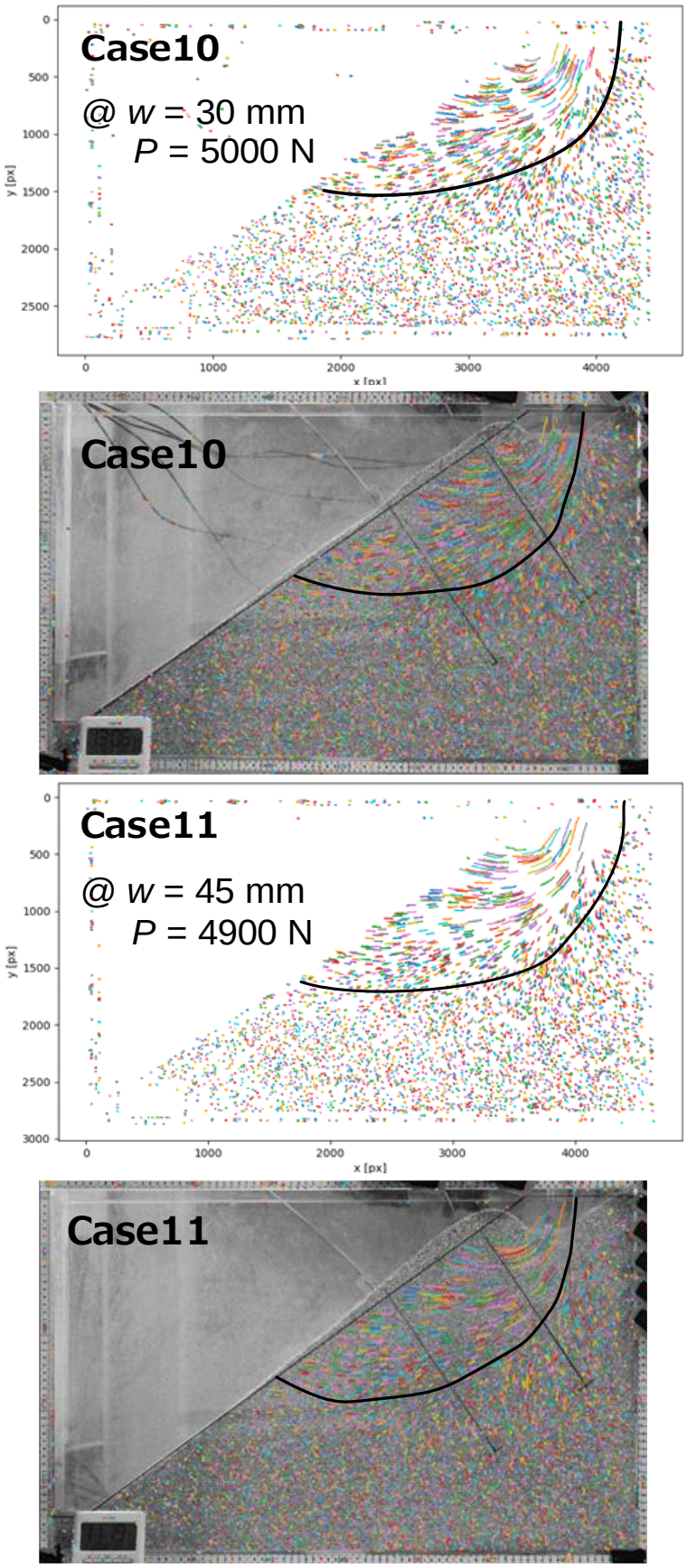

Fig. 6.14. Displacement vector (slip lines) of sand particles observed in the experiments.

Figure 6.15 shows p vs. w (a-1, b-1, c-1) or P (a-2, b-2, c-2) for Case10 and 11, respectively. The slope reinforcement effect was confirmed even when reinforced with actual flip anchors. No notable difference was found between Case 10 and 11. And no notable difference of the results using actual flip anchors and model anchors was found.

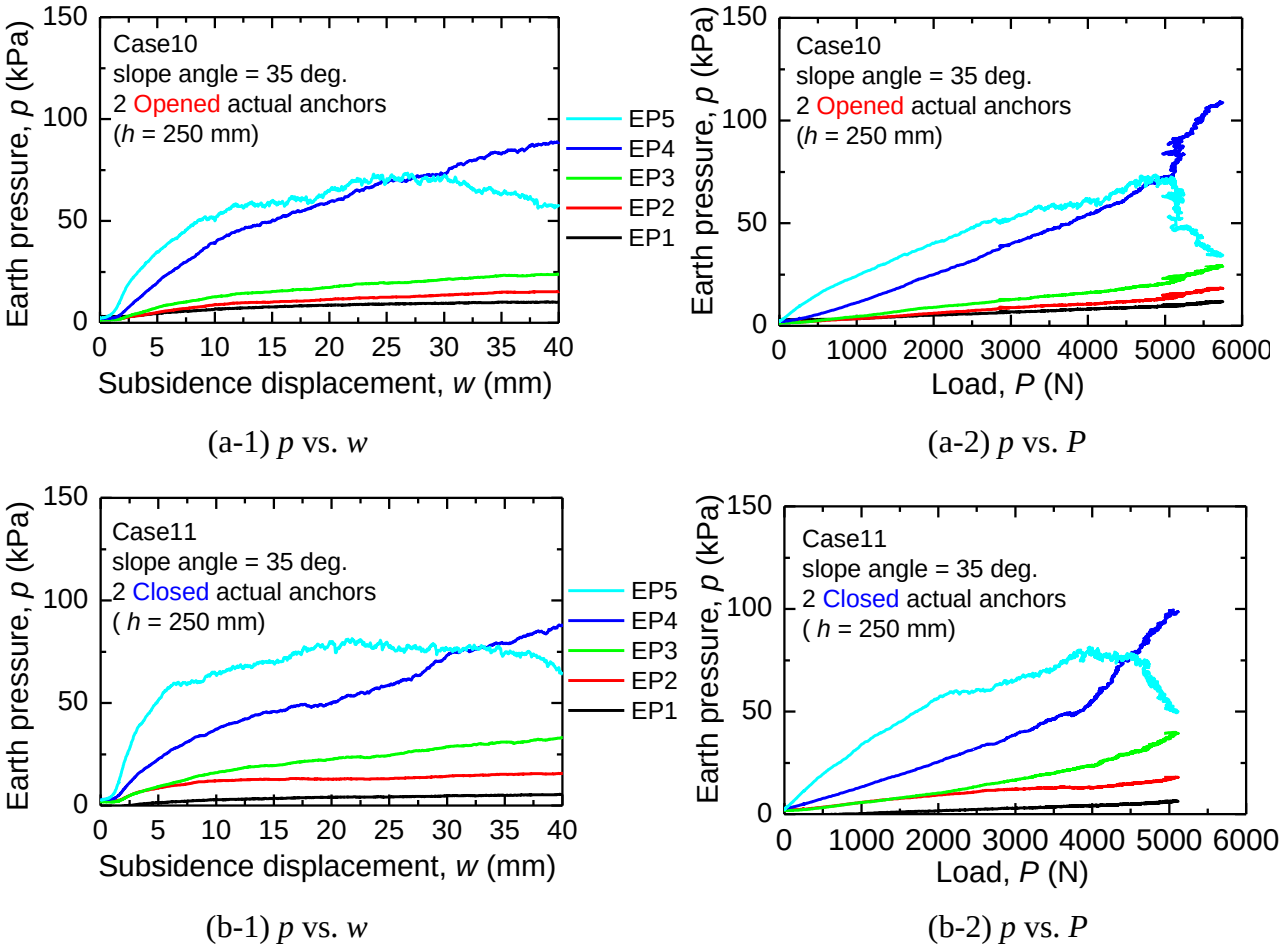

(a-1) p vs. w (a-2) p vs. P

(b-1) p vs. w (b-2) p vs. P

Fig. 6.15. Lateral earth pressure p vs. displacement w or vertical load P.

6.2.3 Discussion of Section 5.2

In this section, the application of flip anchors to slope stability was examined by the experiments using model plate anchors in a plane strain condition, and actual flip anchors in a three-dimensional condition. In both conditions, the anchors were effective for slope stability. Interestingly, Closed flip anchors were effective as well as Opened anchors if larger w was allowed.

The slope reinforcement effect of the anchors was found from the relationship between P and w, and the depth or shape of the slip lines. When the ground began to displace and push the bearing plates, the anchor plates resisted not to be pulled out, and T began to acted on the anchor rods. It is consistent with the mechanism of such as soil nails in term of that T acts oafter the ground is displaced.

If the slope reinforcement effect by flip anchors can be designed efficiently, it may be widely applied as an easy construction method with immediate effect for slope stabilization. The displacement of the ground and reinforcing effect of the anchor depend on the installation position

and a length of the anchor. That can be effectively analyzed by finite element method (FEM). Thus, in the next section, the experiments were simulated by FEM.

6.3 Numerical analysis (FEM)

6.3.1 Outline of FEM analysis

In this section, the loading experiments on the slope was simulated by numerical analysis. FEM analysis software Plaxis 3D was used for the simulation. The ground with a height of 470 mm, a length of 800 mm, and a width of 98 mm that was the same as the model ground (Fig. 6.1) was modelled. As the displacement boundary conditions, the horizontal displacement of the side surface and the vertical displacement of the bottom surface were fixed. The Mohr-Coulomb model was applied to the soil constitutive law.

Procedure of the FEM analysis

The FEM analysis were conducted according to the following procedures (Fig. 6.16).

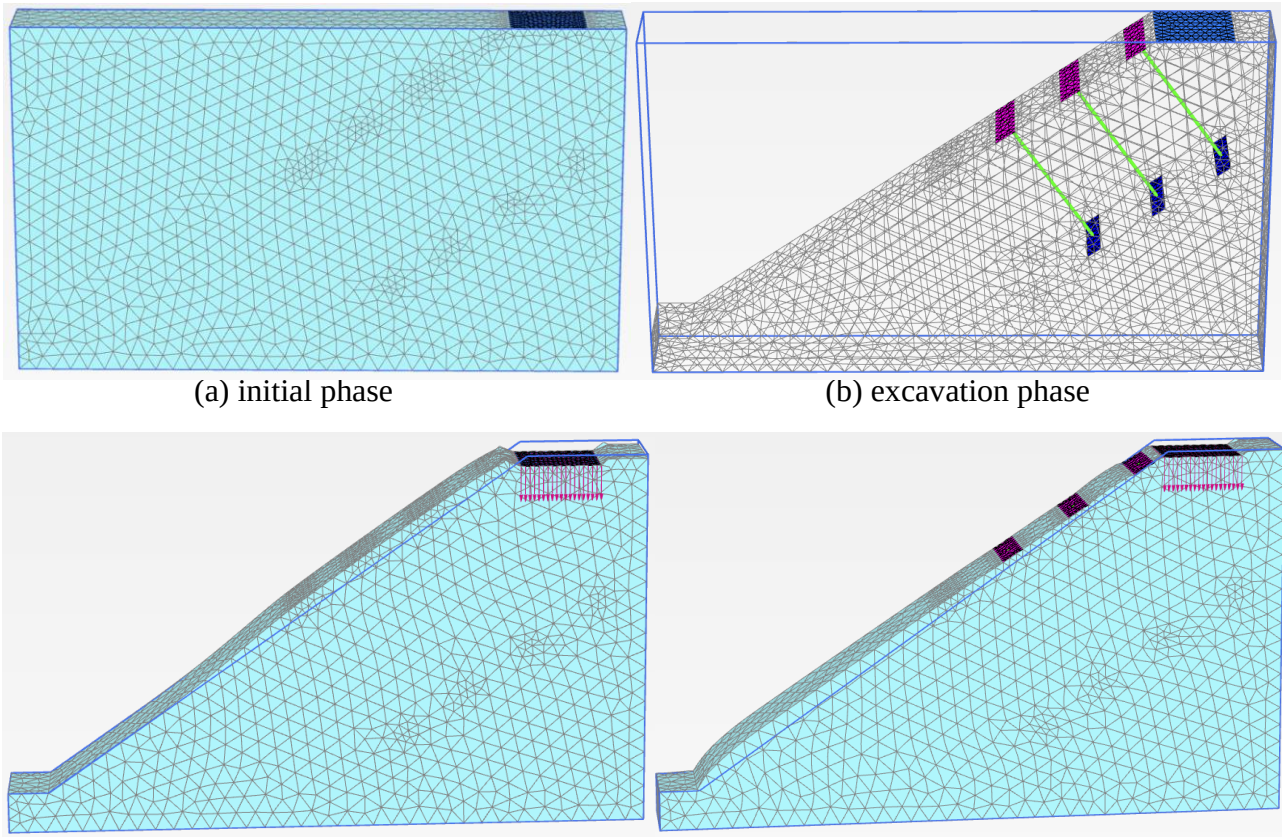

(a) initial phase (b) excavation phase

(c-1) loading phase (w/o anchor) (c-2) loading phase (w/3 anchors)

Fig. 6.16. Procedures of the simulation of the loading experiments on the shoulder of the slope by FEM.

a) Initial phase: K_0 self-weight analysis of horizontal ground was performed with K_0 = 1.2 to simulate the slope made by tamping in each layer. In the experiments in Section 4.3, K_0 = 1.2 was measured.

b) Excavation phase: By excavating the ground, a slope with an angle of 35° was made, which is the same as in the experiment. In this phase, a loading plate and anchor systems were installed for reinforced cases. By setting the phases (a) and (b), the slope condition where the anchors were embedded and compacted was able to be simulated.
c) Loading phase: A vertical prescribe displacement was applied to the loading plate.

Parameters of the material

Table 6.3 shows the ground parameters based on the parameters of the model ground in the experiment from triaxial compression (CD) tests. The constrained modulus E_c was approximated by Eq. (6.1) based on the results of the one-dimensional consolidation test.

$$E_c = E_{cref}\left(\frac{\sigma'}{\sigma'_{ref}}\right)^n \tag{6.1}$$

where σ'_{ref} = 100 kPa, E_{cref} = 90 MPa, n = 0.5. E_c = 20 MPa was obtained by assuming that the typical value of the vertical stress σ'_v was 5 kPa.

In the numerical simulations, the unreinforced slope Case 06 was analyzed first to adjust the ground parameters to match the experimental results. Comparing the experimental and analytical results of Case 06, the ground parameters were finally determined as shown in Table 6.3. After that, Case 07 (h = 200 mm) and Case 09 (h = 250 mm) were analyzed under the same ground conditions as in Case 06.

The parameters of the anchor material are shown in Tables 6.4 & 6.5.

Table 6.3. Parameters of the model ground for FEM analysis.

Item	Value
Unit weight of the unsaturated soil, γ_{unsat} (N/mm^3)	14.8×10^{-6}
Initial void ratio, e_{init}	0.741
Constrained modulus, E_c (MPa)	10.10
Poisson's ratio, ν	0.30
Effective cohesion, c' (kPa)	8.0
Int. friction angle, φ' (deg)	42
Dilatancy angle, ψ (deg)	33
The earth pressure coefficient at rest, K_0	1.2

Table 6.4. Parameters of anchor and bearing plates for FEM analysis.

Item	Value
Unit weight, γ (N/mm^3)	76.93×10^{-6}
Thickness, d (mm)	3.0
Young's modulus, E (GPa)	205
Poisson's ratio, ν	0.30

Table 6.5. Parameters of node to node anchors for FEM analysis.

Item	Value
Axial stiffness, EA (N)	643.7×10^3

6.3.2 Results of the FEM analysis

Measured vs. calculated P vs. w

Figure 6.17 shows measured and calculated (by FEM) *P* vs. *w*. The FEM analysis successfully simulated the reinforcing effect of the anchors. The experimental and calculated results of Case 07 agreed. In Case09 in the experiment, if the loading was able to be continued, larger value of *P* could be obtained equivalent to the analysis.

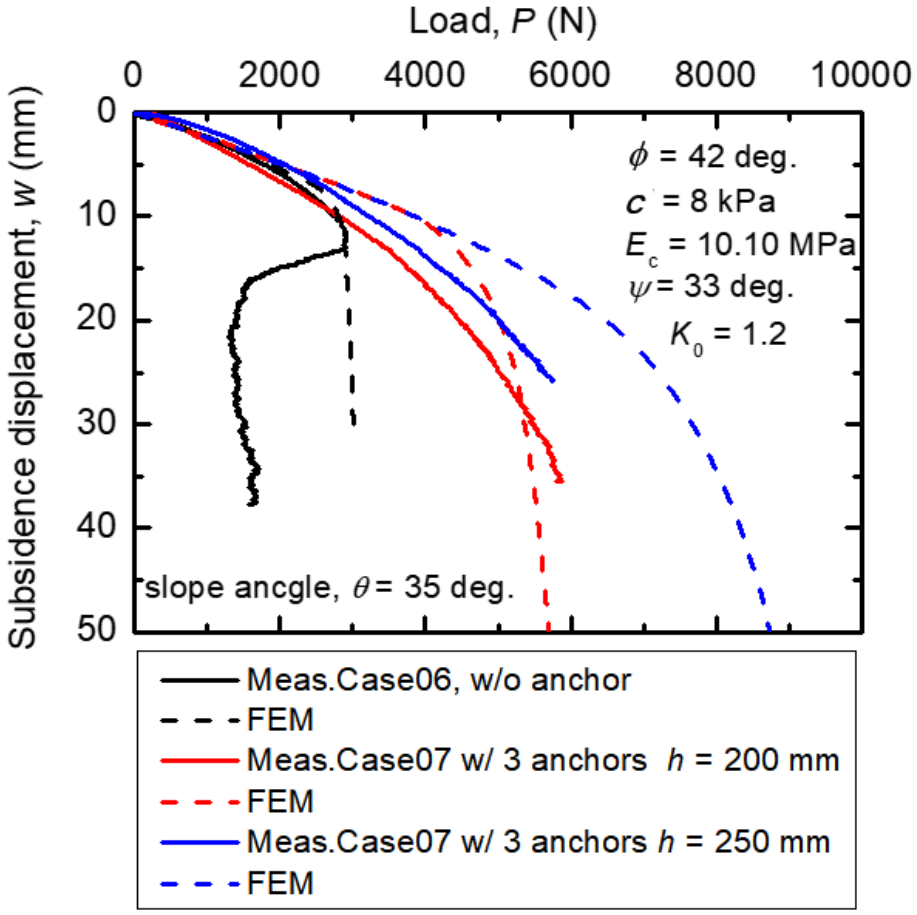

Fig. 6.17. Relationships between measured *P* vs. *w*, and *P* vs. *w* by FEM.

Analysis of the ground failure

Figures 6.18-20(a) shows the displacement vector of the sand particles by the image analysis at maximum values of *P* in Case 06, 07, 09. Figures 6.18-20(b) shows displacement vector by FEM analysis at the same *w*. Figure 6.18-20(c) shows incremental deviation strain distribution by FEM analysis.

From the results of image analysis (Fig. 6.18a), in Case 06 without anchor, shallow slip failure occurred near the shoulder of the slope. In the FEM analysis (Fig.6.18b, c), sand particles near the shoulders displaced, and a slip line was generated. In the results of Case07 (Fig. 6.19), the movement of sand particles was larger than that in Case06, and the slip line was generated deeper in both measured and FEM analytical results. The results of Case 09 were similar to those of Case 07.

Image analysis (Fig. 6.19a & 20a) did not clearly show the difference in Case 07 and 09, but the FEM analysis results (Fig. 6.19b & 20b) show a large difference in the amount of displacement of soil particles. In Case 07, larger displacement of soil particles was observed than in Case 09. This indicates a difference in the reinforcing effect depending on *h*.

The displacement was small at the upper part of the slope where the anchors were installed. In contrast, the lower part of the slope where the anchors were not installed had a large displacement and swelled (Fig. 6.19b & 20b). The displacement of the ground was suppressed by the anchors.

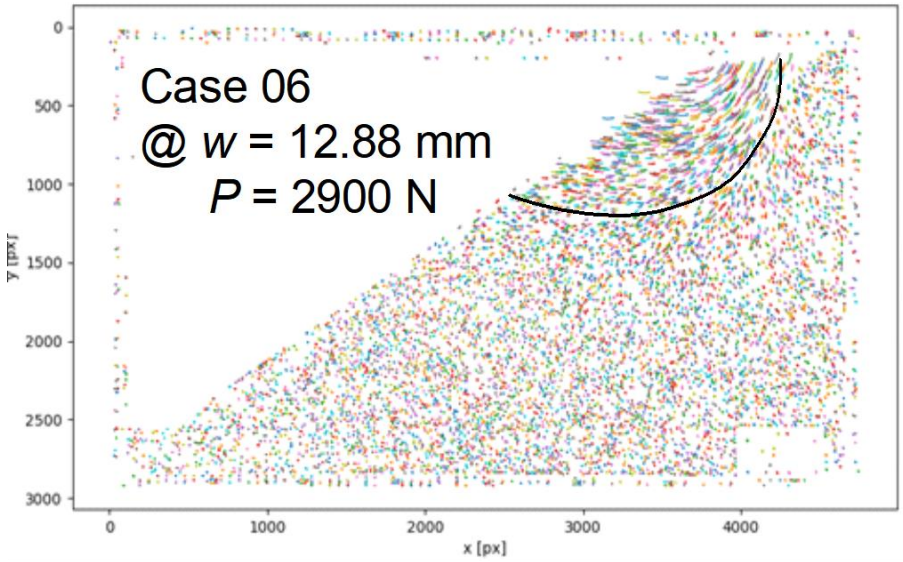

(a) Displacement vector of sand particles by image analysis in Case 06

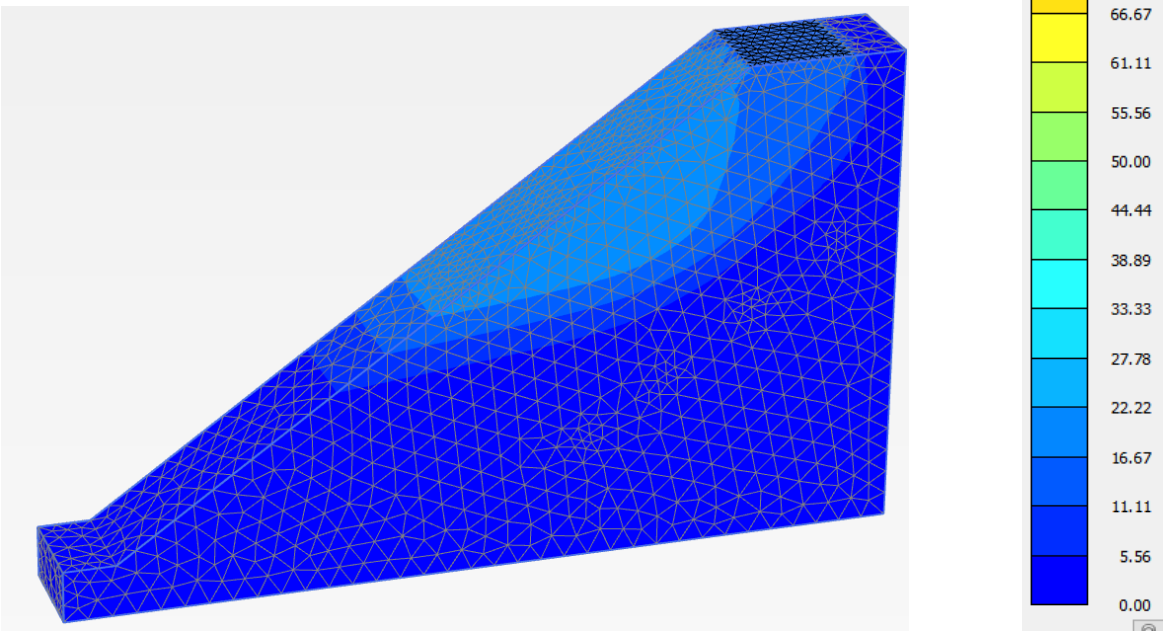

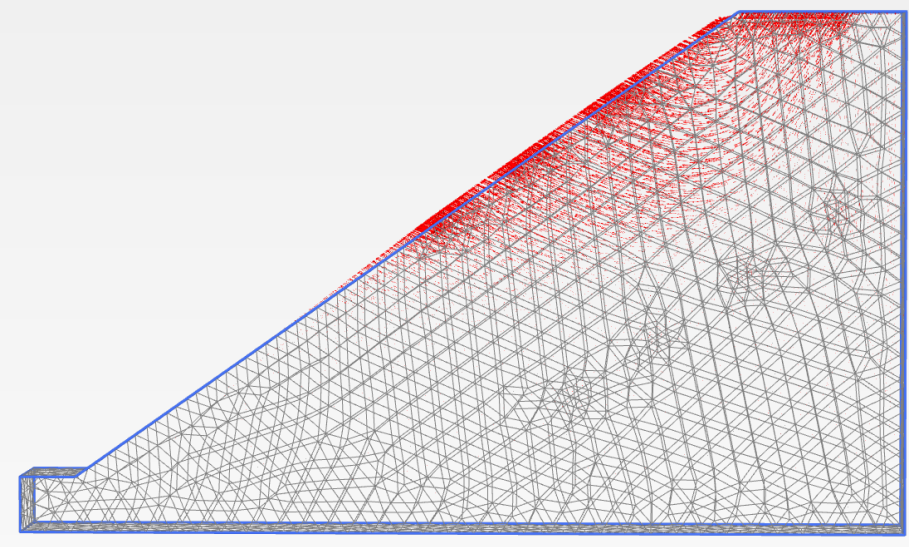

(b) Total displacement and displacement vector of the ground by FEM analysis for Case 06 at w = 13 mm, scaled up 0.5 times

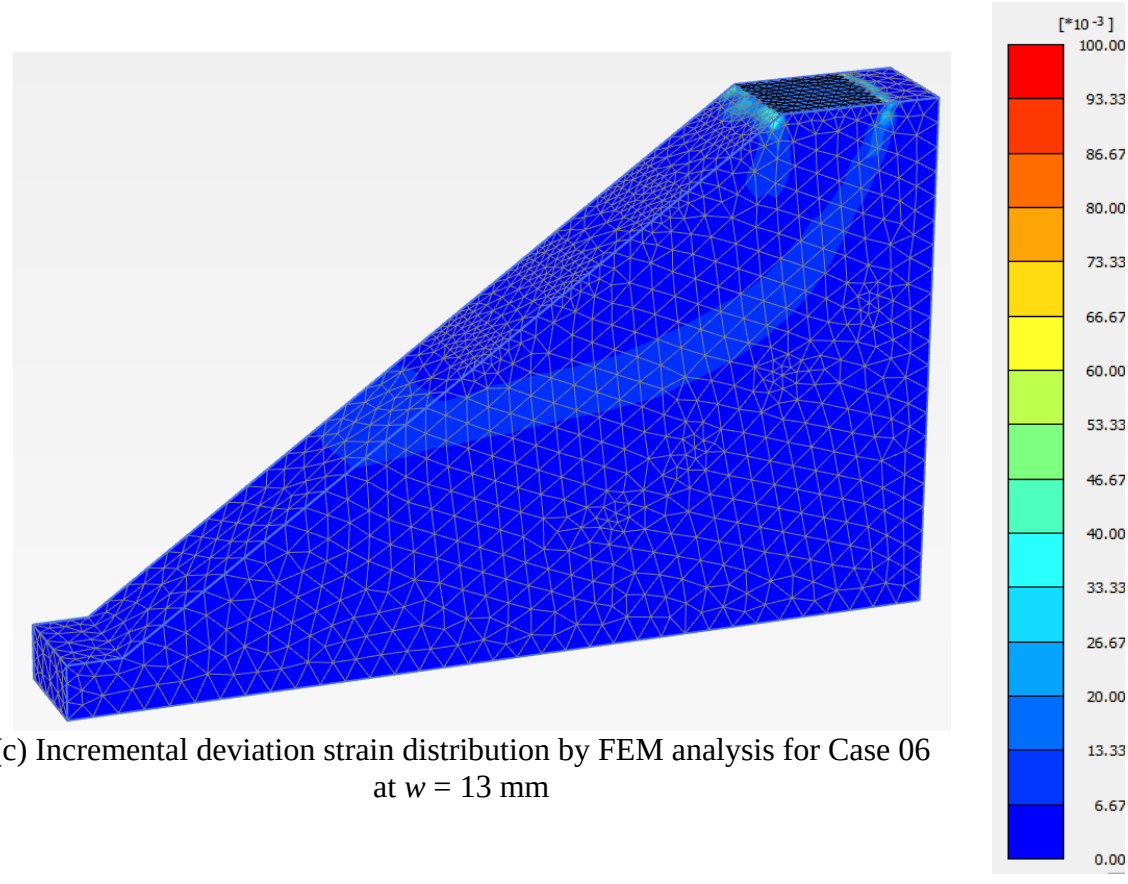

(c) Incremental deviation strain distribution by FEM analysis for Case 06 at w = 13 mm

Fig. 6.18. Ground behavior by the observation and FEM analysis (Case 06).

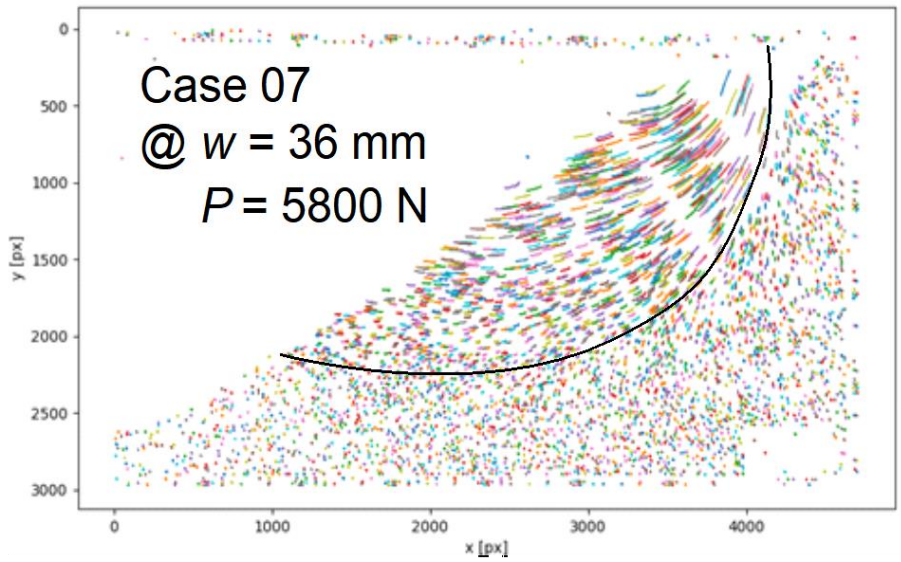

(a) Displacement vector of sand particles by image analysis in Case 07

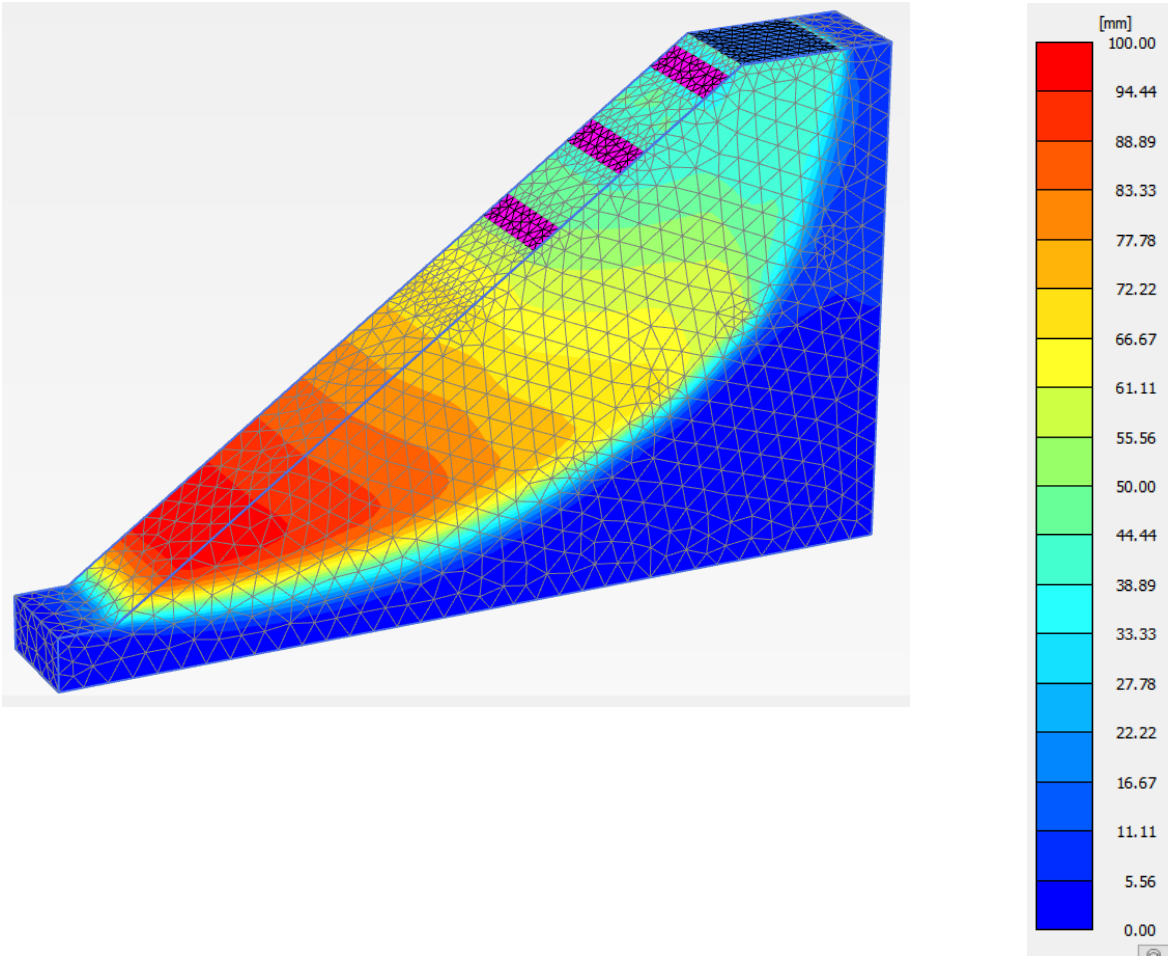

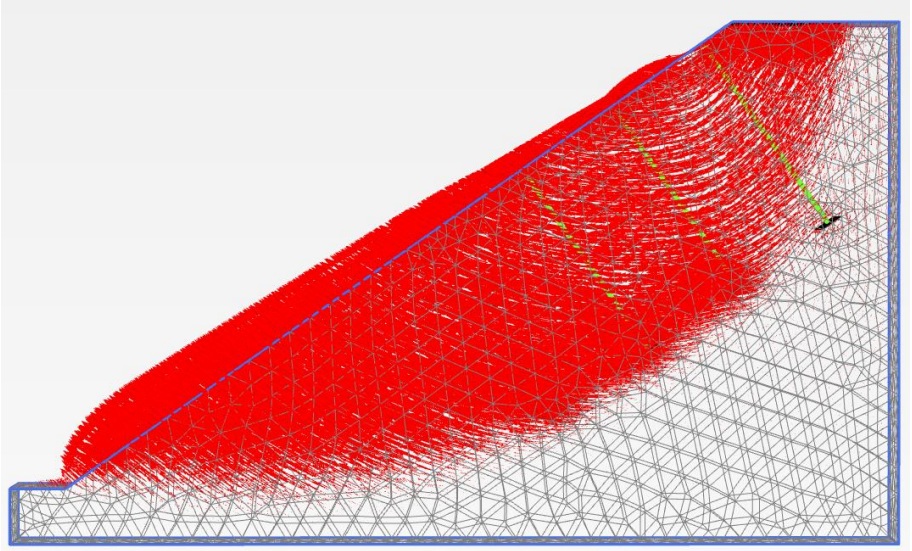

(b) Total displacement and displacement vector of the ground by FEM analysis for Case 07 at w = 37 mm, scaled up 0.5 times

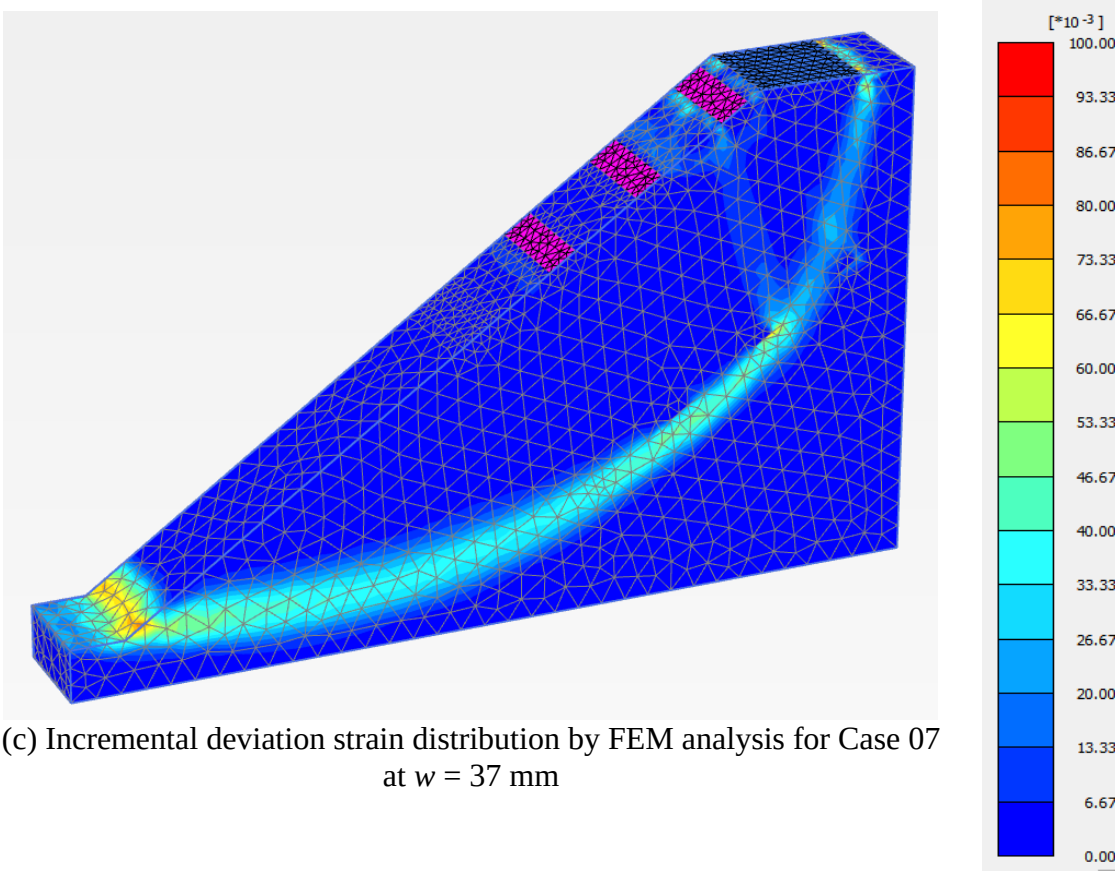

(c) Incremental deviation strain distribution by FEM analysis for Case 07 at w = 37 mm

Fig. 6.19. Ground behavior by the observation and FEM analysis (Case 07).

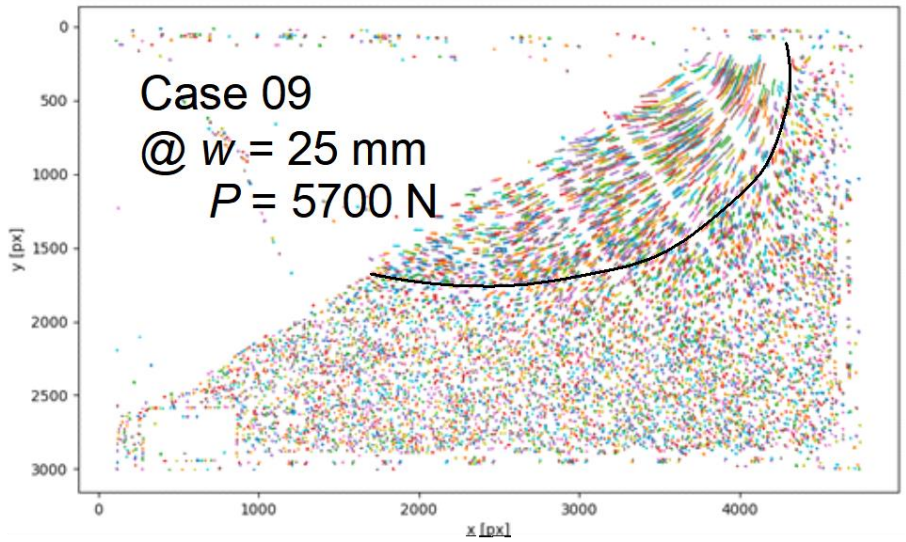

(a) displacement vector of soil particles by image analysis in Case 09

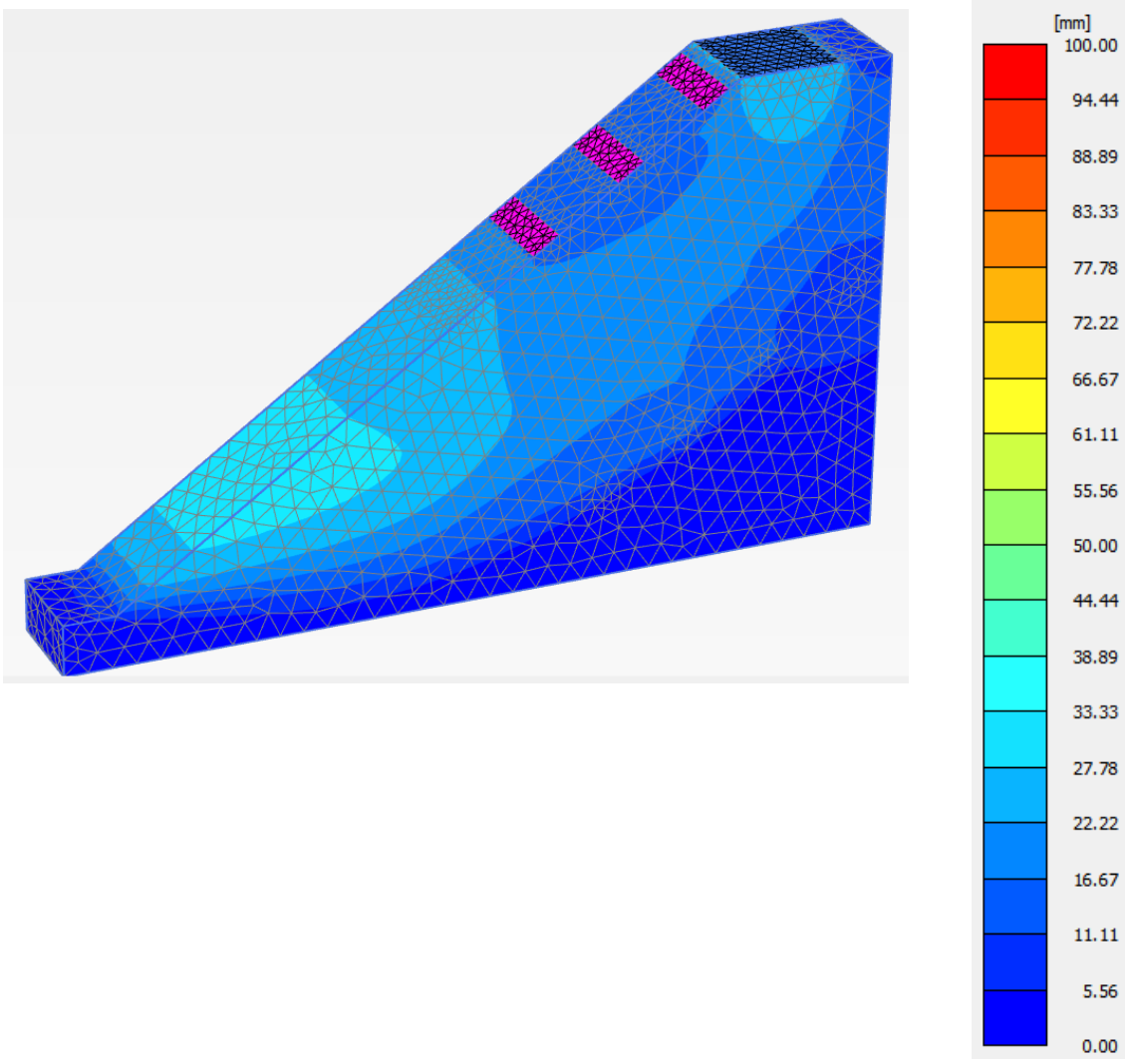

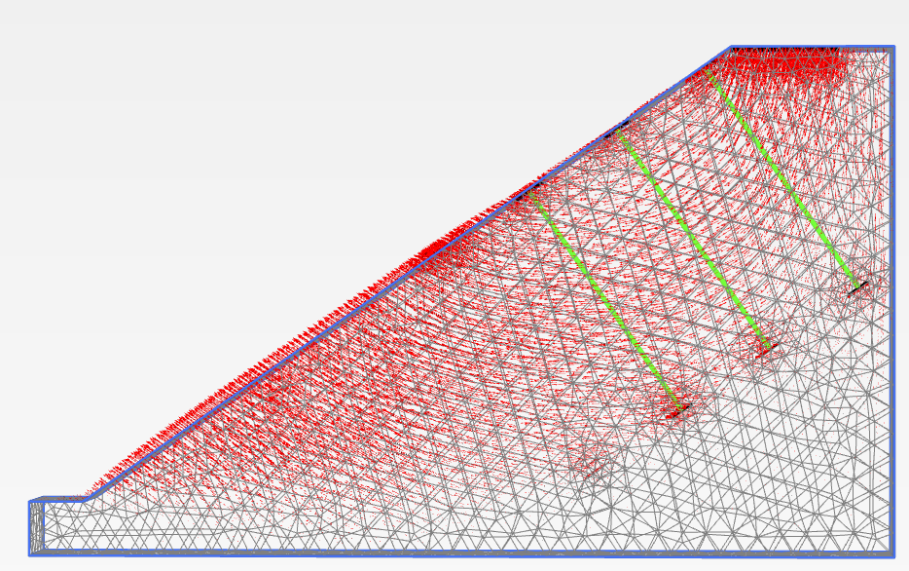

at w = 26 mm, scaled up 0.5 times

(b) Total displacement and displacement vector of soil particles by FEM analysis for Case 09

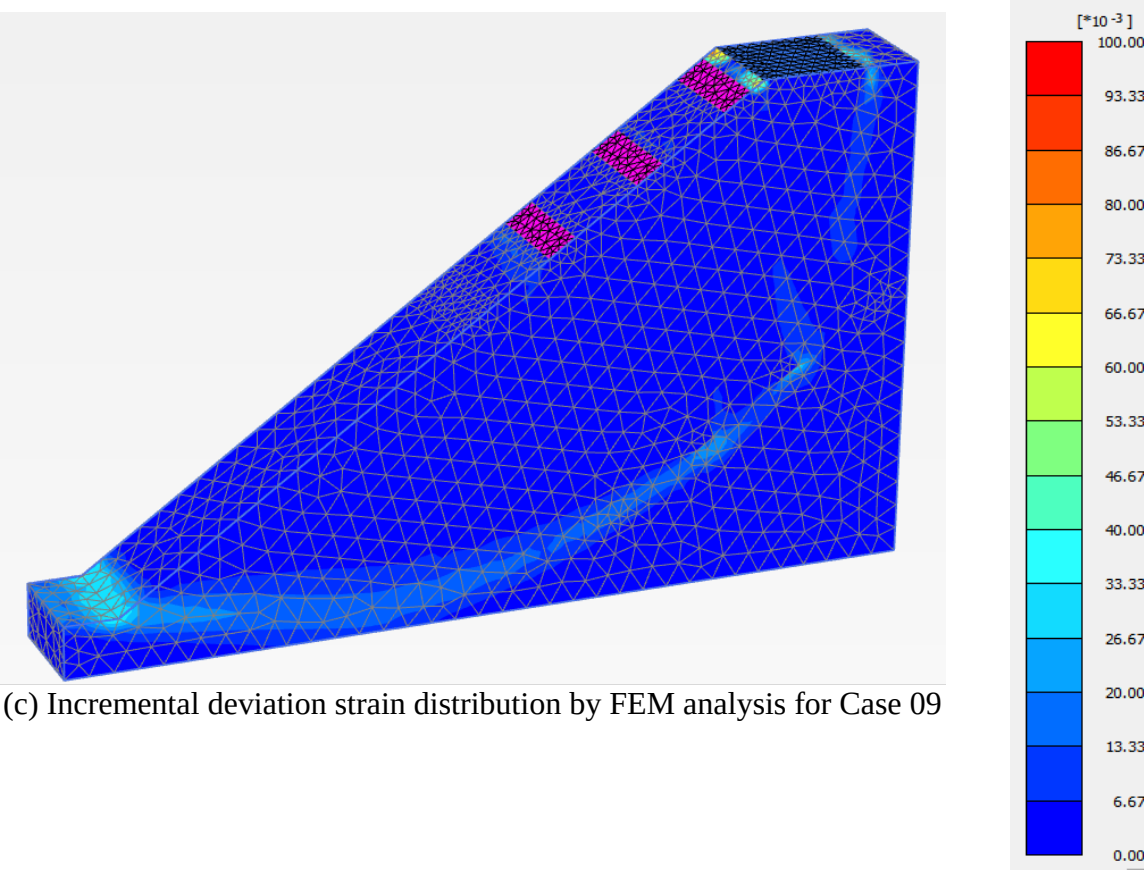

(c) Incremental deviation strain distribution by FEM analysis for Case 09

Fig. 6.20. Ground behavior by the observation and FEM analysis (Case 09).

Figure 6.21 shows the total displacement of the ground at *w* of 13 mm. In the unreinforced Case 06 (Fig. 6.21a), the displacement of the ground was larger than that in (b) Case 07 and (c) Case 09. And *P* in (a) was much smaller than that in (b) and (c). Because the total displacement in (c) was smaller than (b), the larger *h*, the greater the reinforcing effect is.

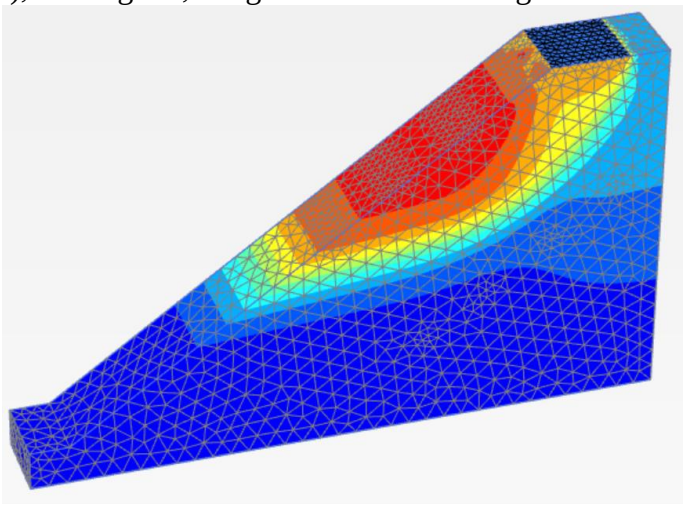

(a) Case 06: *w* = 13 mm, *P* = 2900 N

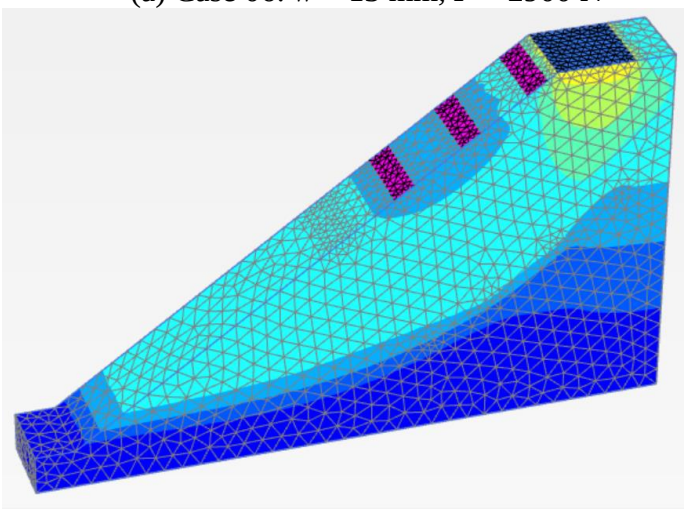

(b) Case 07: *w* = 13 mm, *P* = 4400 N

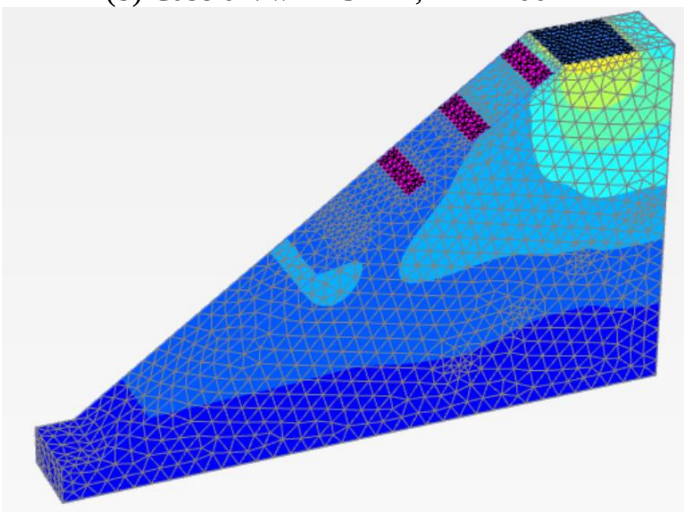

(c) Case 09: *w* = 13 mm, *P* = 4700 N

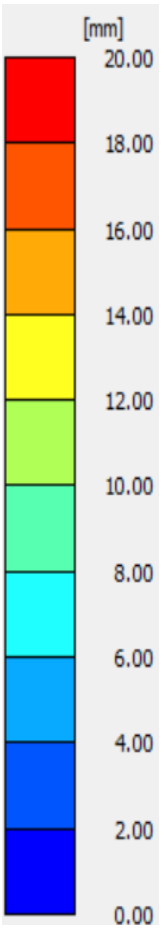

Fig. 6.21. Total displacement of the ground at *w* = 13 mm.

Tensile force acting on anchor rods

Figure 6.22 shows the FEM analytical results of T acting on the anchor rods. In both Cases 07 and 09, as w or P increased, T increased.

In the FEM analytical results of Fig. 6.22a in Case07, T on Rod 1 was the largest; whereas in the experiment, T of Rod 2 was the largest (Fig. 6.12a). It is possibly because that the shape of the ground failure and the slip lines were slightly different between the experiment and the analysis. In the FEM analysis, compressive force worked only on Rod 1. In case 9, T on all rods were equivalent.

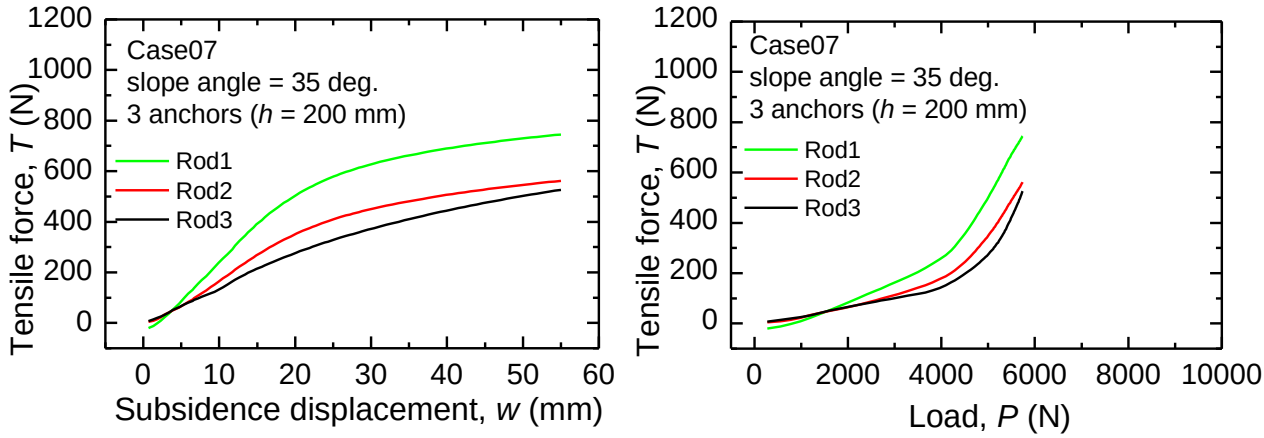

(a) h = 200 mm

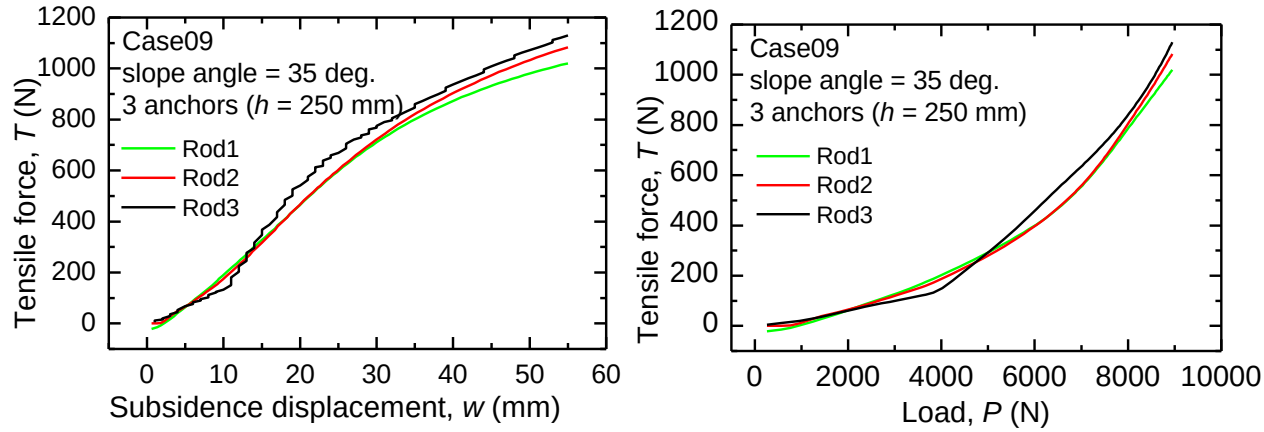

(b) h = 250 mm

Fig. 6.22. T vs. w or P by FEM simulations.

6.3.3 Discussion of Section 6.3

By FEM analysis using the Mohr-Coulomb model, reinforcement effect of flip anchors for slope stability can be simulated well. Not only the reinforcement effect but also the displacement of the soil and T acting on anchor rods were well obtained by FEM analysis.

The analytical results are greatly affected by the ground parameters. In particular, it is necessary to carefully set the dilatancy angle because it greatly affects the results as much as c and ϕ.

6.4 Conclusions of Chapter 6

In this chapter, the effectiveness of the application of flip anchors to slope stability was demonstrated. The main experimental and analytical results were as follows.

1) Flip anchors are effective in reinforcing slopes against slope failure.
2) The deeper the flip anchor is installed, the greater the slope reinforcement effect is.
3) Closed flip anchors are effective as well as Opened anchors if a larger displacement of the ground is allowed.
4) When the ground displaces, flip anchors resist against tensile force by the anchor head.
5) When a slope is reinforced with flip anchors, because small failure near the shoulder of the slope does not occur, slip lines occur at deeper than in that in unreinforced slope.
6) Slope reinforcement effect of flip anchors can be estimated by FEM analysis using the Mohr-Coulomb model.
7) Not only the reinforcement effect but also the displacement of the ground and tensile force acting on anchor rods can be well obtained by FEM analysis.
8) At the position where the flip anchors are installed, the displacement of the ground is suppressed.
9) In case of slope reinforcement, the dilatancy of the soil greatly affects the reinforcement effect of flip anchors.

References in Chapter 6

Rocscience Inc. (2021).
https://www.rocscience.com/help/slide2/slide_model/support/end_anchored.htm.

Chapter 7
Summary, conclusions, and recommendations

7.1 Introduction

To investigate fundamental performance of flip anchors under sandy or clayey ground conditions, experimental and numerical studies were conducted in this research. Based on the results, the some methods to design pull-out resistance of flip anchors were proposed.

Firstly, a series of pull-out experiments were conducted using actual or model flip anchors under sand ground condition. To take into account the unique feature of flip anchors that the anchor head rotates and opens in the ground, three installation conditions: Opened, Closed, and Driven, were applied to the experiments on sand. Comparing the results of pull-out experiments in each installation condition, pull-out resistance of flip anchors can be studied, and the differences from ordinary plate anchors were able to be compared.

Then, based on the results of pull-out experiments on flip anchors, ground failure patterns with an uplift of a flip anchor in a plane strain condition were modelled, and compared with those of plate anchors. To estimate pull-out resistance of flip anchors in sand ground, the two-dimensional model was extended to three-dimensional model, considering the influence of embedded depth on ground failure patterns. Based on the model, an estimation method of pull-out resistance of flip anchors was proposed. Moreover, as an alternative, an estimation method using finite element method (FEM) was also proposed, and calculated results using both methods were compared with those of a typical estimation method using f_q for plate anchors.

Moreover, a full-scale pull-out experiment of flip anchor in a field of clay ground was also conducted. The flip anchors were installed under only Driven condition that is a practical way to install flip anchors. Based on the experimental results, an estimation method of pull-out resistance of flip anchors in clay was proposed.

Finally, to investigate the application of flip anchors to slope stability, experimental and numerical studies were also conducted. From the experiments and analysis, the effectiveness of flip anchors for slope reinforcement was confirmed.

7.2 Summary of each Chapter

In **Chapter 1**, the background and motivation of the research, the objectives of the research, and the thesis structure were presented. The expected growing demand for convenient anchors in the future, and the variation of anchors were introduced. Among the anchors, there are extremely few research cases on flip anchors.

Chapter 2 is a review of literature related to flip anchors and case studies of application of flip anchors by mainly some private companies. Research on plate anchors have been published for more than half a century. Although there are many research on pull-out resistance of plate anchors on sand and clay grounds, they are mainly laboratory model experiments including centrifuge experiments. Full-scale field experiments are rarely conducted. Though there are case studies of flip anchors

applied in the field, there are still few experiments investigating the basic performance of flip anchors.

In **Chapter 3**, pull-out experiments using actual flip anchors were conducted. Pull-out experiments on sand grounds were conducted in a model ground in a laboratory, and subsequently conducted in a field. The following findings are derived from the experimental results in sand.

1) Pull-out resistance of flip anchors increase as A or H increased.
2) F_{max} of flip anchors will be at least about 80% of F_{max} of horizontal pre-embedded plate anchors.
3) Pull-out resistance of flip anchors do not soften immediately when H/L is 5 or more.
4) The larger A is, the larger F_{max} is; whereas the smaller A is, the larger p_{max} (= F_{max}/A) is.
5) w required for a flip anchor to open sufficiently is the same as L or about 1.5 times L

The pull-out experiment was also conducted on the clayey ground. The following findings are derived from the experimental results of the pull-out experiments of flip anchors in clay.

1) In clay, F_{max} is proportional to A.
2) The estimation method invoked form the interpretation of T-bar penetration test is a promising way to estimate F_{max} of flip anchors in clay.
3) Although overburden pressure does not directly affect F_{max} of a flip anchor in clay as much as that in sand, the anchor should be installed deeper than $(H/L)_{cr}$ to obtain maximum N_b (F_{max}).

In **Chapter 4**, push-up, and vertical & diagonal pull-out experiments of model plate or model flip anchors in dry sand grounds under plane strain conditions were conducted while observing the ground failure pattern. The main findings are below.

1) F_{max} become larger as A become larger; whereas p_{max} (= F_{max}/A) become larger as A become smaller.
2) α, as well as β, do not significantly affect F_{max}.
3) Ground failure pattern accompanied with the vertical pull-out of a flip anchor was simply modelled as a 2D model. F_{max} calculated from the proposed 2D ground failure model, which is similar to that of a horizontal plate anchor, agree well with measured F_{max} of flip anchors of any pull-out condition.

In **Chapter 5**, based on the experimental results in Chapter 3 & 4, three-dimensional ground failure models were modelled by extending 2D model in Chapter 4. F_{max} of flip anchors can be calculated based on the 3D models as a limit equilibrium method. To verify the performance of proposed method, the calculated values were compared with the values calculated by empirically using breakout factor f_q for plate anchors. Furthermore, F_{max} and behavior of flip anchors were also estimated by numerical analysis (FEM). The bellows are main findings.

1) The ground failure models of flip anchors should be considered as “Shallow anchor” model or “Deep anchor” model separately according to H/L.
2) F_{max} of flip anchors at $(H/L) < (H/L)_{cr}$ increases exponentially; whereas at $(H/L)_{cr} \leq (H/L)$, F_{max} increases linearly.
3) $(H/L)_{cr}$ can be reasonably determined according to the empirical values of Meyerhof and Adams (1968).

4) F_{max} of flip anchors can be reasonably estimated by the 3D models or f_q.
5) F_{max} of flip anchors can be reasonably estimated by FEM.
6) By FEM, the behavior of the ground affected by the pull-out of flip anchors, and relationship F vs. w can also be observed.
7) The calculated F_{max} by the three estimation methods agree well with each other.
8) In FEM analysis, F at $w = L/2$ is defined as F_{max} in the deep anchor condition.
9) When driving flip anchors into the ground, the amount of w equal to L or 1.5 times L that is required for flip anchors to open sufficiently, need to be added to designed H as the installation depth before pulling the anchor.
10) The calculation methods of F_{max} of flip anchors can be based on that for the plate anchor that has abundant studies, and thus the reliability is improved.

In **Chapter 6**, an effectiveness of application of flip anchors to slope stability was verified by experimental and numerical study. The followings are main conclusions.

1) Flip anchors are effective in reinforcing slopes against slope failure.
2) When the ground displaces and push the bearing plate installed on the surface, flip anchors resist against tensile force acting on the anchor rods by the anchor head.
3) At the area of slope where the anchors are installed, the displacement of the ground is suppressed.
4) The deeper the flip anchor is installed, the greater the slope reinforcement effect is.
5) Even if a flip anchor is driven in, and without being pulled to be opened, the (Closed) anchor still has reinforcement effect. In that case, it is necessary to allow the amount of displacement of the ground that gradually displaces while the anchor is opening.
6) In case of slope reinforcement, the dilatancy of the soil greatly affects the reinforcement effect of flip anchors. In dense grounds, dilatancy behaviors of the soil may occur when external loads are applied. By installing flip anchors, the dilatancy behavior of soil is restrained, turning to an increase in the principal stresses within the slope, thus increasing the stability of the slope.
7) Slope reinforcement effect of flip anchors can be estimated by FEM analysis using the Mohr-Coulomb model.
8) Not only the reinforcement effect but also the displacement of the ground and tensile force acting on anchor rods can be well obtained by FEM analysis.

7.3 Recommendations

In this study, the fundamental behavior of flip anchors in sand or clay was verified by a seriese of basic research. Based on the experimental results and observed ground failure patterns, design methods of pull-out resistance of flip anchors were proposed in both sand and clay.

It was confirmed that the theories of pre-embedded plate anchors can be employed in the design of flip anchors, as long as the displacement of flip anchors to sufficiently open are taken into consideration. Thus, many studies on plate anchors can support application of flip anchors. For conditions not considered in this study, those studies on plate anchors can be referred to.

Because flip anchors are effective for reinforcing slopes, the application of flip anchors for small-scale construction, emergency work, or restoration work is expected. Reinforcing of slopes by flip anchors can also be designed by FEM. By the shear strength reduction (SSR) method, safety

analysis can be performed for practical uses. By designing with FEM, it is possible to consider not only the reinforcement effect but also the behavior of the ground during construction, and the design can be examined flexibly even during the construction.

As a countermeasure against slope failure caused by heavy rain or fall down of structures due to strong wind, practical applications of flip anchors are expected.

References in Chapter 7

Meyerhof G. G., and Adams J. I. (1968). The ultimate uplift capacity of foundations. Canadian Geotechnical Journal, 5(4), pp. 225-244.